A Novel Plasma Etching and Emission Monitoring System (PEEMS) to Assess Protein and Lipid Spoilation for Hydrogel Contact Lenses

Udkhar Singh-Gill

Doctor of Philosophy

The University of Aston in Birmingham

October 1997

A Novel Plasma Etching and Emission Monitoring System (PEEMS) to Assess Protein and Lipid Spoilation for Hydrogel Contact Lenses

A thesis submitted for the degree of Doctor of Philosophy
to
The University of Aston in Birmingham
by

Udkhar Singh - Gill
October 1997

Summary

The work presents a new method that combines plasma etching with extrinsic techniques to simultaneously measure matrix and surface protein and lipid deposits. The acronym for this technique is PEEMS - Plasma Etching and Emission Monitoring System.

Previous work has identified the presence of proteinaceous and lipoidal deposition on the surface of contact lenses and highlighted the probability that penetration of these spoilants will occur. This technique developed here allows unambiguous identification of the depth of penetration of spoilants to be made for various material types. It is for this reason that the technique has been employed in this thesis. The technique is applied as a 'molecular' scalpel, removing known amounts of material from the target. In this case from both the anterior and posterior surfaces of a 'soft' contact lens. The residual material is then characterised by other analytical techniques such as UV/visible and fluorescence spectroscopy.

Several studies have been carried out for both *in vivo* and *in vitro* spoilt materials. The analysis and identification of absorbed protein and lipid of the substrate revealed the importance of many factors in the absorption and adsorption process. The effect of the material structure, protein nature (in terms of size, shape and charge) and environment conditions were examined in order to determine the relative uptake of tear proteins. The studies were extended to real cases in order to study the patient dependent factors and lipoidal penetration.

Keywords: Hydrogels, Plasma Etching and Emission Monitoring System (PEEMS), UV/visible Spectroscopy, Fluorescence Spectroscopy, Proteins, Lipids.

This work is dedicated to my mother who has dedicated so much to me……

And in loving memory of 'V' Aunty, Kamla Aunty and Uncle Dennis

Acknowledgements

As this will be my first and last thesis (I don't think I could go through it again!) , I would like to extend my thanks to all of those who helped me during its gestation.

Kind thanks are due to:

- Professor B. J. Tighe, my supervisor, for his valuable advice, help, guidance, support and patience during this project.
- Dr. E. Smith for his guidance and "chewing the cud", particularly with the complex mathematics modelling .
- Dr. P. Sariri for her assistance in electrophoretic analysis and Mr. G. Snellings for the supply of polyurethane samples.
- Dr. M. Yasin for his help with computational and photographic matters, also his patience in proof reading.
- The CEAC staff for their many hours of hunting for helpful "bits and pieces" and especially Dr S. J. Moss who played a major role in the development of the rigs.
- My fellow postgraduate friends who all proved to be friendly, supportive and constructive.
- My family and friends for their constant encouragement and unfailing support thorough this challenging period.
- To Gohar Yusuf, for his many cups of tea and midnight snacks, coupled with thoughtful counsel.

Finally, I would like to acknowledge the financial support given by the Science and Engineering Research Council (SERC) and Vistakon, U.K.

Table of Contents

Table of Figures

Chapter 2

Chapter 3

Chapter 4

Chapter 5

Chapter 6

Chapter 7

Chapter 8

Table of Tables

Chapter 6

Chapter 7

List Of Abbreviations

A	Absorbance
Å	Angstrom
Ar	Argon
DC	Direct Current
ELISA	enzyme - linked immunosorbent assay
EGDM	ethylene glycol dimethacrylate
ESCA	Electron Spectroscopy and Chemical Analysis
EWC	equilibrium water content
FDA	Food and Drug Administration (USA)
G	Gibbs Free Energy
GPC	Giant Capillary Conjunctivitis
HEMA	hydroxy ethyl methacrylate
HF	High Frequency
HPLC	high performance liquid chromatography
IgG	immunoglobulins G
kD	kilo Dalton
LIF	Laser Induced Fluorescence
MAA	methacrylic acid
MHz	Mega Hertz
µg	microgram
µ	micron
MMA	methyl methacrylate
NVP	N - vinyl - 2 - pyrrolidone
OES	Optical Emission Systems
PCLM	Prototype Contact Lens Material
PE	Polyethylene
PEEMS	Plasma Etching and Emission Monitoring System
PEG	Poly ethylene glycol

PU	Polyurethanes
pHEMA	Poly hydroxy ethyl methacrylate
PMMA	Poly methyl methacrylate
PTFE	Poly tetra fluoroethylene
POTF	Pre-ocular tear film
PPG	Poly propyl glycol
PS	Polystyrene
PTMO	Poly tetra methylene oxide
PU	Poly urethane
PVC	Poly vinyl chloride
RF	Radio Frequency
SEM	scanning electron microscopy
SIMS	Secondary Ion Mass Spectroscopy
UHMWPE	Ultra High Molecular Weight Polyethylene
UV / VIS	ultra violet / visible
XPS	X-ray Photoelectron Spectroscopy

Chapter 1
An Overview of the Problem

In the last 30 years there has been considerable interest in protein (and more generally, biological) interaction with solid surfaces[1-3]. It is a phenomenon found in many areas of work (Table 1.1): the fouling of membranes used in biochemical separations, marine fouling, the formation of plaque, the clotting of blood on foreign surfaces and the deposition of tear debris on contact lenses, causing many acute problems[4-7] . This work will concentrate on the effect that the biological medium has on contact lenses within the ocular environment.

The ocular compatibility of contact lens biomaterials depends upon a series of complex biochemical events. Initially, contact lens wear produces a marked change in the environment of the anterior eye and corneal metabolic function. During a period of time deposits accumulate on the lens surface which may not only impair vision, but also result in adverse immunological events[5-6]. Tripathi termed this process 'spoilation'[4]. The success of contact lens wear depends on limiting the degree of metabolically induced change, whilst the eye adapts to a reduced oxygen environment, and in controlling the accumulation of the deposition during lens wear. Clinical studies have shown, there is evidence of ocular adaptation to materials of differing physical properties, making the diffusional and bio-interfacial phenomena of particular interest[1,7].

Extensive studies using a wide variety of methodologies have been reported for monitoring protein deposits on the surface and within the matrix of hydrophilic 'soft' contact lenses. These studies have attempted to characterise the deposition processes that occur during contact lens wear and to identify ways of reducing deposit formation. Some of the more common reported methods for characterising lens deposits are listed in Table 1.2.

It has been well documented that the higher water content lenses (Food and Drug Administration (FDA) classification Group II and especially the ionic Group IV lenses) form protein deposits to a much greater extent than the low water content lenses (Group I and III), (Table 2.5). It is clear from the studies appearing in the literature, that no method has been developed that can simultaneously measure matrix and surface deposition profiles and relate these to the lens material. Fowler and co-workers[17] have

suggested a greater (unspecified) surface deposition on high water content lenses as compared to low water content lenses over a short wearing period.

Field	Role of Adsorption
◆ Medical devices (cardiovascular)	Interactions with the surrounding fluids leads to protein adsorption and other interfacial processes. Occurring in blood coagulation, complement activation and the interaction of tissues to artificial implants
◆ Pharmacy	Interaction of peptide and protein agents with container surfaces leads to the depletion of the active agent from solution. The controlled delivery of peptides and proteins by drug delivery devices is also dependent on protein-solid interactions.
◆ Protein Processing	The separation and purification of proteins (from plasma or other complex media) is usually accomplished by solid-liquid chromatography. Protein and lipid chromatography depends on the interaction of the protein or lipid with the support - generally by hydrophobic, ion exchange, or charge transfer mechanisms.
◆ Biotechnology and cell culture	Cell culture *in vitro* usually requires cell-surface adhesion which is mediated by an interim layer of adsorbed protein. Biotechnology industries, depend in part on mass cell culture and on protein separation and purification by chromatographic means.
◆ Filtration	Water treatment: Clarification is often done by filtration processes. The long-term function and stability of the filters depends on the adsorption properties of proteins and other macromolecules in the solutions treated.
◆ Fouling	The attachment of marine and micro-organisms to materials is often mediated by protein interactions. It is often necessary to minimise fouling, such as on naval ships, underwater structures, etc.
◆ Sensors and Diagnostics Products	Solid-phase immunoassays often depend on the adsorptive immobilisation of antigen or antibody.
◆ Directed Drug Delivery	The use of liposomes or other particles as targeted drug delivery devices depends on the adsorptive and /or covalent immobilisation of tissue and organ-specific immunoglobulins.

Table 1.1: Common Methods For Characterising Biological Deposits On Biomaterials[1,8]

Technique	Principle	Information
◆ Fluorescence Spectroscopy	Intrinsic (Trp) or extrinsic (label) fluorescence-transmission or total internal reflection.	Local environment influences wavelength and intensity of fluorescence. Some conformational information. Difficult to quantify.
◆ UV-visible Absorption Spectroscopy	Tyrosine-Tryptophan environments.	Bulk presence of absorbing ligands or impurities.
◆ Gel Electrophoresis	Molecular transport by current due to charge	Nature of surface charge; requires individual particles or high surface area.
◆ X-ray photoelectron spectroscopy (ESCA)	X-ray induced surface photoelectron.	Elemental analysis and chemical bonding nature of surface. Need dried surface. Not feasible for direct solid-water studies. Variable angle studies useful for determining homogeneity of adsorbed layers. Extrinsic factors (Silicon from packaging) can inhibit results (Fig. 2.1).
◆ Secondary Ion Mass Spectroscopy (SIMS)	Produces an ion beam to sputter fragments of the sample from the surface.	Fragments are analysed in a similar way to the fragments in a conventional mass spectrometer. Similar problems to XPS, but may also alter samples' chemistry before analysis. Its main advantage over ESCA is its superior surface sensitivity and molecular selectivity which enables a much greater level of structural information to be obtained.

Table 1.2: Some Methods Used to Study Biological Interfacial Behaviour[8-11]

Sack and associates[12] examined the lens-bound protein layer on various worn hydrogels and found a much thicker surface layer on higher water content, ionic lenses compared to lower water content, non-ionic materials. In contrast, Myers and co-workers[13] found a nearly equal distribution of visible protein deposits appearing on the surface of Group I and IV lenses yet a significantly greater total protein accumulation was observed (in agreement with many other studies) for Group IV materials. This later finding suggests a significant matrix deposition since the visible protein deposits primarily represent surface accumulation of tear proteins.

A need exists to understand clearly the matrix-surface deposition behaviour, since these patterns are believed to influence the more troublesome contact lens complications (e.g. giant papillary conjunctivitis (GPC) and non infectious keratitis) along with less significant, although no less clinically important, problems such as lens wear discomfort. Although exact mechanisms have not been defined, it is possible that greater surface protein accumulation might create a mechanical stimulus to GPC[14]. Alternatively, significant matrix protein accumulation in certain lens types may be the more probable causal factor. By having a clearer picture of the deposition processes we can go some way in improving the development and production life-cycle of medical devices and reducing the incompatibility of these devices with the biological host.

The technique to be discussed in the following pages is based on plasma etching. It allows removal of micron layers from the surface of a sample, as a 'molecular scalpel', and in conjunction with spectroscopic techniques of absorption (UV) and fluorescence, can reconstruct a depth profile that penetrates many microns within the sample's matrix. Although plasma technology has been around for a numerous number of years, it has only recently been applied in the area of biomaterials, mainly in studies concerning surface modification.

Chapter 2

This chapter describes the application of polymeric biomaterials and focuses specifically on the role of contact lenses produced from hydrophilic polymers, known as hydrogels. The chapter describes the host site for implantation, the eye, and details the biocompatability of a biomaterial within the ocular environment and the tolerability shown by a contact lens on implantation.

Chapter 3

This section will outline the basic terminology and processes which are prevalent in plasma etching. Because of the importance of the plasma to the process of etching, plasma properties are initially described. The general plasma etch process is also described along with major process influences. The chapter then goes on to describe the basic chemistry involved in gas plasma etching for an oxygen-polymer system.

Chapter 4

This chapter will detail the development work undertaken. Initially, the intrinsic plasma system parameters, design and operating procedures are discussed. The extrinsic development techniques that are run either concurrently (Optical Emission Spectroscopy (OES)) or in conjunction (UV and fluorescence spectroscopy) with plasma etching are

described. They are collectively known as the plasma etching and emission monitoring (PEEMS).

Chapter 5

The aim of this series of experiments was to study, for a given etchant, the influence of three process parameters - gas flow, chamber pressure and applied RF power - on the etch rates of Polymacon and Etafilcon A over a wide range of values of the process parameters, and to study the corresponding gas-phase chemistry using optical emission spectroscopy. Three etchants - air, oxygen and argon - commonly used in plasma etch processes, were chosen for investigation. Orthogonal relationships were employed both to maximise the amount of useful data generated from the minimum necessary number of experiments in the parameter space, and to assist in a comparison of the results from the etchants through modelling.

Chapter 6

The studies detailed below look at two classes of polymeric materials, hydrogels (HEMA copolymers) in Section 6.2 and polyurethanes (poly ethyleneglycol (PEG) copolymers) in Section 6.7. Section 6.13 goes on to discuss a terpolymer system comprising of HEMA:PEG:MAA

Chapter 7

An initial view of the data suggests that very high protein concentrations arise in thin layers close to the polymer surfaces of Group I and IV lenses. This chapter describes progress to date and summarises the methods used in data analysis and typical results.

Chapter 8

Describes an enhancement technique for PEEMS using Mass spectrometry. This chapter describes the laboratory set-up and potential data generation through MS and improved OES.

Chapter 9

Concludes the findings procured through PEEMS and suggests future work that maybe undertaken from findings generated in Chapters 5-8.

Chapter 2

Introduction

This chapter describes the application of polymeric biomaterials and focuses specifically on the role of contact lenses produced from hydrophilic polymers, known as hydrogels. The chapter describes the host site for implantation, the eye, and details the biocompatability of a biomaterial within the ocular environment and the tolerability shown by a contact lens on implantation.

2.1 Application of Polymeric Biomaterials

The development of artificial organs and prostheses has contributed immeasurably to the welfare and health of the human race and animals, with over 2,500 million devices being used annually[15] (Figure 2.1), contributing to some of the most valuable remedies in present medical armoury.

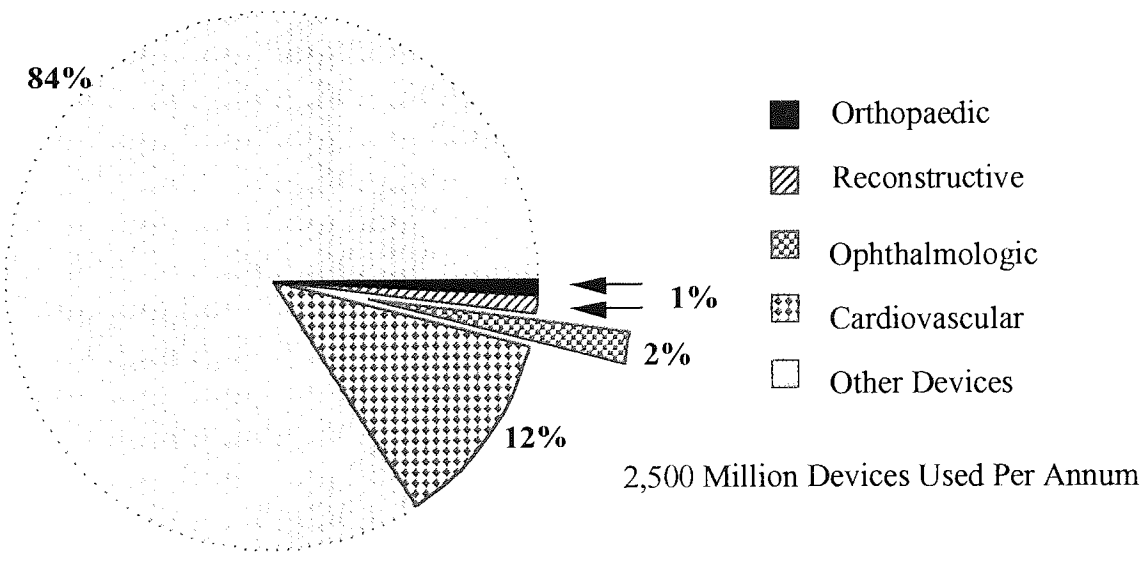

Figure 2.1: Selected Biomedical Applications of Polymers

Figure 2.2 illustrates the diversity of applications of biomaterials as prostheses in humans. With the widespread usage of these materials, one would presume the success rate of these devices to be high. This is true in some cases, but in others, high failure rates are common. Some examples illustrate this situation[16].

(a) One million intraocular lenses (IOL's) are implanted in US citizens every year, largely to replace a natural lens after significant cataract formation has degraded vision. Because this procedure restores vision to most recipients within hours of implantation and most IOL recipients have suffered degraded vision for years prior to the implant, the efficacy of this operation is generally praised. However, the failure rate for IOL procedures hovers around 1%. Many of these failures can be attributed to material related issues. A 1% failure rate translates to 10,000 impaired eyes (in the US alone).

(b) Vascular prostheses for peripheral arteries are implanted in thousands of individuals each year. The failure rate for these synthetic polymeric implants within the first 18 months may be as high as 50%. Failure of the device often necessitates amputation of the limb.

(c) It is estimated that over 100, 000 US adults could benefit from a total artificial heart to replace their own natural hearts. Although only a relatively small number of people have undergone artificial heart implantations the ratio of success of this device (presuming long term circulatory support to be the appropriate performance standard) is low, with significant problems attributed to biomaterial-related infection and thromboembolic complications.

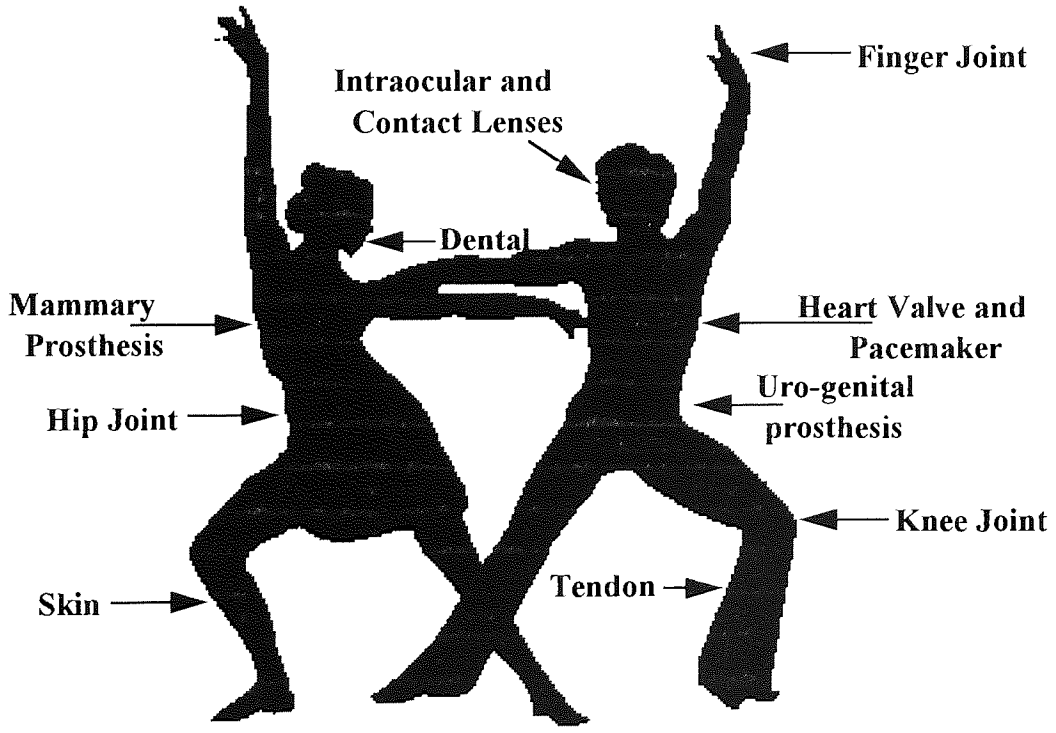

Figure 2.2: Clinical Applications of Biomaterials

Fundamental research on biological reactions to implanted synthetic materials continues with increasing interest and effort to the present day. The actual role of a biomaterial is for repair, restoration and replacement of damaged or diseased tissue and to interface with the physiological environment. Although the synthetic implant device does have a low success rate, at present they do supply some degree of functionality and often an improved quality of life, to an individual who might otherwise have a curtailed activity level or life expectancy.

CLASS	MATERIALS
Metals[23]	Stainless steels, cobalt-based alloys, gold, titanium and its alloys.
Ceramics[18]	Aluminium oxide, hydroxyapatite, glass, carbon.
Composites[19-20]	Ceramics coated materials, carbon coated materials.
Polymers[17,21-22]	Hydrogels, acrylics, polyurethanes, silicones, nylon, Teflon.
Biological Materials[21]	Porcine skin and heart valves, bovine arteries.

Table 2.1: Classes Of Biomaterials

Biomaterials may be of natural origin or synthetically produced (Table 2.1). One of these groups of biomaterials, polymers, shows great processing diversity and application (Figure 2.1 and Table 2.2) allowing great scope for investigative work[24-26]. The general biomedical principle of designing a material to give a balance of properties appropriate to a particular environment is of prime importance. For example, in ophthalmics, the contact lens can be considered as an extension of the cornea. Thus, the lens must allow the cornea to respire normally, it must resist the deforming force of the eyelid and it must permit a continuous tear film to be maintained on the lens, whilst minimising the accumulation of deposits. One of the classes of polymeric materials associated with contact lens design has been the hydrogel.

2.2 Synthetic Hydrogels

Hydrogels are defined as polymeric materials that have the ability to swell and retain a significant fraction of water within their three dimensional network[24]. They represent the first class of materials to be designed and developed with medical applications in mind[26]. Table 2.3 lists the various applications of hydrogels as biomaterials to date, taken from a comprehensive review by Ratner and Hoffman[16].

MAJOR FIELDS	POLYMERS
• Ophthamological	• PMMA, PVP, PHEMA
• Cardiovascular	• PP, PTFE, PVC, Teflon, PU
• Reconstructive	• Silicone Rubber, PE, Teflon, PU
• Dental	• PMMA, Silicone Rubber, Nylon
• Orthopaedic	• UHMWPE, PP, PMMA
• Disposable articles or extra corporeal materials	• PVC, PE, PP, PS, PU, PHEMA

Table 2.2: Biomedical Applications Of Polymers [16-26]

Polymethylmethacrylate (PMMA), Polyvinylpyrrolidone (PVP, Polyhydroxyethylmethacrylate (PHEMA), polypropylene (PP), Polytetrafluoroethylene (PTFE), Polyvinylchloride (PVC), Polyurethane (PU), Polyethylene (PE), Ultra High Molecular Weight Polyethylene (UHMWPE), Polystyrene (PS).

COATINGS	BULK MATERIALS	SYSTEMS
Sutures	Contact Lenses	Enzyme Therapeutic Devices
Catheters	Artificial Corneas	
Inter-Uterine Devices	Vitreous Humor Replacements	
Blood Detoxicants	Soft Tissue Substitutes	Drug Delivery
Sensors (electrodes)	Bone Growth Sponges	
Vascular Grafts	Dentures	Artificial Organs-dialysis
	Synthetic Cartilage	

Table 2.3: Biomedical Applications Of Synthetic Hydrogels[27-28]

The biomedical interest in hydrogels stems from a number of real and hypothetical advantages for these polymers[26-28]. It is these hydrogel characteristics which can be used to help maximise tolerability of implants.

(a) They have an inherent permeability and diffusion for small molecules, waste products and salts just as soft tissue in the body.

(b) This permeability has an added bonus, in allowing artefacts of polymerisation (i.e. excess initiator, monomer, products and solvents) to be eliminated prior to the hydrogels coming into contact with living system. Post polymerisation leachates have been cited as a cause of inflammation and ultimate rejection of biomaterials.

(c) Their soft, rubbery nature minimises mechanical and frictional irritation to surrounding tissue.

(d) Another distinct structural advantage of hydrogels, is that it is possible to incorporate drugs into their gel-network, which when implanted or administered, will give controlled release of the drug.

(e) Hydrogels have low interfacial tensions which may be exhibited between a hydrogel surface and an aqueous solution. These low interfacial tensions should reduce the tendency of the proteins in the bodily fluids to absorb, or to unfold upon adsorption. Surface adsorption and denaturation of proteins have been shown to elicit a thromobogenic response.

2.2.1 Contact Lenses

There are two main classes of contact lenses which are, hard (polymethylmethacrylate (PMMA), rigid gas permeable (RGP)) and soft[29-30] is the latter classification which is relevant, being manufactured from hydrogels. Although there are essential chemical differences between the classifications, there is also a physical difference. It is the manner in which the lens fits the eye. PMMA contact lenses and RGP lenses require a relatively thick tear film between their surfaces and the cornea. Soft hydrogel lenses adhere closely to the cornea. This fitting criteria in itself has made soft lenses popular, because they are more comfortable and better tolerated by the eye[29-30].

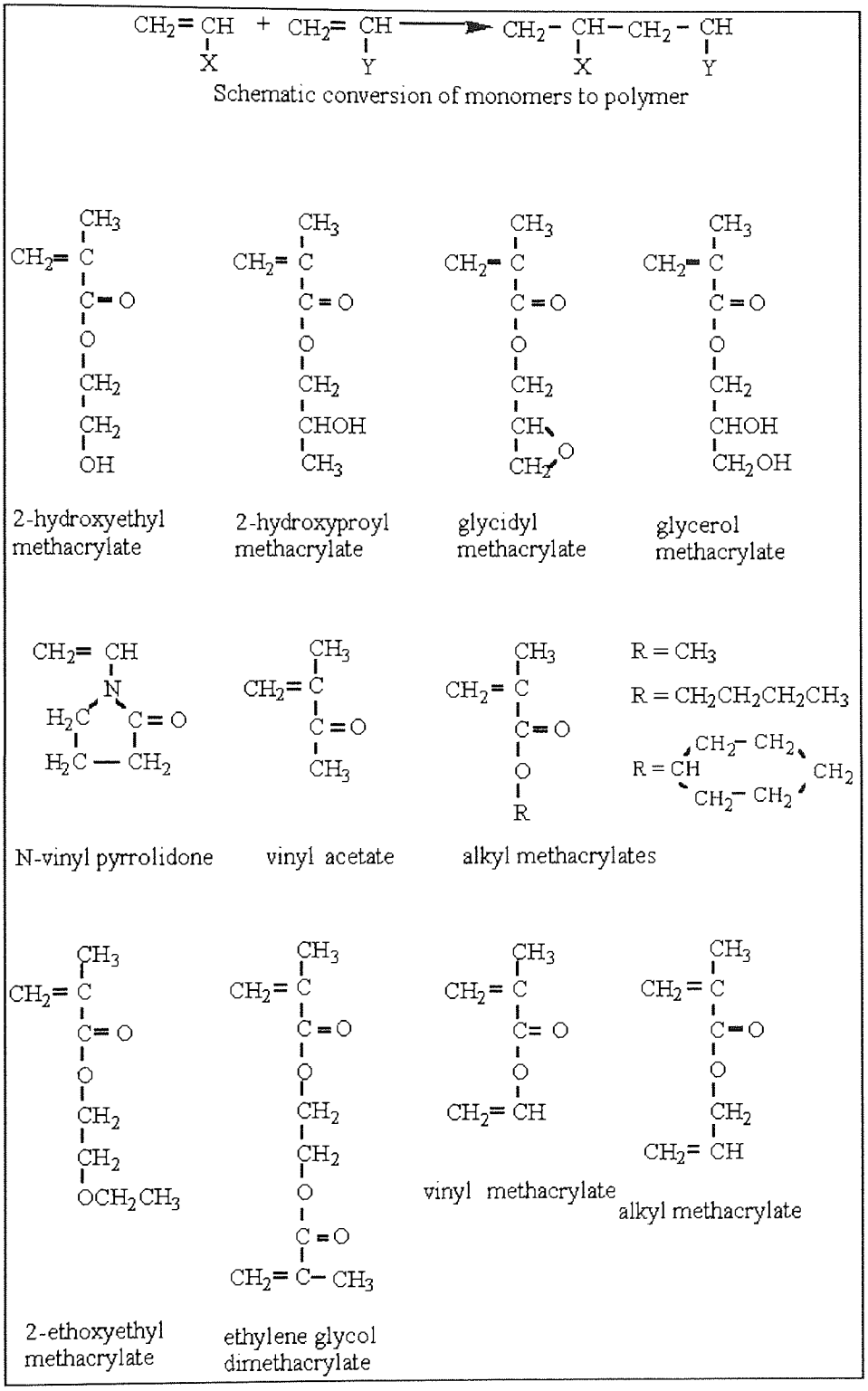

Figure 2.3: Structures of some monomers used in hydrogel synthesis[30-34]

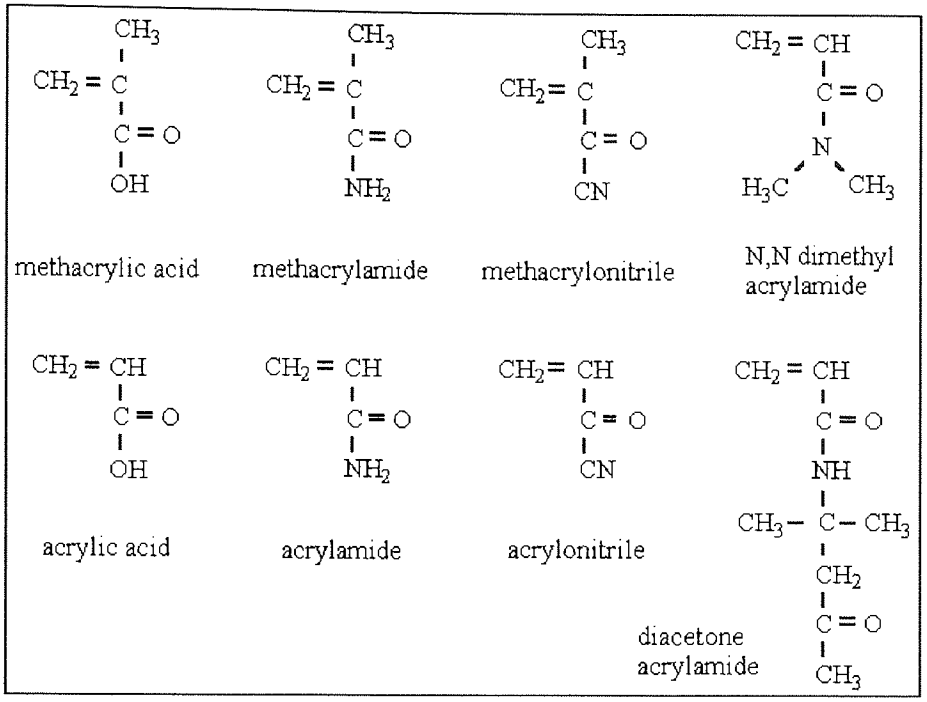

Figure 2.4: Monomers used in hydrogel synthesis (continued).

Common hydrogel materials consist of constituents such as poly(2-hydroxyethylmethacrylate (HEMA), and copolymers of this with methylmethacrylate (MMA), N-vinylpyrrolidone (NVP) glycerol methacrylate (GMA) and methacrylic acid (MAA). Figures 2.3 and Figure 2.4 shows a range of monomers used in hydrogel synthesis. Cross-linking agents are typically added to produce mechanical strength and thermal stability. All of these hydrophilic monomers, with the exception of methacrylic acid, yield non-ionic polymers that interact with the polar molecules of water without generating a formal electrostatic change on the molecule. Low water content lenses of this type usually have water contents of 38-50%. High water content lenses, that are mostly vinyl pyrrolidone-based polymers, have water contents of 50-80%. These lens materials constitute the low and high water content non-ionic lens groups. On the other hand, ionic lens materials with low or high water contents are made using methacrylic acid, a charged, ionic monomer. Table 2.4 shows some examples of commercially available soft hydrogel lens materials.

Name	Principal Component(s)	Water Content (%)	Manufacturer Supplier	FDA Class.	USAN Nomenclature
Acuvue	HEMA, MA	58	Vistakon	Group IV	Etafilcon-A
Gentle Touch	MMA, NDMA	65	Pilkington Barnes-Hind	Group	Netrafilcon-A
Classic	HEMA, VP,	42.5	Pilkington Barnes-Hind	Group I	Tetrafilcon-A
Excelens	PVA, MMA	64	Ciba	Group II	Atlafilcon
SeeQuence	HEMA	38	Bausch & Lomb	Group I	Polymacon
Medalist 66	HEMA	66	Bausch & Lomb	Group	Alphafilcon
Surevue	HEMA, MAA	58	Vistakon	Group IV	Etafilcon-A

Table 2.4: Examples of commercially available soft contact lenses and lens materials.

Since hydrogel lenses adhere very closely to the corneal surface, the amount of oxygen transferred to the cells of the cornea by tear flow is very small and the oxygenation of the cornea is largely through diffusion of gas across the lens[29,35]. From this design parameter has evolved not only the daily-wear lens but also the extended-wear lens. The principal difference is that the latter must be more permeable to oxygen than the former. Extended-wear lenses must transmit sufficient oxygen to maintain corneal health; the requirement is estimated at 2-5 $(mm^3h^{-1})cm^{-2}$ of corneal surface[34], even when the eye is closed for sleep.

Daily-wear regimes provide a rest period in which the cornea can repair from the day's anoxia. The relatively high oxygen transmissibility of soft extended-wear lenses is achieved by making the lens thinner than daily-wear lenses or by a higher water content, or both. If insufficient oxygen reaches the cornea, corneal swelling (œdema) occurs causing much discomfort to the patient.

2.3 Nature of the Problem - Spoilation

Any polymer from which contact lenses are made, has to meet a set of structure-based requirements[21]. The polymer must be chemically stable, optically clear, with a stable and appropriate refractive index, a smooth surface that has a low surface energy and low contact angle (the angle between the lens surface and a drop of water on it, a contact angle of zero implies complete wetting of the surface).

The biological environment is a diverse and complex system. Implanting a polymer requires the scientist or clinician to have a thorough understanding of the physiological functions and conditions under which the device must operate. The natural performance standard is that provided by the natural tissue or organ (Table 2.7 and 2.8). As the successful application of a biomaterial requires both an acceptable biological response to the implanted material and the absence of physiological induced damage, the concept of biological performance (biocompatability) has emerged[8]. This is a measure of the overall interaction between biomaterials and the living systems and includes local and systematic host responses to the implant and the material's response to the physiological environment[33,37]. Therefore, all biomaterials must meet certain criteria and regulatory requirements before they can be qualified for use in medical applications, as illustrated in Table 2.5.

Several advantageous points were listed for the use of hydrogels as biomaterials in Section 2.2, but unfortunately hydrogels have disadvantages as well, e.g. hydrogel contact lenses are more easily damaged than hard lenses and require greater hygienic care because of bacterial attack. Additionally, once in contact with the tear film the contact lens immediately becomes coated with the tear components[29,36-42].

- Can be purified, fabricated and sterilised easily by conventional methods.
- Free from leachable impurities, additives, and compounds e.g. (initiators, stabilisers, emulsifiers, unreacted monomers or oligomers, plasticisers, fragments or fillers)
- Meets desired biomechanical properties (in tension, compression and shear).
- Has desirable physical structure (e.g. crystallinity, entanglement density, equilibrium swelling).
- Has other desirable properties (hydrophobicity/hydrophilicity, wettability, surface charge, polarity, heterogeneity in the distribution of reactive chemical groups, surface energetics, mobility of the surface molecules and smoothness).
- Maintains its properties and function *in vivo* over desired time period (e.g. 1h, 1 day, 1 or 10 years).
- Does not induce undesirable host reactions (e.g. thrombosis, inflammatory reactions, tissue necrosis, toxicity, allergenic reactions, carcinogenic).

Table 2.5: Criteria For Selection Of Biomaterials [24,43]

This is not necessarily bad, because it can contribute to improved biocompatability of the contact lens (Section 2.2 (e)). Thus, the problem is not that a contact lens adsorbs proteins and other biological species, but the consequential build-up that occurs thereafter. The

nature of the initial biological species' adsorption[1, 39-49] is influenced by a combination of factors related to the contact lens biomaterial, such as the smoothness of the contact lens surface, the surface charge, the wettability, the chemical structure of the polymer surface, the elasticity of the lens material, and other factors such as tear flow and rate of blinking. Additionally, build-up may have more to do with the quality of the tear film and the blinking habits of a given patient than with the chemical nature of the contact lens material. Future developments in the contact lens field will result in lenses that are not only permeable to oxygen, but those that are also more resistant than currently available lenses to the build-up of proteins, lipids and other foreign materials. The aim is to minimise the irreversible processes, such as conformational changes in proteins (denatured) and to attain reversible deposition.

2.3.1 Nature And Occurrence Of Lens Spoilation

It is the nature and extent of the interaction between tear fluid and lens material that reflects the degree of spoilation (biocompatability). When a hydrogel is in an aqueous solution at equilibrium swelling, many low molecular weight solutes and ions in the solution are distributed between the aqueous phase and the external environment. Certain molecules of variant nature, deviate from this behaviour. Some substances show a greater affinity for the polymer matrix than for the aqueous solution, and so concentrate on and in the lens, to form a pellicle and eventually form complex compositional structures, called white spots[79]. Subsequent release of components from the absorbed molecular structure back into the eye is a possible hazard, since these substances maybe toxic to the host tissues, e.g. preservatives in disinfection solutions, denatured protein. Lens spoilation is the term used to encompass physical and chemical changes in the nature of contact lenses, and various extraneous deposits which may impair the optical properties of the lens or produce symptoms of discomfort and intolerance to the wearer[44-46]. The extent of the situation may be appreciated by considering the reported incidence of lens spoilation[45-70]. Lens spoilage may occur in some cases as early as 48 hours of wear, whilst the majority of cases are 3-6 months of daily or extended wear[71]. It is convenient in a review of this type to divide the observed types of spoilation into different classes. It must be appreciated, however, that such a classification is largely artificial[37] with considerable overlap between the classes, and systematic analysis of the results of spoilation are rarely undertaken. Therefore, the classification is best regarded, as a grouping of various related types of clinically observed phenomena and is shown in Table 2.6.

COMPLEX DEPOSITS	LENS COATINGS	MICROBIAL	DISCOLOURATION
Discrete elevated deposits - "White spots"	Proteinaceous Films. Granular Deposits. Calcium Deposits	Fungal and Bacterial Contamination	Eye make-up. Rust spots

Table 2.6: Clinical Observed Manifestations Of Hydrogel Lens Spoilation[3,7,38-40,59,61]

It is essential to appreciate fully the area of implantation and the interactions occurring within the tear film and between it and the surface of the eye. Only with this information as a working base will it be possible to decipher the steps involved in the spoilation process and aid in alleviating the symptoms encountered by the patient. The next section will describe the ocular environment: the host (eye) and the biological media (tears).

2.4 The Host - The Eye

In a normal eye, a ray of light from an object diffracts through the cornea and the lens of the eye and falls on the retina (Figure 2.5), the signal is then transmitted down the optic nerve to the brain. When the eye is abnormal in vision, the object is focused either in front of the retina or behind the retina. The function and design of the contact lens and fitting techniques employed convert the abnormality by enabling the image to be found on the retina, as in a normal eye[73-75].

As in other body sites the tissues within the eye undergo similar processes of degeneration and regeneration. Nutrition and waste disposal are requirements continually fostered throughout the body, and in the eye this is maintained by tears, vitreous and aqueous humour and vascular system. The exterior portions exposed to the surrounding environment are the conjunctiva and cornea (Figure 2.5). The cornea is the first structural line of defence for the eye and damage or destruction of the cornea can lead to blindness for many people. When the cornea is damaged, the tear fluid and aqueous fluid are insufficient to meet the eye's new requirements and corneal vascularisation may occur. (If this leads to irreparable damage, a hydrogel may be used as a replacement for the cornea[32]). The cornea is separated from the lens of the eye by the aqueous humour, and on the other side, from the atmospheric air by a layer of tear fluid known as the pre-ocular tear film (POTF)[76].

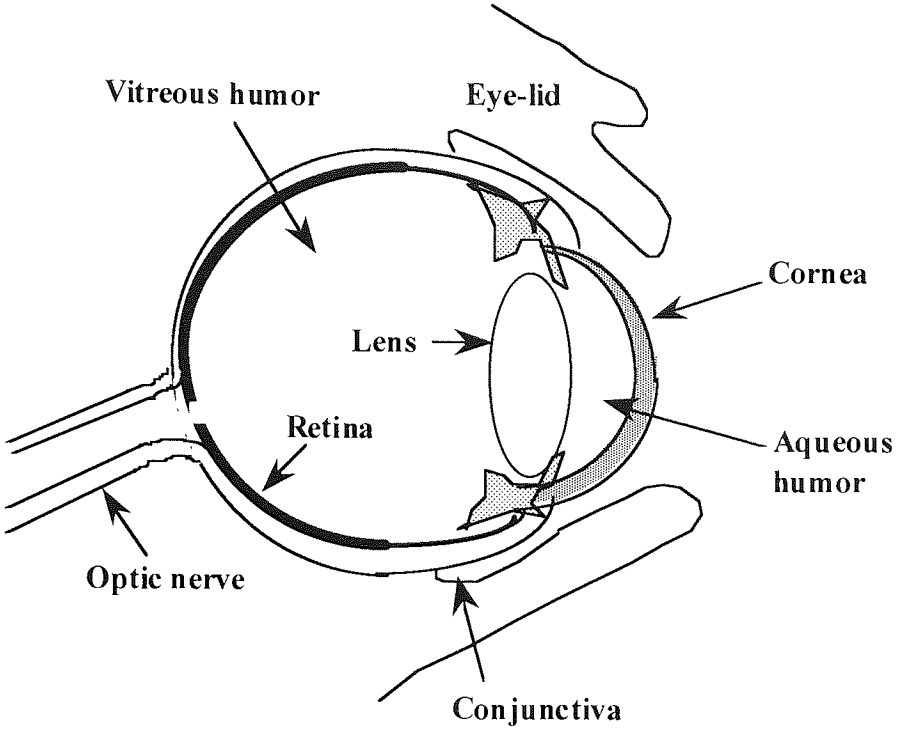

Figure 2.5: Cross-sectional Structure of the Eye

Component	Value
Water Content	~ 81%
Critical Surface Tension	~35 mN/m
Refractive Index	1.37
Mechanical Properties	~ 1.3 x 10^7 N/m^2
Oxygen Permeability (stroma)	~ 300 x 10^{-10} cm^3/mm/cm^2/s/cmHg
Oxygen Consumption	3.5-7 x 10^{-6}/1 cm^2/h
Minimum oxygen tension for corneal clarity	12-18 mm Hg
Normal oxygen tension in Tear Fluid	155 mm Hg (open eye); 55 mm Hg (closed eye)
Deforming Force of Eyelid	~2.6 x 10^3 N/m^2

Table 2.7: Some Properties of the Cornea and its Environment [30,77-79]

The general biomedical principle of designing a material to give a balance of properties appropriate to a particular environment is of prime importance. The contact lens can be likened to an extension of the cornea. Thus, the lens must allow the cornea to respire normally, it must resist the deforming force of the eyelid and it must permit a continuous tear film to be maintained on the lens, whilst minimising the accumulation of deposits.

2.5 The Biological Medium - Tears

The pre-ocular tear film (POTF) is probably the most regularly arranged fluid to be found within the body, having a tri-laminar structure as shown in Figure 2.6, with an outer superficial lipid layer, an intermediate aqueous phase, and a tertiary mucoid layer.

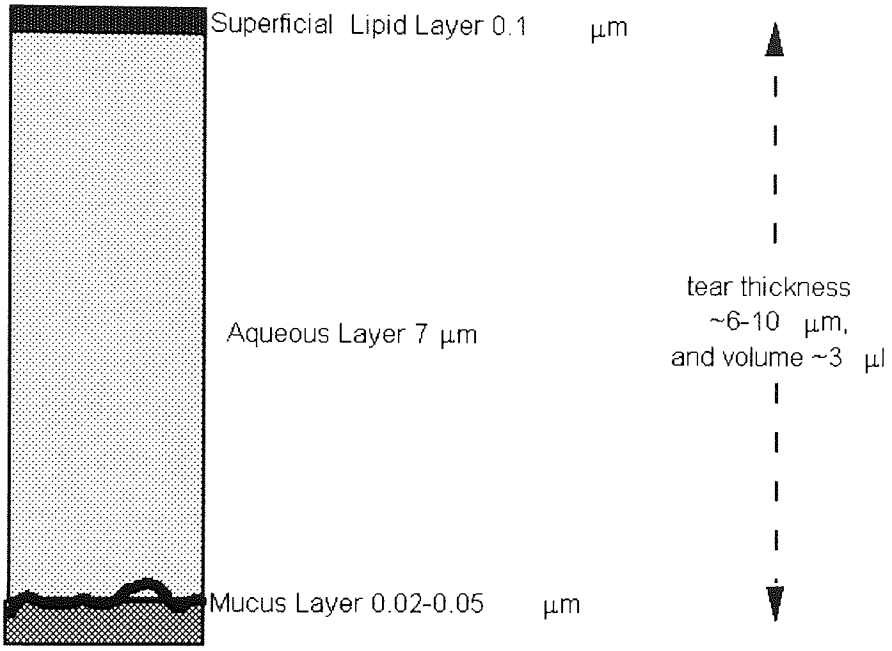

Figure 2.6: Schematic Representation Of Tear Film [30,80-83]

2.5.1 Physical Properties

Derived from a number of sources (Table 2.9), the tear film fulfils several roles. The presence of a continuous tear film significantly increases the optical resolution of the eye by 'smoothing' the many fine irregularities of the corneal surface. As well as providing the major oxygen source of the vascular cornea, the tear film acts as a lubricative agent, allowing the eyelids to remove cellular debris from the cornea, by sweeping across its surface. The tear film also ensures the necessary degree of hydration required for a fully functioning cornea, and defines the transport characteristics across the cornea. By the provision of a wide spectrum of anti-microbial proteins, the tear film provides powerful and effective protection of the cornea.

Volume	3μl
Production Rate	1.2 μl /min
Thickness	6-10 μm
Break-up Time (BUT)	5-45 s
Eyelid Closure Time (between blinks)	0.4 s
Surface Tension	40-42 dyne cm^{-1}
Temperature	30 °C
pH	7.6 ($\pm$0.4)

Table 2.8: Physical Characteristics of Tears[76-78]

Table 2.8 shows some of the tears' physical properties before lens insertion. The tear film is not evenly distributed over the ocular surfaces, but forms a distinct meniscus at the lid margins; the marginal tear strips, or lakes. The volume of tears in this area is approximately 3 μl, while the volume covering the cornea is about 1μl and a further 3 to 4 μl are distributed in an even manner over the conjunctiva[30,32]. There is some disagreement about factors affecting normal tear secretion[71]. Most researchers find a decrease in secretion rate with age. Some studies, however, have reported no correlation of tear secretion with age[71], and suggests that these findings could be because older eyes are less sensitive to stimuli. Furthermore, data may vary because there is a significant difference in composition between the tear film in closed and open eyes[83], making time of day for data retrieval from patients an added criteria in the assessment of lens related problems.

Although it is possible to ascribe differing volumes to the tear film located in differing parts of the anterior surface of the eye, the tears are not static. The act of blinking has a substantial effect upon the film and the marginal strips. Holly[80,83] has described the dynamics of the tear film due to blinking. As the upper lid moves downwards, the superficial lipid layer is compressed. As it thickens, it begins to exhibit interference colours. When the eye opens, at first the lipid spreads in the form of a monolayer against the upper eyelid. In this spreading process, the limiting factor is the motion of the eyelid. The spreading of the excess lipid follows, and in about one second the duplex (multi-molecular) lipid layer is formed. The spreading lipid drags some aqueous tears with it, thereby thickening the tear space film. The magnitude of this effect is controlled by the size and the shape of the tear meniscus, a local thinning adjacent to the meniscus takes place, which effectively prevents further fluid flow from the meniscus to the tear film.

2.5.2 Chemistry of the Tear Film

Although easily accessible, tears are relatively little understood or studied[160] probably due to the small volumes available. Reports on tear composition are diverse, widely scattered and technique-dependent. One of the most comprehensive descriptive studies of the structure and composition of tear fluid was that by Larke[30,85-86]. Based on this review a dissemination of the tri-laminar layers is given in Table 2.9.

Tear Film Composition	Superficial Lipid Layer	Aqueous	Mucus
Origin	Tarsal Meibomian Glands.	Main lacrimal gland & accessory lacrimal glands of the conjunctiva.	Conjunctival Globlet Cells.
Components	Cholesterol esters and other ester waxes.	Inorganic Electrolytes, Proteins & Water.	Glycoproteins, plasma proteins.
Major Role	Produces a hydrophobic barrier-contains the tears, reduce tear evaporation, enhances the optical properties of the tear film and tear film stability.	Houses the major components of the tear film; to aid in functionality and protection of the eye.	Interfaces between tears and epithelium. Removes tear contaminants.

Table 2.9: Tear Film Composition[30,79,84]

The tear film possesses a complicated chemical structure which contains many proteins, lipids and a number of inorganic substances. It is these components which will now be discussed in further detail, as these are the 'players' in the process of spoilation.

2.5.2.1 Lipid phase

The composition of human tear lipids was probably first described in 1897 as cholesterol, fatty acids and fat[83,87-90]. However, the large size and number of meibomian glands suggest that the eye has a considerable requirement for fatty materials. Lipids are required to prevent wetting of the skin of the lids adjacent to the eye and to contain the tears. Some lipids are spread over the tear film surface forming the outermost layer of the film and reducing evaporation. This spreading action may be aided by the particular nature of the fatty acids found in lipids which form an unusual group of high molecular weight

compounds. It has been suggested that considerable variations in lipid composition exist between different individuals[73].

However, there are considerable technical difficulties in the analysis of the very small samples that can be obtained from subjects and the close similarities between post-mortem samples of human and bovine fluid suggest that the requirement for lipid on the eyelids of man and animals is similar. Table 2.10 shows the lipid composition for bovine and human meibomian samples.

Lipid Composition	Bovine	Man
Esterol esters	31.7	29.5
Weak acid esters	31.2	35.0
Material in the diester region	11.4	8.4
Triacyl glycerol	1.6	4.0
Material in the post-triacyl glycerol region	2.8	3.2
Free estrols	3.0	1.8
Free fatty acids	5.1	2.1
Polar lipids	13.3	16.0

Table 2.10: Comparative lipid composition for bovine and human meibomian samples (all values % by weight) [83,98-99]

2.5.2.2 Aqueous phase

The aqueous phase of the tears forms the major component of the film, comprising about 98% of its total thickness. It is a complex dilute solution of both inorganic electrolytes and low and high molecular weight organic substances.

The main cation found in the aqueous phase of the tear film is sodium, and its concentration is similar to that found in serum. Potassium is another principal cation found in tears, but its concentration is about 3-6 times higher than its concentration in serum. Calcium and magnesium cations are also found in small quantities in tears. The two principal anions in tears are chloride and bicarbonate ions, and their concentrations are very similar to those found in serum. Table 2.11 compares the concentrations of tear and serum electrolytes.

Glucose is present only in very low concentrations. Raised glucose levels may occur in diabetes, but these values are attributable to the raised tissue fluid levels rather than raised tear levels.

Electrolyte	Ionic Radii (Å)	Tears	Serum
Na^+	1.02	80-170	140
K^+	1.38	6-42	4.5
Ca^{++}	0.99	0.3-2.0	2.5
Mg^{++}	0.72	0.3-1.1	0.9
Cl^-	1.81	106-135	100
HCO_3^-	2.32	26	30

Table 2.11: Average concentrations (mmol/l) of human tear and serum electrolytes and their Ionic Radii [91-93]

The total free amino acids present in tears have not been identified, but may be present in a concentration that is three to four times the serum levels. The concentration of urea in tears is similar to that of blood plasma (20-40%). This suggests an unrestricted passage of urea across the blood/tear barrier of the lacrimal gland.

The aqueous phase of tears contain a remarkably complex mixture of both locally produced and serum derived proteins. Using the cross immuno-electrophoresis technique, Gachon et al[95] have identified at least sixty protein components, some of which are immunologically indistinguishable from serum homologous, while others are clearly distinguishable and of specific tear origin. Table 2.12 lists some identified tear proteins.

Although a complex mixture of proteins have been identified, the major tear proteins are lysozyme, lactoferrin, albumin, tear specific pre-albumin and globulins.

Component	Average Concentration (mg/100ml)
Total protein	751
Lysozyme	236
Albumin	130
Tear specific pre-albumin	123
Lactoferrin	184
Immunoglobulin A	30
IgG	12.6
IgM	0.086
IgE	0.01

Table 2.12: Average concentrations of important tear proteins [94-95]

2.5.2.3 Mucous phase

The major source of mucus is the conjunctival goblet cell. The essential function of mucoid layer over both corneal and conjunctival surfaces is to render this hydrophobic surface hydrophilic. In addition, mucus plays a role in removing lipid and debris from the surface of the anterior eye[95-100]. The effect of the surface bound mucous is to increase the surface tension to a level at which surface wetting will occur (about 42 x 10^{-5} N/cm).

Mucus is made up of high molecular weight glycoproteins. Each polypeptide chain has, at about every tenth residue, a carbohydrate chain, which are about ten saccharide units long. Moore and Tiffany have separated the glycoprotein component of mucus[96]. The principal mucin complex GP1 (molecular weight > 2 x10^6) and its subunit GP3M (Mw~200,000) were detected in a saline extract of mucus. Reduction of disulphide bonds in the extract gave rise to GP3 (Mw > 1.3 x10^6), but considerable patient variation was detected. The ocular mucus is composed of mucin-type glycoproteins, many of the tear components found in the aqueous phase are also found in mucus. The presence of some components such as IgA, lysozyme and lactoferrin in the mucin layer provide it with bacteriostatic properties.

From the components of the trilaminar structure involved within the tear film we can see that there are three major culprits that could be responsible for spoilation: proteins, lipids and/or mucin. The work to be discussed is principally based on proteins, with marginal overlap with the action of lipids. The next section discusses possible mechanisms of interaction between surfaces and biological species for proteins.

Chapter 3

Gas Plasma Etching: The Process

There are numerous publications on the preparation, structure and applications of hydrogels and it is evident from the literature that one of the most significant problems in the design of a biomaterial is the reactions that occur at the interface between the synthetic device and the biological environment (see Chapter 2). For example, in the design of artificial arteries surface interactions might cause the deposition of debris from the blood, this in turn might lead to thrombus formation within the artery, resulting in a potentially fatal sequence of events. In the case of a contact lens, surface interactions may lead to the deposition of tear proteins and lipids which reduce the quality and comfort of vision experienced by the wearer and subsequently may even lead to eye infections. The nature and extent of the interaction between tear fluid and lens material is reflected by the types of spoilation (Table 2.6).

It is therefore necessary to have an understanding of the underlying surface chemistry which will dictate the liable extent of spoilation. It is this information that will provide a platform to develop subsequent biomaterials which are less disruptive to the biological system.

- Amount of biological species adsorbed ?
- Amount adsorbed versus time-adsorption isotherm ?
- Conformation of adsorbed proteins, bound segments ?
- Thickness or extension of adsorbed layer ?
- Heterogeneity of adsorption ?
- Amount of biological species absorbed ?
- Depth of penetration of biological species ?
- Thickness or extension of adsorbed layer ?
- What are the protein's desorption properties ?
- How do protein mixtures interact with the surface ?

Table 3.1: Some Desired Information Pertaining to Contact Lens Spoilation

There are many techniques available for assessing phase interactions within the fields of spectroscopy, microscopy and chromatography all yielding important specific information

to the enquiring mind. But as questions are answered, newer more intriguing questions are generated (Table 3.1). *'Necessity being the mother of Invention'*, compels the researcher to devise tools to generate answers to these questions. This can be done by modification of existing techniques or the development of new ones. The techniques which are available to study spoilation are limited and generally do not provide all the information desired (Table 1.2). They can be expensive and adaptability is complicated requiring complementary techniques to detail experiments. For example, surface analysis techniques such as XPS and SIMS have been around for a number of years and have been applied to many areas of surface science looking at minute sample areas. The techniques analyse the outermost atomic layers of a material and can identify the chemical state of the surface, assessing the bonding states of the 'visible' molecular bonds. To date the literature has shown minimal explanatory information produced by XPS although it is cited as a technique used to explore the interfacial phenomena experienced by biomaterials[111].

- Adhesion Promotion
- Bioadsorbable Polymers
- Chemical surface Modification
- Catheters
- Cell Culture
- Controlled Release Delivery Systems
- Diagnostic Biosensors
- Disinfection and Sterilisation
- Ocular Prostheses
- Separation Membranes

Table 3.2: Biomedical Applications of Plasma Technology

One technology being employed in a vast number of medical applications is plasma science for surface modification (Table 3.2). It is being used to control tissue adhesion, reduce drag, provide thromboresistance or infection resistance, and act as immobilising agents for biomolecules[104-112]. The work described in chapters 4-6, use plasma as a means of assessing a materials behaviour within a biological media, by using a concept that originated in the semi-conductor industry, where plasma is used to etch surfaces, and reveal the underlying layers.

This following section will outline the basic terminology and processes which are prevalent in plasma etching. Because of the importance of the plasma to the process of

etching, plasma properties are initially described. The general plasma etch process is also described along with major process influences.

3.1 Plasma Physics

Plasma is a partially ionised gas comprising of equal numbers of positive and negative charges, photons and neutrons. The positive charges are usually ions and the negative charges predominantly electrons, although in some discharges negative ions[109] maybe significant e.g. SiF_6.

Plasma formation maybe most readily understood by considering the case of a simple gas, argon. When an electric field of sufficient magnitude is applied between two parallel electrodes to a low pressure gas, the gas starts to breakdown. Unless the gas is at absolute zero, free electrons will already be present in the gas due to processes such as field emission or photoionisation. The free electron is accelerated in the applied electric field and gains kinetic energy. However, as it proceeds through the gas, it looses energy in collisions with gas atoms. Collisions can be either elastic or inelastic. Elastic encounters with neutral species only serve to deflect the path of the electron with little energy loss, due to the large mass difference. If the electrons have sufficient energy, inelastic collisions such as excitation may occur, causing the plasma to 'glow', or ionise. Ionisation frees another electron which is then accelerated within the electric field, and the process continues.

The most important inelastic, electron-impact reaction mechanisms for plasma formation can be described as excitation and relaxation; and ionisation and recombination[110-111]. For example, in an argon discharge this would involve:

Excitation $$e^- + Ar \rightarrow Ar^* + e^-$$ (Eqn 3.1)

Relaxation $$Ar^* \rightarrow Ar + h\nu$$ (Eqn 3.2)

Ionisation $$e^- + Ar^* \rightarrow Ar^+ + 2e^-$$ (Eqn 3.3)

Recombination $$e^- + Ar^+ \rightarrow Ar$$ (Eqn 3.4)

where h is Planck's constant and ν is the frequency of the emitted photon and Ar* indicates an argon atom in an excited state.

This process continues while the applied field voltage exceeds the systems' breakdown potential, causing the gas to be rapidly ionised throughout its volume, an 'avalanche' process. The ions are accelerated towards the cathode, strike it and produce secondary electrons, which sustain the process. Through these processes the discharge reaches a self-sustaining steady state where ion/electron generation and loss processes are in equilibrium. (Note A third body, usually the chamber wall, is required for simple recombination of small species to occur).

Due to the large mass difference between electrons and ions, electrons attain much higher mean speeds and therefore also much higher temperatures than ions. Typical values for an argon discharge are shown in Table 3.3[112]:

Species	Mass (x 10^{23}g)	Speed (x 10^{2}ms^{-1})	Temperature (K)
Electron	9.1x 10^{-5}	9.5x 10^{-3}	23200
Ion	6.6	5.2	500
Neutral	6.6	4.0	300

Table 3.3: Particles mass, speed and temperature values for an argon plasma.

Electron densities for the plasmas of interest are in the range 10^{9} to 10^{12} cm^{-3}. As the density of gas molecules at 1 torr is approximately 10^{16} g cm^{-3} it is obvious that these discharges are only weakly ionised. Average gas temperatures are near ambient despite mean electron temperatures of around 10^{4} to 10^{5} K [ref 6].

If a small electrically isolated substrate were suspended into plasma, the substrate would be struck by both electron and ion fluxes. Due to the large mass difference between the electrons and ions, the electron flux density to the substrate is far greater than the ion flux density (by a factor of 10^{3}). The substrate will immediately start to accumulate a negative charge, and hence a negative potential with respect to the plasma. This charge build-up disturbs the quasi-random motion of the charged particles in the vicinity of the substrate. The negative charge on the substrate starts to reduce the flux of negative charge to the substrate and attracts positive ions. This repulsion is sufficient to balance the fluxes of charged particles to the substrate. The area of positive space charge around the substrate is known as a sheath or dark space. Sheath thickness is related to the Debye length, λ_D, which is a measure of how a plasma will react to oppose potential disturbance from a floating substrate. It has units of length and can be described as[113]:

$$\left(\lambda_D = \frac{kT_e\varepsilon_0}{n_e e^2}\right)^{\frac{1}{2}} \qquad \text{(Eqn 3.5)}$$

where k is Boltzmann's constant, T_e is the electron temperature, ε_0 is the permittivity of free space, n_e is the electron density, and e is the charge on an electron. The Debye length shows how rapidly a potential disturbance is attenuated by the discharge, and over a length λ_D the perturbation is reduced to 0.37 of its original value. The substrate is then said to have developed a floating potential (Figure 3.1), V_f, which is negative with respect to the plasma potential, V_p. The potential difference V_p - V_f will repel electrons leaving a net positive charge, a sheath, around the substrate (insulator to outside influences). There will therefore be fewer electrons to cause excitation by electron impact, and the plasma will glow less brightly - the substrate is surrounded by a dark space. Similarly, sheaths are formed at both electrodes (Figure 3.2).

The simplest plasma is a glow discharge in which a DC potential is applied between two metal electrodes in a sealed chamber containing a low-pressure gas. The discharge is spatially non-uniform and consists of a series of glowing and dark regions as shown in Figure 3.2[114].

Both electrodes in a DC discharge must be conductors. If, during the discharge process, either electrode becomes covered with an insulating layer, then the surface of the insulator charges up capacitivley. As the capacitor charges up, the net current through the plasma falls to zero, extinguishing the discharge.

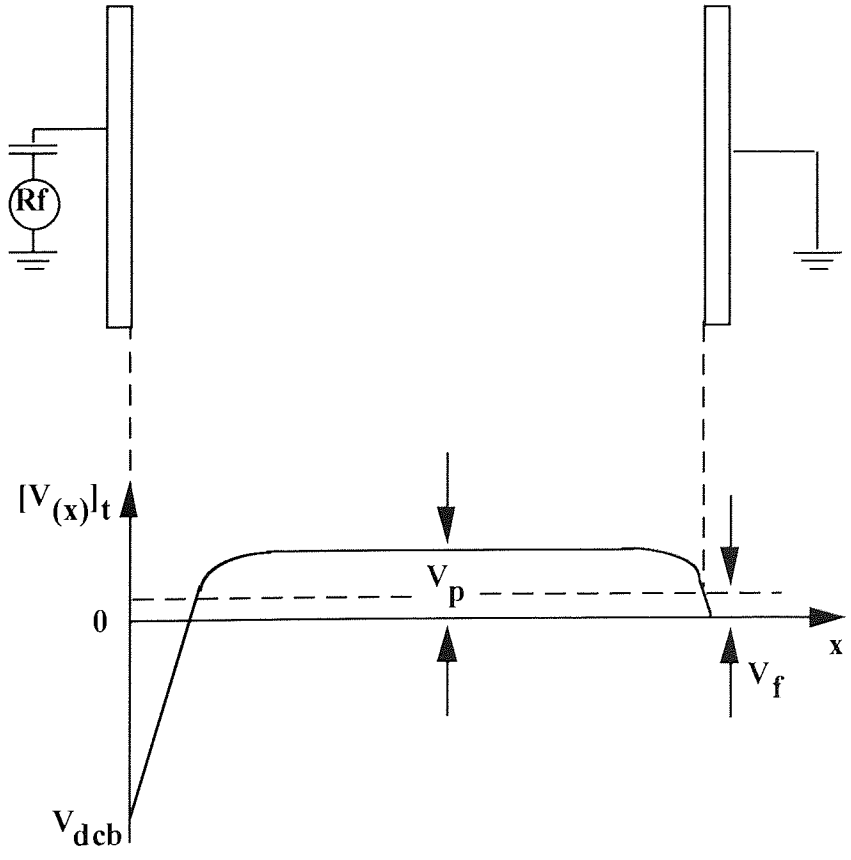

Figure 3.1: The time averaged resolved potentials which occur for RF plasma[115].

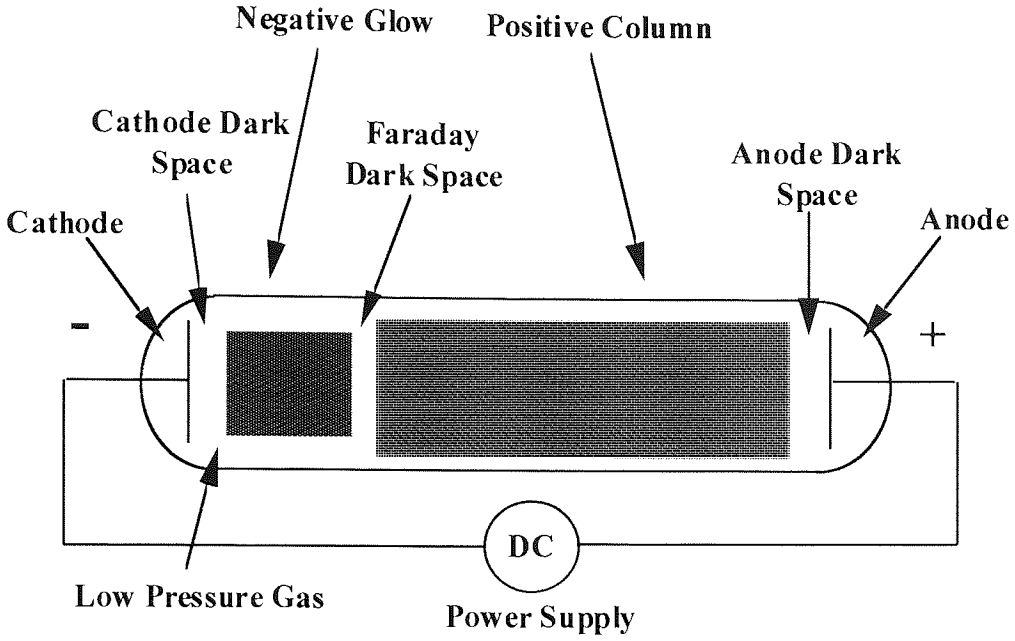

Figure 3.2 : Schematic view of a typical glow discharge at low pressure, showing the most prominent regions[5]

If a low frequency alternating field (< 10^4 Hz) is applied to the circuit shown in Figure 3.3, then the effects discussed above will remain unchanged except for the reversal every half cycle of anode and cathode. Ion and electron distributions can both equilibrate with the changing field and the cathode and anode dark spaces also change position every half cycle. As the applied field frequency is increased, a point is reached when the period of oscillation is less than the time required for plasma equilibrium. Initially positive ions cannot be fully extracted from the cathode sheath areas before the field is reversed. As the frequency is increased further, the electrons are unable to travel to the anode during the half cycle. These electrons then oscillate in the inter-electrode gap and collide with gas molecules. Frequencies of > 1 MHz must typically be applied for oscillation of electrons to occur.

The radio frequency (RF) generated discharge has fewer regions than the DC discharge. It consists of a negative glow insulated from the electrodes by dark spaces at the powered electrode and the earthed electrode. These dark space sheaths are similar in composition to the cathode sheath in a DC discharge, with regions of positive space charge being formed.

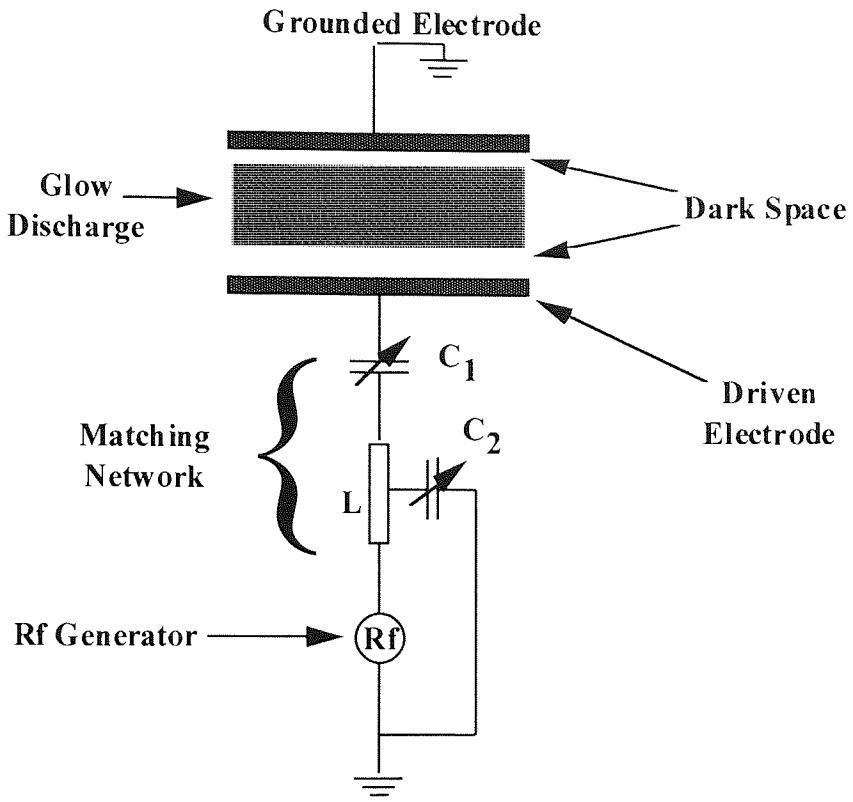

Figure 3.3: A schematic view of a RF plasma discharge where the power is supplied by a matching network.

At RF frequencies the ion (massive) may be regarded as stationary, and the electrons (light) as oscillating between, but not necessarily reaching the electrodes. The electrons may gain sufficient energy in their oscillations to cause ionisation, removing the dependence on secondary electron emission. Further the ionisation process becomes more efficient with increasing frequency allowing lower operating pressures. Most commonly a frequency of 13.65 MHz (an allocated frequency) is used. Typical plasma characteristics of a parallel plate electrode system are given in Table 3.4[116-117]:

In RF plasma systems the largest self-bias voltage develops at the driven electrode. This is because there is an impedance matching network between the driven electrode and the RF power supply, as shown in Figure 3.3. A DC isolating capacitor exists in the circuit between the RF supply and the plasma. A large DC self bias (V_{dcb}) develops between the powered electrode and the negative glow due to the action of this capacitor, and is inversely proportional to the size of the two electrodes.

Pressure	10^{-3} - 1 torr
Frequency	50 kHz - 50 MHz
Electrode Separation	1-10 cm
Power Density at Electrode	0.01 - 1 Wcm^{-3}
Number density of ions and electrons	10^{8} - 10^{11} cm^{-3}
Ion Density	10^{16} m^{-3}
Degree of Ionisation	10^{-6} - 10^{-4}
Electron Mean Energy	0.1-10 eV
Ion and Neutral Mean Energy	0.03 - 0.05 eV
Debye Length	10^{-4} - 10^{-2} m

Table 3.4: Some typical parameters which are characteristic of a glow discharge process.

The dimensions of the reactor chamber play an important role in the determination of the plasma potential V_p the self-bias potentials, and therefore the ion bombardment energy which is incident on the reactor walls and electrodes. The relationship between the plasma potential and the driven electrode potential, V_{dcb} as a function of time with the area ratio R as a parameter (as shown in Figure 3.4[118]). R is equal to A_e / A_d where A_e and A_d are the earthed electrode and driven electrode areas respectively. If the system consists of two electrodes of equal area, the V_p will be very large and both electrodes will be subject to energetic ion bombardment to approximately the same extent, as the sheath voltage drop across all the sheaths will be equal to V_p.

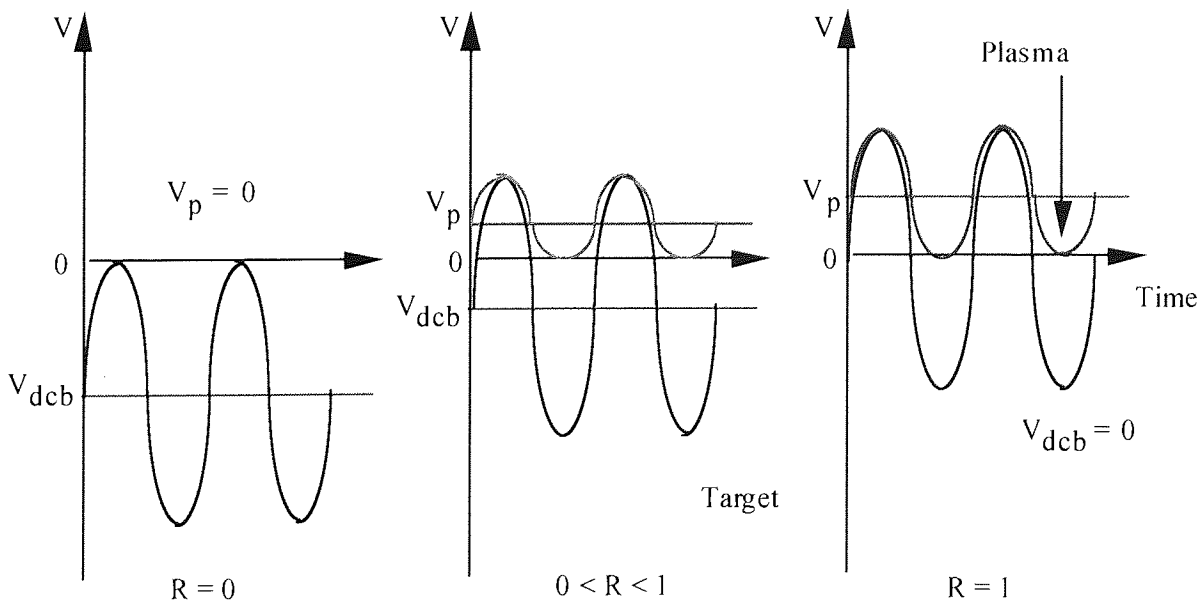

Figure 3.4: Approximate driven electrode and plasma potential waveforms for a glow discharge with grounded chamber walls. R is the ratio of powered electrode to wall area.

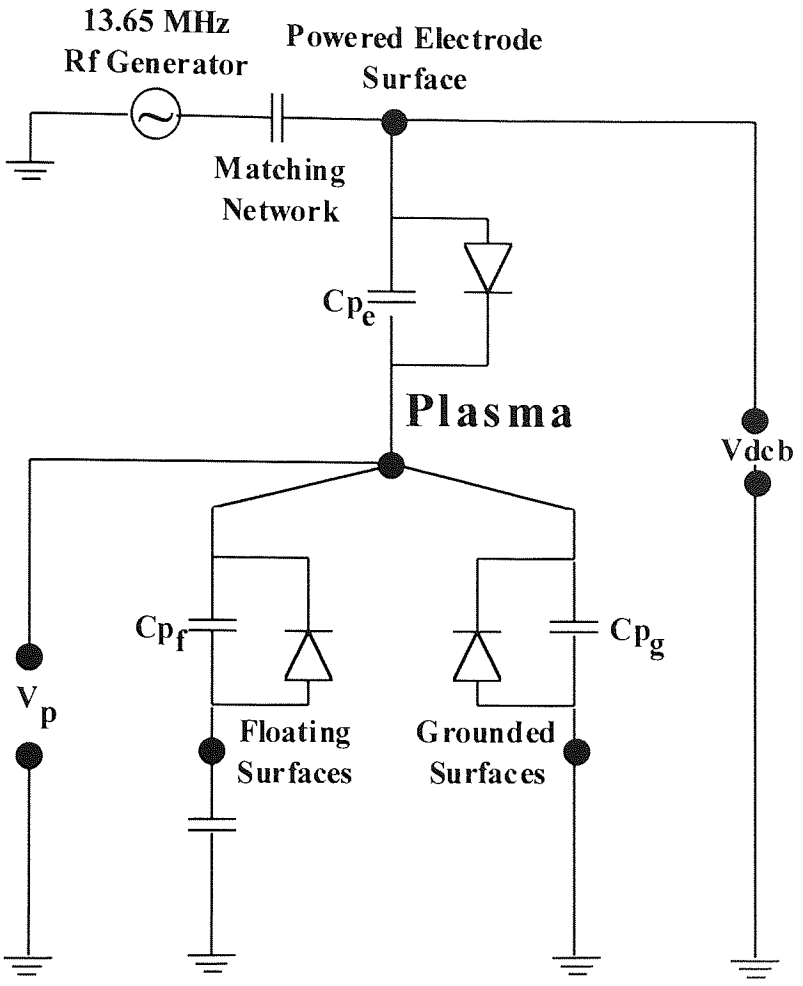

Figure 3.5: Approximate RF plasma equivalent circuit[119].

A typical system will feature $0 < R < 1$. This behaviour is due to the capacitative nature of the ion sheaths. From the approximate equivalent circuit for a discharge shown previously in Figure 3.5, it follows that V_p is determined by the relative magnitudes of the sheath capacitances. This is effectively capacitative voltage division, which in turn depends on the relative areas of the cathode electrode and other surfaces in contact with the plasma. An early theory of plasma characteristics predicts[120]:

$$\frac{V_d}{V_e} = \left(\frac{A_e}{A_d}\right)^4 \qquad \text{(Eqn 3.6)}$$

where V_e and V_d are the voltage drops across the earthed and driven electrode sheaths respectively. This model was originally developed for sputtering systems operating at a few mtorr, and some problems occurred when applying this reaction in higher pressure scenarios, as outlined in the literature[121]. In fact, for the plasmas which are used in etch processes, there is evidence to suggest that the voltage ratio varies as the first, and not the fourth power of the area ratio [122].

3.2 The Basic Mechanisms of Plasma Etching

Plasma etching is an extremely complicated process with many parameters contributing to the etch process. Even at a basic level, these parameters encompass a wide range of interactions. Much progress has been made in the last two decades, with many of the ideas and understanding being developed in the semiconductor industry. Although not completely understood the etching mechanisms can be grouped into four categories: sputtering, chemical etching, energy-driven ion-induced etching and inhibitor protected-side wall ion-enhanced etching[123-126].

Referring to Figure 3.6 during sputtering (a and b), particles (usually positive ions which are accelerated across the sheath) collide energetically with the substrate. If the energy transferred to the surface is greater than the atomic binding energy, then some surface atoms are ejected leading to net material removal. The sputtering yield is the number of target atoms ejected per incident ion, and is dependent on the relative masses of the atoms and the incident energy, and is typically less than one. This is a purely mechanical interaction.

Chemical etching (c), occurs when gaseous active species encounter a surface and react with it to form a volatile product. The criterion of product volatility is essential to stop reaction products coating the surface, thus inhibiting the etch process by preventing etchants adsorbing to the surface ((d) and (e)), shown experimentally in Figure 5.2 deposition profile. Chemical etching using plasma is usually carried out by free neutral radicals and has no directionality, leading to isotropic profiles.

In energy-driven ion-induced etching (f), there is usually little or no etching when the substrate is exposed to neutral etchants alone. The rate-limiting step in this case is product formation. The ion bombardment component enhances the reaction rate by creating 'damage' sites on the surface of the substrate, by virtue of the ion impact energy. Ion bombardment makes the substrate surface more reactive to neutral radical flux. 'Damage' includes the formation of reactive dangling bonds, disruption of lattice structure and formation of dislocations.

Ion bombardment (g), plays a different role in inhibitor protected-side wall ion-enhanced etching. Neutral etchant species from the plasma can spontaneously etch the surface, but etch resistant polymers are also deposited on the surface during the reaction. This 'protective' inhibitor film can only be removed from horizontal surfaces and receives a vertical bombardment component of energetic ions. Vertical walls of masked features retain their protective film because they only interact with the small number of ions, which are scattered, as they cross the sheath. Sidewall film deposition allows the etch profile to become highly directional.

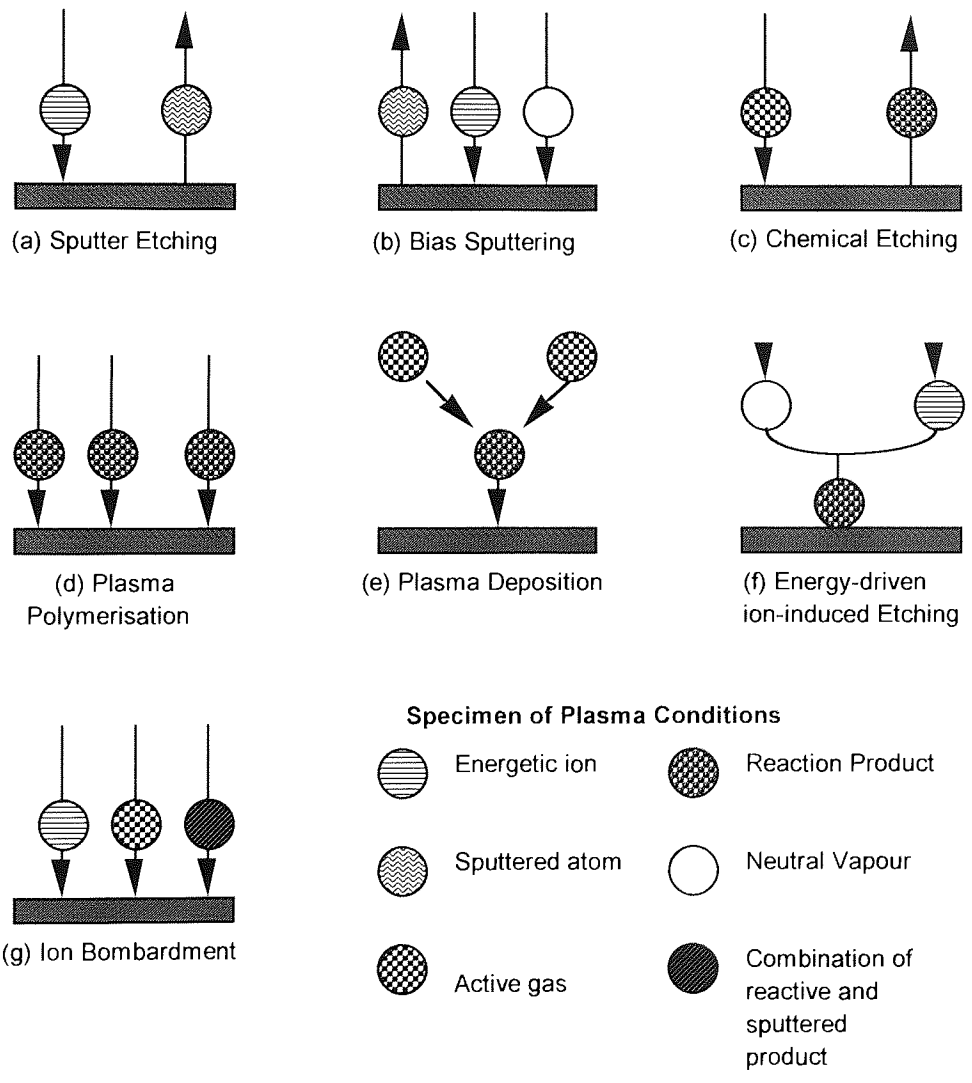

Figure 3.6: Major processes by which etching takes place: sputtering; etching; ion-induced energy driven etching; inhibitor protected - side wall ion-enhanced etching[124]

3.3 Fundamentals of Polymer Chemical Etching

Etching can be defined as the removal of a solid material from a substrate through chemical reaction. Many different types of reactions are possible in a glow discharge[13-15] but for successful etching, the RF discharge must act as a source of species that engage in or catalyse etching. For these species to occur it is necessary that dissociation of the molecular feed gas takes place. Dissociation occurs as a result of electron impact reactions in the negative glow:

Dissociation $$e^- + O_2 \rightarrow 2O + e^-$$ (Eqn 3.7)

Dissociative Ionisation $$e^- + CF_4 \rightarrow CF_3^+ + F + e^-$$ (Eqn 3.8)

Fragmentation of the feed gas in this way is essential, as the gases themselves are mostly unreactive with the substrate. Radicals created during dissociation processes are atoms, molecules or complexes that contain one or more unpaired electrons, such as O and F in the examples above[16]. Long and short-lived radicals play a major role in the etch process due to their highly reactive nature. The resulting RF glow discharge is a mixture of ions, neutrals, radicals and electrons. If a polymeric sample is exposed to this flux some of the surface will evaporate, thereby etching the substrate. The reactive plasma etch process can therefore be summarised by the following sequence:

(i) Dissociation of the feed gas (es).
(ii) Adsorption of the reactant to the surface.
(iii) Product formation by surface reactions.
(iv) Desorption and product removal.

Any one of these steps has the potential to be the slowest, and thereby become the limiting step in terms of etch rate[125-126]. The two necessary conditions for chemical etching of a polymeric substrate are:

(i) the formation of volatile reaction products, and
(ii) an exothermic reaction[127].

The volatility of a substance is controlled by its vapour pressure P_v, with a temperature dependence given by [128-129].

$$\log P_V = \frac{-\Delta H_V}{2.3RT} + \text{constant} \qquad \text{(Eqn 3.9)}$$

where $^{-\Delta H_V}$ = heat of vaporisation, and R = gas constant, 8.314 $JK^{-1}mol^{-1}$.

Initially, referring to the above system, evaporation/desorption of etch products is seemingly dependant on lowering operating pressures and using elevated temperatures, which would be detrimental to any biological system we wished to observe in this study. Actually, it is the partial pressures of the product that is the key factor, this is reduced by lowering the residence time[128]. Many other factors such as supply of reactant and sample damage must also be taken into account.

Returning to the specific case of a carbon-based polymers and considering possible volatile reaction products, the following candidates in Table 3.5 maybe identified:

Compound	Boiling Point (°C)
CH_4	-161.5
CF_4	-128
CO_2	-78
CCl_4	76.4

Table 3.5: Boiling Points of Selected Carbon Compounds [130]

Whilst the first three compounds may readily be considered volatile, this is also holds true for the fourth case, which has a vapour pressure of $2*10^{-3}$ torr at room temperature, which rises considerably higher at elevated temperatures.

The other condition for spontaneous etching is that the volatile products must be more stable than the reactants products. Carbon is etched according to the complete reaction:

in Oxygen

$$C_nH_{2n} + \frac{3}{2}O_2 \rightarrow nCO_2 + nH_2O \qquad \text{(Eqn 3.10)}$$

where X= H, F, Cl, Br, I

$$C + 4X \rightarrow CX_4 \qquad \text{(Eqn 3.11)}$$

The requirement is therefore for the breaking of -C-C- bonds in a polymer and the formation of a C-X bond to be exothermic. The comparison of energies in a glow discharge with the typical bond energies in molecules (Table 3.6) shows that the energies of species in such plasma are sufficient to break covalent bonds in molecules exposed to this environment.

Energy	**eV**
In Glow Discharge	
electrons	0-20
ions	0-2
metastables	0-20
UV-visible	3-40
In Bonds	
C-H	4.3
C-N	2.9
C-Cl	3.4
C-F	4.4
C=O	8.0
C-C	3.4
C=C	6.1

Table 3.6: Energies in a Glow Discharge Compared to Typical Bond Energies[131]

Since CF_4 is the most volatile of the halogenated carbons, and its formation is the most exothermic, it is not surprising that fluorine chemistry has been frequently used for plasma etching of carbon. However chlorine or oxygen chemistry, are in fact more widely used due to control of other features such as selectivity, anisotropy, damage etc.

3.3.1 The Oxygen Plasma

In the oxygen plasma system, O_2 dissociates to form many species including $O^+, O_2^+, O^-, O_2^-, O^3p, O_2(1\,g), O^1D$ and free electrons. Metastable molecules have also been identified, e.g. O_2^* probably in the ^1g state, and are present in relatively large concentration. Battey[127] measured the etch rates of several polymeric resists and found them to be a function of the oxygen atom concentration, and thus concluded that the $O(^3p)$ atoms are the main oxidising species in plasma stripping of resists[127]. He also showed that the strip rate did not depend upon the combination of pressure and power used to produce the atomic oxygen but only upon the concentration itself. Benson and Cook, using electron paramagnetic resonance (EPR) spectroscopy showed that $O_2(^1g)$ was not consumed in the stripping process and confirmed Battey's conclusion that oxygen atoms were the rate determining etchant. The highly reactive ground state oxygen atoms, i.e. O(3p) reacts with the resist so that chain scission occurs. The photoresist, which is mainly a polymeric hydrocarbon with some functional groups, is oxidised and the final products are CO, CO_2 and H_2O. The general stripping mechanism of polymers in an oxygen plasma is given below:

$$O\,(^3p) + RH \rightarrow R^{\bullet} + HO^{\bullet} \qquad \text{(Eqn 3.12)}$$

$$HO^{\bullet} + RH \rightarrow R^{\bullet} + H_2O \qquad \text{(Eqn 3.13)}$$

$$R^{\bullet} + O_2 \rightarrow ROO^{\bullet} \qquad \text{(Eqn 3.14)}$$

$$ROO^{\bullet} + RH \rightarrow ROOH + R^{\bullet} \qquad \text{(Eqn 3.15)}$$

$$ROOH \rightarrow RO^{\bullet} + HO^{\bullet} \qquad \text{(Eqn 3.16)}$$

$$2ROOH \rightarrow ROO^{\bullet} + RO^{\bullet} + H_2O \qquad \text{(Eqn 3.17)}$$

$$ROOH + RH \rightarrow RO^{\bullet} + R^{\bullet} + H_2O \qquad \text{(Eqn 3.18)}$$

$$RO^{\bullet} \rightarrow \text{Chain scission} \qquad \text{(Eqn 3.19)}$$

Taylor and Wolf[224] studied relative rates of polymer film loss when subjected to an oxygen plasma environment. They postulated that the rates of removal are correlated with structural factors, which enhance or retard removal. These factors are:

(i) The presence of strong backbone and backbone-side chain bonds confers plasma stability.

(ii) Weak backbone-side chain bonds afford enhanced degradation and activate the main chain.

(iii) Weak bonds not immediately pendant to the main polymer chain have little effect.

(iv) Removal may be catalysed by active species such as F or Cl produced either in the plasma or as a result of the polymer removal process.

(v) Stability is conferred on an otherwise reactive material by capture with species forming higher energy unreactive groups.

(vi) Aromatic and polar functional groups promote stability perhaps by enhancing radiationless deactivation of normally reactive species.

(vii) Ultimate protection is found for these organometallic polymers containing moderate to high percentages of metals forming refractory oxide products, e.g. poly(dimethyl siloxane) has no appreciable etch rate in an oxygen plasma.

Gokan et al[158] studied the dry-etch resistance of polymers, and measured etch rates under Ar ion-beam, O_2 ion-beam, and oxygen plasma etching conditions. The etch rate under ion bombardment has a linear dependence on a factor that relates the total number of oxygen atoms in a monomer unit. The resistance to ion bombardment is determined by the effective carbon content. This implies that the etching mechanism under ion bombardment differs from that by plasma discharge.

Moss et al[159] have studied plasma stripping of poly methyl methacrylate, polystyrene and copolymers of the two. They pointed out that the interaction between an oxygen plasma and a polymer is a complex process in which comprised of four distinctive stages:

(i) Surface bombardment by photons, electrons, ions, atoms and excited species.

(ii) Reactions of free-radical sites on the polymer with molecular oxygen.

(iii) Chain cleavage leading to the primary volatile species.

(iv) Gas-phase reactions of the primary volatile products in the plasma.

They observed that the stripping rates of copolymers of methyl methacrylates and styrene did not vary linearly with composition. They showed that only a very small amount (10-15%) of styrene reduced the relative stripping rate of the copolymer. Primarily due to the aromatic ring of polystyrene which reacts with O(3p) to form phenols. Consequently, they may or may not trap other free radicals. Another explanation of this unexpected behaviour may be formed on the basis of different mechanisms, as shown in Figure 3.7.

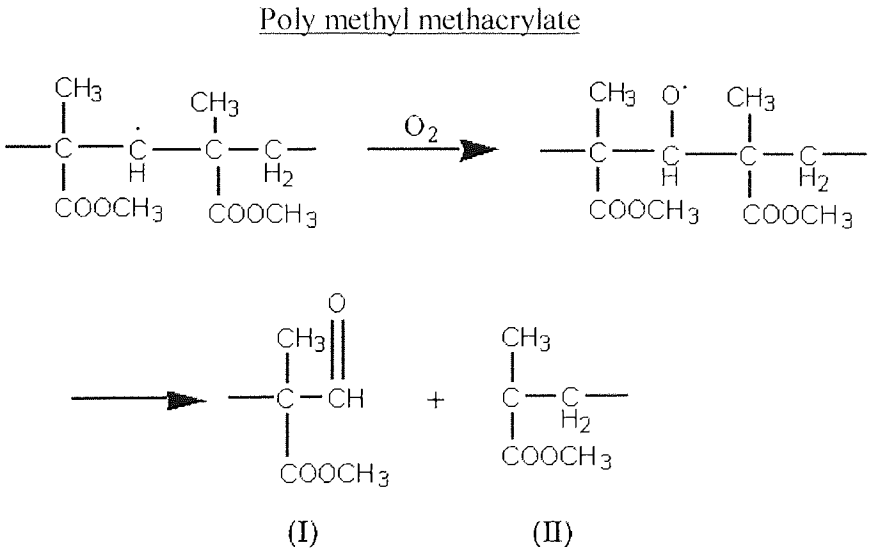

(I) is stable

(II) may partly polymerise and react with oxygen

Figure 3.7(a): Proposed Free Radical Mechanism for Gas Plasma Etching in Oxygen for PMMA, PS and PSMMA

Polystyrene

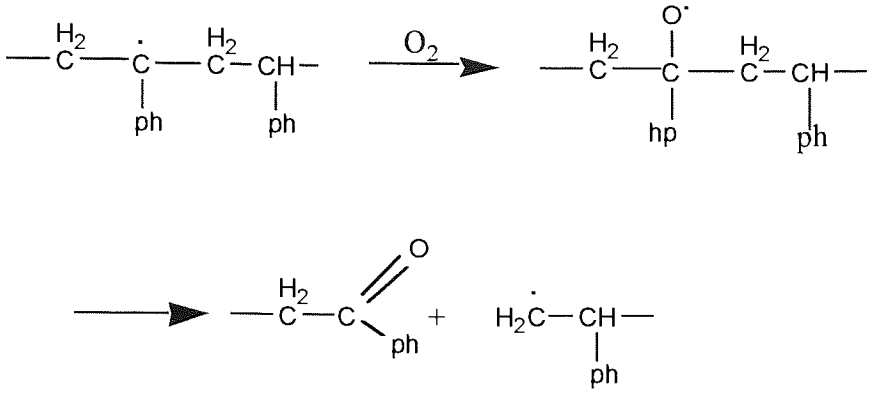

(III) (IV)

(III) is stable

(IV) reacts mainly with oxygen to give 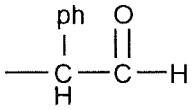

Figure 3.7(b): Proposed Free Radical Mechanism for Gas Plasma Etching in Oxygen for PMMA, PS and PSMMA

Poly (styrene-methyl methacrylate)

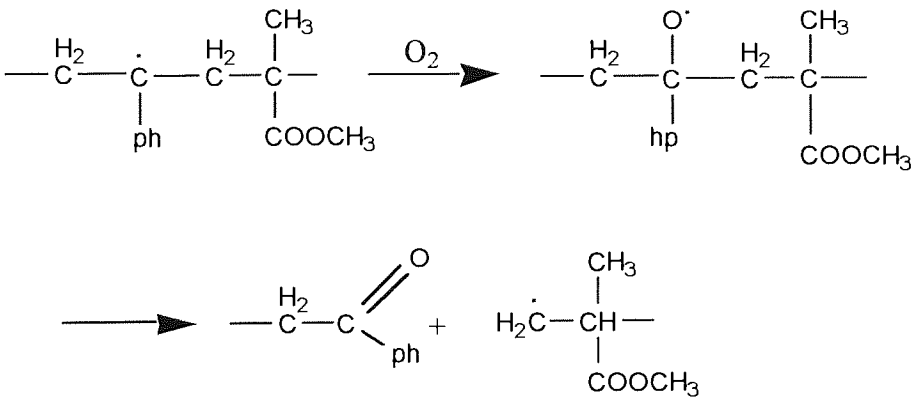

(V) (VI)

(V) is stable

(VI) react with oxygen (depolymerisation is unfavourable)

Figure 3.7(c): Proposed Free Radical Mechanism for Gas Plasma Etching in Oxygen for PMMA, PS and PSMMA

Many aspects need to be considered, bearing in mind the major problems of etching are the sensitivity of the plasma, coupled with a basic lack of understanding of the fundamental physical and chemical variables. For control purposes, machine parameters or discharge variables, such as power, pressure, etc. are used to alter the fundamental operations. Characterisation of the process with respect to discharge parameters is not at all straight-forward.

Chapter 4 looks at the development of an experimental set-up to determine protein penetration and location within a biomaterial. The refinement of the system parameters and the diagnostic techniques which have been implemented for surface characterisation are also described. Additionally, the sensitivity of the technique is also addressed.

Chapter 4

The Development of Gas Plasma Based Diagnostic Techniques For Surface Characterisation

This chapter will detail the development work undertaken. Initially, the intrinsic plasma system parameters, design and operating procedures are discussed. The extrinsic development techniques that are run either concurrently (Optical Emission Spectroscopy (OES)) or in conjunction (UV and fluorescence spectroscopy) with plasma etching are described. They are collectively known as the plasma etching and emission monitoring systems (PEEMS). The operative system took 20 months to commission, calibrate, validate and to attain an adequate etch process.

4.1 The Systems' Parameters and Set-up

One of the major obstacles to the routine implementation of plasma etching is the extensive parameters that are associated with the process, and the difficulty involved in directly measuring most of the fundamental variables.

Many process parameters, e.g. choice of gases, flow, pressure, power, electrode temperature, dc bias, electrode spacing, determine the performance of the system, e.g. etch rate, selectivity, anisotropy, of a plasma etcher. As the process parameters (Figure 4.1) may also be interactive, the one-parameter-at-a-time approach to a process optimisation can require very many experiments, as well as giving potentially misleading results. It is therefore better to take an orthogonal axes approach based on a statistical experimental design methodology, designed in the 1950's. In this approach the factors (parameters) of interest are represented as orthogonal axes in space. The limits of the axes are the physical maximum and minimum possible parameter settings. Responses (experimental results) are then systematically measured within the defined space. These in turn are fitted to a polynomial equation which models all the defined space, but not beyond (see Chapter5).

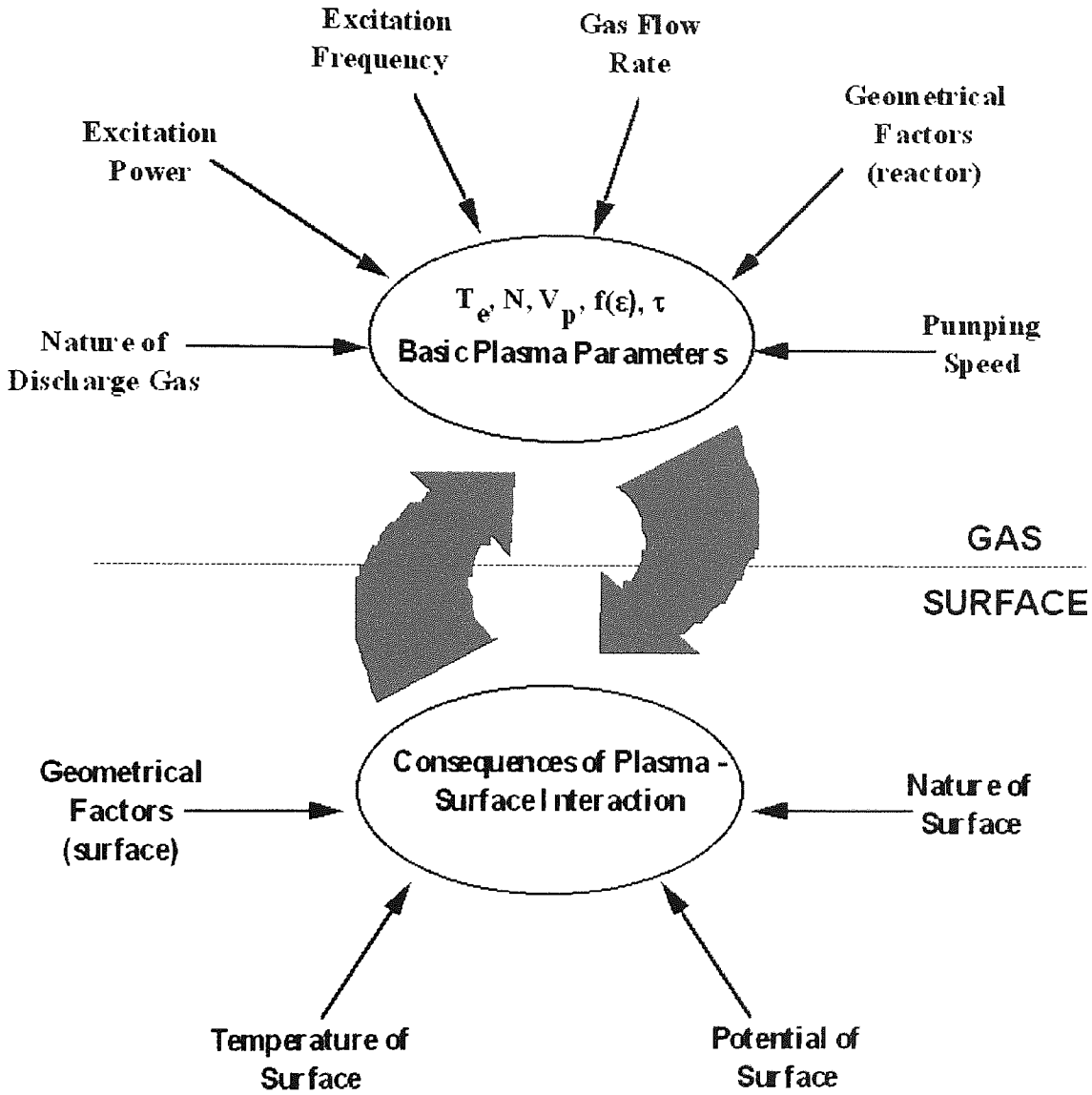

Figure 4.1: The system parameters associated with the plasma etch process, where T_e is the electron temperature, N is the plasma density, V_p is the plasma potential, f(ε) is the electron energy distribution function and τ is the gas particle residence time[144-156].

4.2 Components of Plasma Etching System

4.2.1 Plasma Chamber

The reaction vessel was based on a capacitively coupled barrel reactor (Figure 4.2a), with four equivalent area copper electrodes (Figure 4.2b) connected to a RF power supply. The electrodes assume a negative potential with respect to the discharge, and positive ions are accelerated towards the sample because of its induced negativity. The electrodes are 128 cm^2 in area. The inter-electrode gap is 85 mm.

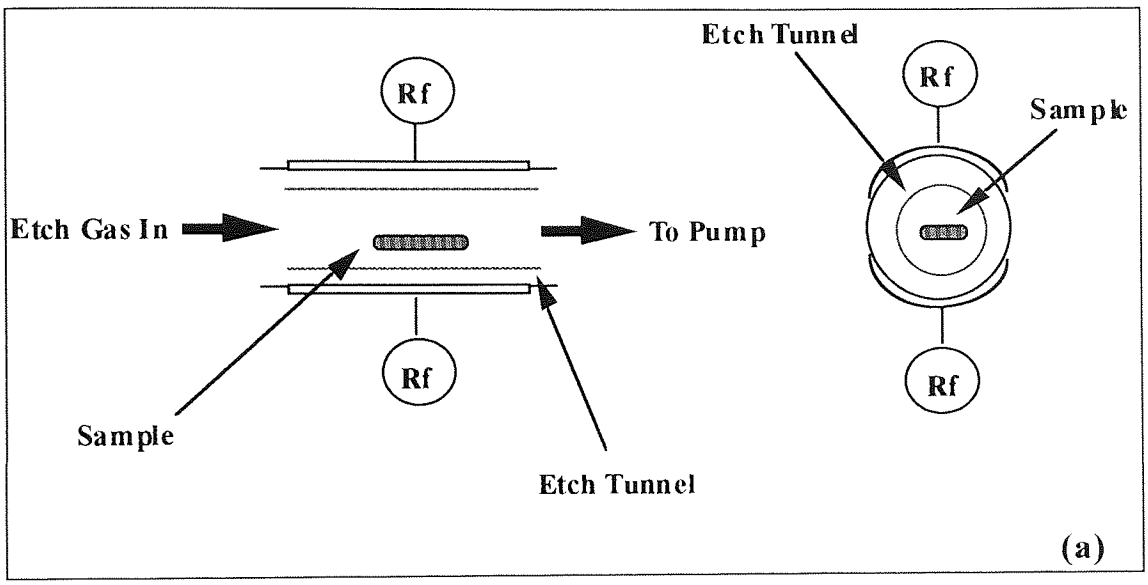

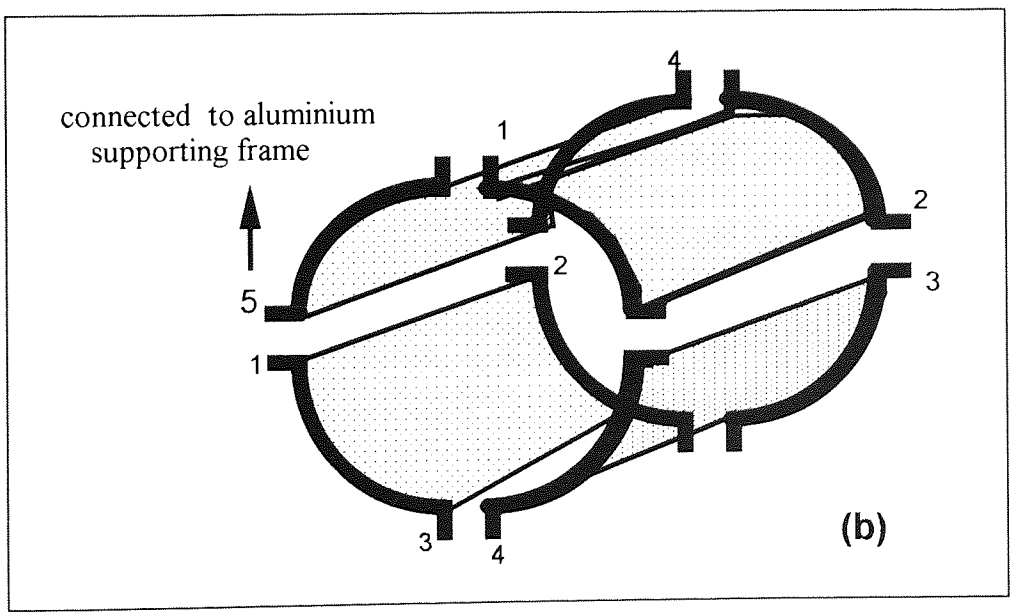

Figure 4.2: (a) Barrel etch reactor with capacitively coupled RF power.(b) Copper Plate Arrangement around glass plasma reaction vessel. The numbered electrode terminals correspond to the location of the wires.

The plasma chamber itself was made of Pyrex in a cylindrical design, of internal diameter 75mm and length 250mm. The chamber volume was ~ 4.4 dm^{-3}, giving a gas residence time of ~ 18sec at $3cm^{-3}s^{-1}$ flow and 0.15 torr pressure.

A micro force balance was centrally housed within the chamber as depicted in Figure 4.3 to monitor material depletion, maintain reproducibility and validity of the process during etching.

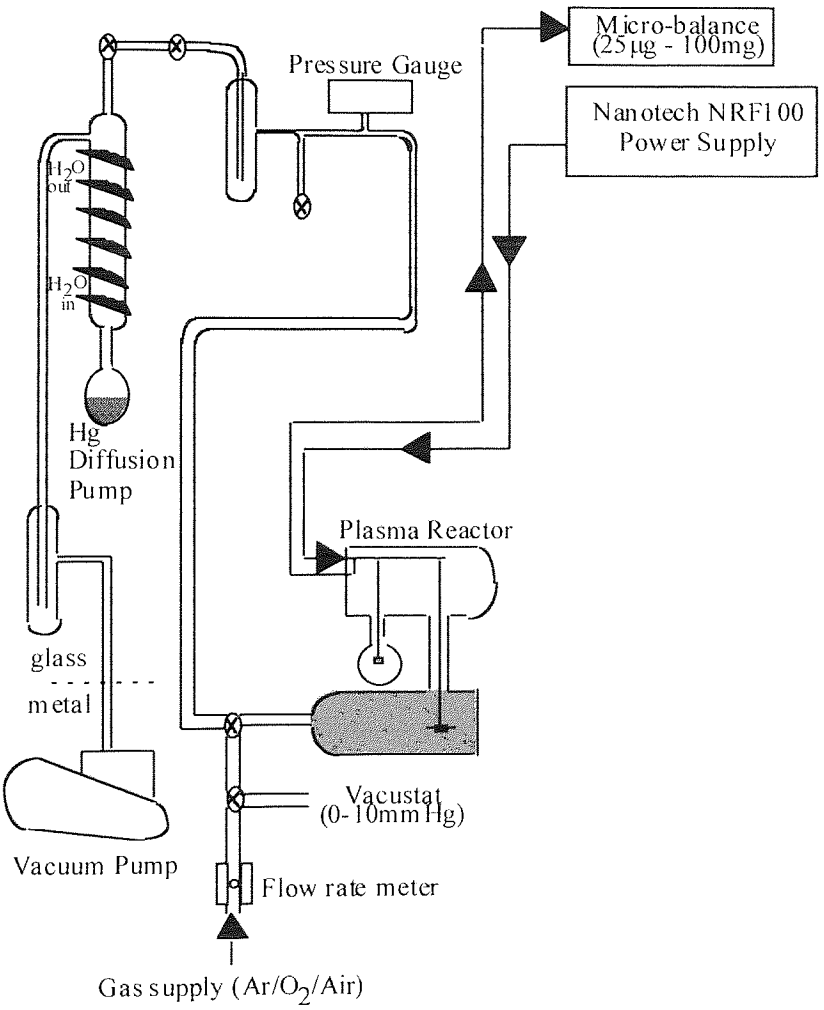

Figure 4.3(a): Schematic Representation of Plasma Etching System's Set-up

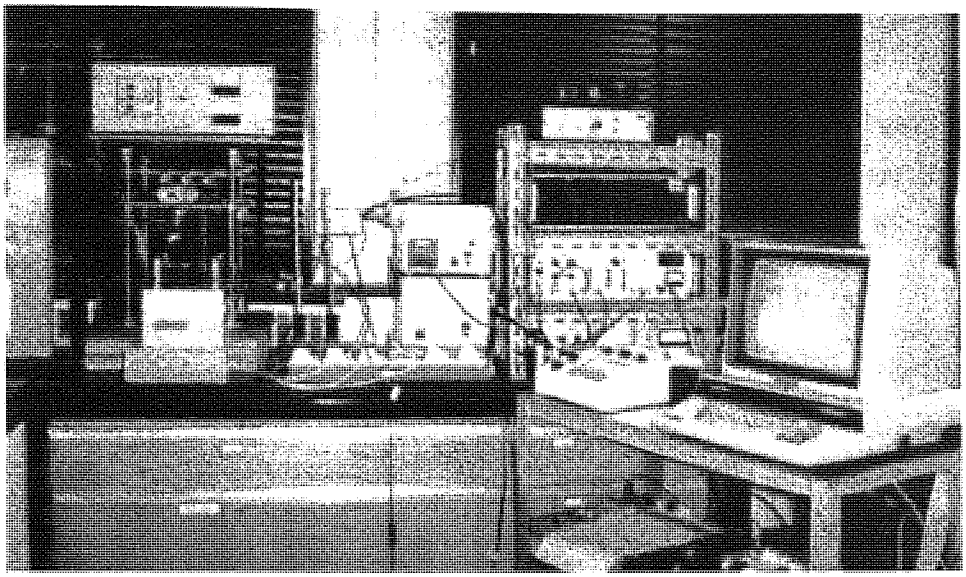

Figure 4.3(b): Photograph of Laboratory Set-up of Plasma Etching System.

4.2.2 Pumping System

It has been noted[142] that when choosing a pump for etching processes, one must consider process contamination (the effect of the vacuum pump on process contamination), vacuum pump deterioration, and most importantly operator safety. Not all the primary gases used in plasma etching are toxic (e.g. halocarbons), but many of their by-products are dangerous to breathe[151]. Some gases (e.g. oxygen), pose a hazard (explosion) when in contact, in high concentration with hot hydrocarbon oils.

Some by-products may readily cause pump corrosion, and the chemistry of by-product/hydrocarbon pump oil interactions is essentially unknown. For these and other reasons inert synthetic pump fluids, perfluoroether, and oil free ('dry') pumping systems are often employed[61].

The etching system was equipped with an Edward's rotary pump running on conventional mineral oil. The rotary pump was ballasted and oil conditions were assessed by visual inspection at the sight glass, and the oil was then changed when required. The pump was capable of bringing the chamber from atmospheric pressure to <5% of the operating pressure (e.g. from atmospheric pressure to <3 mtorr prior to an operating pressure of 15 mtorr), in 10-15 minutes. Slightly lower pressures could be obtained if the necessity arose by using a diffusion pump, housed within the vacuum system (Figure 4.3a).

4.2.3 Pressure Measurement and Control

Pressure measurements were made initially using an Edward's Speedivac Pirani Gauge and then replaced by a high resolution MKS Baratron absolute pressure transducer with pressure control by a VG automatic pressure controller situated between the chamber and pumps.

The Baratron is a diaphragm gauge and measures pressure differences by deflection of a metal diaphragm. Changes in the position of the diaphragm are detected electrically by measuring the capacitance between the diaphragm and the fixed flat electrode. The gauge measures total pressure, and the reading is independent of the type of gas used. The calibration of the Baratron used in these studies was checked by comparison with readings obtained from a similar gauge.

4.2.4 Mass Flow Controllers

Gases were bled into the evacuated chamber through the Brooks flow meter. In later work, improved gas flow was obtained by using a mass flow meter and MKS Instruments 254 Flow Ratio Controller, (by by-passing the Brooks flow meter). The calibration of the mass flow controller was checked at 10 points over the entire range using a bubble flow meter. Due correction was made for room temperature, but errors due to variations in atmospheric pressure were ignored.

4.2.5 Power Supplies and Matching Networks

RF power was supplied by a 100W, 13.65 MHz generator - Nanotech Model NRF-100 or NRF 1-2, as available. In both cases the indicated generator power output was checked with a in-line watt meter, whilst the generator was coupled to a 50 ohm dummy load, and was found to be accurate. The indicated generator power output was relied upon for all experimental work.

A matching network was placed between the power supply and the electrodes in order to increase the power dissipation in the discharge, and to protect the power supply. The network was used to match the generator impedance to the discharge impedance. It contained two variable capacitors, in a parallel configuration, which were adjusted manually to give maximum forward and minimum reflected power.

4.2.6 Gravimetry

The development of this process was specifically to remove molecular layers from the surface of polymeric materials within a plasma, and so acting as a 'molecular scalpel'. In order that the most reliable results be obtained from a gravimetric balance, the balance should be capable of recording weight changes with adequate capacity and sensitivity. A C. I. Electronics microforce balance was employed. At the heart of the micro-force balance is an electronic bridge circuit maintained in continuous balance by a servo system. The 'head unit', made with the precision of a galvanometer, electro-magnetically balances the torque produced by the sample weight. A current flows through the head in exact proportion to the applied weight and this current operates the 'indicating meter' and provides an electrical output (i.e. output to a recorder or a computer interface). Both the sample and counterweight are suspended from two rigid lattice arms, which offer uniform expansion at elevated temperatures. The electronic components of the head are coated with PTFE due to the possible corrosive nature of the system. The movement and framework are nickel plated with fixing points for mounting onto a framework to alleviate excessive vibration.

Figure 4.4 illustrates the construction of the MK 2 vacuum head. A small displacement of this arm causes an excess current flow through a photocell, this is amplified and passed through the movement coil restoring it to its original position.

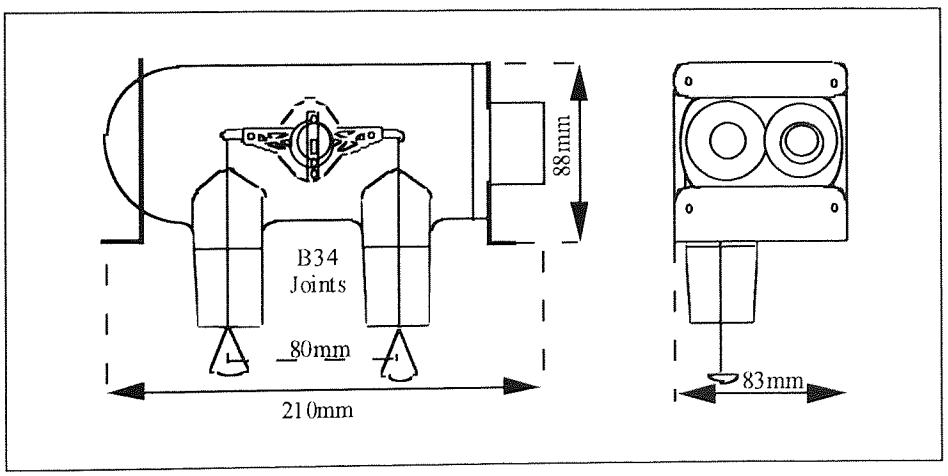

Figure 4.4: Micro-force Balance Head Unit Design (MK 2 Vacuum Head)

The balance has an electrical range of 25μg to 200mg with independent range selectors of: Range 1 (0-25μg), Range 2 (0-250μg), Range 3 (0-2.5mg), Range 4 (0-10mg) and Range 5 (0-100mg), for direct switching.

The design incorporation of the microforce balance within the plasma chamber required attention to eliminate extraneous parameters., such as vibration, electro-magnetic interference, any thermal interference etc.

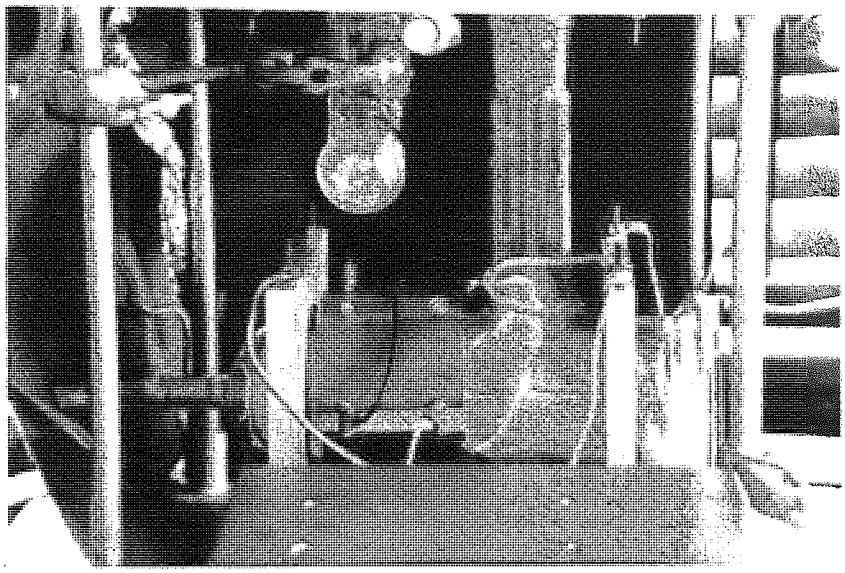

Figure 4.5: Plasma Chamber and micro-force balance

4.2.7 Data Acquisition

The ease and convenience of collecting data through a computer interface has untold advantages, especially in a system where the read-out (micro-force balance) is voluminous yet assessment is required virtually as the data is generated. The signal has to be converted from an analogue format to a digital format for the processor to acknowledge the information and this is done through an A-to-D (analogue to digital) converter, as shown in Figure 4.6. (Any unstable signals were damped and amplified before passing through to the a to d converter). The data will only be collected into a meaningful output through software. The software was written in a computing language called, Visual Basic so that the input data could be sampled every second, alternating between two serial ports: one for the micro-force balance, the other for the monochromator during OES (Section 4.3).

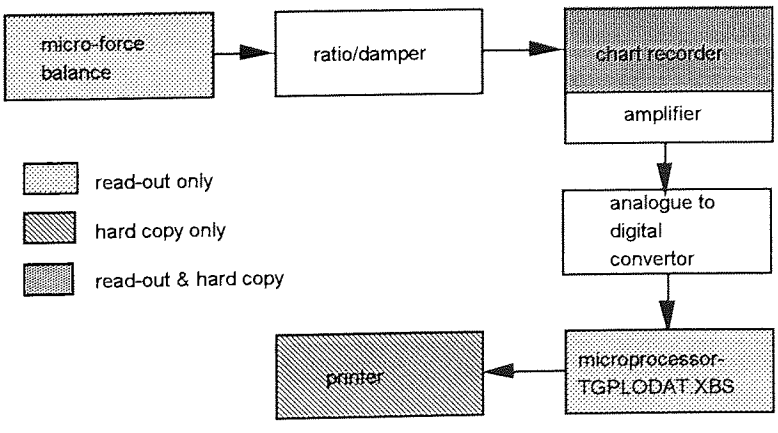

Figure 4.6: Flow Diagram of the Data Acquisition System

4.3 Extrinsic Techniques For Surface Characterisation.

Once having set-up the apparatus to remove material from the surface by etching, the next stage was to monitor the residual layers produced and the species generated. The layers produced were determined using UV and fluorescence spectroscopy, and the generated species were determined using gravimetry and optical emission spectroscopy.

4.3.1 Optical Emission Spectroscopy

Optical emission spectroscopy (OES)[160] is one of the several optical diagnostic techniques used for plasma discharges. It has the advantages of being non-invasive, capable of operating in real-time, and of being relatively straightforward to implement. The emissions from a plasma are characteristic of those species present in an excited state. OES is used to record the intensity of those emissions as a function of wavelength, most usually in the UV/visible region. The resultant spectra may, if they have suitable emission, be fully analysed to unequivocally identify atoms, ions, free radicals and molecular species present in the plasma.

4.3.1.1 Spectrometer

A diffraction grating[11] is most commonly employed as the dispersion element in OES. In modern instruments subsequent analysis of light intensity as a function of wavelength is carried out in one of two ways:

(i) the grating is rotated to scan the spectrum, and the dispersed light. It samples at a fixed position; or,

(ii) the grating is stationary and the light falls on a diode array.

The former potentially offers high resolution at the expense of relatively lengthy scan times, and the latter rapid response but lower resolution even when used over a narrower spectral range - there are typically 1024 diodes in an array. The requirement for high resolution (0.2nm) over a wide range (200-850 nm) made use of a scanning instrument essential for these studies.

The spectrometer used was a Bentham M300 scanning monochromator, controlled by a Bentham 215 stepping motor. The spectrometer contained a 1800 groove/mm grating blazed at 300nm, and was coupled to a photo multiplier and Optonic model radiometer. Output could be monitored on either a Bentham 223 lock-in amplifier and/or a Servi chart recorder. Quartz, rather than glass, optics were used in order to be able to study emissions in the region 200-320 nm. The spectrometer was aligned for maximum signal intensity.

4.3.1.2 Methodology

The spectrometer was calibrated with a Hg-lamp, and its resolution determined by scanning a Hg doublet at 131.1 nm. The system was capable of 0.018nm resolution, but was operated at ~ 0.2nm resolution (150μm entrance and exit slits). This represented a compromise between resolution and signal to noise ratio. Scan rates of 0.25 nm/s were used. Higher rates gave a significant loss of signal (> 10%). Full spectral scans were run between 200-850nm and therefore took almost 45 minutes.

4.3.2 Ultra Violet Absorption Spectroscopy (UV)

Materials absorb radiation at varying wavelengths, because of structural features within their molecular makeup (chromophores). This absorption occurs due to the fact that all molecules possess electrons which can be excited (raised to a higher energy level)[160]. Many of these electrons are excited by radiation of UV or visible wavelengths, but others are only excited by radiation within the vacuum ultraviolet range.

The quantity of proteins deposited on hydrogel lenses can be calculated by UV. spectrophotometry. Nearly all proteins exhibit an absorption peak near 280 nm due to conjugated grouping , but specifically the aromatic amino acid moieties when analysing proteins. Measurement of UV absorbance is an interesting, direct method which allows quantitative studies, but background absorbance of the material sometimes interferes with the reading. This can be minimised by using a blank of exactly the same lens in the reference cell. Lipids cannot be analysed by this means because lipids absorption wavelengths coincide with that of the polymer materials under observation, typically 320nm.

4.3.2.1 Ultra Violet Spectroscopic Measurements of Protein Deposition.

The protein concentration present on the contact lenses or in the storage solution was measured using UV absorbance. A dual beam U-2000 spectrophotometer (Hitachi) was used during the course of this work. The measurement is carried out in matched quartz 1 cm cells, against an unworn contact lens of the same material type, at 280nm. The contact

cells, against an unworn contact lens of the same material type, at 280nm. The contact lenses were mounted on the bottom of the cell so that they faced to the detector (Chapter 7).

Concentrations are obtained using the combined Beer-Lambert Law (Chapter 7). In order to apply this simple law and determine the concentration of an unknown analyte species, it is necessary to first construct a calibration graph of absorbance versus concentration using standard solutions of known concentration of the analyte species. The absorbance of the unknown can then be measured and the concentration interpolated from the calibration graph.

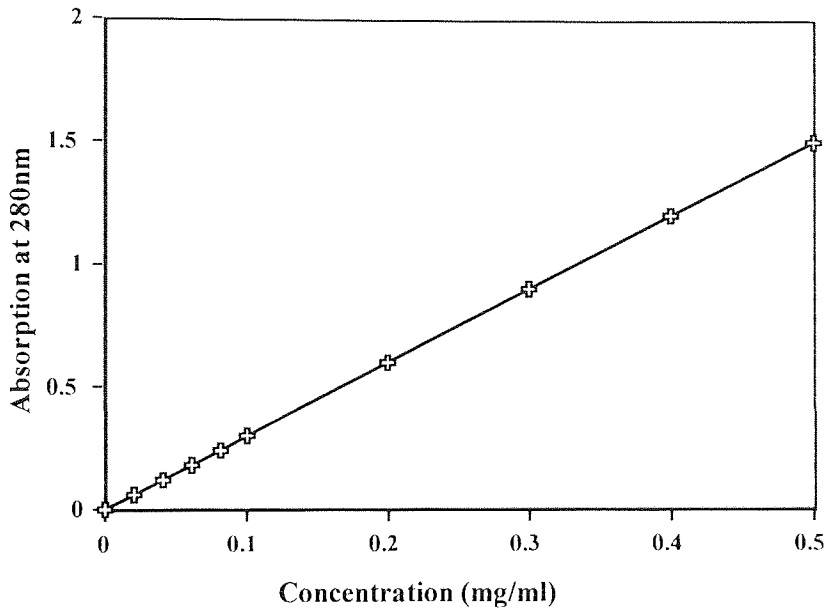

Figure 4.7: Calibration curve for the UV absorption of standard lysozyme solutions.

The instrument was zero adjusted using the blank. A calibration curve was produced by measuring the absorbance (A) of a series of lysozyme solutions with known concentrations C (ranging from 0.01 to 0.5 mg/ml), and plotting A against C (Figure 4.7). Similar calibration curves were also obtained for other individual and mixtures of proteins used for the spoilation studies. The calibration curves obtained for each protein and for the mixture of proteins were stored in the memory of the instrument for further measurements of the unknown samples. The UV absorption spectrophotometry was then used in experiments to quantify the amount of protein absorbed and adsorbed on and in the soft contact lenses. Samples were placed vertically within the quartz cuvettes as shown in Figure 4.8, against the wall of the cuvette, and the absorbance measured, and then calculated by the instrument to give a concentration value.

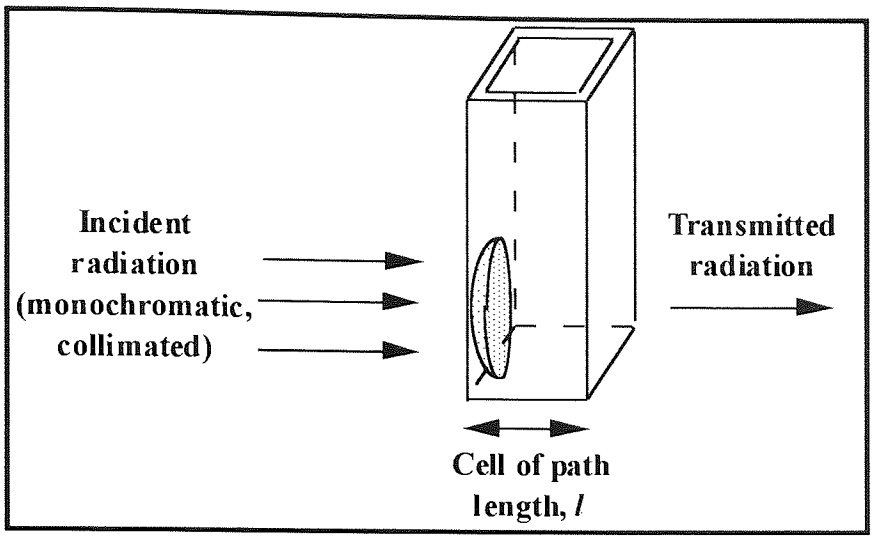

Figure 4.8: Schematic Representation of Sample Analysis for UV Spectroscopy

4.3.3 Spectrophotofluorimetry

Spectrophotofluorimetry[111,160-161] is another simple and direct method for the identification of adsorbed proteins and lipids on to the surface of a hydrogel contact lens. Similar to aspects in UV spectrometry, molecular structure is the determinant for the emitting wavelength observed and the concentration.

In fluorescence the excited molecules do not return to the ground state after excitation, but remain in the excited state for typical times in the order of 10^{-8}s. This is represented in the Jablonski Diagram (Figure 4.9).

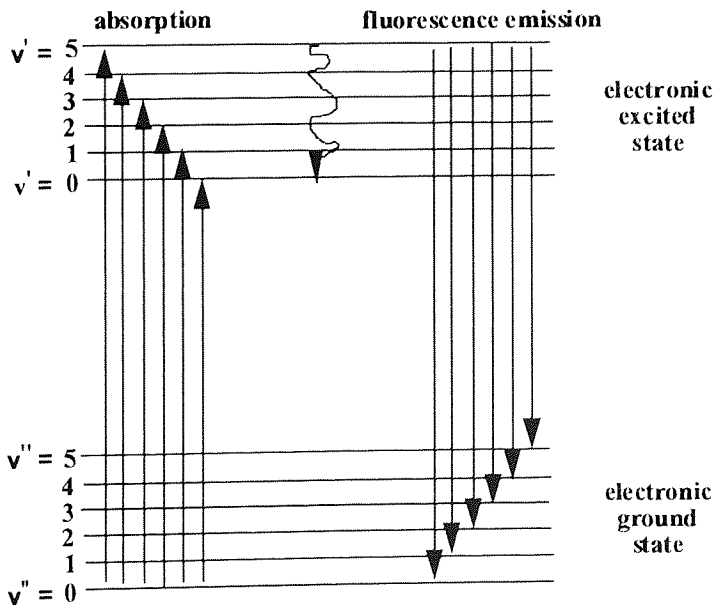

Figure 4.9: A Simple Energy Level Diagram Showing Molecular, Electronic and Vibrational Levels[160].

This 'lifetime' of the excited state, though apparently very short, is in fact very long compared with other events on the molecular scale, some of which are listed below in Table 4.1.

Lifetime of Events	Time (sec)
Transitions between electronic states	10^{-15}
Time period for molecular vibrations	10^{-14}
Time period for molecular rotations	10^{-11}
Av. time between collisions for a molecule in the liquid phase at room temperature.	10^{-12}

Table 4.1: Lifetimes for Molecular Events[162]

4.3.3.1 Fluorescence and Molecular Structure

Not all molecules which absorb ultra-violet or visible radiation are fluorescent. Only a small proportion of organic compounds fluoresce. Molecular structures which fluoresce are termed fluorophores. Fluorescent molecules are typically aromatic or contain multiple-conjugated double bonds with a high degree of resonance stability. Both classes of substances have delocalised π-electrons that can be placed in low-lying excited singlet states. Some typical molecules which exhibit fluorescence are shown in Figure 4.10.

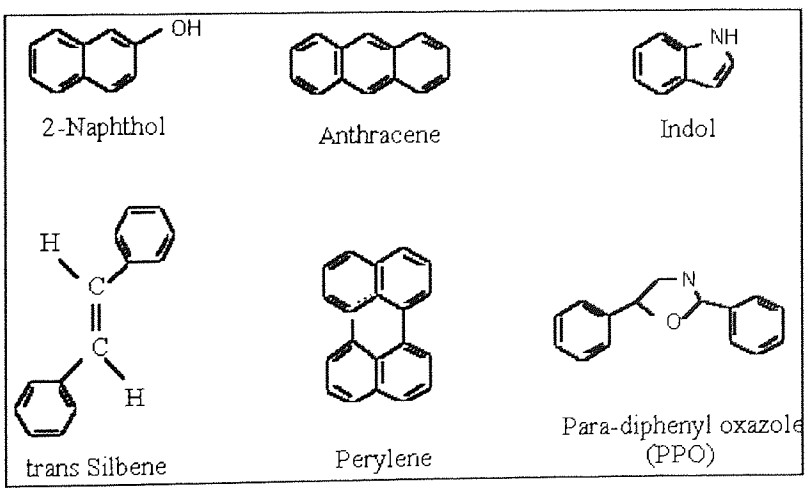

Figure 4.10: Typical fluorescent molecules[162]

The intrinsic fluorescence of most of the proteins is due to the presence of the fluorescent amino acids, tryptophan (ex. 280nm, em. 345nm), and tyrosine (ex. 280nm, em. 308 nm). Some proteins may also contain a fluorescent coenzyme such as reduced nicotinamide-adenine dinucleotide (NADH), flavine-adenine dinucleotide (FAD), or pyridoxal phosphate (Figure 4.11).

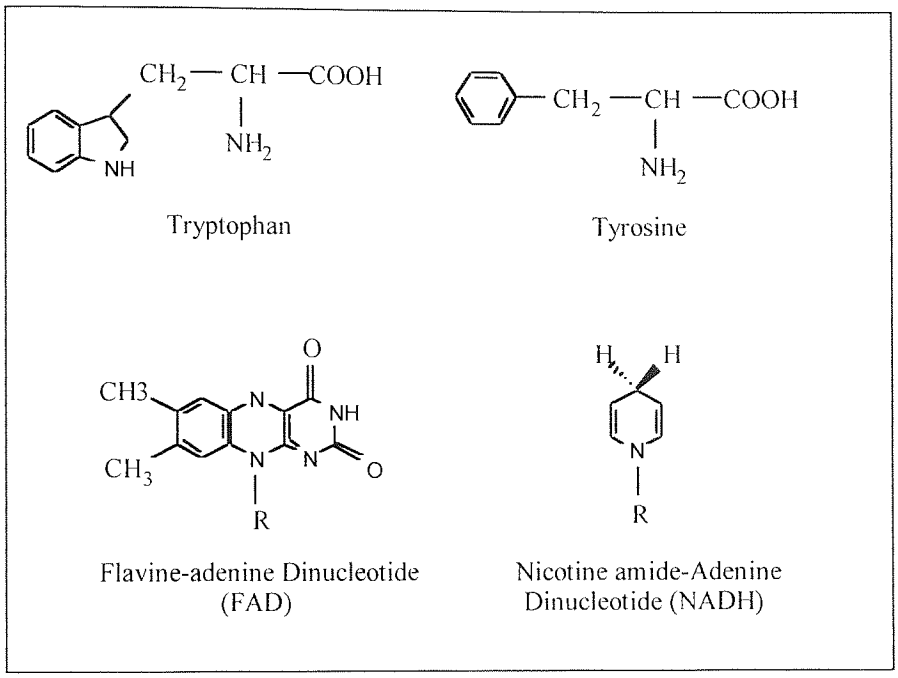

Figure 4.11: Intrinsic biological fluorophores (in the case of NADH and FAD, only the fluorescent part of the molecule is shown)[162]

It is possible to add intrinsic fluorophore labels to the substances which do not contain an appropriate natural fluorophore, such as FITC. The emission of the molecule is sensitive to the polarity of the surrounding environment, which was detected in preliminary fluorescent tagging experiments.

4.3.3.2 Surface Fluorescence Analysis of Gross Spoilation Profiles.

Spectra (of the lens placed in the 8 mm diameter cylindrical cell with the centre of the lens facing the light beam) were recorded with a modified Aminco-Bowman Fluorescence Spectrometer at excitation wavelengths of 360 nm and 280 nm since the emission from adsorbed proteinaceous and lipoidal components on the lens surface most commonly occur at these excitation wavelength. The emission spectra are recorded between 200 and 800nm. Excitation at 280nm produces emission centred around 360nm (Figure 4.12), which provides the best measure of surface protein, (recorded at 0.3 on % full scale) and aqueous lipid at 430 nm. Whereas excitation at 360nm produces the measure of gross lipid from the meibomian glands (Figure 4.13)[62], (recorded at 0.1 on % full scale).

The instrument was checked every week with standard cells. The excitation spectra were taken at 280 nm emission. For convenience the terms "meibomian" and "aqueous" are used throughout this section of the report to refer to the groups of lipids assayed by these two excitation wavelengths. Similarly the term "absorption" is used to encompass the components adsorbed onto the surface and absorbed within the surface layers of the lens.

Chapter 5 assesses the optimum working conditions of the PEEMS system and devises a standard protocol for sample preparation and machine operation during sample analysis. Further work detailed in Chapter 6 studies two classes of polymeric materials, hydrogels (HEMA copolymers) in Section 6.2 and polyurethanes (poly ethyleneglycol (PEG) copolymers) in Section 6.7. Section 6.13 goes on to discuss a terpolymer system comprising of HEMA:PEG:MAA. This chapter looks at the possible biological compatibility of these materials. Chapter 7 then goes on to look at the possible mechanism for deposition of the protein moieties. An initial view of the data suggests that very high protein concentrations arise in thin layers close to the polymer surfaces of Group I and IV lenses. This chapter describes progress to date and summarises the methods used in data analysis and typical results.

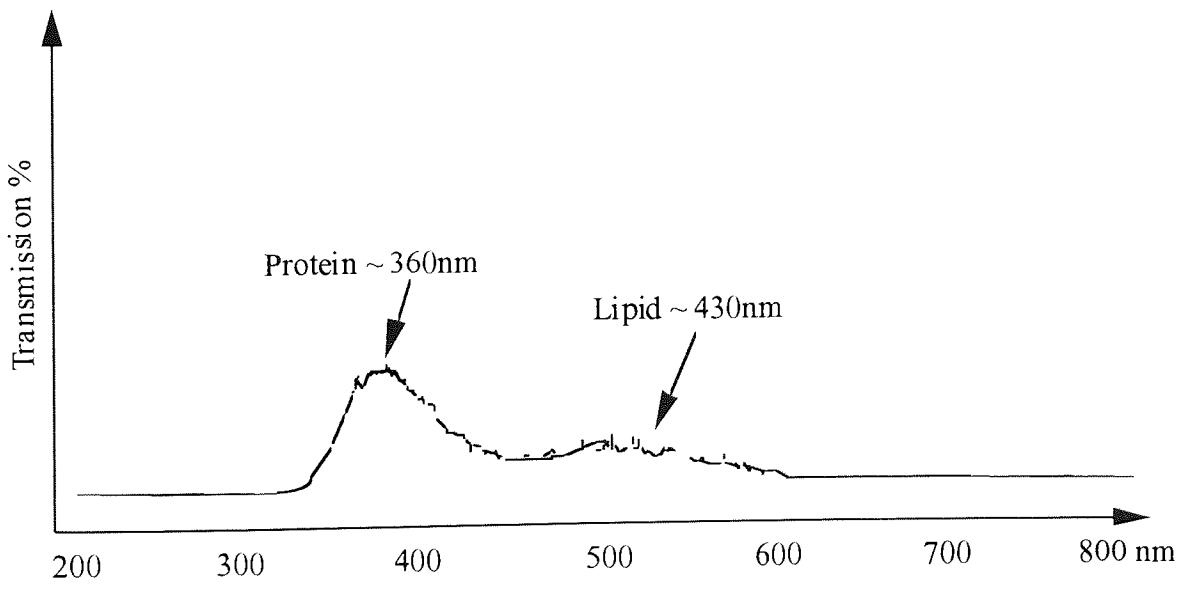

Figure 4.12: The fluorescence spectra of a spoiled Acuvue™ lens excited at 280nm.

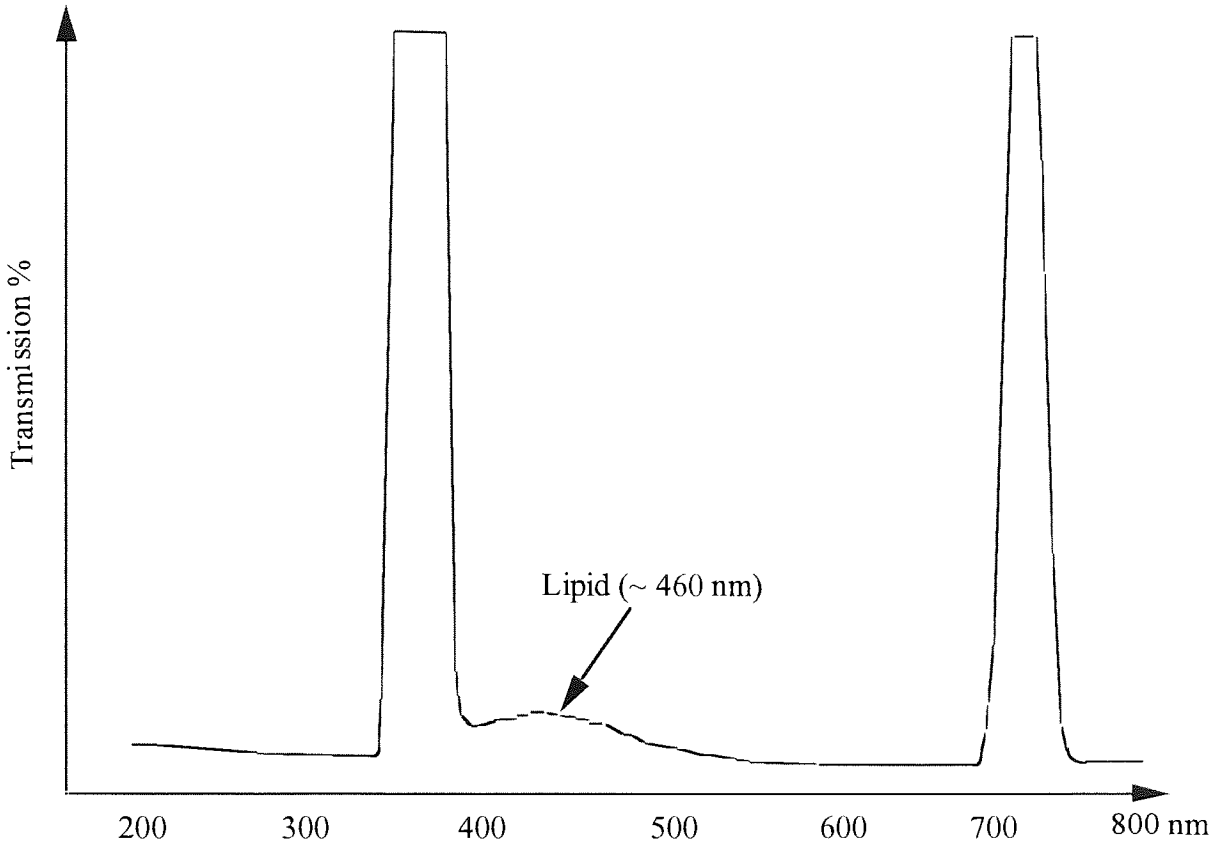

Figure 4.13: The fluorescence spectra of a spoiled Acuvue™ lens excited at 360nm.

Chapter 5

Gas Plasma Etching: Results

Initially a series of experiments were set up to study, for a given etchant, the influence of three process parameters - gas flow, chamber pressure and applied RF power - on the etch rates of Polymacon and Etafilcon A materials over a wide range of values of the process parameters, and to study the corresponding gas-phase chemistry using optical emission spectroscopy. Three etchants - air, oxygen and argon - commonly used in plasma etch processes were chosen for investigation. Orthogonal relationships were employed both to maximise the amount of useful data generated from the minimum necessary number of experiments in the parameter space, and to assist in a comparison of the results from the etchants through modelling. The chapter then goes on to look at possible detrimental effects caused by gas plasma etching and sample preparation.

5.1 Response Surface Methodology: Experimental Design

Many process parameters e.g. choice of gases, flow, pressure, power, electrode spacing, temperature, dc bias, determine the performance e.g. etch rate, selectivity, anisotropy of a plasma etcher. As the process parameters may also be interactive, the one parameter at a time approach to process optimisation can require very many experiments, as well as giving potentially misleading results.

Response surface methodology is a statistical experimental design technique developed in the 1950's that has recently become popular for the study of plasma processes. In this approach the factors (parameters) of interest are represented as orthogonal axes in space. The limits of the axes are the physical maximum and minimum measured within a defined space. Responses (experimental results) are then systematically measured within defined space, but not beyond.

The number of levels (settings) used for each factor determines the complexity of the model which can be produced. A three-level design is needed in order to include

quadratic terms for curvature as well as linear, two-factor interactions. For example, a three- factor, three level design gives a model of the form:

$$Y = c_o + c_1X_1 + + c_2X_2 + c_3X_3 + c_4X_1X_2 + c_5X_1X_3 + c_6X_2X_3 + c_7X_1^2 + c_8X_2^2 + c_9X_3^2$$

where Y is a response, e.g. etch rate; X_1, X_2 and X_3 are factors, e.g. flow, pressure and RF power; and c_o - c_9 are coefficients to be determined.

In this work, a Box-Behnken[162] experimental design was used. It consists of replicated centre points and the set of points lying at the midpoints of each edge of the multi-dimensional cube that defines the region of interest. The three-factor design requires fifteen experiments- the midpoint of each of the 12 edges of a cube, and replicates of the centre point in order to assess the experimental error. The chosen values of the factor were scaled by normalisation about their respective means. Thus high, middle and low settings were represented by 1, 0 and -1. Comparison of the magnitude of the coefficients obtained from modelling then provided an estimate of the relative importance of each parameter in the model. The 15 experiments needed covered the ranges in Table 5.1, and were carried out in a randomised order.

Setting	*-1*	*0*	*1*
Parameter			
Flow (ml/min)	1	2	5
Pressure (mtorr)	15	100	150
RF Power (W)	50	100	150

Table 5.1: Parameter Settings

The data generated was analysed using least squares regression analysis, with the aid of a commercially available package - Excel/Design Ease- run on a personal computer. The software also provided statistical information on the model produced. The statistical significance of each term in the model is given by its F-ratio. The F-ratio is the ratio of the variation in the response accounted for by the model term to the residual error (the variation between the model and the data). A larger F-ratio value indicates a greater statistical significance of that term. Critical values have been tabulated for the F-ratio,

with 1 and n-p-1 degrees of freedom (n = number of data points; p = number of model terms), above which the model term is statistically significant for a given confidence level- typically 95%. The software used here allows the stepwise inclusion of significant terms into a model.

The success of the final model can be assessed in a number of ways. The correlation coefficient, R^2, gives a measure of how well the model fits the experimental data. It is defined as the ratio of the sum of squares due to regression to the total sum of squares:

$$R^2 = \Sigma_I (\hat{Y}_I - \dot{Y})^2 / \Sigma_I (Y_I - \dot{Y})^2 \qquad \text{(Eqn 5.1)}$$

where Y_I are observed values, $\hat{Y}_I$ predicted values and $\dot{Y}_I$ mean values.

The values of R^2 vary between 0 and 1, a value of 1 indicating a perfect fit.

The standard error s, is given by:

$$s = (R_I (Y_I - \dot{Y})^2 / (n-p))^{0.5} \qquad \text{(Eqn 5.2)}$$

The requirements here are for the standard error to be significantly smaller than the magnitude of the response.

As the individual terms, the statistical significance of the model may be tested by determining the F-ratio (the ratio of regression mean square to the residual mean square). However, it is also important to know whether any inadequacies in the fit of the model are due to experimental error or are inherent in the model itself. As the experimental design included repeated points, the experimental error and the lack of fit can be compared. This is termed analysis of variance, (ANOVA). An F-ratio, the ratio of replicate error to the lack of fit mean square, is calculated and compared with critical values as before.

The results of the experiments to determine the Group I (Polymacon) and Group IV (Etafilcon A) etch rates are given in Table 5.2. The randomised experimental order was: 6, 5, 2,14,11, 3, 12, 9, 4, 10, 1, 13, 15, 8, 7.

Expt.		Settings		Etch Rate ($*10^{-10}$g/s) in Oxygen		Etch Rate ($*10^{-10}$g/s) in Air		Etch Rate ($*10^{-10}$g/s) in Argon	
#	Flow	Pressure	Power	Group I	Group IV	Group I	Group IV	Group I	Group IV
1	1	1	0	2400	40	115	76	42	36
2	1	-1	0	1560	40	100	76	17	10
3	-1	1	0	2220	32	166	66	102	37
4	-1	-1	0	1640	45	126	74	27	10
5	1	0	1	2740	80	168	120	51	33
6	1	0	-1	960	9	26	22	14	20
7	-1	0	1	2800	94	200	140	85	4
8	-1	0	-1	1040	7	30	38	25	18
9	0	1	1	3600	75	214	132	56	61
10	0	1	-1	840	7	80	5	23	34
11	0	-1	1	2100	90	200	108	34	13
12	0	-1	-1	900	14	40	28	8	7
13	0	0	0	2280	46	130	76	35	23
14	0	0	0	2300	44	118	70	42	23
15	0	0	0	2360	48	108	78	37	13

Table 5.2: Group I and Group IV etch rates in Oxygen, Air and Argon

Prior to modelling the air, oxygen and argon systems, it is immediately apparent from comparison of the results that there are considerable differences between the three systems. Most dramatic is the oxygen : air systems where there is a ten-fold increase in the Group I etch rates.

Table 5.3 summaries the results of statistical analysis of the model. The adjusted R^2 term shows that the data is reasonably well represented, e.g. 96% of the variation in the polymer etch rate for air, is accounted for by the model. The adjusted R^2 value of 61% for the Argon-Group IV etch is disappointing. Nonetheless, the regression F-ratios all show statistical significance of all the models at a 95% confidence level. As the systems parameters were standardised to a common range of values (-1, 0, 1), a number of features of the models may be identified by examination of the relative size of the coefficients in Table 5.3. In all cases, other than argon-Group IV (where the modelling was least successful), a positive, linear power-term was dominant.

Interestingly, the etch rate increased with increased pressure and decreased flow of air. A number of interactive terms can be seen. Here the relative influence of one parameter on a response varies according to the setting of another parameter. The oxygen system results were generally of a higher quality (Table 5.3) than those of air, as evidenced by the adjusted R^2 and F-ratio values. Consideration of standard errors, s, and the replicate errors shows that this was due to an improved set of experimental results. Thus the lack of fit F-ratio values are even smaller than those for air, and although the models are statistically significant, their residual error is due to lack of fit rather than experimental error. This suggests that additional terms, such as third-order interactions, need to be included in the models.

Model	R^2_{adj}	**F-ratio** (Regression)	**s**	**Replicate** (mean value)	**F-ratio** (lack of fit)
Group I $_{oxygen}$	0.99	243	79	2310 ± 50	0.08
Group IV $_{oxygen}$	0.97	187	6	46 ± 2	0.11
Group I $_{air}$	0.96	91.0	12	119 ± 11	0.85
Group IV $_{air}$	0.96	177	8	75 ± 5	0.24
Group I $_{argon}$	0.82	14.0	14	38 ± 4	0.09
Group IV $_{argon}$	0.61	22.7	9	19 ± 6	0.33

Table 5.3: Evaluation of Air Plasma Models

The etch rates for the systems were proven to be better for air and oxygen, but not Argon. Oxygen gave a very rapid etch system whereas argon was more subdued, the intermediate etch system of air was chosen, as submicron levels could be removed within a workable time span.

Having assessed the optimum working conditions a standard protocol of sample preparation and machine operation was devised for analysis purposes.

5.2 Standard Operating Procedures Used for Etching System

Prior to any series of experiments the plasma chamber was cleaned by using a detergent/abrasive cloth, followed by rinsing in distilled water and acetone, and finally subjecting the chamber to a hot air stream, so warming the reaction vessel and allowing solvent evaporation under vacuum. Trace carbonaceous material was then removed by striking an oxygen discharge - the plasma colour changed from blue (characteristic of CO/CO_2 species) to pale pink. The propanol/oxygen plasma treatment sufficed for minor contamination and helped to maintain reproducible etch rates.

Up to three process gases could be used - oxygen gas, an additive argon and air. When any new process gas was selected, or after a gas cylinder was changed, the gas lines were evacuated. This procedure served the dual purpose of both removing trace contaminants, and leak checking lines prior to pressurisation with a process gas.

The steps necessary prior to striking a plasma were:
(i) evacuation of chamber to base pressure (10-15 mins),
(ii) admittance of process gases,
(iii) pressure adjustment,
(iv) stabilisation of flow and pressure (2-3 mins),
(v) stabilisation of balance (10-15 mins), and
(vi) setting forward RF power level (power supply and matching unit).

When the chamber was to be used for the first time after cleaning 'conditioning' was necessary before spectroscopic or gravimetric measurements could be carried out. This involved running a plasma of the desired process parameters for ~ 15 minutes.

Finally, the plasma chamber was fully evacuated after any discharge in order to remove potentially noxious gases.

The system is regularly standardised using a 14mm diameter dehydrated sample of etafilcon A (trade name is Acuvue, supplied by Johnson & Johnson), which has an etch rate of $0.007\mu g/sec \pm 4\%$). Figures 5.1 and 5.2 show typical traces obtained for sample during reproducibility studies: Figure 5.1 is a typical etch profile for an Acuvue Lens, Figure 5.2 is an extreme case of incorrect usage of the system, where deposition is occurring. This may occur because the flow rates or reflected power are not suitably set, which would consequently affect the pressure, temperature and forward power of the system. Balance instability can be caused due to electrical field interference, earthing should be consequently checked.

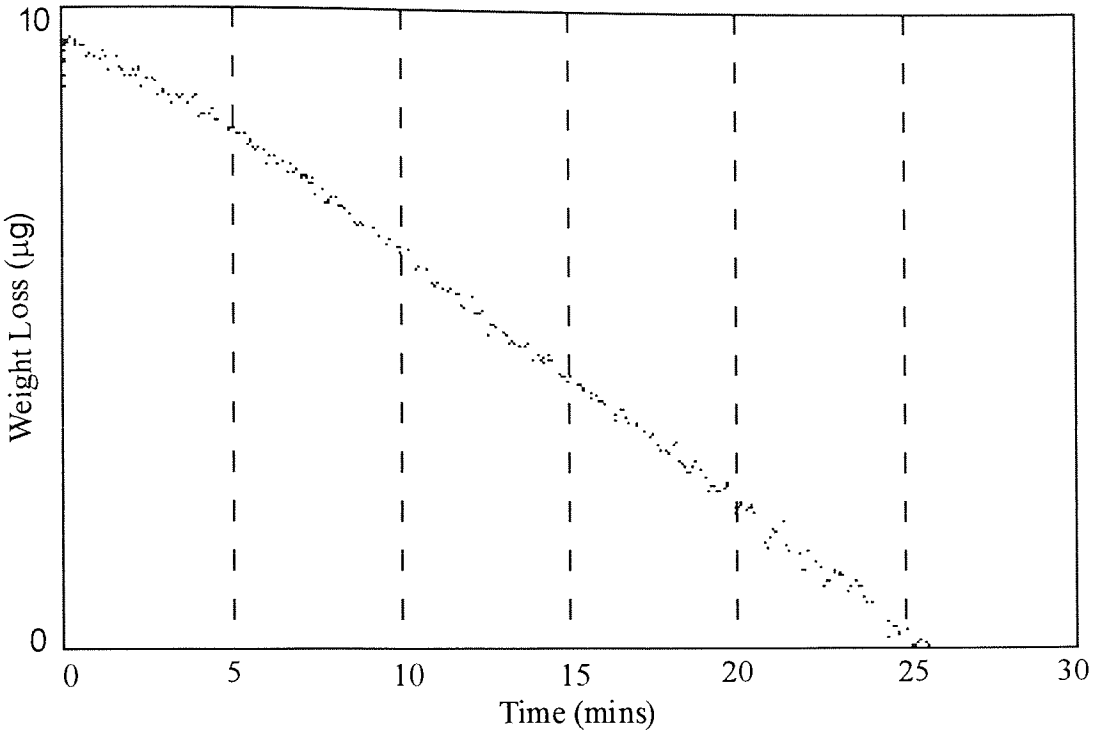

Figure 5.1: Typical Etch Profile for etafilcon A (Acuvue) Material

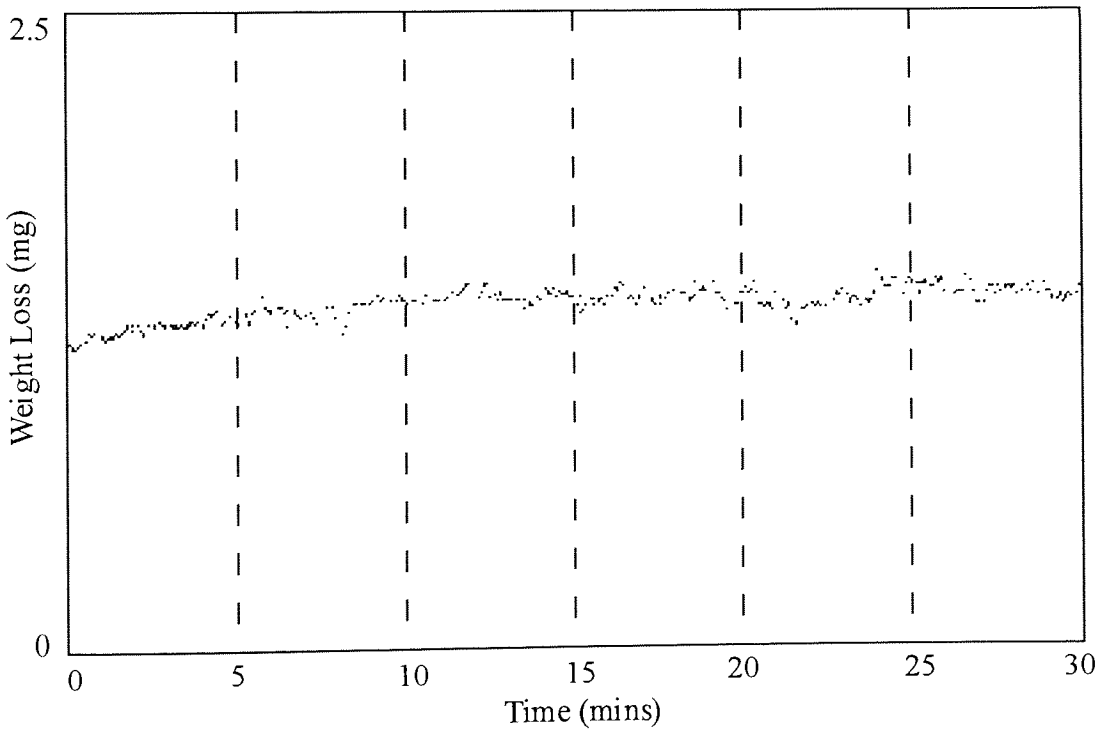

Figure 5.2: Deposition Occurring in Reactor Using an etafilcon A (Acuvue) Material

Table 5.4 lists typical operating conditions used for plasma etching of an etafilcon A (Acuvue) lens. These parameters were employed for consistency when comparing data unless otherwise stated.

Parameter	Setting
Power (forward)	100 Watts
Power (reflected)	3 Watts
Pressure	0.1 Torr
Flow Rate (air)	2 cm^{-3}/s

Table 5.4: Optimum Plasma Etching Conditions

A number of plasma emissions from both atomic and molecular species were unequivocally identified. The species given in Table 5.5[163], and typical spectra are shown in Chapter 8.

Species Monitored	Wavelength (nm)	Reference
N_2O	283.3	78
CO	297.7	79
OH*	308.9	78
N_2*	337.1	79
CN*	387.1	79
CO*	483.5	79
CO*	519.5	79
H*	656.3	78
N*	674	78

Table 5.5: Common species and emission wavelengths

* indicates a species in an excited state.

Within the above mentioned groups using OES, it is usually straightforward to follow qualitative changes in discharge properties. However, the minute concentrations of species evolved when etching a small cross-sectional area of 1.4 cm^2 within a vessel of ~ 4.4 dm^3 is hardly above that of background levels. To overcome this, as the technique proved reliable and uniform it was considered feasible to etch en masse (several lenses) to see if concentrations were of a detectable level. Reasonable results were obtained when 22 lenses were placed within the chamber, (21 arranged in three's on the grounded electrode and one on the cradle of the micro-force balance). This would allow maximum coverage of etchable area without causing loading effects. Peaks were observed for CO*, OH* and NO*, but the system proved temperamental not allowing duplication, and unfortunately time did not permit enhancement techniques of the system to be followed up at this stage (Chapter 9).

5.3 Plasma Etching and Emission Monitoring (PEEMS)

The incorporation of both intrinsic and extrinsic diagnostic techniques for surface characterisation is collectively known as PEEMS. The surface and bulk distribution of protein and lipid are analysed using the PEEMS system which generates a gas plasma that serves as a "molecular scalpel" to remove the protein and lipid absorbed on the contact lens surface.

5.3.1 Methodology

Samples are initially rinsed in distilled water to remove excess spoilant, and placed in acidic solution, to 'freeze' the system. At physiological pH and above, the pore size of hydrophilic hydrogels (typically Group IV) is larger than the spherically proportioned lysozyme molecule and so allows movement of the protein through the matrix. To inhibit mobility of these species the lenses are placed in an acidic solution (e.g. hydrogen peroxide, pH 3.56). pH values lower than the isoelectric point of a protein provides a higher charge density (Table 5.11), in this case rendering the protein more positive in nature, and absorb to a greater extent onto the negatively charged polymer surface. The lenses are then dehydrated by microwave (10 minutes, 650 Watts) and etched for 30 minutes to reveal the underlying matrix layer.

The lenses are then rehydrated in acidic solution and the exposed layer is then analysed for lipid and protein spoilants using both surface analysis (fluorescence spectroscopy) and bulk matrix analysis (ultra-violet spectroscopy). As mentioned at the beginning of section 4.5, improvements in sensitivity of the OES system would concurrently have yielded data on the evolving species during etching.

The process is repeated progressively to ascertain the composition of the remaining unetched matrix layers and graphically represented as a penetration profile (Figure 5.4).

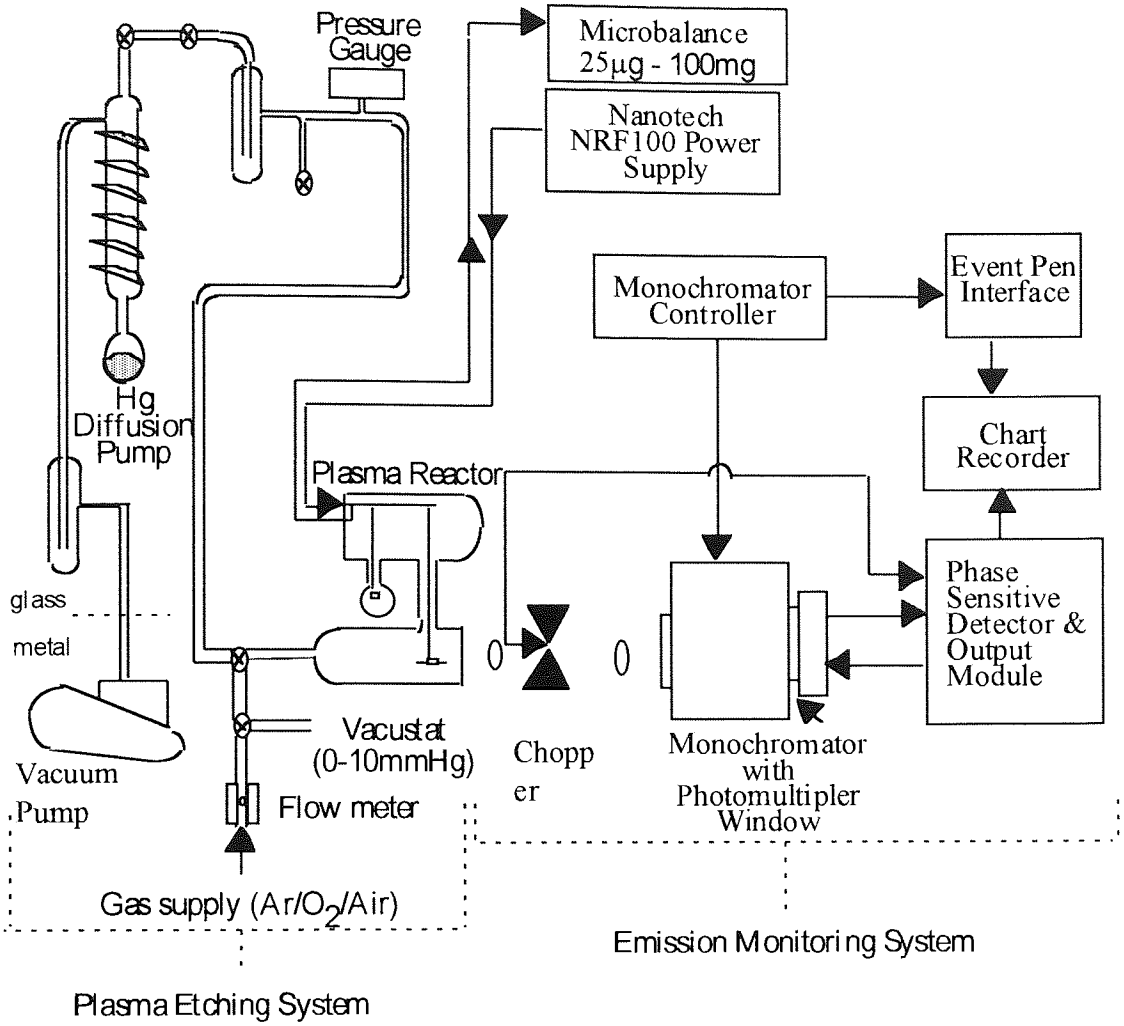

Figure 5.3: Experimental Set-up of Plasma Etching and Emission Monitoring System

From this initial data plot (Figure 5.4) with each etch it can be seen that the protein concentration reduces progressively, and with weight loss readings viewed in conjunction with material removal the location of the spoilation debris can be determined. Simple calculations give an idea of the amount of sample that is removed per etch, and this can then be translated into depth of material removed per etch, assuming that there is uniform etching, detailed in Chapter 7.

The next stage is to assess whether this observation is due to the removal of protein during etching or a modification to the sample. The next section details investigative work undertaken to assess the legitimacy of the technique for the detection of proteins.

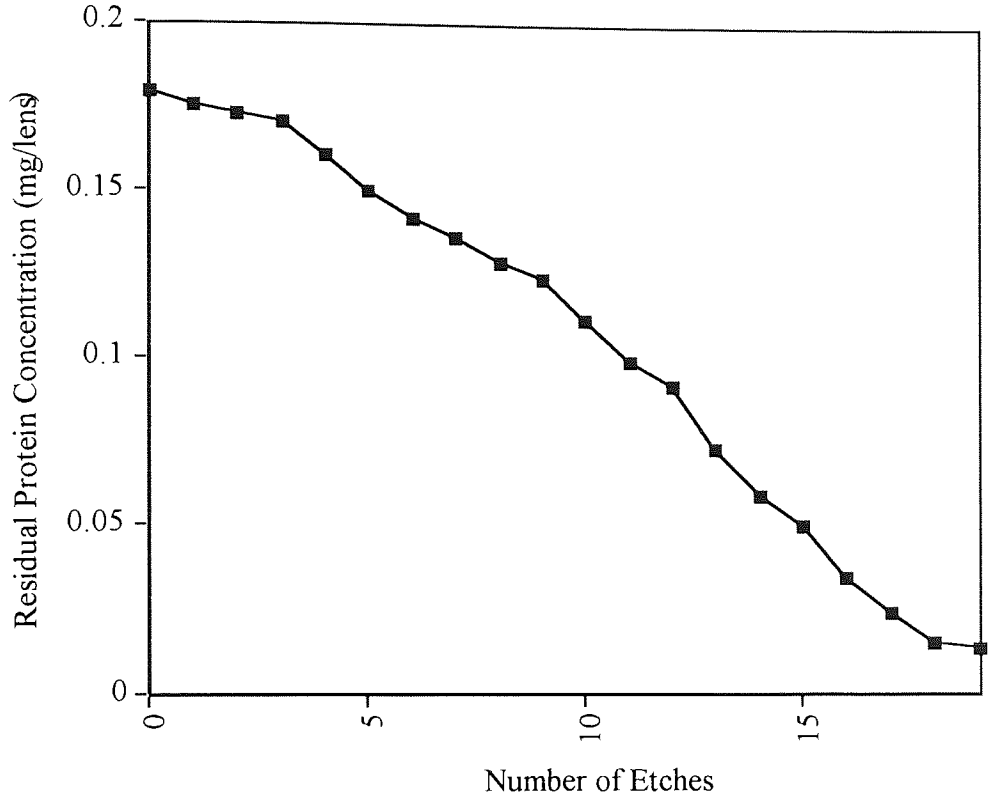

Figure 5.4: Lysozyme Penetration on FDA Group IV (Acuvue) Contact Lens

5.4 Detrimental Effects of Plasma Etching on Contact Lens Samples

When treating samples within a gas plasma environment, the process is that of bombardment, dislodgement and/or cleaving. The initial sample preparation employed for this technique (dehydration) is liable in itself to cause proteins to denature before the sample is even treated within a plasma environment, but proteins such as lysozyme are quite resistant to extreme conditions[164]. But breaking bonds through etching would cause the production of smaller chained peptides to be formed. Two established techniques, gel electrophoresis and activity measurements were used to assess the extent of protein denaturing with lysozyme as the marker, because of the high incident rate for spoilation with this protein.

5.4.1 Electrophoresis

Proteins are amphoteric compounds which contain both acidic and basic groups, the net charge of a protein being determined by the pH of the medium. The pH at which proteins have no net charge is called the isoelectric point (pI) (Table 5.6). At a pH above the isoelectric point, proteins are negatively charged, and at pH values below their isoelectric point they have positive charge. This protein behaviour makes them suitable to be separated by electrophoresis.

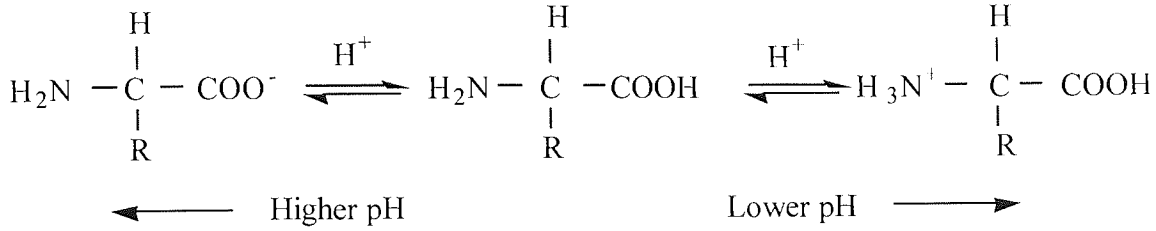

Electrophoresis is a method whereby charged molecules in a buffer solution migrate in an electric field. Therefore, if the pH of the buffer is higher than the pI of a specific protein, it is negatively charged and migrates towards the anode, similarly, if the pH of the buffer used is lower than the pI of the protein it will migrate towards the cathode. The rate of migration depends on the strength of the field, the net charge, size and shape of the molecules and also on the viscosity, ionic strength and temperature of the medium.

Protein	Molecular Weight (kD)	Isoelectric Point (pH units)	Relative Overall Charge
Lysozyme	12.6	11.0	(3+)
Lactoferrin	74	9.6	(2+)
Albumin	65	4.6	(2-)

Table 5.6: Characteristics of Major Tear Proteins

5.4.2 Densitometry of the Gels

Densitometry is a quantitative method for assessment of the amounts of colour present in each part of a stained gel can. The accuracy depends on whether the proteins bind to the dyestuff to the same degree or not. However, if this bind is not similar, only an estimation may be used to calculate the amount of the proteins. A LKB Ultrascan Laser densitometer was used to measure the density of the stained proteins on polyacrylamide gel, which was interfaced to an Apple II EuroPlus computer. The absorption spectra were obtained with the position and intensity of each peak representing a specific protein.

Figure 5.5 shows the electrophoresis gel with a series of standard lysozyme solutions with different concentrations which were stained with BBG.

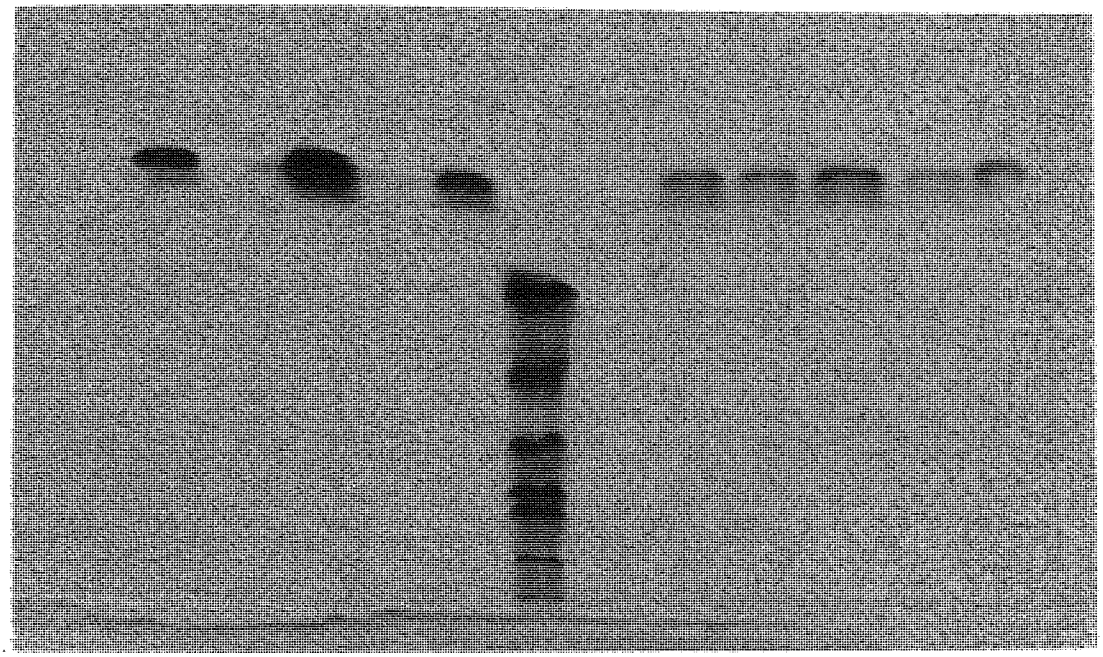

Figure 5.5 A Brilliant Blue stained gel containing: Etched Samples, Sigma High Molecular Weight Standards, 0.25-2.0 mg/ml Lysozyme Solutions.

5.4.3 Quantitative determinations

A set of standard solutions of lysozyme were prepared and run on a polyacrylamide gel and the resulting gel was stained using Brilliant Blue G technique (Figure 5.5). The intensity of the dye on each of the bands on the gel were measured by the use of the densitometer and a standard curve obtained by plotting the concentrations of the lysozyme samples against the height of the peak on the densitogram (Figure 5.6). The standard curve was used to calculate the quantity of the lysozyme in the remaining on etched contact lenses to determine the denaturing effect of plasma etching.

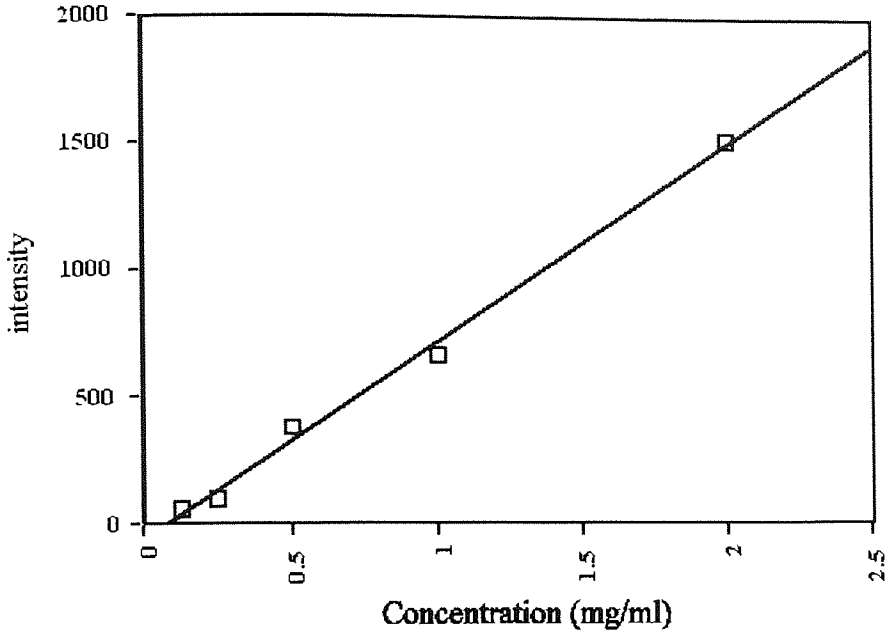

Figure 5.6: Calibration curve for Densiometry

5.4.4 Results

From the stained gels produced and under densitometry measurements, there were no detectable levels of low molecular weight peptides. Figure 5.8 is the densitograms of the lysozyme solutions in each well.

Figure 5.7: Photograph of Gel produced from electrophoretic run of the standard lysozyme solutions in each well.

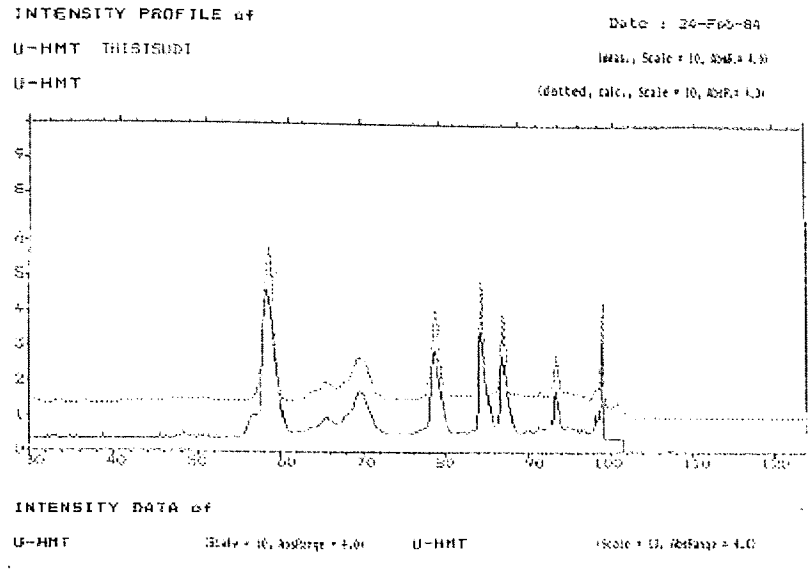

Figure 5.8: The densitogram of lysozyme solutions from the gel in Figure 5.7.

5.4.5 Measurement of Lysozyme Activity

The following technique, which is based on the decrease in turbidity (A_{580}) following lysis of a suspension of *Micrococcus lysodeikticus* (this is the substrate for enzymatic action of lysozyme)[165].

5.4.5.1 Materials and solutions

1.Phosphate buffer (pH 6.2, M/15)
9.08 grams of anhydrous potassium dihydrogen phosphate (BDH, 29608) was dissolved in 1000 ml of distilled water (solution "a"). 9.47 grams of anhydrous disodium hydrogen phosphate (BDH, 10248) was dissolved in 1000 ml of distilled water (solution "b"). 815 ml of solution "a" was mixed with 185 ml of solution "b", and the pH was checked with a pH meter.

2.Buffered substrate
15 mg of dry *Micrococcus lysodeikticus* (Sigma, M-3770) was dissolved in 10 ml of saline solution (0.9 % NaCl) and diluted to 100 ml with phosphate buffer. The solution was aged overnight at room temperature.

3.Lysozyme standard solution (0.4 mg/ml)
20 mg of lysozyme was dissolved in 50 ml of 0.9% NaCl solution.

5.4.5.2 Procedure

5.0 ml of the substrate was equilibrated at 37 °C for about five minutes in two test tubes. 0.5 ml of each standard solution and extracts were added to each appropriate tube. To obtain the most possible extractable protein from the surface and matrices of the contact lenses ReNu™ multi purpose solution was used, with the summarised extraction procedure below:

1. Cut the contact lenses in quarters and shake them vigorously in 1ml of the extraction solution.

2. Leave the whole lens in 1ml of the extraction solution while shaking on a low speed (set on 150) vibrator (IKA-Vibrax-VXR) for 24 hours.

3.Cut the lenses into 8-10 small pieces, add 0.5ml of the extraction solvent and centrifuge for 15 minutes at a high speed.

The UV absorption was recorded at 540 nm after exactly thirty seconds (first reading) and after three minutes reaction at 37 °C in the water bath (second reading). The blank used was 0.9% NaCl and it was also equilibrated in 37 °C bath for at least five minutes. To avoid any errors, each sample was determined individually.

5.4.5.3 Calculation of lysozyme activity

The change in absorbance (ΔA) was calculated from the following formula:

$$\Delta A = A\ (540\ nm)\ \text{at}\ 30\ \text{seconds} - A\ (540\ nm)\ \text{at}\ 3.0\ \text{minutes}$$

The concentration of active lysozyme in the unknown samples was measured from the U.V absorbance:

$$C = \frac{\Delta A_T}{\Delta A_S} = \times\ 0.40 \qquad \text{(Eqn 5.3)}$$

Where C is the concentration of lysozyme in the unknown sample, A_T and A_S are the absorbance of the unknown and the standard lysozyme solutions respectively, and 0.4 is the concentration of the standard solution of lysozyme.

5.4.5.4 Results

As shown in Table 5.7, the effects of prolonged plasma etching and repetitive hydrating and dehydrating, does decrease the activity of lysozyme to ~80% when allowing for experimental errors. By microwaving the sample initially there is ~10% decrease in the activity of lysozyme. So the actual activity of lysozyme has actually only fallen by ~10%, after repetitively etching the sample. This implies that during etching the underlying lysozyme layers, whether on the surface of the material or below- within the polymer matrix- are not extensively damaged by the bombarding plasma particles.

No. of Etch Sequences	Activity (%)
0	89.1
1	90.1
3	88.9
5	87.2
10	85.8
15	83.9
20	82.8

Table 5.7: The Effect of Etch Sequence On Activity of Lysozyme

5.4.6 Dehydration Systems

A trial was set-up to assess the best means of drying the sample without altering it's spatial configuration. Three methods were tried: Vacuum Oven, Critical Point and Microwave.

Drying Methodology	Activity (%)
Vacuum Oven	95
Critical Point	85.4
Microwave	89.1

Table 5.8: The Effect of Drying Conditions on the Activity of Lysozyme

From Table 5.8 we can see that each technique had comparably the same effect on reducing the lysozyme activity, vacuum drying being considerably better than critical point and microwave drying lying centrally between these. The swifter of the three to operate was microwave drying and ease of handling, and this became the preferred method.

5.4.7 Excitation Frequency

The mass difference between electrons and ions results in the electrons being accelerated to higher velocities than the ions in the presence of an electric field. In particular high frequencies (HF) and radio frequencies (RF) systems the electrons can reach much higher energies than the ions because of their smaller mass and the rapidity of the field change. Therefore there are many advantages of RF discharges over the DC discharges, as shown below:

(i) RF plasma can be excited and sustained using either conductive or non-conductive electrodes, while DC discharges require the electrodes to be conductive throughout the process.

(ii) RF plasma can be sustained with internal as well as external electrodes, while DC discharges require the electrodes to be inserted inside the reactor and be in direct contact with the plasma. Use of external electrodes is sometimes required when the gases of the discharge are corrosive or when contamination levels are required to be low so reducing levels from the electrodes.

(iii) RF plasma are characterised by higher ionisation efficiencies than are the DC plasma.

(iv) RF plasma can be sustained at lower gas pressures than are DC plasma.

(v) In RF plasma the energy of the ions bombarding the sample is controlled by the negative bias, which can be adjusted over a wide range of values. Samples placed on the cathode of the DC discharge are exposed to bombardment of high energy ions that are accelerated at voltages that have to be above the minimal breakdown voltage. This can cause damage to sensitive substrates.

Radio frequency power generator from Nanotech (13.56 MHz) was used, which operates within the range of 0-1000 Watts. A Electrotech RF generator operating at 6 GHz was also employed to see the varying effects of excitation frequency on etching. The etch rates increased by 20% with all other parameters kept constant, but through SEM, excessive surface damage was assessed as 'pit-holes', formed during etching, as seen in Figure 5.9.

Activity measurements tabulated in Table 5.9, showed extensive damage to samples of lysozyme, implying damaged to imbibed protein, as shown in Table 5.8, unlike the system shown in Table 5.8 where damage is limited mainly to the drying technique rather than the etch process.

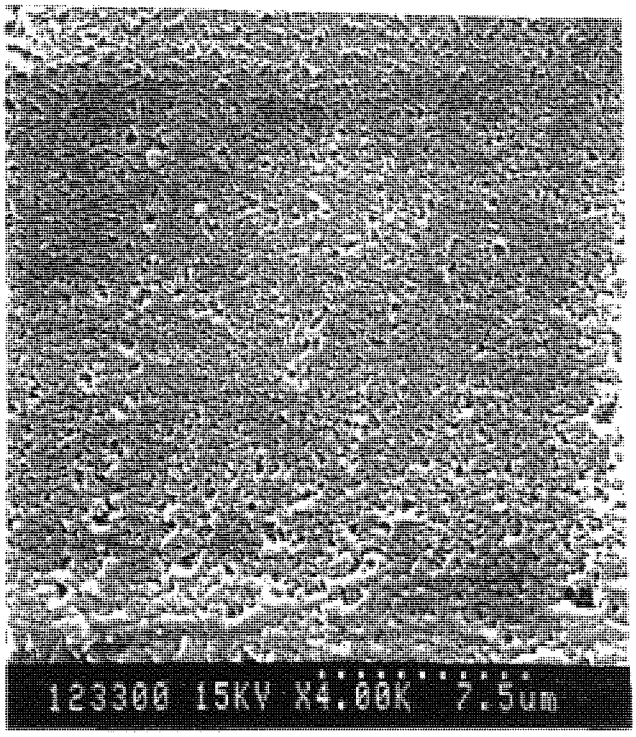

Figure 5.9: Surface Damage of Etafilcon A Hydrogel Material Using a 6 GHz RF Generator

No. of Etch Sequences	Activity (%)
1	30
2	10
3	0

Table 5.9: The Effect of Etch On Activity of Lysozyme

Any surface immersed in a glow discharge will be subjected to fluxes of ions, electrons and photons. This bombardment tends to increase the rate of subsequent reactions and heat the surface. The optical radiation emitted by a plasma spans the ultra-violet to the infra-red regions of the electromagnetic spectrum. Ultra-violet radiation is strongly absorbed by polymers producing free radical sites at large penetrations. Impinging ions damage the polymer producing active sites extending several monolayers below the surface, the depth of penetration and number of active sites produced are determined by the ion energy. Electrons having high energy, produce damage at large depths in the polymer structure. But it must be noted that bombardment by ions, electrons and photons plays a secondary role in the stripping process since removal rates in an inert gas plasma, under similar conditions are low, as shown later in Section 5.1.

5.4.8 Temperature

The energetic species in a plasma -including ions, electrons, metastables, and photons- collide with the surfaces of the polymer substrate in the plasma chamber and excite the molecules at the surface layers. The energies in the plasma, constitutes equal or exceed the bond energies of many common chemical bonds. Hence, low-temperature plasma can break chemical bonds. Because the plasma treatment is conducted in a vacuum, it tends to be completely pervasive and is capable of treating surfaces of complex shape.

Because the system was being devised for examination of biological species, the working temperatures had to be assessed, to reduce detrimental damage (denaturing) to the spoilants on the contact lens material. Polyurethane samples with known Tg's (melting points, 78°C) were taken (Chapter 6, Section on PU's), and etched for 30 minutes within the plasma reactor at desirable operating conditions that would produce gentle removal of the substrates surface. The samples were cut to the same size as a contact lens with a no 10 cork borer and thickness of 0.1 mm. A thin groove was impressed on the samples' surface. The samples were then individually subjected to either a microwave or varying conditions in a plasma reactor. SEM of the samples were then run to ascertain whether the sample underwent physical damage within the plasma chamber or microwave, the results are depicted in Figure 5.10.

From the pictures in Figure 5.10 it can be seen that a 10 minute exposure of a polyurethane sample produced sample flow, whereas for the 30 minute etched sample, the sample seemed physically undisturbed. For sustained etching of 2 hours there was signs of flow as sections of the material started to merge together, but not to the same extent as the microwaved sample. Therefore temperatures at the sample stage within the plasma don't seem to exceed 78 °C, for short periods of etching. After 2 hours of continuous etching, the sample starts to warm from plasma species bombardment. Therefore in the case of biological samples etching should be carried out for limited periods to maintain a 'cool' plasma. Or substrate cooling is could be used to protect the sample during etching against thermal deterioration and flow. Substrate cooling can also give consistent etch rates during etching since the sample can be kept at a constant temperature. But in this case, it was considered not necessary, as the sample temperatures did not seem to rise above 78°C, as there was no visible flow within the low Tg value.

5.4.9 Conclusion

It was possible to produce a stable system, with operating conditions that were not detrimental to the biological samples under inspection. Operating at these conditions did not raise the sample temperature above 78°C for a 30 minute etch. The activity level of

lysozyme did not fall below 90% and electrophoresis did not yield any data on fragmented particles produced during plasma bombardment.

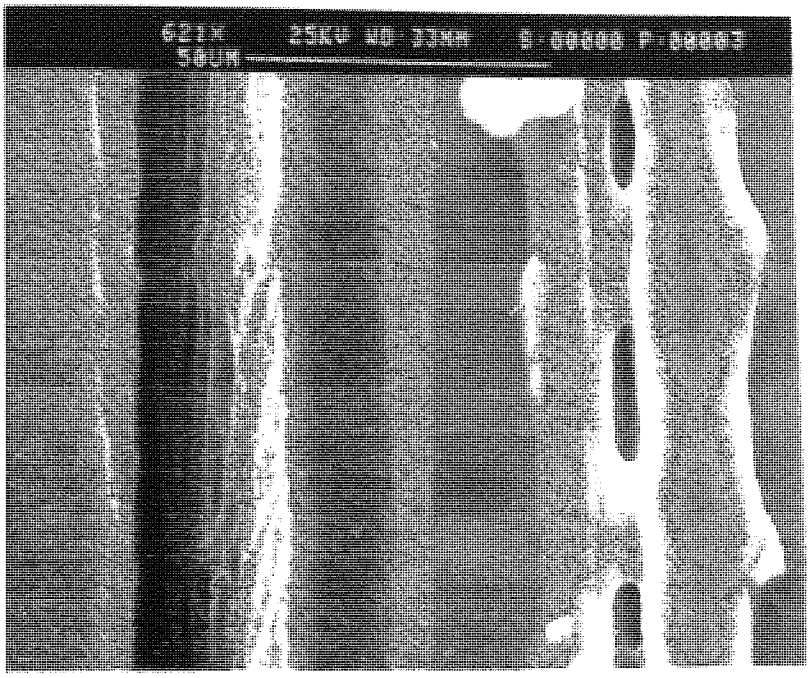

(a) (c)

(b)

Figure 5.10: SEM of Polyurethane samples (a) untreated, (b) 30 minute etched sample and (c) 10 minute microwave treated sample.

It is important to keep such plasma controls as a consistent as possible as damage may occur if extreme conditions are employed. Although dehydration causes protein reduction in activity the system has to be under vacuum. The next chapter will discuss various calculations undertaken to assess protein penetration levels, from *in vitro* and *in vivo* data obtained by PEEMS.

5.5 Key Points

- The etch rates for the systems were proven to be more suitable for an air and oxygen, but not Argon. Oxygen gave a very rapid etch system whereas Argon was more subdued, the intermediate etch system of air was chosen, as submicron levels could be removed within a workable time span.

- To assess the efficacy of PEEMS as a system to monitor biological deposition a number of experiments were run to see the effect of drying systems, excitation frequency of the generator and temperature on the substrate and spoilants. From the stained electrophoretic gels produced and under densitometry measurements, there were no detectable levels of low molecular weight peptides. Concluding that within the detection limits of the experiment PEEMS is not an "aggressive technique" using the standard operating procedure.

- A successful, reproducible operating system was obtainable by working through a series of designed experiments to ascertain the optimum settings.

- Intrinsically the microforce balance proved to be an effective way to monitor deposition, but unfortunately, the OES was a more difficult system to acquire meaningful results from. From the initial design the chamber volume proved to be too large for the sample size under investigation.

- In conjunction with the microforce system two extrinsic techniques proved to be adequate in providing information about location and deposition species. These techniques were fluorescence spectroscopy and ultra-violet spectroscopy.

- An initial view of the data suggests that very high protein concentrations arise in thin layers close to the polymer surfaces.

Chapter 6

Experimental and Commercially Available Biomaterials

6.1 Introduction

A biomaterial is a suitable material, designed to fulfil a role within a physiological environment, without insult. It repairs, restores and replaces damaged or diseased tissue. There are large arrays of polymer materials devised for this use, but with varying success rates. Rejection may be manifested in many ways depending on the biological environment of the implanted material. For example, a material rejected at a blood interface may cause thrombosis in a patient, whilst an inadequate contact lens material may promote tear protein and lipid deposition that will impair the quality of the lens and also give discomfort to the wearer. An ideal vascular graft material should remain smooth with no build up of biological material on the interior surface while for synthetic articular cartilage tissue growth into the implant would be encouraged. Biocompatability is primarily concerned with the physiochemical interactions that occur between materials and body fluids and the physiological responses to these materials. The chemical interactions that occur between the biomaterial and its working environment are dominated by initial events at a molecular level at the interface, as discussed in Chapter 7. The studies detailed below look at three classes of polymeric materials, hydrogels (HEMA copolymers) in Section 6.2-6.4, polyurethanes (poly ethyleneglycol (PEG) copolymers) in Section 6.5 and a terpolymer system discussed in Section 6.6 comprising of HEMA:PEG:MAA

6.2 HEMA Co-polymers

The versatility of hydrogel polymers[183] and their numerous potential applications in the field of biomedicine stems from the extensive range of hydrophilic monomers available (Table 1.3) for their formation and from the ability to control the extent and nature of water binding within the polymer matrix. The most commonly used monomer is undoubtedly 2-hyroxyethylmethacrylate (HEMA). The polymer poly (HEMA), has a number of limitations when used as a biomaterial; even when highly crosslinked the poly (HEMA) matrix has relatively poor mechanical properties restricting their usage. There is also the additional problem of bioincompatability.

This is illustrated in HEMA's use as a soft contact lens material, where even though it is found to be mechanically adequate, ocular incompatibility ('spoilation') is observed leading ultimately to the formation of 'white spot deposits' on the lens surface (Table 2.6).

Despite these disadvantages, poly(HEMA) is still the most commonly used material for contact lenses. In the ocular environment[2] poly(HEMA) has the advantage of a high oxygen permeability coefficient of 145 * 10^{-10}cc (STP) $mmcm^{-2}s^{-1}$ $cmHg^{-1}$ related to its adequate water content of 39% , at 34°C. Additional advantageous points for these hydrogels have been raised in Section 2.2, assessing their high degree of tolerability in the body. As our technology improves, it provides further scope for the extended life-cycle of a biomaterial.

This first section of work (Section 6.3) describes the *in vitro* surface deposition of individual proteins onto different lens materials. The materials have been used to study the effect of hydrogel structure on the nature and quantity of protein absorbed into the lens matrix. In Section 6.4 we look at the 'competitive' *in vivo* environment and the effect of polymer composition.

6.3 Polymer Composition - *in vitro* study

6.3.1 Materials

The major tear proteins, lysozyme, lactoferrin and albumin were used (Table 6.2) to spoil representative contact lenses from FDA Groups I and IV (non-ionic and ionic polymers respectively) for comparative studies between different lens materials (Table 6.1).

Properties	SeeQuence	Acuvue
EWC (%)	38	58
Monomers	HEMA	HEMA & MAA
USAN	Polymacon	Etafilcon A
FDA Classification	Group I	Group IV
ACLM Category	Filcon 1a	Filcon 1b
Manufacturing	Spun-cast	Wet Moulded

Table 6.1: The Characteristics of Commercially Available Group I and IV Contact Lenses Used In Study

Protein	Ellipsoid Dimensions (Å)	Molecular Weight (kD)
Lysozyme	45 * 30 * 30	14
Lactoferrin	55 * 42 * 42	78
Bovine Serum Albumin	140 * 38 * 38	86
IgG	235 * 44 * 44	160
Fibrinogen	450 * 90 * 90	400

Table 6.2: Structural Parameters of Proteins[190-196]

6.3.2 Method

The lenses were soaked individually in 3.0ml of 0.2mg/ml solutions of each protein at room temperature (15 $\pm$ 2 ^{o}C). They were constantly shaken on a low speed shaker for 24 hours. The deposited lenses were then rinsed with distilled water and the quantity of protein deposited was measured using UV spectrometry, and calculated against a reference material- an unworn lens of the same type and optical power.

6.3.3 Results and Discussion

Figure 6.1 shows graphically the absorption levels of each material type with different protein types. Figure 6.2 shows the rate of deposition of each protein.

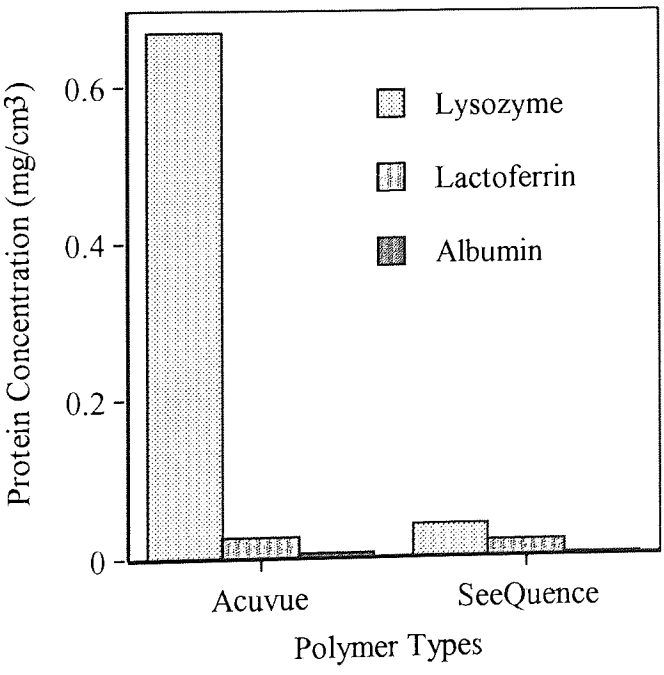

Figure 6.1: The Effect of Lens Material on the Deposition of the Major Tear Components

From the data obtained above it can be seen that material composition and type of protein have an effect on material absorption. This may be expected as it is the outermost surface atoms of a membrane (or implant) material that directly interface with the surrounding media. The absorption follows a pattern, where Group I materials (low water content, non-ionic) have a lower absorbance for all the proteins studied, compared to Group IV materials (high water content, ionic) (Figure 6.2). The trend with both material types is that a small, highly charged molecule, lysozyme, has a higher degree of attraction than (Figure 7.5(c) and Table 6.2), lactoferrin and then albumin.

Compared to lysozyme, lactoferrin is molecularly five times larger, with a lower charge distribution, and albumin is a magnitude larger than lysozyme with a smaller, negative charge density (Table 5.6 and 6.2).

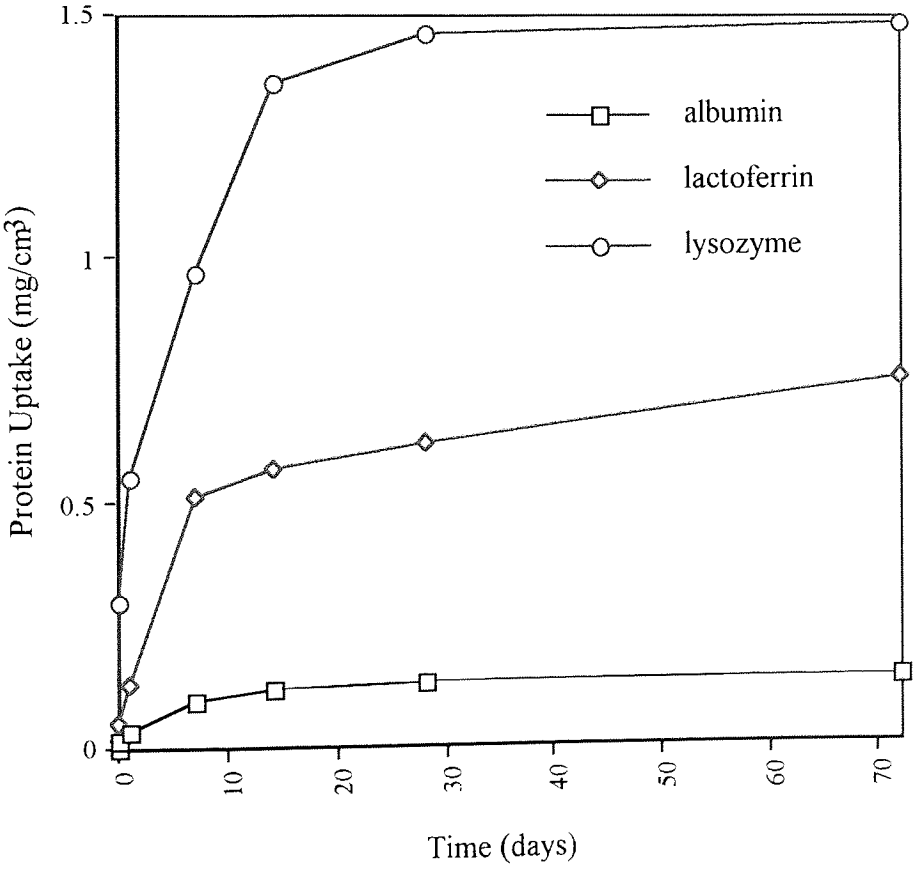

Figure 6.2: The Effect of Size and Charge of the Major Tear Proteins on Uptake by a Group IV *in vitro* Spoilt Lens Material

6.3.4 Assessment of Protein Penetration

The samples from the above study were then plasma etched according to the procedure stated in Chapter 5. Initial concentration readings were taken using UV spectroscopy and samples were etched for 30 minute intervals until there was no detectable levels of protein by UV spectroscopy (50μg) measured on the Hitachi Spectrofluorimeter (Figure 6.3). An average penetration profile was drawn for Residual protein concentration after each stage versus the number of etches (Figure 6.3).

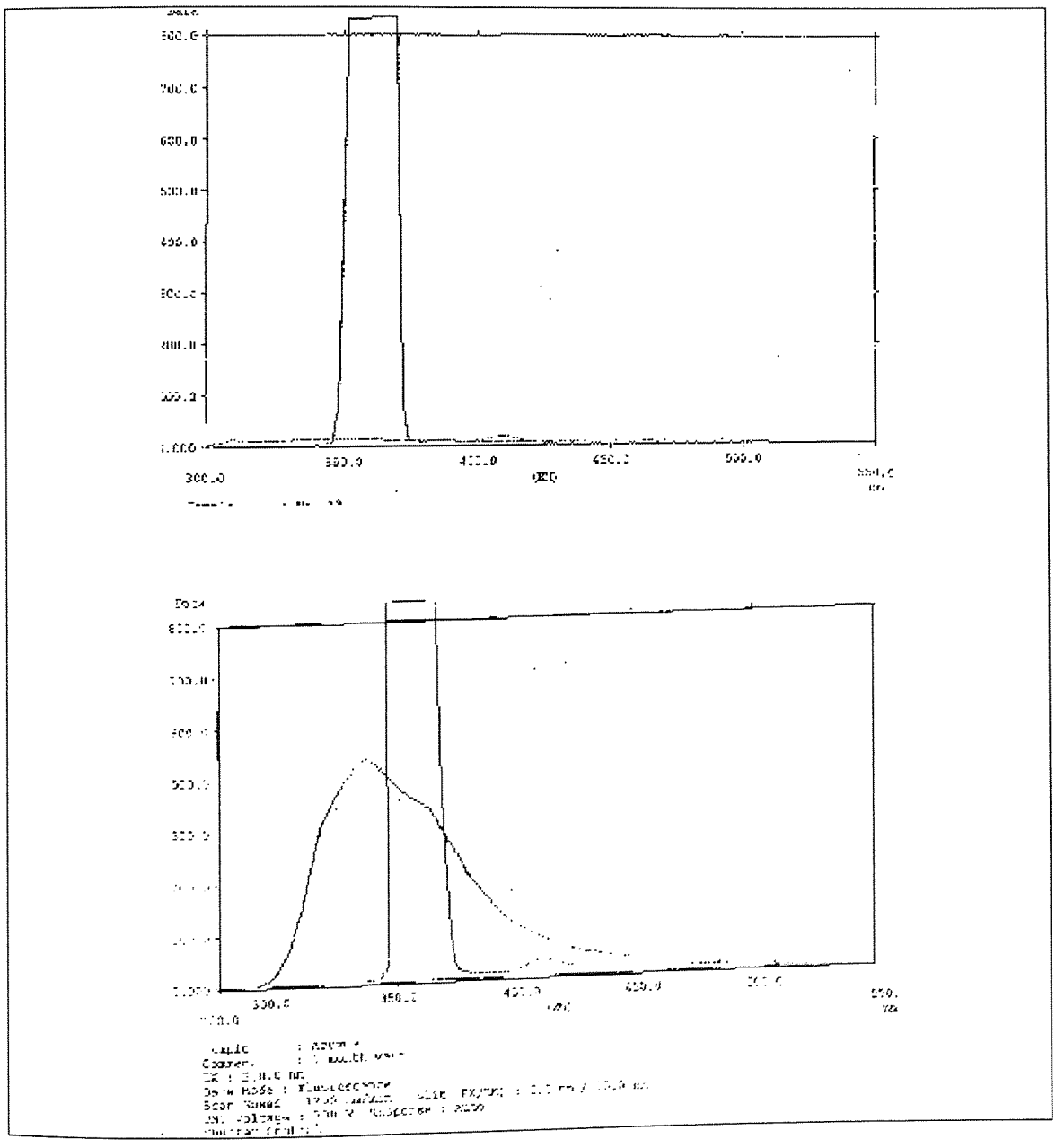

Figure 6.3: Detectable Limits for Protein Using the Hitachi Spectofluorimeter

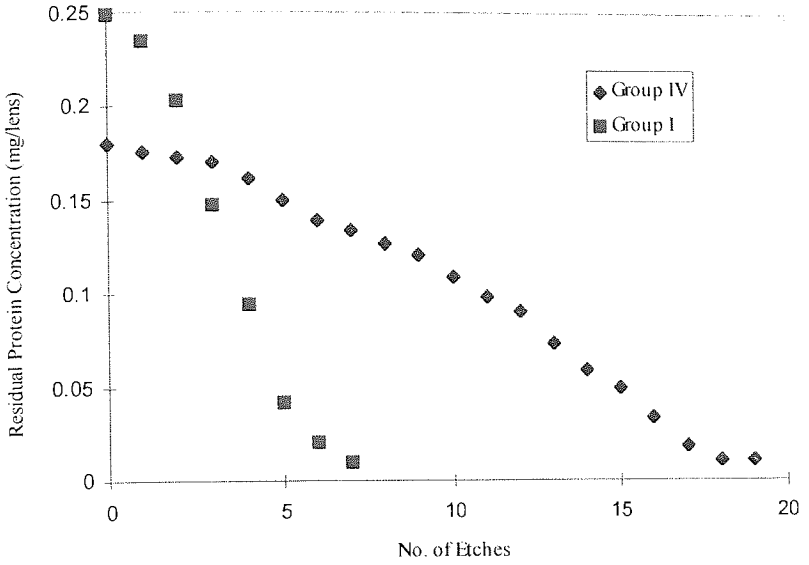

Figure 6.4: Lysozyme Removal by Sequential Plasma Etching for FDA Group IV (Acuvue) and Group I (SeeQuence) *in vitro* Spoilt Contact Lenses

From Figure 6.4 we can see the removal of subsequent layers from the lens (exterior surface to bulk matrix) in unison. There is a progressive removal of protein as we etch deeper into the surface. This plot is an average between five similarly spoilt - etched lenses. The removal of protein for a Group I material is more rapid when compared to that of a Group IV material. The total removal of protein is 8 etches for the Group I material as compared to 20 for a Group IV material. This rapid reduction in protein levels for Group I materials imply an exposed layer of protein not tightly bound to the substrate, probably only a surface coating of submicrons in depth. During progressive etching after this point the etch rates drastically altered from that of surface borne protein (0.014ug/sec) to that of the bulk polymeric material (0.007ug/sec). Whereas with the Group IV lens material the removal of protein was slower although the concentration of protein present when assessed by UV/visible Spectroscopy was less than that on a Group I lens material. This is probably due to the varying nature of the surfaces and the impenetrable nature of the matrix for lysozyme with Group I materials. The slower more sustained removal of protein from the material shows the depth of penetration which is also supported by the changes in etch rate as steady progression is made through the network. If we now overlay the samples weight loss for the Group IV lenses with each etch as shown in Figure 6.5. There is a distinctive difference in the gradient observed from the graph. The gradient reduces as the number of etches increases, as we probe further into the substrata.

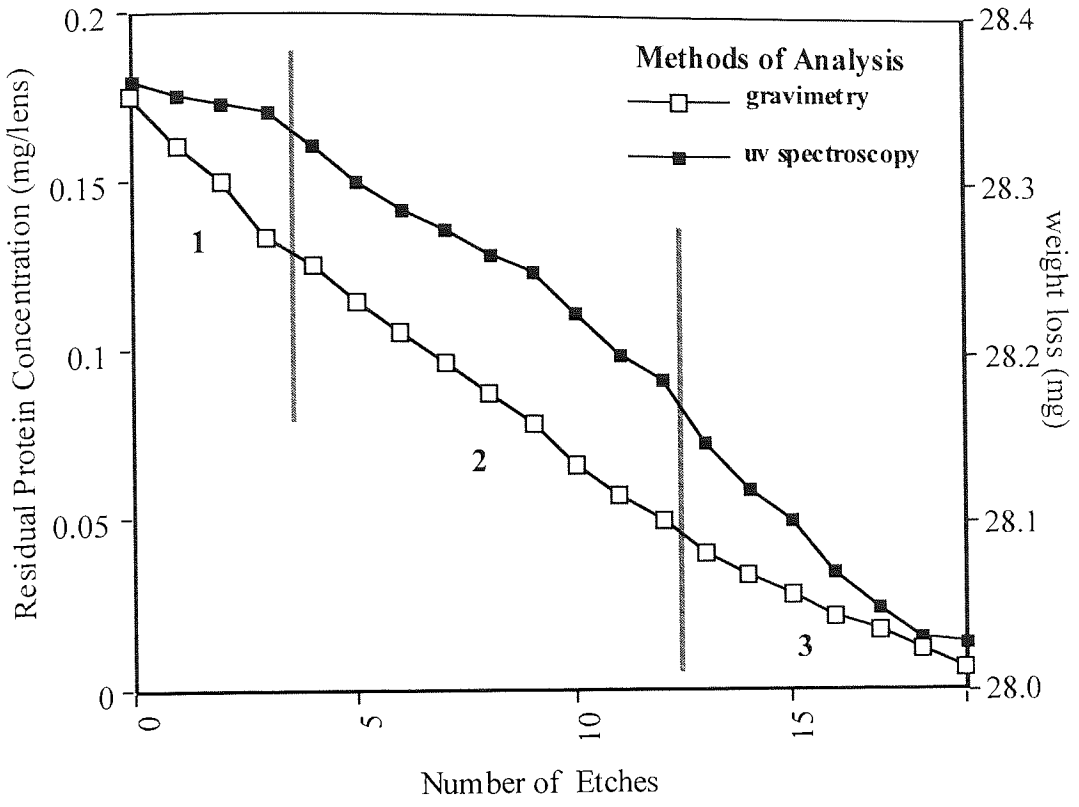

Figure 6.5: Assessment of Lysozyme Deposition on FDA Group IV (Acuvue) *in vitro* Spoilt Contact Lenses

If we now look closer at the removal of protein on a Group IV material we see three distinct regions assessed by their varying etch rates (or gradients). From the weight loss profile in Figure 6.5 there are three distinctive regions: Region 1 has a steeper gradient (~0.014μg/s) compared to Region 2 (~0.0095μg/s) as compared to Region 3 (~0.007μg/s). This possible three strata variation has an indication about the absorption process. Region 1 shows a similar etch rate to that of a spun film of lysozyme, and region 3 has an etch rate of that of a blank Acuvue lens. Region 2 is an intermediate area where the sample is both a mixture of protein and polymer. This is borne out in later *in vivo* experiments, where there are clearer regional variations as the spoilants' constituents become more complex with additional proteins and lipids.

In region 1 and 3 following the train of reasoning as for region 2, the actual depth of penetration of lysozyme is tabulated in Table 6.3. Comparative data for lactoferrin and albumin are also shown in Table 6.3:

Protein	Region 1 (microns)	Region 2 (microns)	Region 3 (microns)
Lysozyme	0.2	2.7	0.02
Lactoferrin	0.1	0.04	-
Albumin	0.07	0.02	-

Table 6.3: Depth of Penetration of Major Tear Proteins for Group IV Materials

From this data it can be seen that most of the lactoferrin and albumin interactions are surface bound, with some protein penetration. If this method is repeated for Group I samples also spoiled in this experiment the protein layer is removed within the first two etches (submicron levels), denoting light surface binding. The greater the negative ionicity of the polymer the greater the positive protein penetration as in the case of lysozyme. Whereas the charge distribution is lower in lactoferrin and albumin is a large positively charged molecule.

6.3.5 Conclusion

From the data generated in this initial experiment, we can see that the proteins we have studied (lysozyme, lactoferrin and albumin) having varying absorption levels depending on polymer composition. An ionic polymer (Group IV) absorbs more protein than a non-ionic polymer (Group I). Absorption is dependent on the charge density and overall type of charge that the protein posses, as this is the potential driving force for absorption. The varying amount of water within the polymer may also have an effect, as the polymer possessing a greater percentage of water, absorbed a greater amount of protein (Group IV). This point will be additionally touched on in Section 6.3.6.

6.3.6 Structure, Charge and Mobility

This investigation was designed to establish the effect of different amounts of MAA and cross-linking agent (EGDM) on protein deposition on polymers membrane. A HEMA copolymer already discussed in Section 6.3, etafilcon A (Acuvue), will be a commercial comparator in this experiment.

6.3.7 Materials and Method

A series of HEMA polymers with increasing weight percent (1-5%) of MAA were polymerised. The copolymers were crosslinked by using 1 and 10% of crosslinking agent (ethylene glycol dimethacrylate (EGDM)).

Reagent Type	Name	Molecular Weight (g)	Abbreviation	Supplier
Monomer	2-hydroxyethyl methacrylate	130	HEMA	Ubichem Ltd.
Monomer	methacrylic acid	86	MAA	Aldrich
Crosslinking Agent	ethylene glycol dimethacrylate	198	EGDM	B. D. H.
Initiator	azo-bis isobutyronitrile	164	AZBN	B. D. H.

Table 6.4: Polymerisation Constituents

Membranes were prepared by the bulk polymerisation of the monomer reaction mixture (Table 6.4) in a membrane mould consisting of two polyethylene gaskets (0.2mm thick, with rectangular hole (6 x 11 cm)) sandwiched between two glass plates (8 x 13 cm). The gaskets were separated from the plates by two sheets of melinex (poly(ethylene terephthalate)) that were present to aid the release of the membrane and give it a smooth finish (Figure 6.6) and the complete assembly held together with clips. The reaction mixture was transferred into the mould cavity via the syringe inserted between the melinex sheets. The monomers were then polymerised at 60°C for three days, followed by two hours post-curing at 90°C. On removal from the oven the clips were removed and the glass plates prized off. The gaskets were removed and the melinex sheets carefully peeled from the membrane which was then placed in distilled water to hydrate. The membranes were allowed to fully hydrate in distilled water with frequent changes of water to remove any water soluble residues.

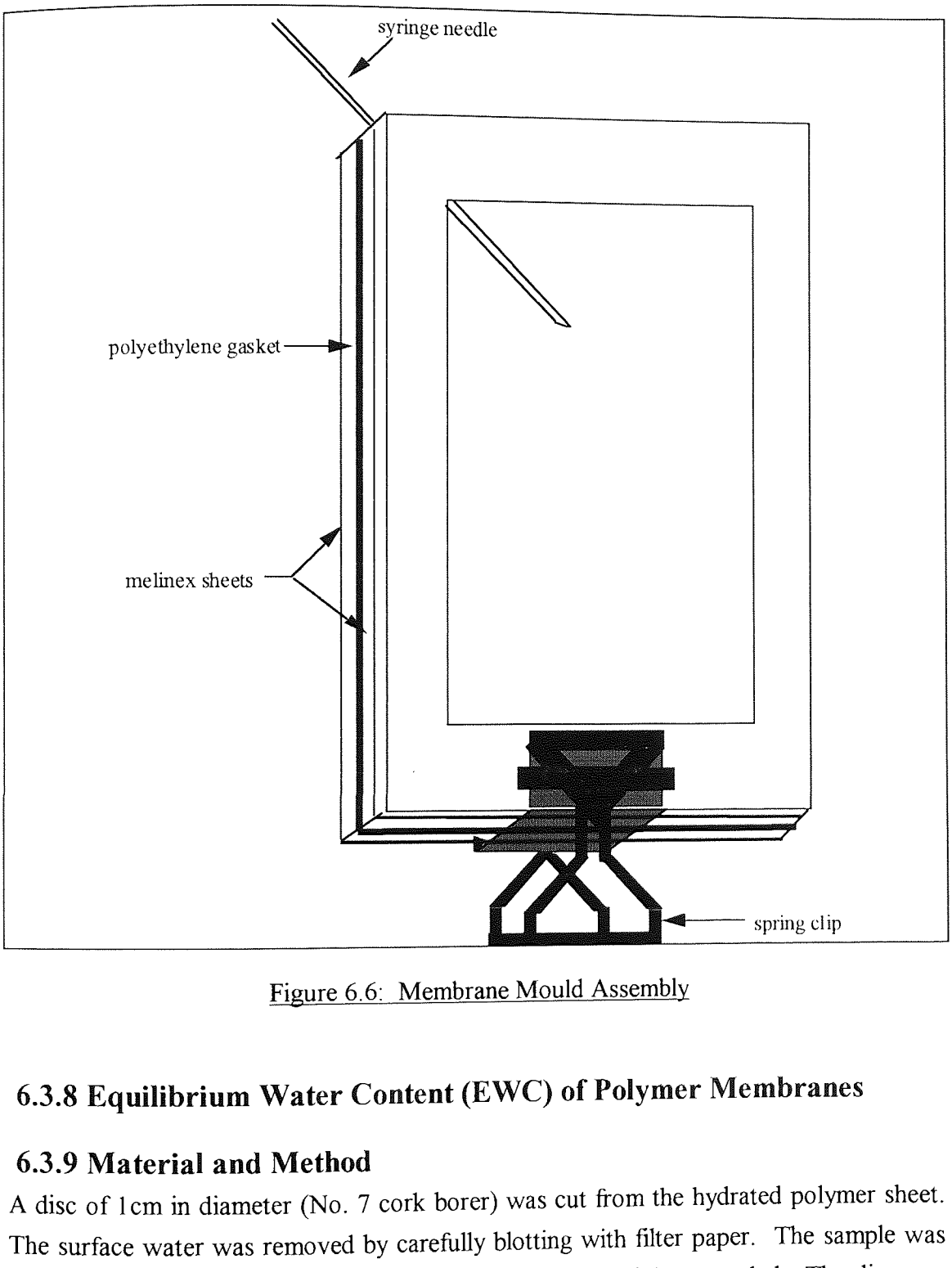

Figure 6.6: Membrane Mould Assembly

6.3.8 Equilibrium Water Content (EWC) of Polymer Membranes

6.3.9 Material and Method

A disc of 1cm in diameter (No. 7 cork borer) was cut from the hydrated polymer sheet. The surface water was removed by carefully blotting with filter paper. The sample was placed in a pre-weighed sample bottle and its hydrated weight, recorded. The disc was dried in a microwave oven for 10 minutes. The Equilibrium Water Content, EWC, was calculated:

$$\% \text{ EWC} = \frac{(\text{hydrated weight - dehydrated weight})}{\text{Hydrated weight}} \times 100 \qquad \text{(Eqn 6.1)}$$

This technique has been extensively used in these laboratories and should provide weights which are correct to within $\pm$ 0.01g. Water content determinations were carried out in triplicate.

6.3.10 Results and Discussion

The quantity of cross-linker used affects the equilibrium water content of the copolymer (Figure 6.7). The equilibrium water contents of the copolymers were comparatively lower in the case of the copolymers produced from 10% cross-linker (18.1- 45.1%) compared to the copolymers produced from 1% cross-linker (33.5 - 67.3%).

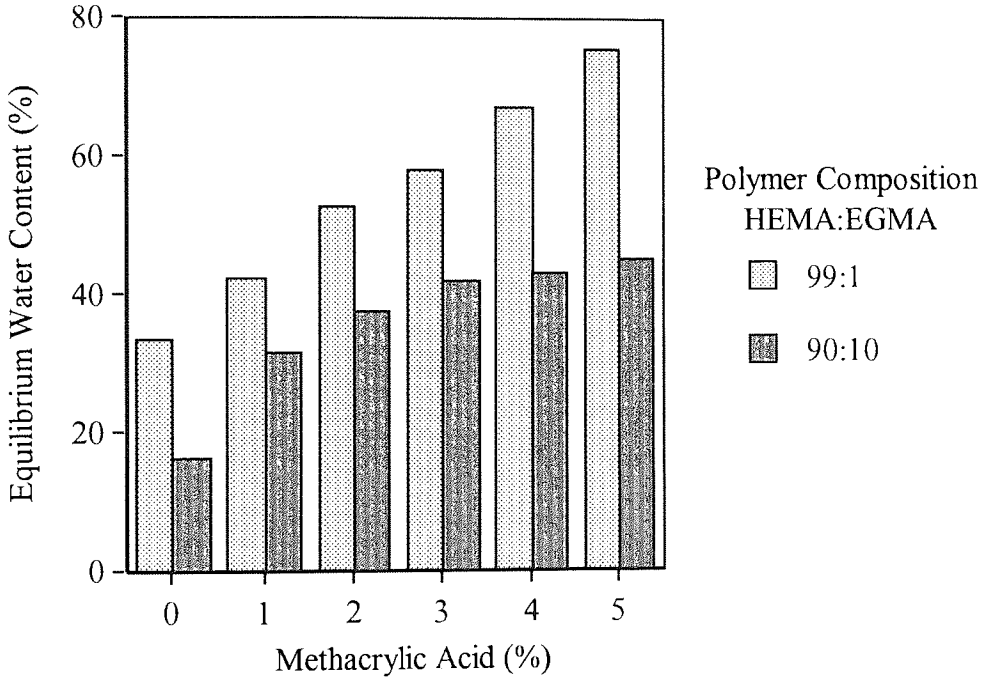

Figure 6.7: Equilibrium Water Content (%) for HEMA Copolymers of Varying Compositions

Methacrylic Acid (%)	99:1 EWC (%)	90:10 EWC (%)
0	33.5	16.1
1	42.2	31.5
2	52.6	37.5
3	57.7	41.8
4	67.1	43
5	75.5	45.1

Table 6.5: Equilibrium Water Content (%) for HEMA Copolymers of Varying Compositions

It can be seen that EWC falls as the proportion of hydrophobic component is increased. Additionally as the proportion of crosslinking agent is increased the spatial components of the polymer restrict inhibiting the proportion of space available for water molecules and the increased rigidity allows minimal room for expansion to accept further packing of water molecules.

6.3.11 Adsorption Studies

A disc of 1cm in diameter (No. 7 cork borer) was cut from the hydrated polymer sheet. They were spoiled at room temperature in 5ml of 0.1mg/ml of individual protein solutions for 24 hours with continual shaking. The quantity of deposited protein was measured by UV spectrometry at 280nm. The absorption of the blanks were measured before the samples were spoiled and values subtracted from the readings for the spoilt samples. The experiment was reproduced in triplicate.

6.3.12 Results and Discussion

The build up of the major tear proteins (lysozyme, lactoferrin and albumin) on the copolymers are shown in Figure 6.8. The graphs show that small, highly charged, compact, lysozyme (Figure 7.10) absorbs very rapidly, especially on the higher percentage MAA polymers. Increasing the proportion of methacrylic acid (1-5%) caused an increase in the concentration of negative charges on the polymer. Comparing the graphs, the reduction in proportion of cross-linker causes an absorption increase for protein with increasing water content (the rigidity of the polymer is reduced). In the case of polymers with 1% cross-linker, the water contents are higher and the amount of lysozyme absorbed is about 2.5 times higher than the lower water content polymers containing 10% cross-linker.

In the case of albumin and lactoferrin, the increase in the absorption of protein with the increase of MAA and water content is less pronounced and the quantities are much lower than lysozyme.

The results obtained lead to the conclusion that in the case of highly positively charged proteins such as lysozyme and lactoferrin, the absorption increases negative surface charge on the polymer increases, due to higher proportions of methacrylic acid.

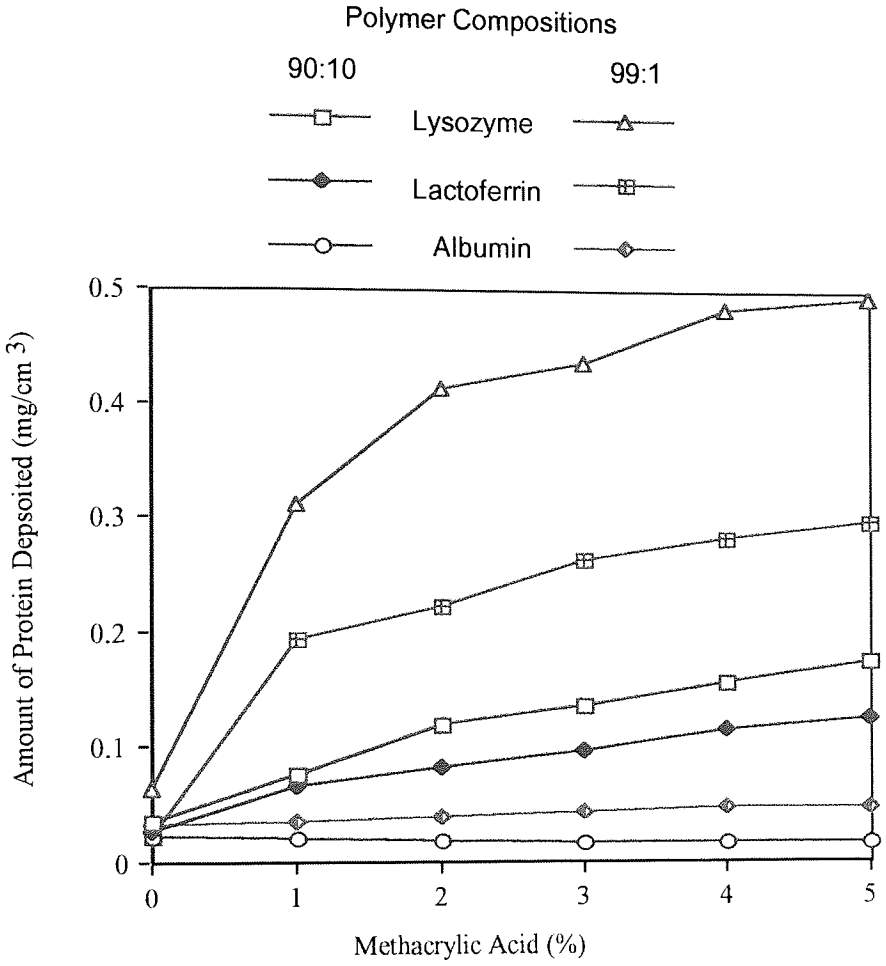

Figure 6.8: The Build-up of the Major Tear Proteins on HEMA Copolymers with Different Proportions of Methacrylic Acid (0% to 5%)

6.3.13 Absorption Studies

Samples produced from the adsorption studies above were then progressively etched, using the method described in Chapter 5. Table 6.6 to Table 6.8 assembles the data obtained, with three typical depth profiles for each protein lysozyme, lactoferrin and albumin.

6.3.14 Discussion

These experiments show the gradual permeation of protein molecules as the percentage of methacrylic acid rises, but as the value of crosslinker is increased comparatively the penetration is reduced due to the rigidity of the system. The increased hydrophobicity of the systems also minimises the driving forces for further penetration.

EGDM / MAA	1%	10%
0%	0.5μ	0.5μ
1%	1.5μ	0.5μ
2%	3μ	0.7μ
3%	4μ	1μ
4%	6.5μ	1.5μ
5%	8μ	2μ

Table 6.6: Comparison of Lysozyme Penetration on HEMA copolymers for Varying Proportions of EGDM and Methacrylic Acid.

EGDM / MAA	1%	10%
0%	< 0.5μ	< 0.5μ
1%	1.μ	0.5μ
2%	2.5μ	0.6μ
3%	3.5μ	0.75μ
4%	4.7μ	1μ
5%	6μ	1μ

Table 6.7: Comparison of Lactoferrin Penetration on HEMA copolymers for Varying Proportions of EGDM and Methacrylic Acid.

EGDM / MAA	1%	10%
0%	< 0.5μ	< 0.5μ
1%	< 0.5μ	< 0.5μ
2%	0.5μ	< 0.5μ
3%	1μ	< 0.5μ
4%	1.5μ	0.5μ
5%	2μ	0.5μ

Table 6.8: Comparison of Albumin Penetration on HEMA copolymers for Varying Proportions of EGDM and Methacrylic Acid.

6.4 Polymer Composition - *in vivo* study

Three materials were studied, supplied by Contact Lens Research Consultants. The supplier classifies the lens wearers as having unstable or stable tear films. An unstable tear film meant that a cohesive tear film could not be sustained for more than 15 seconds. Table 6.9 and Table 6.10, details contact lenses studied and associated wear times.

Trade Name	Principal Monomers	USAN Classification	FDA Classification	EWC (%)
Acuvue	HEMA, MAA (~3.8%)	etafilcon A	IV	58
Focus	HEMA, VP (Graft), MAA (~1%)	vifilcon A	IV	55
Perspective	HEMA, MMA	tetrafilcon A	II	43

Table 6.9: Material Characteristics

Sample Code	FDA Classification	Material Trade Name	Wear Time (days)	TBUT
FAP 1	IV	Acuvue	17	unstable
FAP 2	IV	Acuvue	14	stable
FAP 3	IV	Focus	28	stable
FAP 4	II	Perspective	28	stable
FAP 5	II	Perspective	28	unstable

Table 6.10: Patient Wear Times and Tear Break Up Times

6.4.1 Method

The procedure was run as detailed in Chapter 5. Surface lipid and protein absorption were analysed for proteins and those lipids of aqueous origin (excited at 280nm), and for those lipids produced by the meibomian glands (excited at 360nm). Results are shown and discussed in Sections 6.4.2 and 6.4.3 respectively. Gross protein absorption was also analysed and results are shown in Section 6.4.4 and discussed in Section 6.4.5. Graphically on the x-axis there is a break to signify the inconsistency of the axis, but generally this width signifies approximately 100 microns for all lens. This will vary slightly depending on the manufacturing process undertaken e.g. lathed lenses will be slightly larger and cast moulded lenses are slightly thinner.

6.4.2 Results Obtained From Spectrophotofluorimetry

Figures 6.9 to 6.13 show the penetration profiles for protein and lipid on samples FAP 1-5:

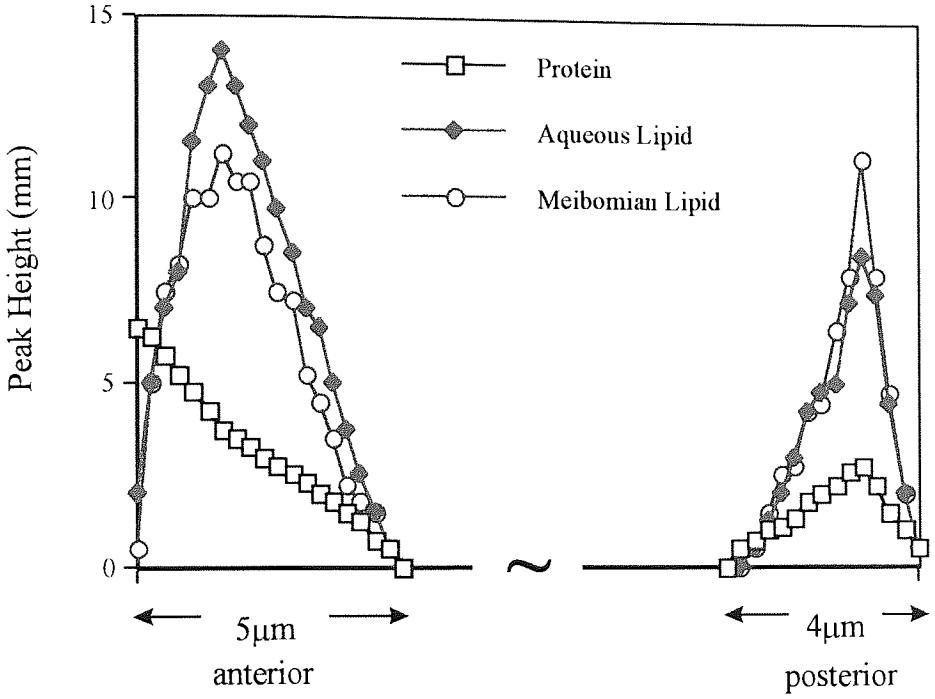

Figure 6.9: Depth of Penetration for Protein and Lipid from Anterior and Posterior Lens Surfaces' for an *in vivo* Spoilt Contact Lens (FAP 1).

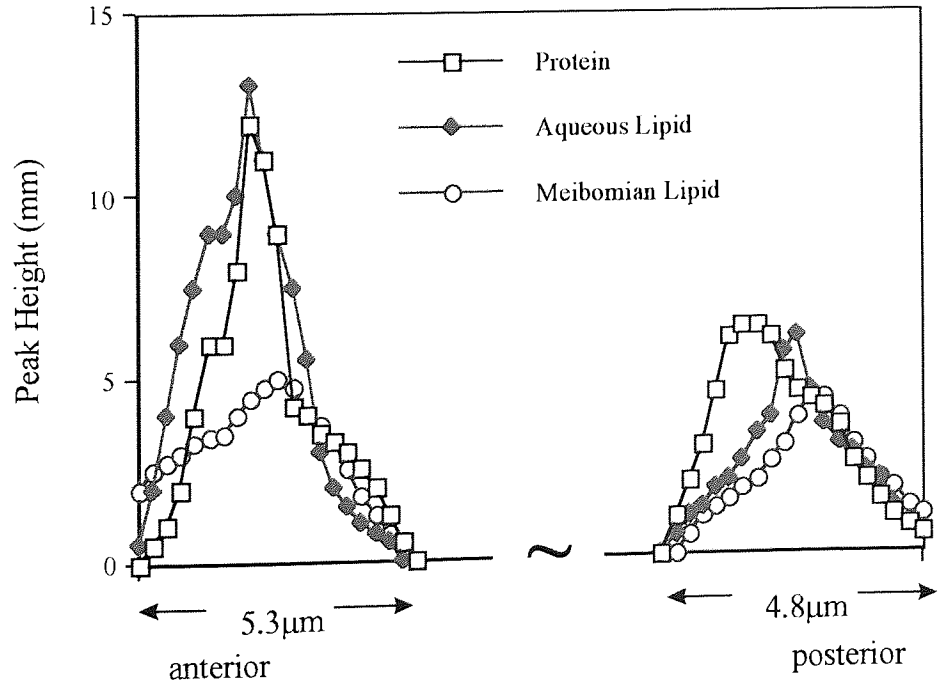

Figure 6.10: Depth of Penetration for Protein and Lipid from Anterior and Posterior Lens Surfaces' for an *in vivo* Spoilt Contact Lens (FAP 2).

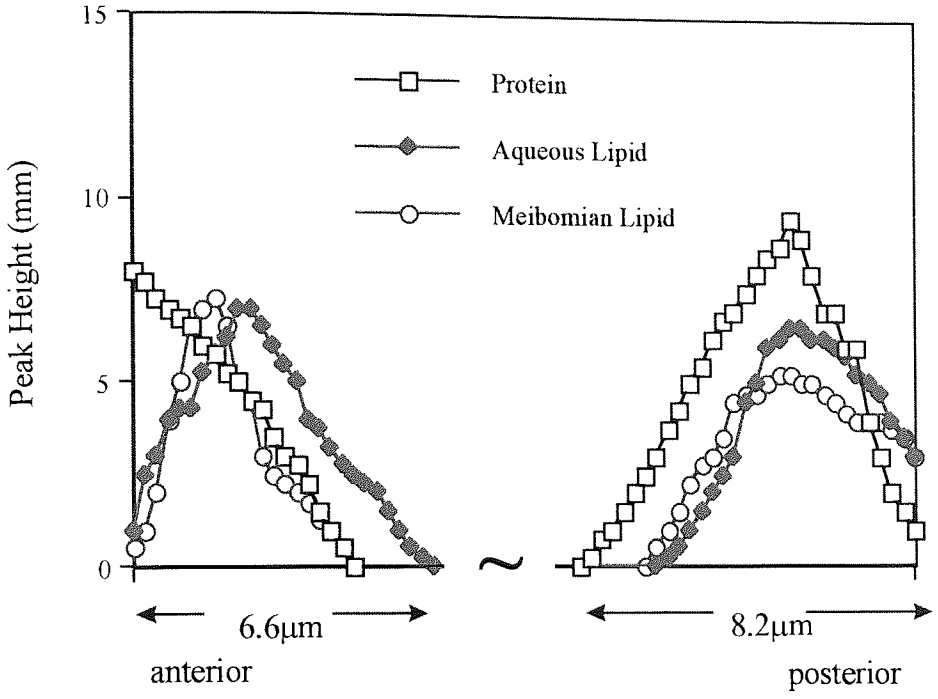

Figure 6.11: Depth of Penetration for Protein and Lipid from Anterior and Posterior Lens Surfaces' for an *in vivo* Spoilt Contact Lens (FAP 3).

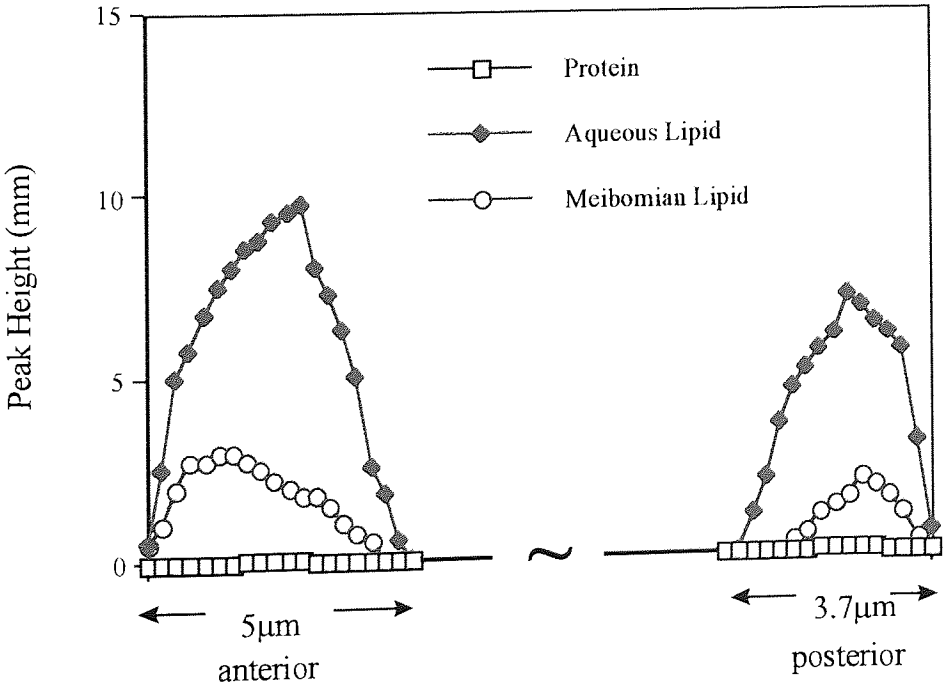

Figure 6.12: Depth of Penetration for Protein and Lipid from Anterior and Posterior Lens Surfaces' for an *in vivo* Spoilt Contact Lens (FAP 4).

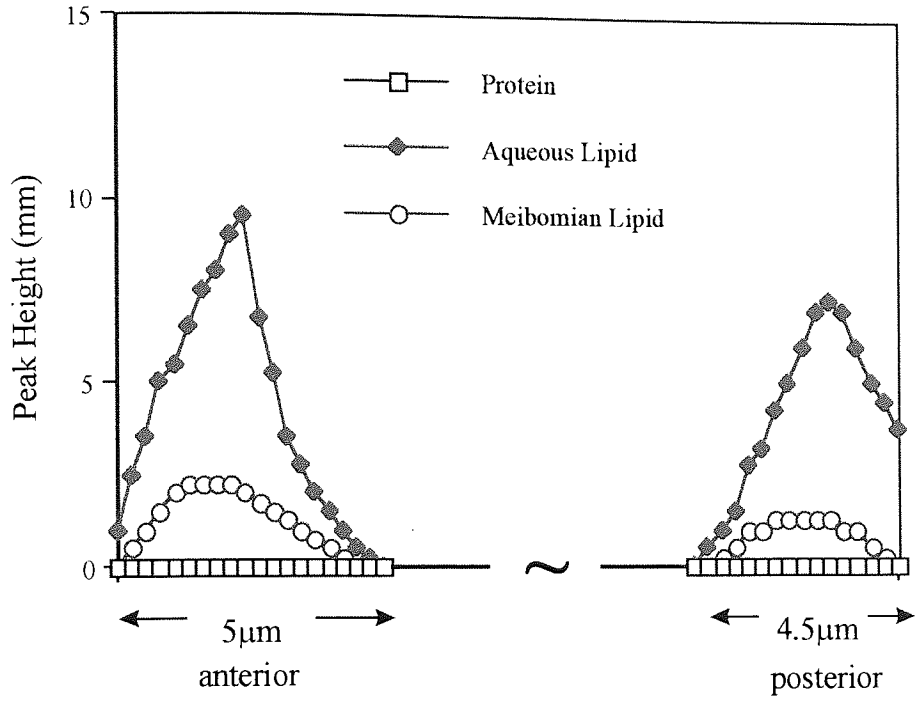

Figure 6.13: Depth of Penetration for Protein and Lipid from Anterior and Posterior Lens Surfaces' for an *in vivo* Spoilt Contact Lens (FAP 5).

6.4.3 Discussion

Figures 6.9-6.13 show that lipid absorption is very similar for Group II and Group IV lenses, with a somewhat greater depth of penetration on the posterior surface than on the anterior surface. The similarity between Group II and Group IV materials is not surprising because of the great similitude of their chemical backbones.

By overlaying the fluorescence spectrum for protein with that of lipid in Figures 6.9-6.13, we see the absence of protein penetration in the Group II lens because of the non-ionic nature of the polymer backbone. These lenses were systematically stored in Renu Multi-purpose solution before analysis. The solution contains a mild surfactant which has reduced the lipid concentration on the lens surface and within immediate surface layers, relative to the bulk. The solutions are retained and analysed for lipid, as they were for protein. This enables a complete picture of the spoilation profile to be assembled. The major reason for the apparently anomalous lipid profile such as cholesterol esters partition, and thus penetrate more effectively into the polymer matrix.

6.4.4 Results Obtained From UV Spectroscopy

Data obtained is graphically represented in Figure 6.14 and penetration depths are tabulated in Table 6.11:

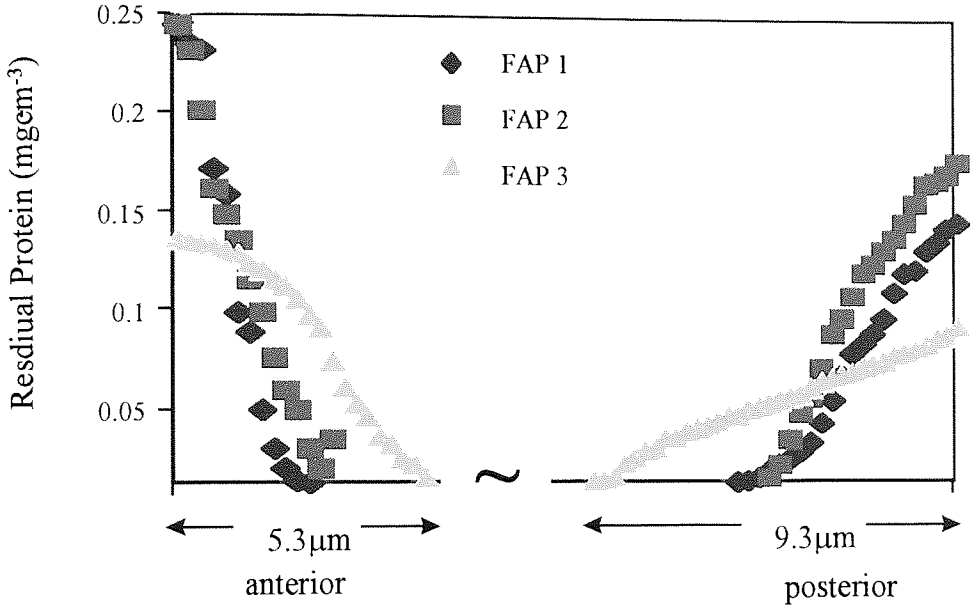

Figure 6.14: A Comparison of the Depth of Penetration of Protein from Anterior and Posterior Lens Surfaces' on *in vivo* Spoilt Contact Lenses

Sample Name	Depth of Penetration (μ)	
	anterior	posterior
FAP 1	4	6
FAP 2	4	6
FAP 3	6	8

Table 6.11: A Comparison of the Depth of Penetration of Protein for both Anterior and Posterior Lens Surfaces' on *in vivo* Spoilt FAP Contact Lenses

6.4.5 Discussion

A study of the two types of group IV lenses showed that the depth penetration in the wear schedules used here equilibrate out for a typical depth of penetration of 6 microns on the posterior surface and 4 microns on the anterior surface (Figure 6.14).

The difference in protein absorption from the two surfaces is probably related to:

(a) tear break-up, which elevates the anterior surface protein concentration in the tear layer through evaporation, and

(b) dehydration, which reduces water content relative to the posterior surface.

On the posterior surface we see the result of a lower, more 'normal', tear protein concentration coupled with little dehydration. As a result the concentration gradient at the posterior surface is lower, but its effectiveness persists further into the matrix. We have studied group IV lenses from several patients in the course of in house work and find this effect consistently.

The protein deposition on Group II lenses was etched away before the lens matrix began to be eroded, illustrating that it is a surface-located protein film.

This initial data yields evidence of a process of adsorption occurring, but can this mechanism be explained by a simple diffusion mechanism or are there other influences to be considered? (Discussed in Chapter 7).

6.4.6 Conclusion

The use of PEEMS technique show a dramatic contrast in the protein location. From these studies it was found that water content of the hydrogel affects most of its potential contamination by protein. Group II lenses have shown an affinity for protein which is greater than Group I, but significantly less than Group IV. However, the non-ionic polymer matrix prevents additional favourable interactions between the protein and the lens.

Lipids in contrast to proteins, are non-water soluble and hydrophobic, and prefer the relatively hydrophobic environment of the polymer, to that of the aqueous tear layer. They therefore partition out of the tear layer into the hydrogel, as if being absorbed by a sponge. Because lipid cannot be measured by UV transmission techniques it is necessary to use surface fluorescence, which gives a useful additional check on the protein profiles.

6.5 Polyurethanes

6.5.1 Introduction

Interest in polyurethanes[108-110] for medical devices stems largely from their excellent mechanical properties, especially their elastomeric behaviour, high tensile strength, low stress relaxation and resistance to long term cyclic flex failure. In addition, their resistance to biodegradation and their blood compatibility have been cited as important factors that have led to their acceptance for use in biomedical devices and implants. These issues will be discussed in more detail below. The medical applications of polyurethanes have been reviewed in a number of collections and articles[1-5].

Many types of polymers have been classified under the generic name 'polyurethane'. The materials of most interest for biomedical applications are segmented block copoly(ether urethanes) (PU's). A general synthetic scheme for these polymers is illustrated in Figure 6.15.

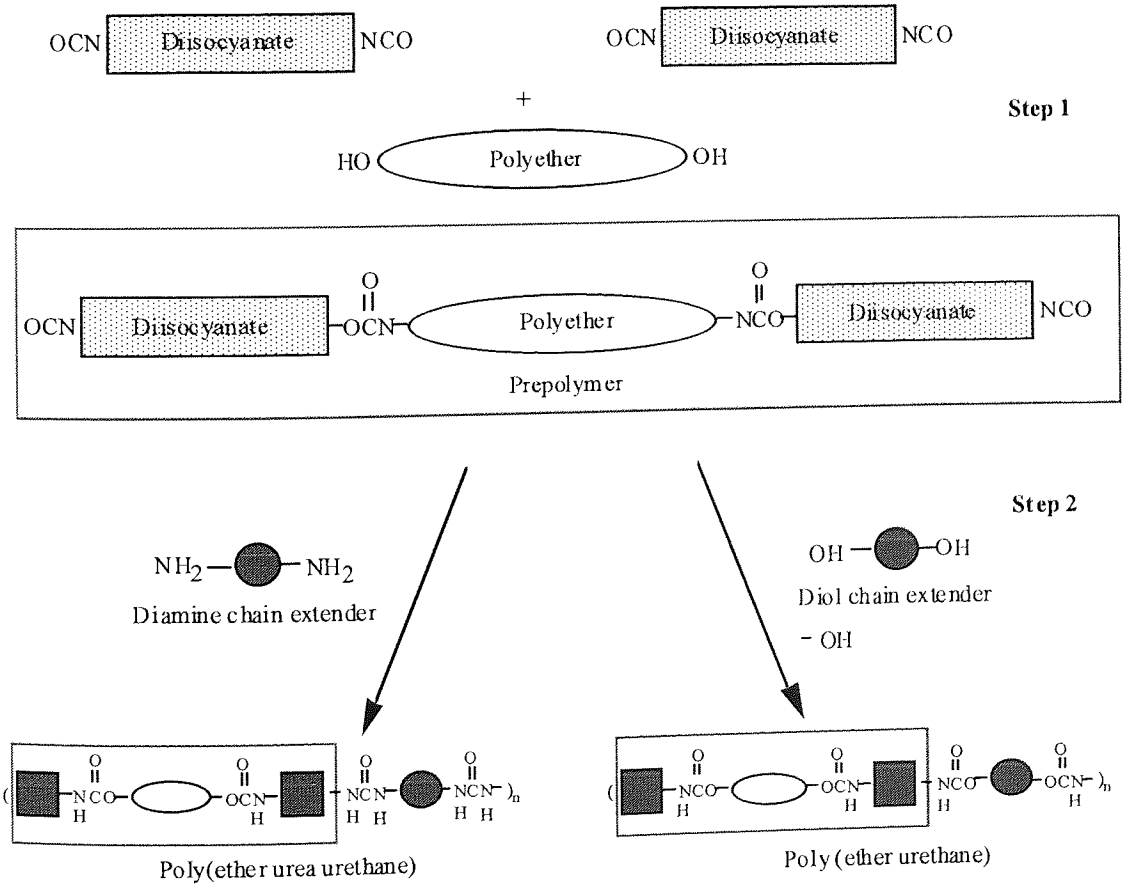

Figure 6.15: A General Synthetic Scheme for the Preparation of Segmented Block Copolyether Urethanes.

A wide range of polymers can be classified as PU's and many have been specifically investigated for medical applications (Table 6.12).

Conventional	Unconventional
MDI:PTMG:ED (Biomer)	MDI:PEG:ED (hydrogel)
MDI:PTMG:BD (Pelletane)	MCHDI:PPG:PEG:BD
HMDI:PTMG:ED (Tecoflex)	MCHDI:PEG:PTMO:BD
MDI:PPG:ED (SRI)	MCHDI:PEG:PPG:BD

(MDI = methylene bisphenyl diisocyanate, MCHDI = 4,4'-methylene-di(cyclohexylisocyanate), PTMG = poly(tetramethylene glycol), PPG = poly(propylene glycol), PEG = poly(ethylene glycol), HMDI = methylene dicyclohexyl diisocyanate, PDMS = poly(dimethyl siloxane), ED = ethylene diamine, BD = butanediol).

Table 6.12: Types of Polyurethanes

The excellent mechanical properties of PU's can be attributed to a phase separation (domain formation) of the polyether component (soft segment) and the urethane component (hard segment). The soft segment contributes to the elastomeric behaviour while the hard segment non-covalently crosslinks the polymer and adds mechanical strength and toughness. Figure 6.16 schematically illustrates this:

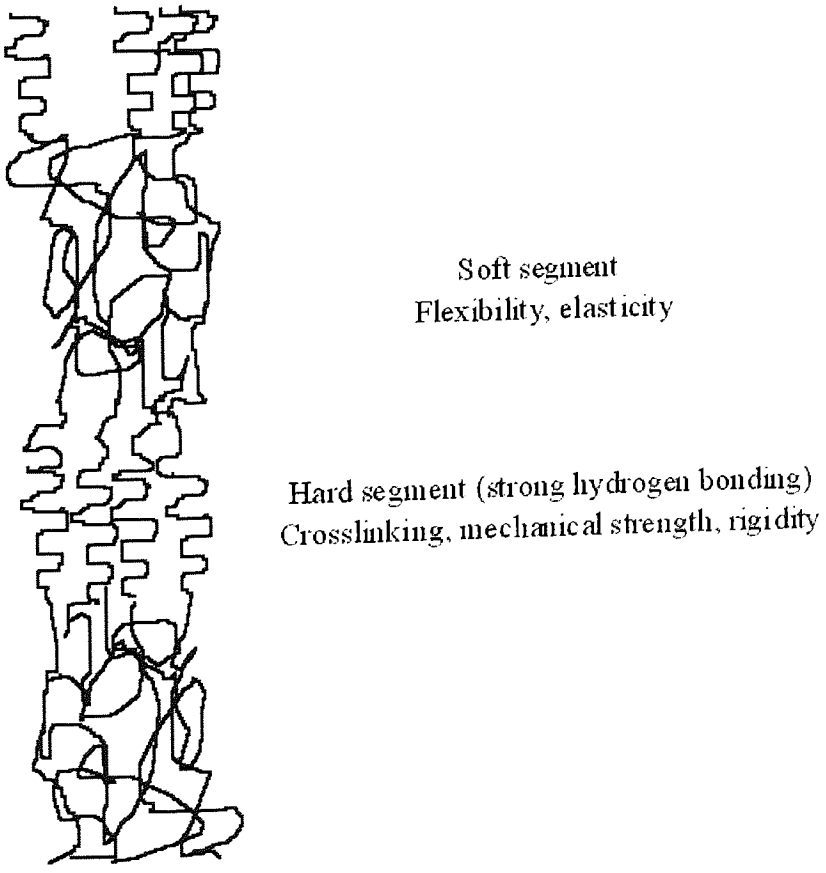

Figure 6.16: The Hard and Soft Segments in Polyurethanes segregate into Domains. The hard Domains Contribute Mechanical Strength and Toughness, while the Soft Domains Result in Elasticity.

Applications of polyurethanes in Medicine
◆ Artificial Hearts
◆ Blood Bags
◆ Catheters
◆ Heart Valves
◆ Pacemaker Leads
◆ Tubing for Blood
◆ Vascular Grafts
◆ Ligament Replacements

Table 6.13: Applications of Polyurethanes in Medicine

The major implant applications of PU's has been in pacemaker leads (Table 6.13). Their use in total artificial hearts and heart assist devices has heightened interest in these polymers. In addition PU's have been proposed for tubular vascular prostheses because of their history in blood contact applications and their compliant nature that can resemble that of the natural blood vessel wall. A number of schemes have been developed for fabricating porous polyurethane vascular prostheses, as summarised in Table 6.14. This table also emphasises the range of options available in processing polyurethanes. In addition to these processing technologies, PU's can, in some cases, be injection moulded or extruded.

Methods of Fabrication of Polyurethanes
◆ Solvent cast
◆ Solvent cast / precipitate in non-solvent
◆ Salt crystal impregnation
◆ Electrostatic spinning
◆ Spin casting

Table 6.14: Fabrication of Polyurethanes Vascular Grafts.

Blood interactions of polyurethanes have received intensive study since the late 1960s. Many studies based upon prolonged of clotting time, platelet adhesion or thrombus accumulation have suggested good blood compatibility for polyurethanes. However, such studies generally do not differentiate between materials that are non-thromobogenic and those that are not only non thrombo-adhesive. Polyurethanes that appear 'blood compatible' in these tests may continuously shed small clots or emboli from their

surfaces, which can lead to significant patient complications. However, studies have demonstrated that PU's containing additives that modify their surface properties can show platelet reactivity, suggesting that blood-compatible PU's can be made.

6.5.2 Materials

Samples were kindly supplied by the Dept. of Organic Chemistry, at the University of Ghent. These samples were jointly tested by a colleague from Ghent and myself.

The aim was to characterise the polymers spoilation characteristics to that of existing polyurethanes. Components used are shown in Table 6.15 and the compositions of the synthesised polyurethanes are shown in Table 6.16:

Reagent Type	Name	Molecular Weight	Abbreviation
Monomer	poly (ethylene glycol)	1000, 2000	PEG
Monomer	poly(tetramethylene oxide)	1000, 2000	PTMO
Monomer	poly (propylene glycol)	1000, 2000	PPG
Diisocyanate	4,4' methylene di(cyclohexylisocyanate)	262	MCHDI
Chain extender	1,4 butanediol	90	BD

Table 6.15: Materials Used in the Synthesis of Polyurethanes

Sample Code (TPU)	Polymer Composition (+ MCHDI + BD)	Mp (°C)	EWC (%)
1a	PEG_{2000}:$PTMO_{2000}$ (1:1)	105	59.8
1b	PEG_{1000}:$PTMO_{2000}$ (1:1)	120	33.1
1c	PEG_{2000}:$PTMO_{1000}$ (1:1)	110	63.7
1d	PEG_{1000}:$PTMO_{2000}$ (1:2)	175	44.7
2a	PEG_{2000}:PPG_{2000} (1:1)	112	67.0
2b	PEG_{2000}:PPG_{2000} (2:1)	129	73.3
2c	PEG_{1000}:PPG_{1000} (1:1)	93	32.9
2d	PEG_{1000}:PPG_{1000} (1:2)	93	27.4
2e	PEG_{1000}:PPG_{1000} (2:1)	93	41.2

Table 6.16: Sample Compositions for Polyurethanes

6.5.3 Processing Method

Approximately 1g of powered samples was placed within a 0.2mm deep Melinex template, and sandwiched between two cellophane sheets. Samples were homogeneously melt processed for two minutes at their respective melting-points under pre-heated metal plates in a Daniel's Press (Table 6.16). They were then pressed under load for three minutes with heat (at their melting point), and then allowed to cool under pressure. The polyurethane films were removed by wetting from the cellophane sheets. Samples were dried under vacuum at 35°C, and cut into 1cm diameter discs using a No.7 cork borer.

6.5.4 Equilibrium Water Content

The underlying role of water is to act as a bridge between the different surface energies of synthetic polymers and body fluids and tissue. The amount of water absorbed is expressed as the equilibrium water content (EWC).

The permeability of the polymers, their mechanical properties, their surface properties, and resultant behaviour at biological interfaces are all a direct consequence of the amount and nature of water held in this way.

From Table 6.16 it is noticeable that for samples from Group TPU1, increasing the ratio proportion of PTMO to PEG increases the water content because of the introduction of longer chain groups (1b and 1d). But the water content has only a marked increase (10%). Actually increasing the proportion of PEG, doubles the water content (1b and 1c), although PEG is only a slightly shorter chain length. Overall, the actual hydrophilic nature of the later case (1b and 1c) has increased, compared to that of the former (1b and 1d), so increasing the amount of imbibed water. A similar trend is also seen with that of samples in Group TPU2. Increasing the proportions of either constituent (2c and 2d) increases the water content, because of increased chain length.

Comparing TPU1 to TPU2, when PPG is introduced into the structure with PEG (instead of PTMO), the water content rises (e.g. 2a (67%) compared to 2b (73.3%). This can be explained by the longer unit of PPG and the pendant methyl group causing steric hindrance within the structure, so reducing packing, and allowing greater swelling.

6.5.5 Adsorption

Because most polyurethanes become opaque in dilute solutions the UV absorbance was measured on dry samples in air at 280nm. The polyurethane discs, were hydrated in distilled water for 24 hours and then dried in a vacuum oven for three hours at a temperature of 35 °C. The samples were then placed in a square reference holder, and the UV/visible absorption was measured against air. The absorbance values obtained were used as the absorbance for the blanks.

6.5.6 Time Experiments

These experiments with lysozyme were carried out to see spoilation as a function of time. The polyurethanes were equilibrated in water for 24 hours before they were put into a 3ml solution of 0.1mg/ml lysozyme. After the respective spoilation time three discs were dabbed with filter paper and dried in a vacuum oven for three hours at a temperature of 35 ^{o}C. The UV absorbance was measured in the same way as described in Chapter 5. The results for three polyurethanes TPU 1b, 2c and 2a, after subtraction of the blanks are shown in Figure 6.17.

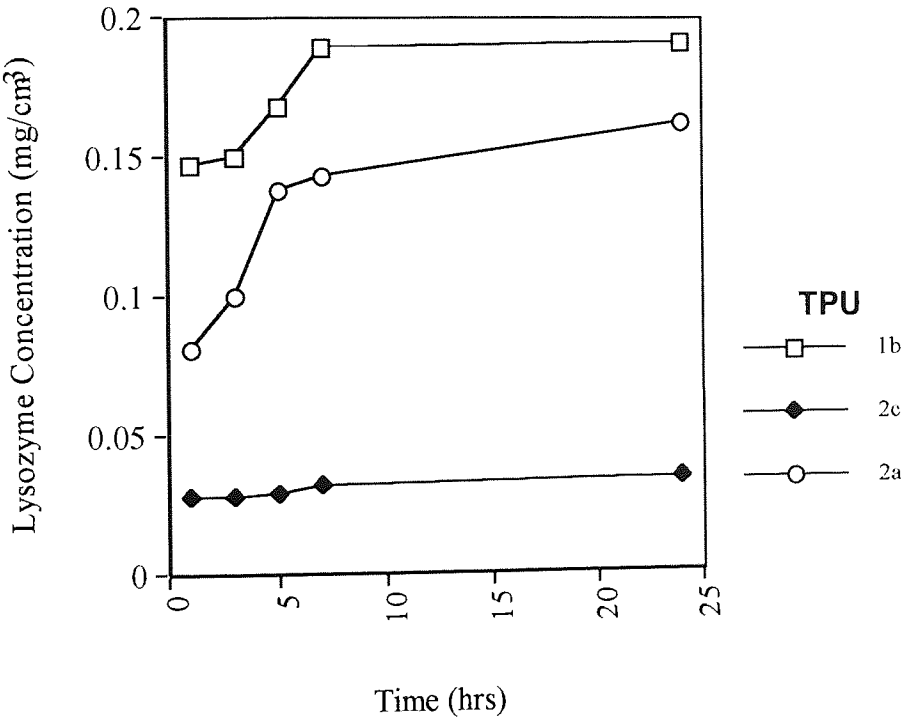

Figure 6.17: Lysozyme Uptake for Three Polyurethanes From TPU1 and TPU2 Groups (PEG:PTMO; TPU 1) and (PEG:PPG; TPU 2).

Figure 6.17 shows the build-up of lysozyme with time on varying polyurethane structures. Polymers TPU 2a and c are PEG:PPG compositions of similar composition but varying molecular weight (2a being 2000 based), whereas 1b is a PEG:PTMO samples. There are variations in protein uptake, with TPU 1b has a greater build up (0.19 mg/cm^3), compared to TPU 2a and 2c (0.15 and 0.04 mg/cm^3, respectively). Comparatively PTMO is highly charged compared to PPG, so causing greater hydrophilic interactions between molecules. Between the PPG samples 2a and c the higher molecular weight sample TPU 2a has reduced protein interaction as the sample is comparatively more hydrophobic in nature, reducing the level of mutual attraction between protein and polymer.

6.5.7 The Influence of Protein Type

Samples were spoiled for 24 hours in 3ml of various tear proteins (0.1mg/ml of lysozyme, lactoferrin or albumin). The data produced is shown graphically in Figure 6.18 and Figure 6.19.

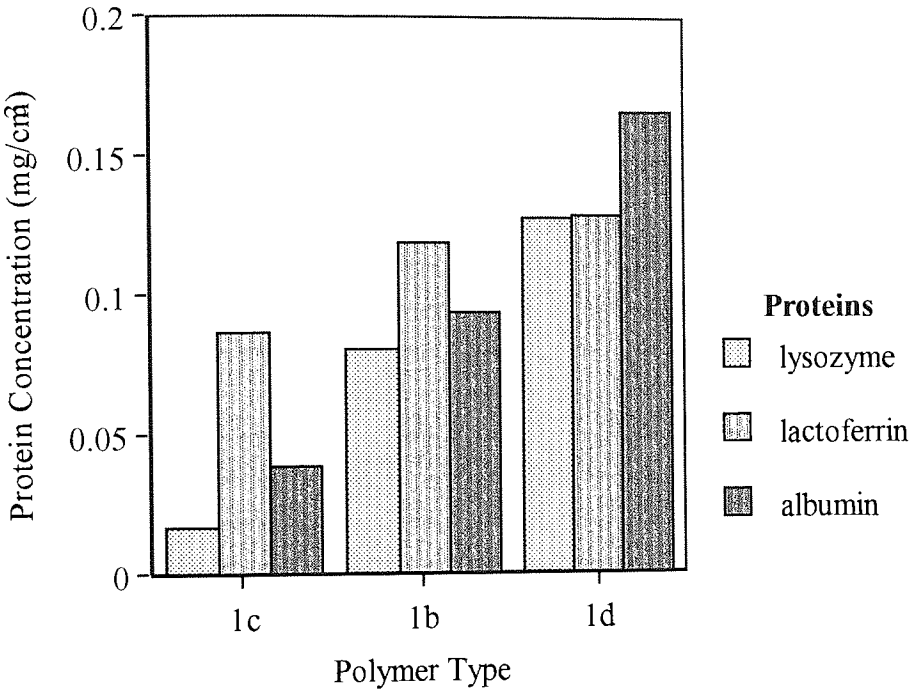

Figure 6.18: Protein Spoilation of TPU 1 Family, Presented in Order of Increasing Molecular Weight for PTMO Ratio

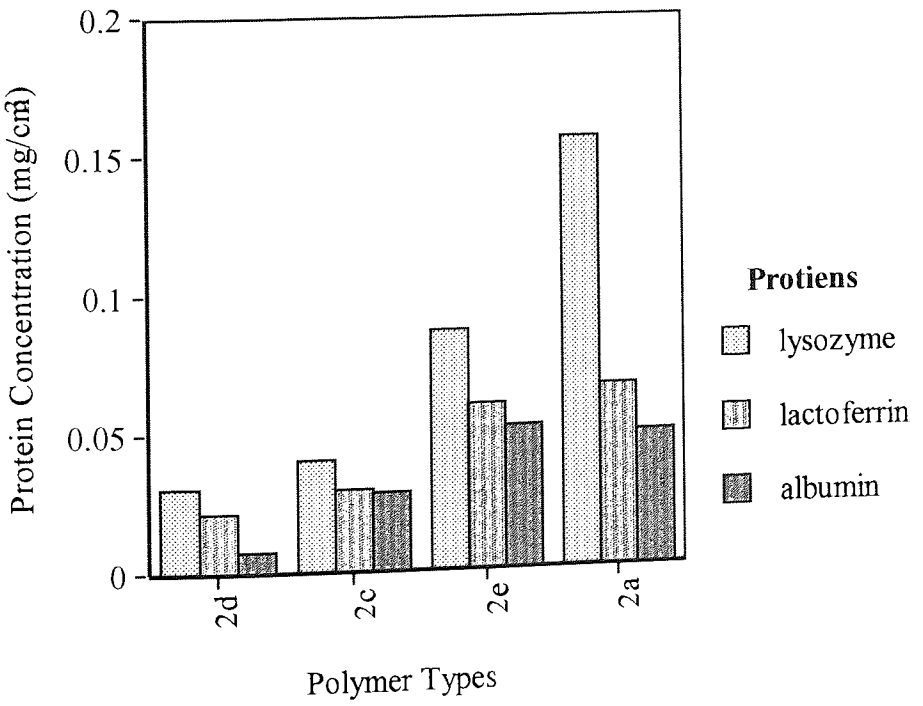

Figure 6.19: Protein Spoilation of TPU 2 Family, Presented in Order of Increasing EWC

By increasing the overall charge of the polymer, there is an increase in the overall protein uptake, shown in Figure 6.18 and Figure 6.19. This is additionally borne out in TPU 2 where the system is highly hydrophobic comparatively to TPU 1, but with increasing water content, there is also a marked protein uptake, because of the increase in hydrophilic interactions. TPU 2 have a similar protein uptake pattern to that of an anionic hydrogel (Section 6.3.3), as there is a greater attraction of lysozyme for the polymer and a continual decrease in attraction for lactoferrin and albumin, suggesting an overall negative charge residing on the polymer. Whereas in TPU 1, the interactions seem more cationic/hydrophobic, with a greater affinity for albumin. This differentiation between the polymer groupings is the amphiphilic nature of the polymers.

6.5.8 Absorption

Samples etched are tabulated in Table 6.17. Chosen on the basis of ease of handling and levels of spoilation. The data generated is assessed on the samples etches rates, as each material has its own unique etch value. Etch rates of unspoiled samples were run first to ascertain the blanks reading.

Sample Code	Polymer Composition	Etch Rate (μg/s)	Mp (°C)	EWC (%)
TPU 2d	PEG_{1000}:PPG_{1000} (1:2)	1.050	93	27
TPU 2a	PEG_{2000}:PPG_{2000} (1:1)	0.597	112	76
TPU 1b	PEG_{1000}:$PTMO_{2000}$ (1:1)	0.363	120	33
TPU 1d	PEG_{2000}:$PTMO_{2000}$ (1:2)	0.061	175	46.5

Table 6.17: Trends in Polyurethane polymer etch rates

From Table 6.17 it can be seen that the etch rate increases with decreasing melting point values, showing that chain scission becomes easier, as bond strengths reduce, because of reduced hydrophilic interactions and increased steric effects.

Samples were spoiled for 24 hours in 3ml of 0.1mg/ml solutions of lysozyme, lactoferrin and albumin. The samples were then vacuum dried in a 35°C oven, and etched for 30 minutes under standard etch parameters.

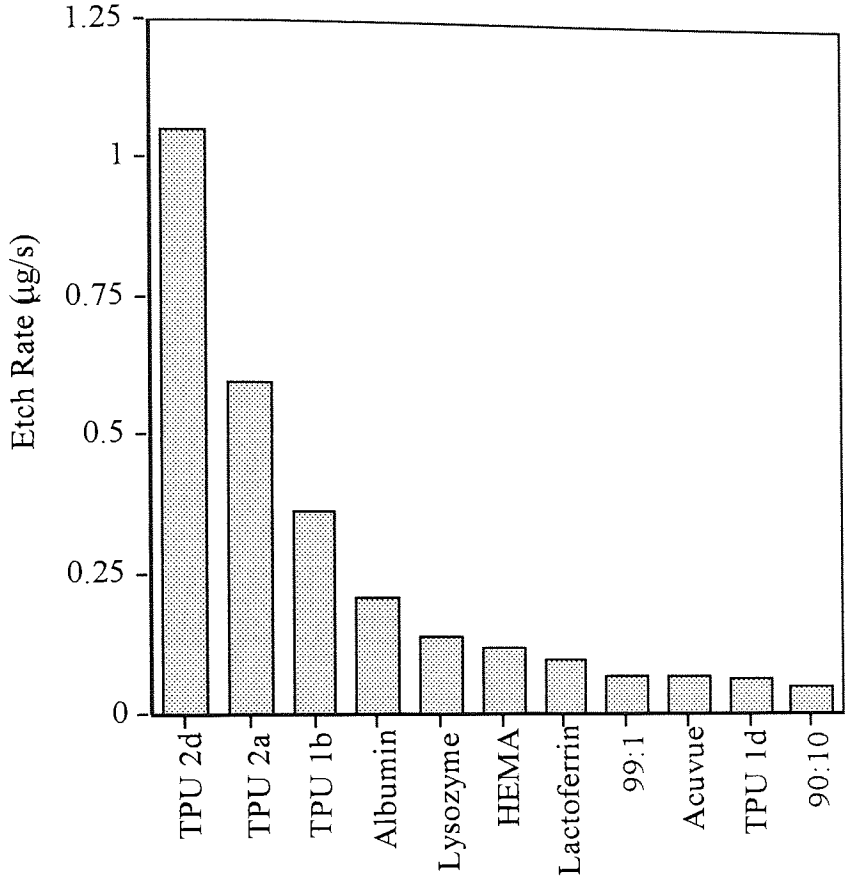

Figure 6.20: Typical Etch Rates for Biomaterials

The original protein levels dropped considerably within the first etch sequence revealing the polymer surface. Figure 6.21, shows the removal of protein within the first 30 minutes (a), and then the increased etch rate in (b) as the polymer is exposed, and is then subsequently etched (c). With some samples, noticeably the TPU 1 group additional etching caused cross-linking occurring on the surface as the sample increased in opaqueness and mass. Mass increase could have been caused by water uptake, but on re-drying, weight loss was not observed, so addition oxidation products must have been formed, that were energetically to heavy to be removed by the plasma parameters employed.

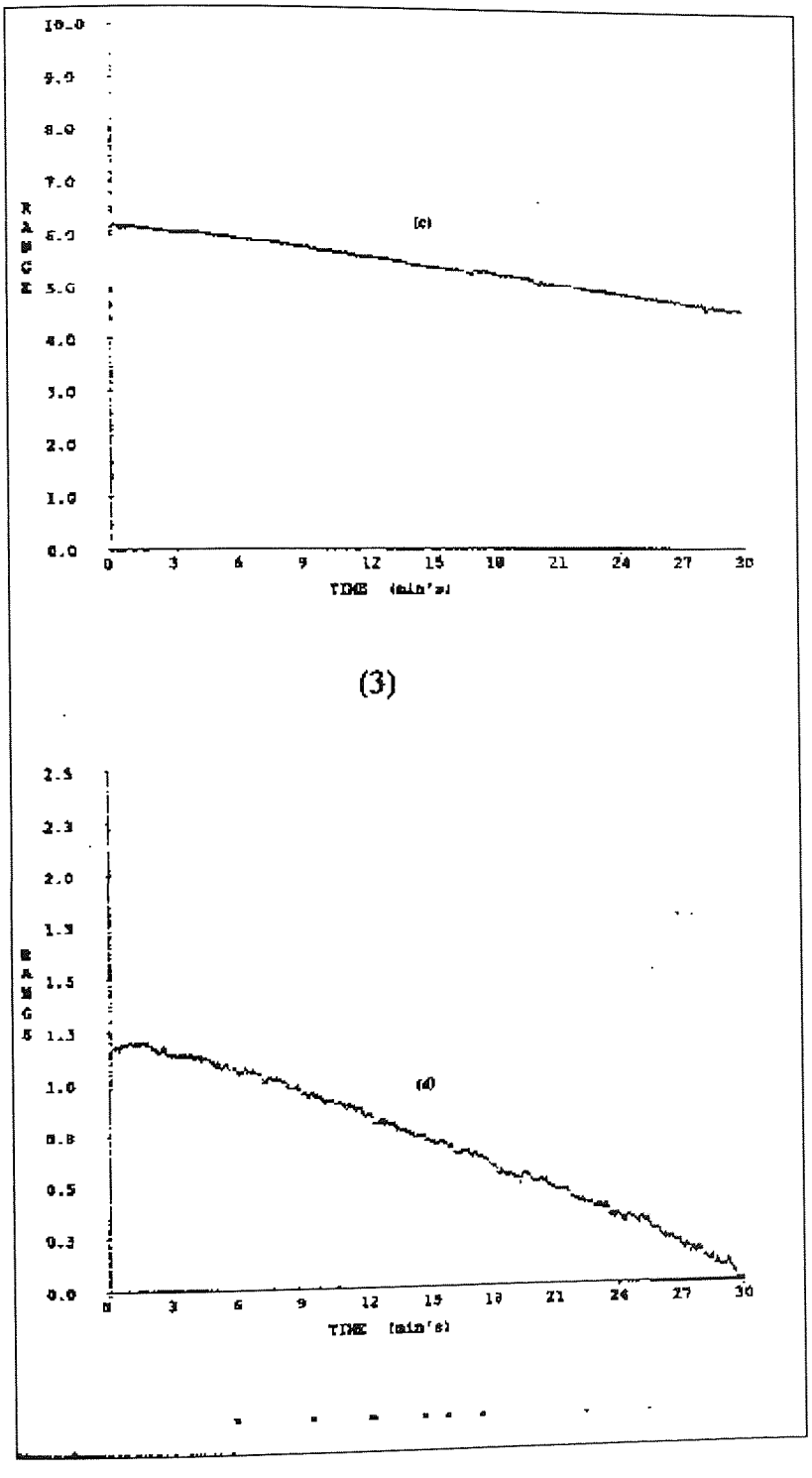

Figure 6.21: Computer Generated Graphs of Weight Loss Against Time for a lactoferrin spoiled sample of TPU 2d: (a) First 30 minute etch removing surface Protein; (b) Second 30 minute Removing Polymer and Protein; (c) Removing Polymer.

6.5.9 Discussion

Polyurethanes show protein adsorption levels to one tenth of that of Group IV materials, with lysozyme and lactoferrin adsorption and limited albumin absorption. There is no protein absorption detectable. PU are impenetrable to protein, and only undergo surface deposition.

The higher the molecular weight of PEG in the PEG:PTMO system, the greater the water content. These affects are due to steric hindrance. The greater the molecular weight of PTMO the greater the protein deposition, due to increased negative charge on the polymer. Additionally, increasing the concentration of PTMO in the copolymer increases the protein adsorption.

The higher the molecular weight of PEG and PPG in the PEG:PPG system the higher the water content, due to steric hindrance. Molecular size did not make a drastic difference in protein deposition for PPG:PEG copolymers, but water content did where an increase in water content saw an increase in lysozyme levels. This is probably due to a more open network caused by steric effects. Increasing the concentration of PEG increased the protein absorption, but increasing the concentration of PPG decreased the protein adsorption.

6.6 Prototype Contact Lens Materials

6.6.1 Materials

A group of materials supplied in the form of lenses which have been used in clinical trials by Contact Lens Research Consultants were studied. They have some protein resistance that is different to that of Group IV contact lens (Acuvue) although exhibits a similar degree of ionicity, but with varying water content. The main polymer constituents of theses materials are HEMA:PEG:MAA. Table 6.18 details the characteristics of the lenses studied.

Material	Ionicity	Water Content (%)
PCLM 13	Ionic	70.5
PCLM 15	Ionic	69.9
PCLM 18	Ionic	68.8
PCLM 25	Non-ionic	64.0
Acuvue	Ionic	58

Table 6.18 : Water Content and Wear Times for PCLM compared to a Typical Group IV Lens (Acuvue)

A series of lenses were selected on the basis of observations in the clinic, that represented relative stable and unstable tear films. In so doing, it was unlikely that within the range of normal tear film behaviour, patterns of spoilation behaviour outside that found with these extremes, would subsequently be encountered. Various lenses were analysed for depth penetration of lipid and protein.

6.6.2 Method

Procedure ran as detailed in Chapter 5. Surface lipid and protein absorption was analysed for proteins and those lipids of aqueous origin (excited at 280 nm), and for those lipids produced by the meibomian glands (excited at 360 nm). Results are shown and discussed in Section 6.6.3 and Section 6.6.4, respectively. Gross protein absorption was also analysed and results are shown in Section 6.6.5 and Section 6.6.6. Graphically on the x-axis there is a break to signify the inconsistency of the axis, but generally this width signifies approximately 100 microns for all lens.

6.6.3 Results Using Spectrophotofluorimetry for Stable Tear Film Production

Material	Depth of Penetration (μ)	
	anterior	posterior
PCLM 13	2.5	2.5
PCLM 15	3	3
PCLM 18	2	2.5
PCLM 25	2.5	2.5
Acuvue	4	6

Table 6.19: A Comparison of the Depth of Penetration of Spoilants for Stable Tear Films from both Anterior and Posterior Lens Surfaces' on *in vivo* Spoilt PCLM and Acuvue Contact Lenses

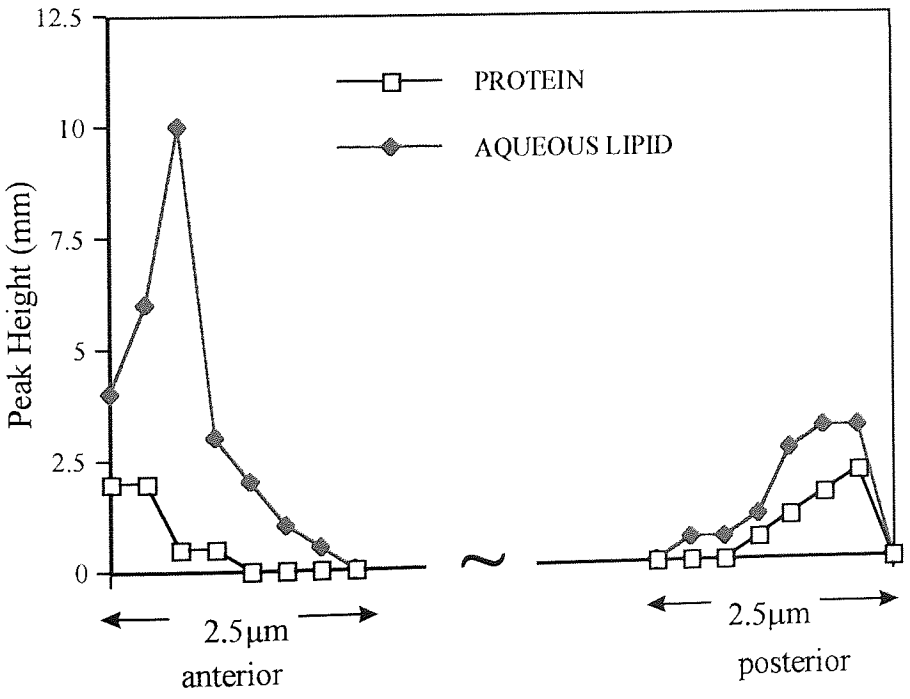

Figure 6.22: Depth of Penetration for Protein and Lipid from a Stable Tear Film for Anterior and Posterior Lens Surfaces' on an *in vivo* Spoilt Contact Lens (PCLM 13).

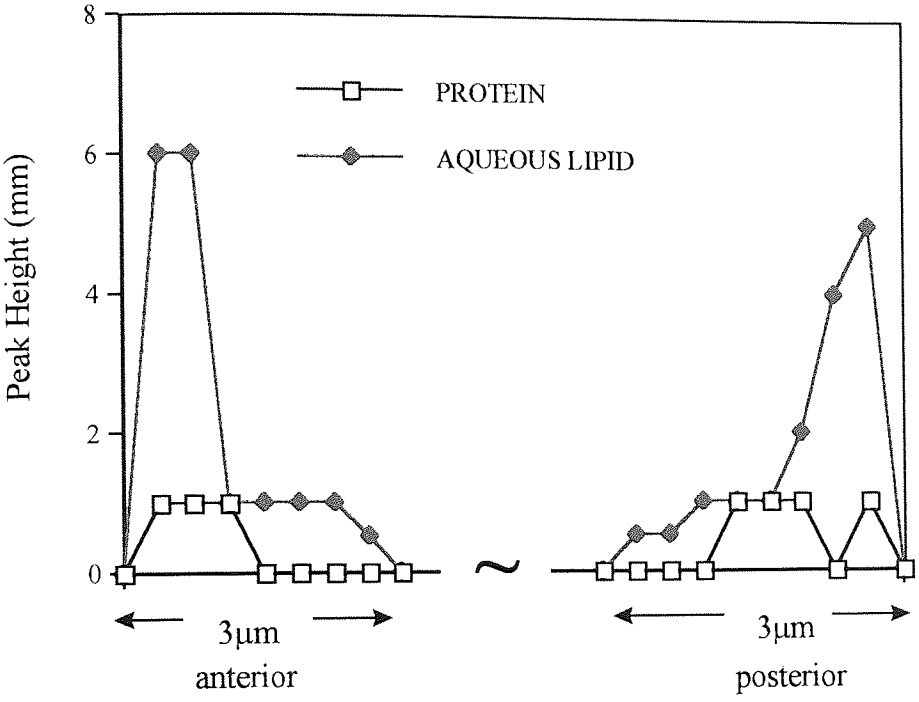

Figure 6.23: Depth of Penetration for Protein and Lipid from a Stable Tear Film for Anterior and Posterior Lens Surfaces' on an *in vivo* Spoilt Contact Lens (PCLM 15).

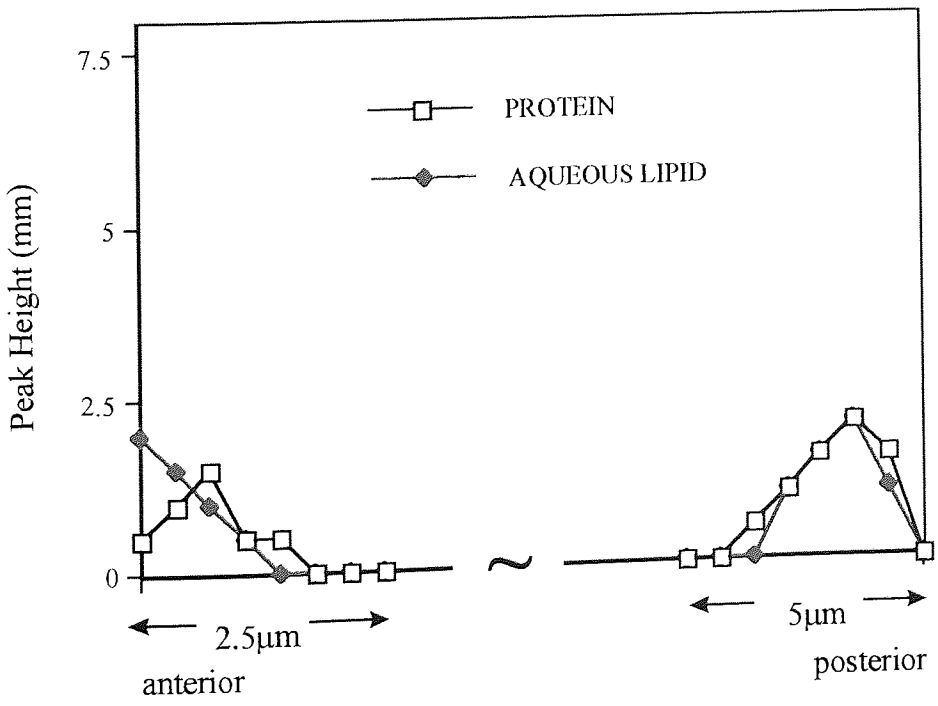

Figure 6.24: Depth of Penetration for Protein and Lipid from a Stable Tear Film for Anterior and Posterior Lens Surfaces' on an *in vivo* Spoilt Contact Lens (PCLM 18).

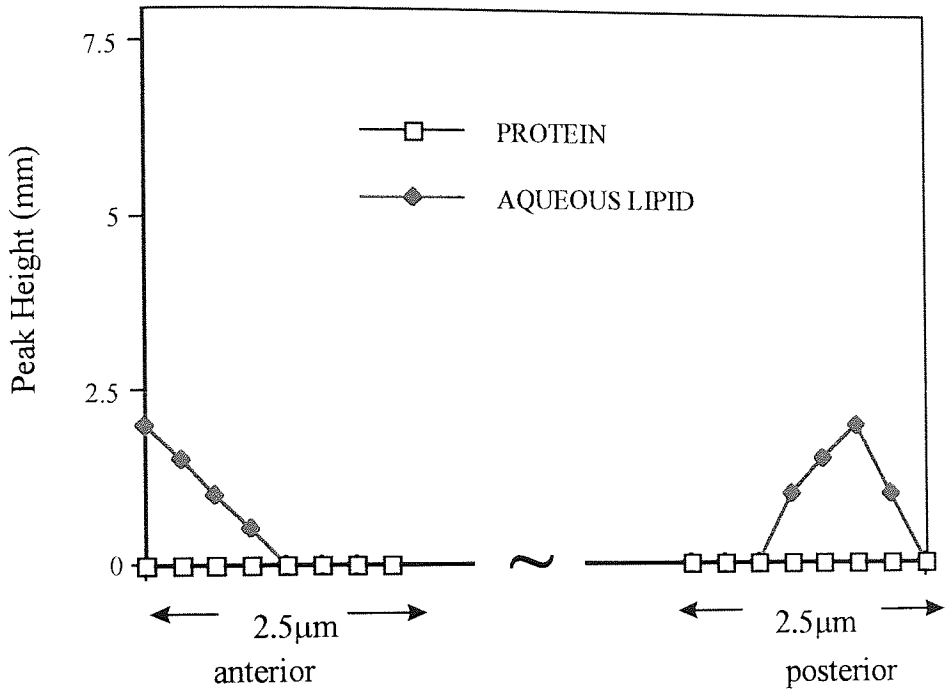

Figure 6.25: Depth of Penetration for Protein and Lipid from a Stable Tear Film for Anterior and Posterior Lens Surfaces' on an *in vivo* Spoilt Contact Lens (PCLM 25).

6.6.4 Results Using Spectrophotofluorimetry for Unstable Tear Film Production

Material	Depth of Penetration (μ)	
	anterior	posterior
PCLM 13	1.5	2
PCLM 15	2.5	4
PCLM 18	2	2.5
PCLM 25	2.5	2.5
Acuvue	3.5	5

Table 6.20: A Comparison of the Depth of Penetration of Spoilants for Unstable Tear Films from both Anterior and Posterior Lens Surfaces' on *in vivo* Spoilt PCLM Contact Lenses

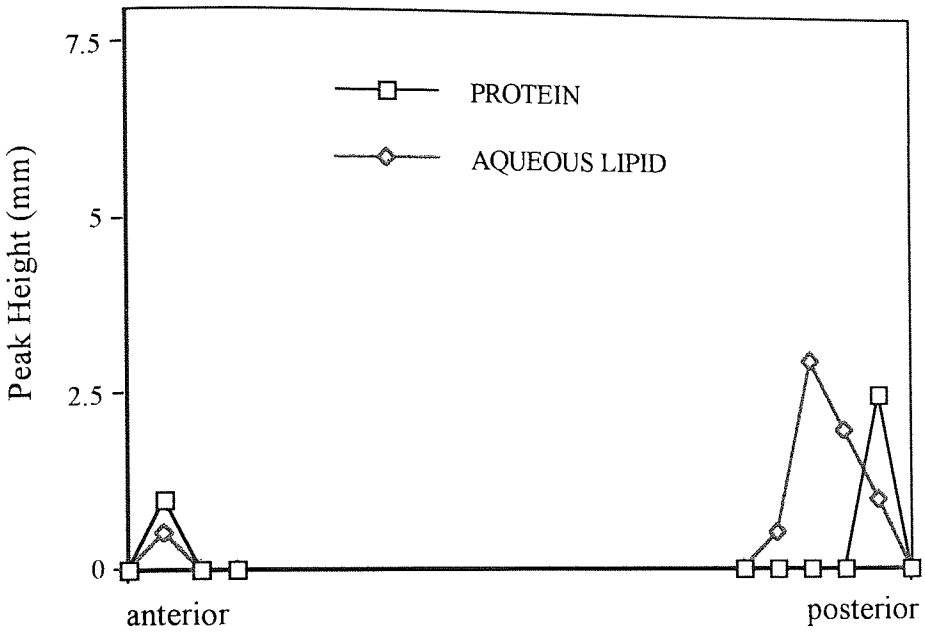

Figure 6.26: Depth of Penetration for Protein and Lipid from an Unstable Tear Film for Anterior and Posterior Lens Surfaces' on an *in vivo* Spoilt Contact Lens (PCLM 13).

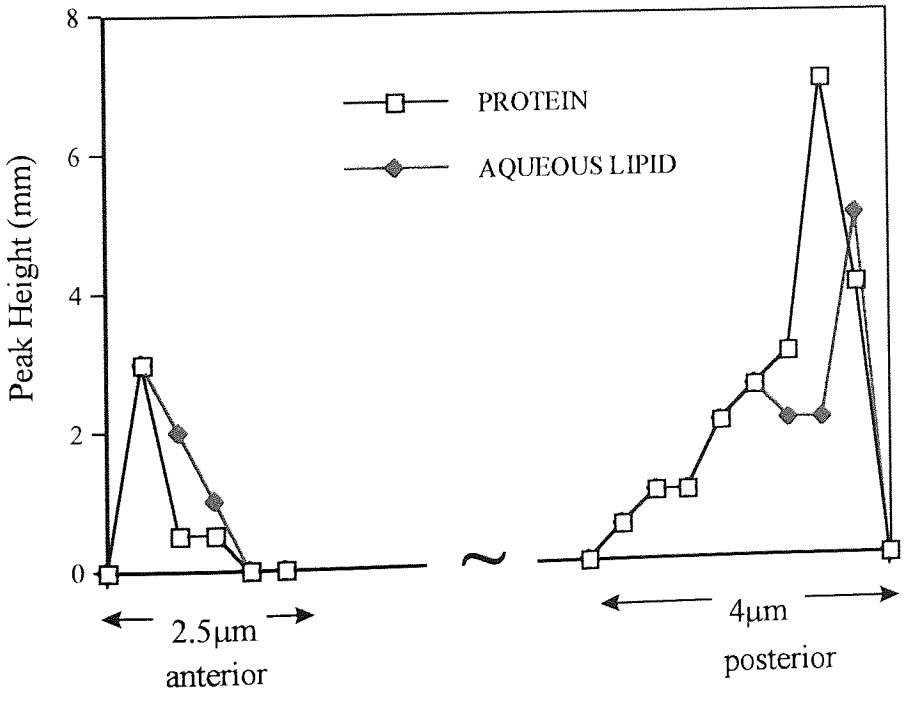

Figure 6.27: Depth of Penetration for Protein and Lipid from an Unstable Tear Film for Anterior and Posterior Lens Surfaces' on an *in vivo* Spoilt Contact Lens (PCLM 15).

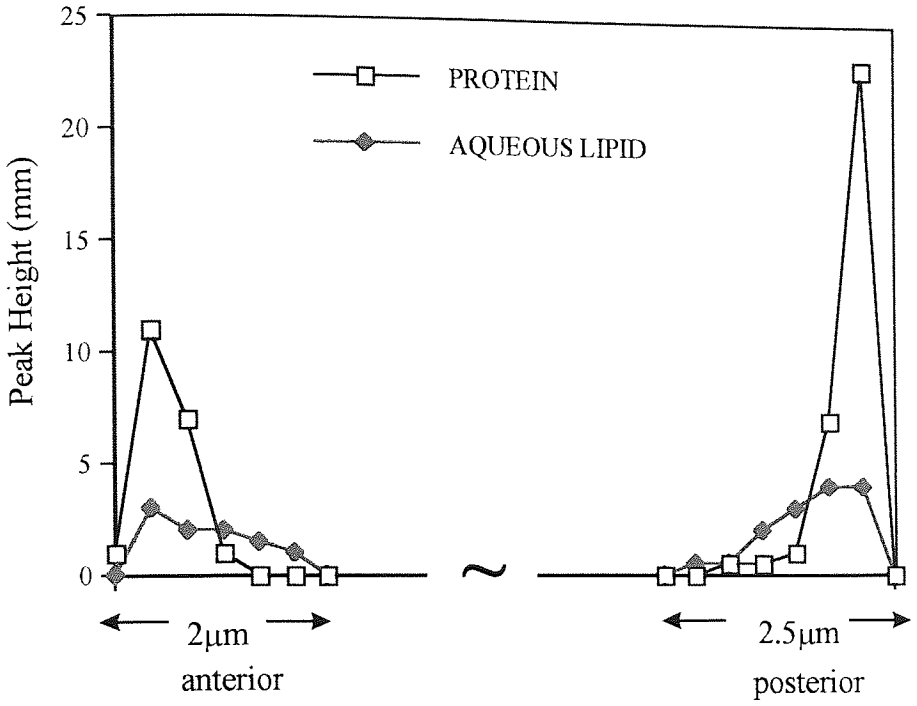

Figure 6.28: Depth of Penetration for Protein and Lipid from an Unstable Tear Film for Anterior and Posterior Lens Surfaces' on an *in vivo* Spoilt Contact Lens (PCLM 18).

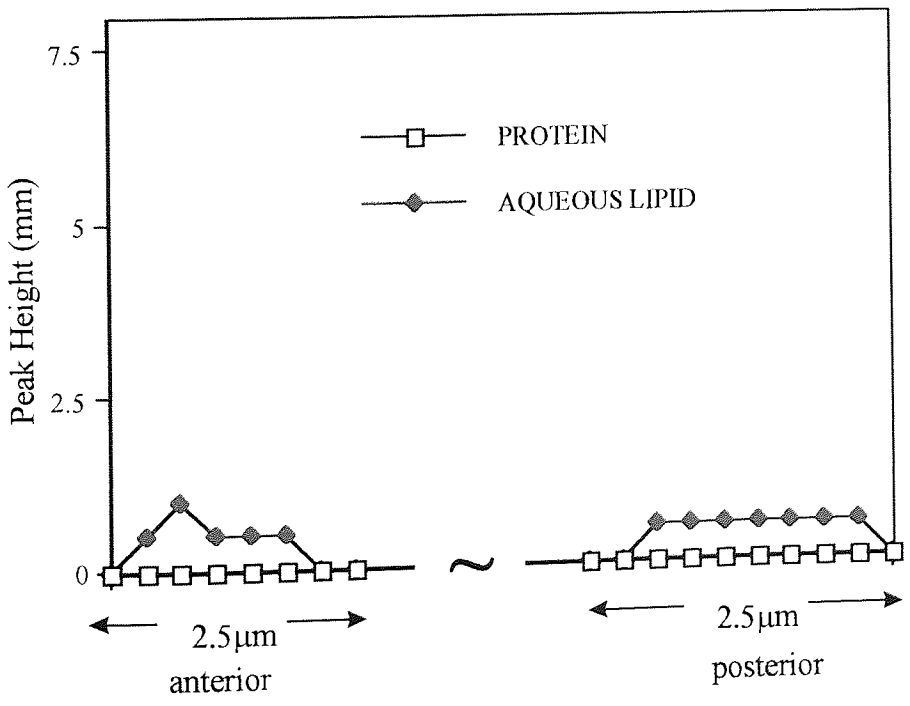

Figure 6.29: Depth of Penetration for Protein and Lipid from an Unstable Tear Film for Anterior and Posterior Lens Surfaces' on an *in vivo* Spoilt Contact Lens (PCLM 25).

6.6.5 Discussion

Figures 6.22 and 6.26 show fluorescence intensity, measured at stages during the etching processes, as a function of depth of penetration. For PCLM13 with stable and unstable tear film respectively. A similar pattern emerges to that observed in Section 6.4, where asymmetry exists between anterior and posterior surfaces due to dehydration. In this case the anterior surface penetration is very slight due to front surface dehydration. Comparing stable to unstable tear film productions, there is an overall reduction of 1- 0.5 microns anterior to posterior respectively.

Figures 6.23 and 6.27 make the same tear film comparison with PCLM15. Here again enhanced tear film stability allows greater, anterior surface penetration as shown in Tables 6.19 and 6.20.

The two PCLM materials, 18 and 25, (shown in Figures 6.24 and 6.28 and Figures 6.25 and Figure 6.29 respectively), both demonstrate relatively modest levels of protein deposition, especially when compared with the wider range of trial materials (Table 6.19-6.20). The differences in their behaviour is seen in Figures 6.28 taken together with 6.29. Figure 6.28 shows, in fluorescence mode, clear protein and lipid penetration occurring with PCLM18 together with the now familiar effect of a unstable tear film on asymmetry. This contrasts with the combination of stable tear film and PCLM25 which produces behaviour shown in Figure 6.29, the major points of which are no protein penetration and enhanced anterior lipid penetration. Although the difference in tear film stability is not as marked as in the earlier comparisons, a drop in lipid fluorescence is clearly visible.

6.6.6 Results Obtained From UV Spectroscopy for Stable Tear Film Production

Material	Depth of Penetration (μ)	
	anterior	posterior
PCLM 13	1.5	1
PCLM 15	2	3.5
PCLM 18	0.2	0.5
PCLM 25	-	-
Acuvue	4	6

Table 6.21: A Comparison of the Depth of Penetration of Protein for Stable Tear Films from both Anterior and Posterior Lens Surfaces' on *in vivo* Spoilt PCLM and Acuvue Contact Lenses

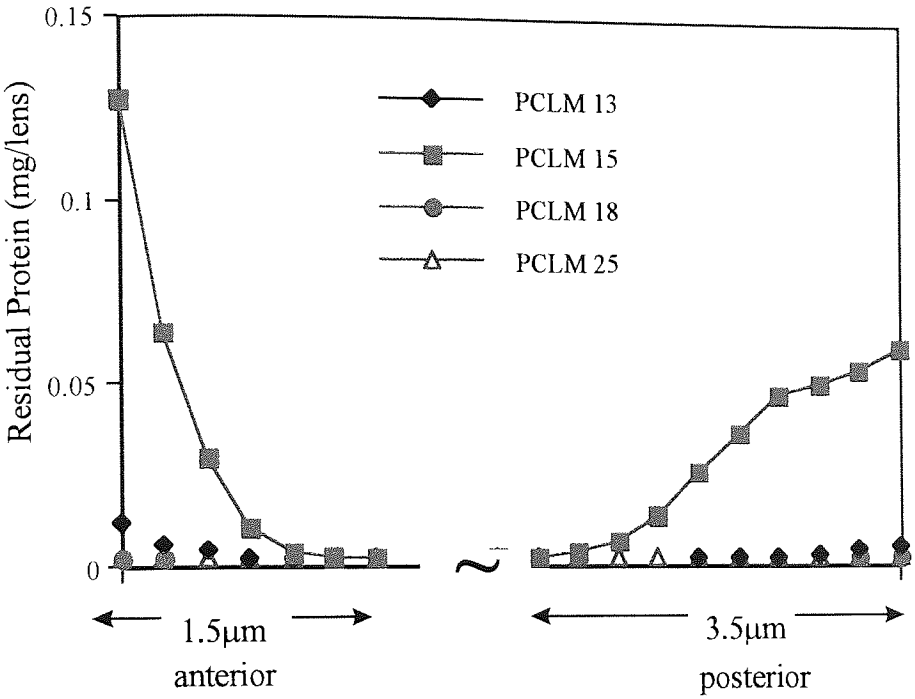

Figure 6.30: A Comparison of the Depth of Penetration of Protein for Stable Tear Films from both Anterior and Posterior Lens Surfaces' on *in vivo* Spoilt PCLM Contact Lenses

6.6.7 Results Obtained From UV Spectroscopy for Unstable Tear Film Production

Material	Depth of Penetration (μ)	
	anterior	posterior
PCLM 13	1.2	1.8
PCLM 15	1.2	1.8
PCLM 18	1	1.6
PCLM 25	-	-
Acuvue	3.5	5

Table 6.22: A Comparison of the Depth of Penetration of Protein for Unstable Tear Films from both Anterior and Posterior Lens Surfaces' on *in vivo* Spoilt PCLM and Acuvue Contact Lenses

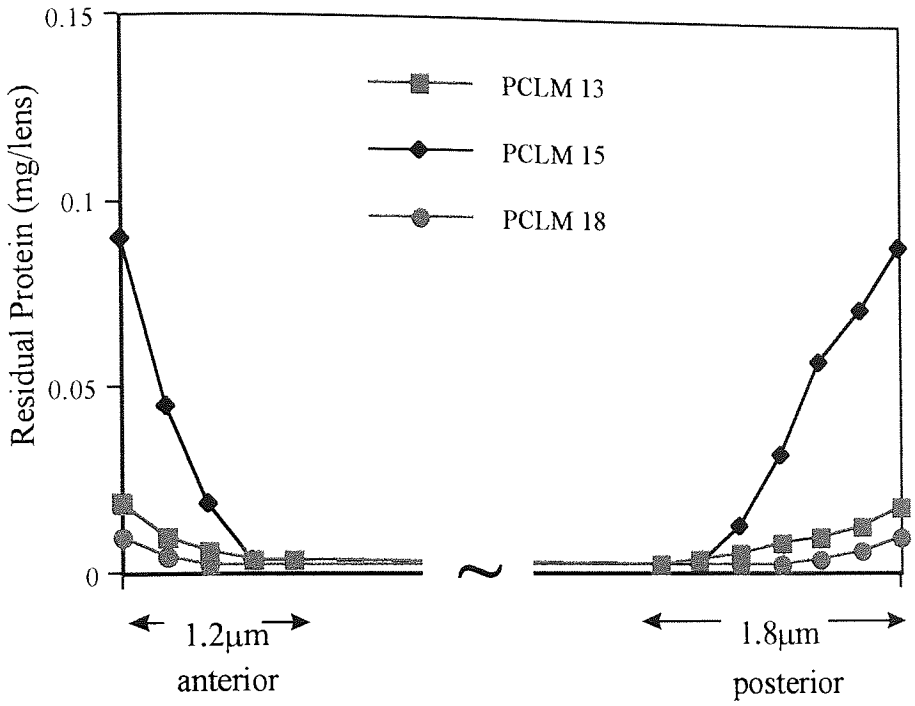

Figure 6.31: A Comparison of the Depth of Penetration of Protein for Unstable Tear Films from both Anterior and Posterior Lens Surfaces' on *in vivo* Spoilt PCLM Contact Lenses

6.6.8 Discussion

Figure 6.21 shows the protein penetration profile for the three ionic PCLM materials for patients with unstable tear films. The comments which followed from the surface to bulk plots for PCLM Unstable tear films (Figures 6.30-6.31) are now put into clear perspective. The fact that of these materials PCLM15 is the only one that shows marked protein penetration underpins quite dramatically the behaviour shown in Figure 6.30. Nonetheless the two ionic materials PCLM13 and PCLM18 both show a degree of penetration. This is confirmed by Figure 6.30 which compares PCLM13 and PCLM15 with two non-ionic materials, PCLM18 and PCLM25. The non-penetration of the two latter materials is quite clear and emphasises the difference between ionic and non-ionic members of the PCLM family.

The additional point of difference in moving from Figure 6.30 to 6.31 lies in tear film stability. Enhanced stability leads to more pronounced asymmetry in the posterior/anterior profiles and a greater anterior penetration. The drier tear film will lead to enhanced front surface dehydration of the lens which will reduce protein penetration through a lower water content.

In summary, the PEEMS study confirms the all ionic PCLM materials are subject to protein penetration and the tear film stability has a clearly discernible effect on spoilation. PCLM materials are all subject to lipid penetration and in broad terms non-ionic PCLM materials resemble Group II materials.

6.7 Conclusions

Build-up of lysozyme, lactoferrin and albumin on the copolymers produced show spoilation characteristics for both high and low water content polymers. The data shows that lysozyme a small positively charged protein absorbs very rapidly, on high water content polymers. Absorption is also highly dependant on the polymers compositions with 1% crosslink density the water content are higher and the amount of lysozyme absorbed is about 2.5 times higher than the low water content polymers containing 10% crosslinker.

In the case of lactoferrin (a positively charged, larger protein), the increase in the absorption of protein with the increase of MAA and water content is less pronounced and the quantities are much lower than lysozyme, but there are still detectable levels of protein penetration. Similar observations were measured for albumin. Due to the negative charge on albumin, the driving force to head for the surface of the lens is less but once having adhered to the surface, it shows signs of absorption, probably due to the hydrophobic interactions.

Polyurethanes show protein adsorption levels to one tenth of that of Group IV materials, with lysozyme and lactoferrin adsorption and limited albumin absorption. There is no protein absorption detectable. The higher the molecular weight of PEG in the PEG:PTMO system, the greater the water content. The greater the molecular weight of PTMO the greater the protein deposition. Increasing the concentration of PTMO in the copolymer increases the protein adsorption. The higher the molecular weight of PEG and PPG in the PEG:PPG system the higher the water content. Molecular size did not make a drastic difference in protein deposition for PPG:PEG copolymers, but water content did where an increase in water content saw an increase in lysozyme levels. creasing the concentration of PEG increased the protein absorption, but increasing the concentration of PPG decreased the protein adsorption. PUs are impenetrable to protein, and only undergo surface deposition.

Tear film stability is clearly discernible within a penetration profile for *in vivo* samples. Non-ionic PCLM materials resemble Group II materials, with no protein penetration, as PUs. The PCLM lenses show lower levels of protein adhesion than typical Group IV lenses, with lower levels of tear debris penetration.

6.8 Key Points

- The higher the material's water content the greater the amount of protein spoilation, (Sections 6.3 and 6.3.6)
- The higher the material's water content the greater the depth of penetration of the protein layer, (Section 6.3.4).
- The greater the negative ionicity of the polymer the greater the positive protein penetration, (Sections 6.3.4 and 6.3.6).
- The greater the positive ionicity of the polymer the greater the negative protein penetration, (Sections 6.3.6. and 6.5.7).
- The hydrophobic polymer backbone attracts the hydrophobic lipids into the polymer matrix, (Section 6.4).
- The higher the material's rigidity the lower the amount of protein spoilation (Section 6.3.6).
- PEEMS shows distinct differences between *in-vivo* and *in-vitro* spoilation, (Section 6.4.6).
- For *in-vivo* wear a distinct difference can be seen between anterior and posterior wear surfaces, (Section 6.4.4).
- Polyurethanes show protein adsorption levels to $1/10^{th}$ that of a high water content, anionic materials (e.g. Group IV). Polyurethanes are impenetrable to protein, and only undergo surface deposition, (Section 6.5.8).
- For polyurethanes as the level of negative moieties (e.g. PTMO) increases so the concentration of protein spoilation increases, due to an increase in overall polymeric charge, (Section 6.5).
- In-vivo studies showed that PCLM materials demonstrated low levels of protein deposition as compared to the heavier spoilers, (Table 6.21).
- Enhanced tear stability shows more asymmetry between anterior and posterior deposition profiles, (Tables 6.19 and 6.20).

Chapter 7

Discussion

From the data generated in Chapters 5 and 6, distinctly different absorption behaviour between material types can be seen e.g. GP I and IV materials (Chapter 5). There has been surface absorption (Group I and PU) and bulk adsorption (Group II and IV). Yet, the adsorption is localised and species do not seem to permeate into the entire bulk of the material. It is interesting to put some interpretation into the mechanism that may govern such behaviour. This chapter searches out the mechanism(s) that may be involved in the absorption and adsorption processes.

Permeation[170] is a phenomenon in which a certain species or component passes through another substance. The driving force for such a process could be a gradient in concentration, pressure, electrical potential or even temperature. Permeation is a general term for mass transmission and covers a number of transport mechanisms, such as reverse osmosis, dialysis, electrophoresis and diffusion.

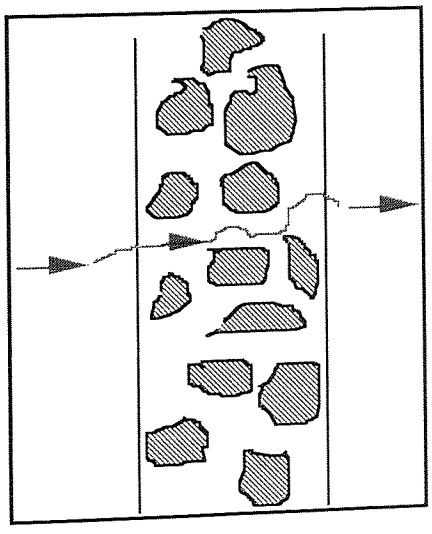

Figure 7.1: Sketch of a typical porous solid, where the size , shape and locality are in a constant state of flux.

7.1 Data Analysis

Since each protein has a unique molecular personality (Figure 7.10) and generally has an unknown three-dimensional structure, it becomes necessary to use approximation techniques to begin to assess protein absorption.

At an initial view of the data suggests that very high protein concentrations arise in thin layers close to the polymer surfaces of Group I and IV lenses. This chapter describes progress to date and summarises the methods used in data analysis and typical results.

According to the Beer - Lambert Law, absorbance and protein concentration are linked by:

$$A_{Total} = \varepsilon . c . l \qquad \text{(Eqn 7.1)}$$

Under normal conditions, l = 1cm and the protein concentration, c, has units of mg/cm^3; ε, is obtained from the calibration curve for the experiment and has a value of 3.3 cm^2/mg (Chapter 4).

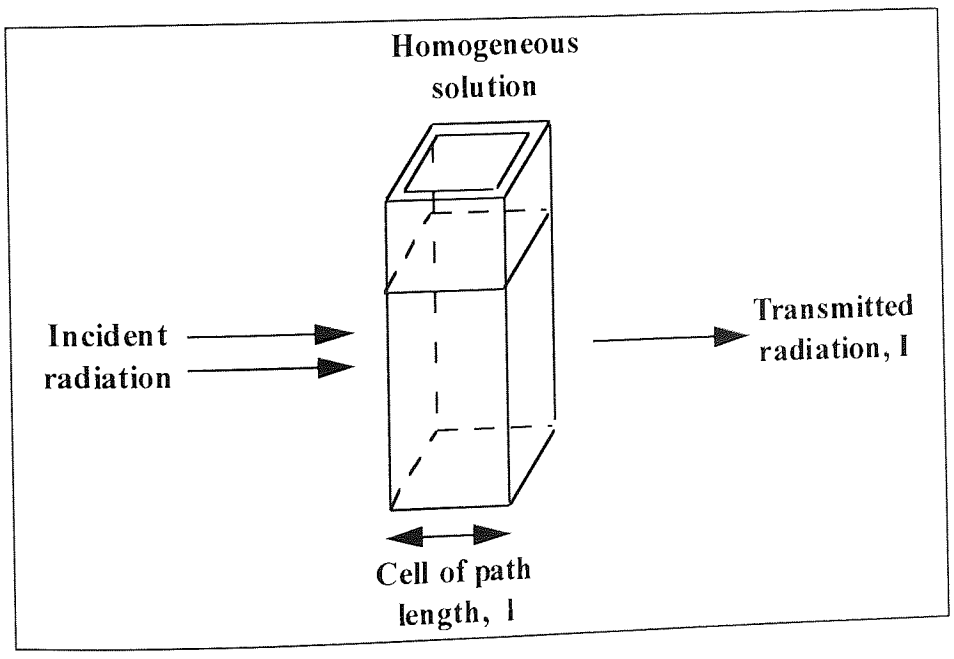

Figure 7.1: Schematic View of Measuring System Employed in UV/visible Spectroscopy

During tests on contact lenses, the so-called "protein concentration" has been calculated as follows:

$$C'_{Total} = \frac{A_{Total}}{\varepsilon . l} = A \times 0.3 \qquad \text{(Eqn 7.2)}$$

The resulting 'concentration' has been reported as mg protein/lens. Strictly speaking, this is the amount of protein in a lens with a cross-sectional area of $1cm^2$; it is not a concentration as such and does not provide a measure of the local protein concentration in a lens, although it does eliminate lens edge effects when viewing varying powered lenses.

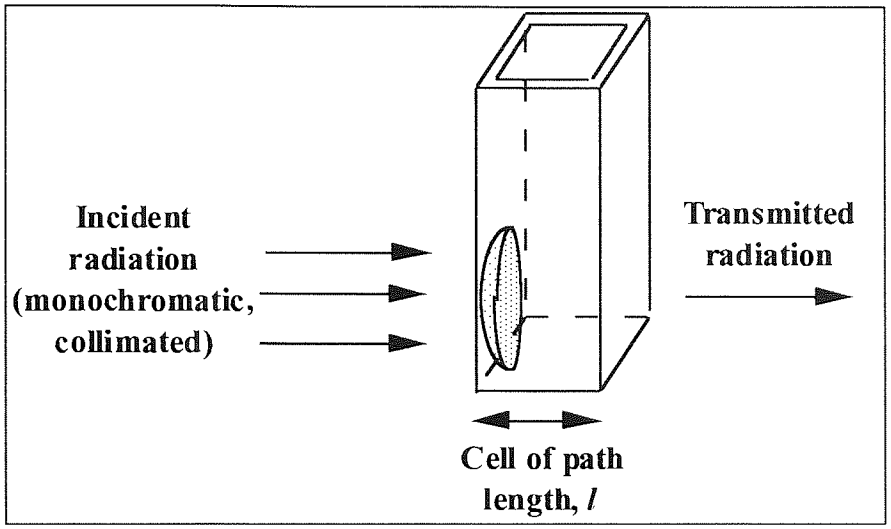

Figure 7.2: Schematic View of Measuring System Employed in UV/visible Spectroscopy with Material Substrate (e.g. contact lens)

7.1.1 Example 1

If we now go to an example of an *in vitro* spoilt lens using the Protein Tear Model, from Section 6.3.

Absorbance reading = 0.597 (for protein on one side of the lens only)

Total protein uptake = $0.597 \times 0.3 \times 2$

= 0.36 mg protein / lens of $1cm^2$ area.

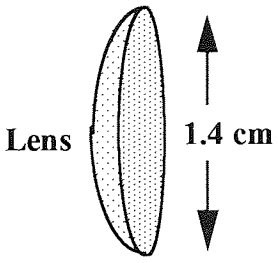

Appendix 5 sets out detailed lens dimensions and using a figure of $0.036cm^3$ for the lens volume and an area of $2.04cm^2$ for the effective cross-section of the lens

Total protein in the lens = $0.36 \times 2.04 = 0.73$ **mg**

and the average protein concentration throughout the lens

$$= \frac{0.73}{0.036} = 20 \text{ mg/cm}^3$$

The average protein concentration, assuming that protein penetration is equivalent to:

$$\frac{\textbf{number of etches} \times \textbf{etch depth (cm)}}{19 \times (3.6 \times 10^{-5})},$$

is found to be:

$$\frac{\frac{0.36}{2}}{19 \times (3.6 \times 10^{-5})} = 263 \text{ mg/cm}^3$$

The above figures reflect typical results obtained from both *in vitro* and *in vivo* studies, demonstrate that:

(i) Protein uptake per lens can be of the order of 1mg.

(ii) Protein concentration in the narrow penetration band can reach levels of around 300mg/cm^3.

These figures should be compared with concentration of protein in tears (about 10mg/cm^3 [43]), and with the amounts of protein adsorbed and desorbed during *in vitro* tests.

Another key aspect of data analysis concerns the apparent protein concentration and depth of penetration (etching). Consider the real protein concentration profile in the outer layer of a lens:

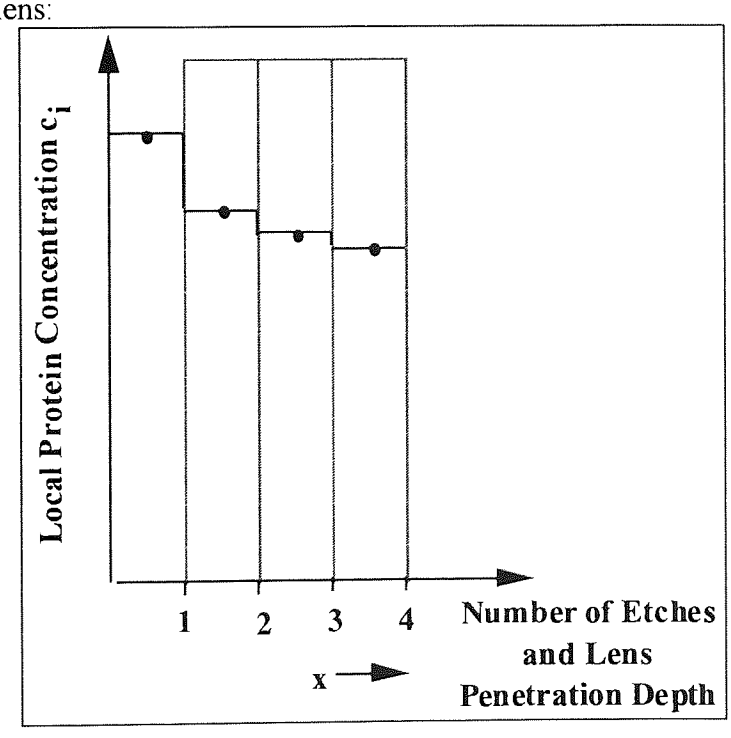

Figure 7.3: Assessment of Local Protein Penetration by UV/Visible Spectroscopy

c_i is the local protein concentration in the *i*th etch layer.

Also, locally $A_i = \varepsilon . c_i . \delta x$, where δx is the thickness of each etched layer.

For the above case:

$$A_4 = \varepsilon . c_4 . \delta x$$

$$A_3 = \varepsilon . c_3 . \delta x$$

$$A_2 = \varepsilon . c_2 . \delta x$$

$$A_1 = \varepsilon . c_1 . \delta x$$

Initially, before any etching has taken place

$$A_{Total} = A_1 + A_2 + A_3 + A_4$$

$$= c_1 + c_2 + c_3 + c_4 . \varepsilon . \delta x$$

An average figure for protein concentration, $\bar{c}$, can then be computed as follows:

$$\bar{c}_{Total} = \frac{A_{Total}}{\varepsilon . (4\delta x)}$$

Alternatively we can compute protein uptake per lens of $1 cm^2$ cross-sectional area:

$$\bar{c}'_{Total} = \frac{A_{Total}}{\varepsilon . 1}$$

Consider now the removal of the first layer:

$$A_{(Total-1)} = A_2 + A_3 + A_4$$

$$= (c_2 + c_3 + c_4) . \varepsilon . \delta x$$

$$\bar{c}_{(Total-1)} = \frac{A_{(Total-1)}}{\varepsilon . (3\delta x)}$$

$$\bar{c}'_{(Total-1)} = \frac{A_{(Total-1)}}{\varepsilon}$$

Clearly,

$$(A_{Total} - A_{(Total-1)}) = A_1$$

$$= c_1 . \varepsilon . \delta x$$

or,

$$\frac{1}{c_{Total}} - \frac{1}{c_{(Total\ -\ 1)}} = c_1 . \delta x$$

C_1, the local protein concentration, can now be readily computed using:

$$c_1 = \frac{c'_{Total} - c'_{(Total\ -\ 1)}}{\delta x} \quad \text{in mg/cm}^3.$$

Also, the amount of protein in each layer can be computed using:

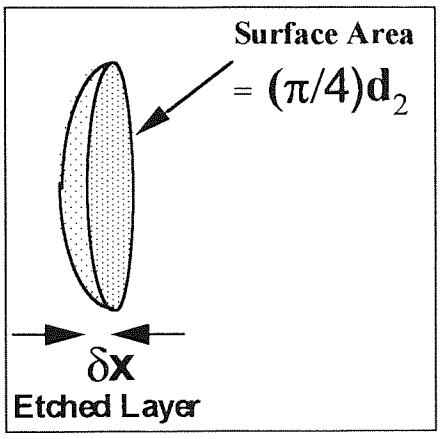

Figure 7.4: Sketch of Dimensional Analysis of a Contact Lens

Volume of etched layer: $(\frac{\pi}{4} . d^2 . \delta x) . c_i$ in mg

7.1.2 Example 2

If we now look at the *in vivo* spoilation of an Acuvue lens (FAP1) as described in Section 6.4 concentration with each etch:

No of Etches i	Initial Protein Concentration (mg/cm^2) $c'_{(Total\ -1)}$	Local Protein Concentration (mg/cm^2) $c_i = c'_{(Total\ -(i-1)} - c'_{(Total\ -i)}$	Amount of Protein per slice (mg/cm^3) $c_i = \frac{c_i}{\delta x}$
0	0.179	-	-
1	0.175	0.004	111
2	0.173	0.002	56
3	0.170	0.003	83
4	0.161	0.009	250
5	0.150	0.011	306
6	0.142	0.008	222
7	0.136	0.006	167
8	0.129	0.007	194
9	0.124	0.005	139
10	0.112	0.012	333
11	0.099	0.013	361
12	0.092	0.007	194
13	0.073	0.019	528
14	0.059	0.014	389
15	0.050	0.009	250
16	0.035	0.015	417
17	0.024	0.011	306
18	0.015	0.009	250
19	0.014	0.001	28

The average concentration over the etched zone $= \frac{0.179}{19 \times 3.6 \times 10^{-5}} = 263\ \mathbf{mg/cm^3}$

see previous example

7.2.3 Qualitative Trends

Initial analysis of experimental data from the *in vivo* study (study 2) with Group II and IV lenses revealed the following qualitative trends.

Lens Code	Relative Depth of Penetration of Protein (Anterior : Posterior)	Relative Average Protein Concentration in Penetration Zones (Anterior : Posterior)
Acuvue 40L	0.58	2.4
Acuvue 39L	0.55	2.9
Focus 28R	0.57	2.7

Also, although fluctuations in local protein concentration are relatively large, it appears that the profiles are not uniform and typically as sketched below. Some similarity can be noted between these profiles and those obtained by fluorescence measurements (Figure7.6).

7.1.3 Protein Penetration

Etched samples reveal that protein penetration depth is typically 10 to 30 etches. Taking the average penetration depth to be $3.6 * 10^{-5}$cm. (see appendix 1), the following figures are obtained:

No. of Etches	Protein Penetration (μm)
10	3.6
20	7.2
30	10.8

If these figures are compared to the hydrated thickness of the lens, typically around 150μm; it suggests that penetration is restricted. A simple diffusion model cannot describe the penetration mechanism alone an additional mechanism needs to be reviewed to assess a more comprehensive mechanism for adsorption. The next section will lead us through possible forces and mechanisms of transport that may be envisaged for hydrophilic porous membranes, in a predominantly aqueous media.

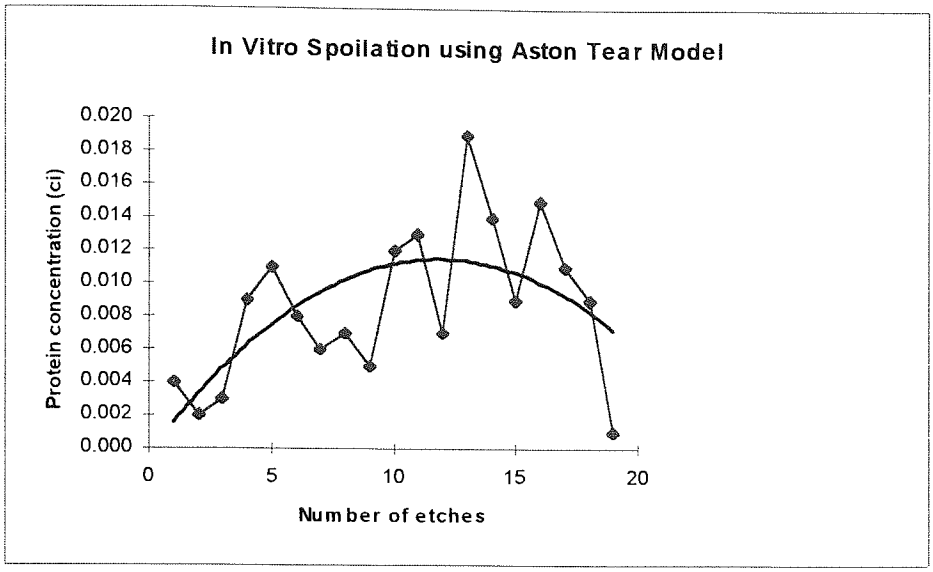

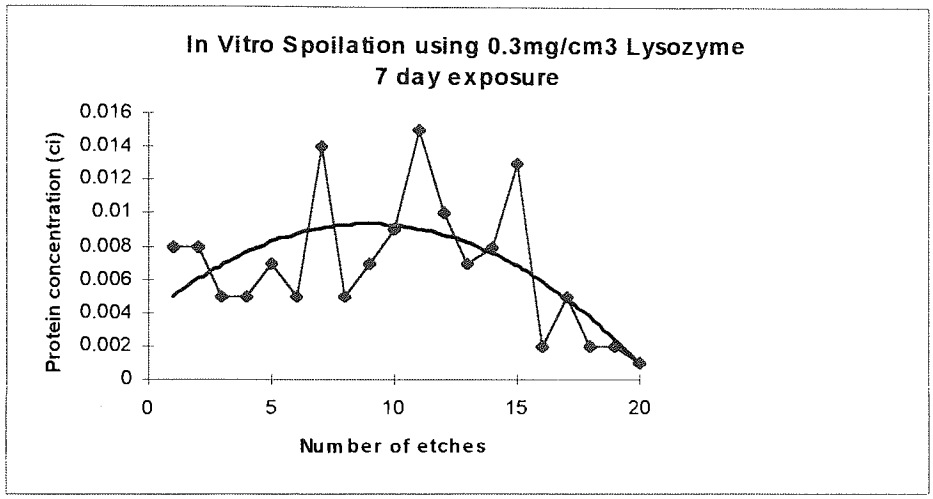

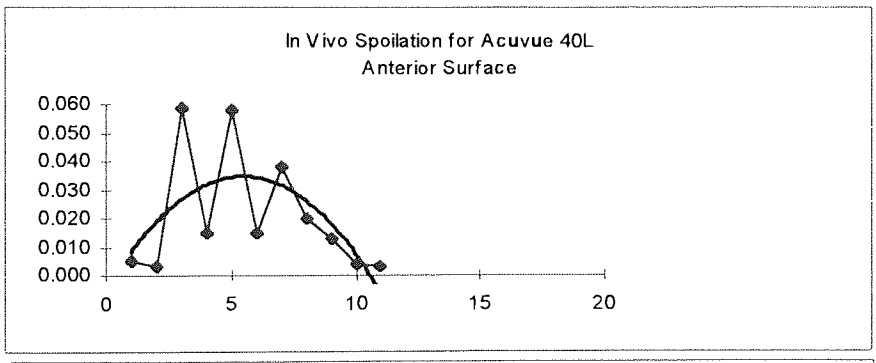

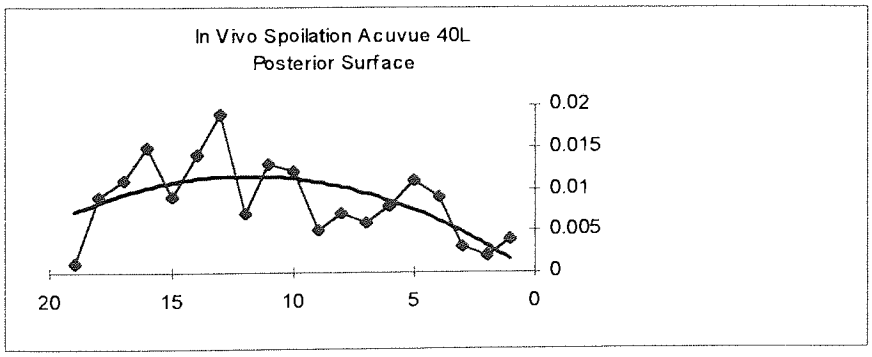

Figure 7.5: Penetration Profiles for FAP1

7.2 Permeation

Permeation[170-173] is a phenomenon in which a certain species or component passes through another substance. The driving force for such a process is complex dependent on many transport mechanisms, such as reverse osmosis, dialysis, electrophoresis and diffusion. It is therefore not possible to develop a model wholly dependent on just protein diffusion. But effort has been directed at analysis and interpretation of raw data obtained from in vivo and in vitro studies. The data suggest that very high protein concentrations arise in the layers close to the anterior and posterior surfaces of Group IV lenses; protein concentration profiles are flatter than expected.

Contact lenses are laminar membranes requiring the passage of oxygen to the cornea to maintain a healthy ocular environment. Since this work is concerned primarily with the transport of water soluble species such as proteins, it may be appropriate to consider a few of the membrane processes used to achieve separation in aqueous media.

7.2.1 Microfiltration

Microfiltration membranes have a heterogeneous porous structure with pore size typically in the range of 0.02 - 10 microns. Such membranes, under a driving force of a pressure differential, in order of a few tens of kilo-newtons, allow for relatively high fluxes of water and dissolved species but retain suspended material such as biological fragments, bacteria and silica. The membranes can be regarded as inert sieves through which the bulk flow of solvent and solute can occur. However, interaction between particles and the membrane surface may occur, especially in aqueous systems due to the presence of electrical double layer effects. Such factors have an influence on membrane lifetime and properties of the membrane.

7.2.2 Ultrafiltration

Ultrafiltration is a means by which large molecules or colloid particles can be separated from solvent and low molecular weight solutes, such as salts. The pore sizes of such membranes lies normally in the range of 1-20nm. Ultrafiltration membranes are classified by the largest molecular weight material that can be transported. This maximum is known as the molecular weight cut-off. Ultrafiltration works in the same way as microfiltration, the difference being a matter of degree rather than kind with respect to the size of particle that can be transmitted.

7.2.3 Reverse Osmosis

Reverse Osmosis is a process whereby virtually all suspended and dissolved material is separated out from solution. This system employs a semipermeable membrane- so called because it allows for the passage of some substances such as the solvent, but not others, such as the solute. Reverse osmosis occurs when the hydrostatic pressure across the membrane exceeds the osmotic pressure, thus resulting in a flow of solvent from the high concentration side to the low concentration side. This is the reverse of what occurs with normal osmosis. To get acceptable solvent flow very high pressures must be employed, typically in the range of 8-10 MPa. Unlike microfiltration and ultrafiltration, a simple sieving mechanism cannot explain the separation processes.

The active layer of a reverse osmosis membrane is isotropic and thus pores have no real physical meaning but are an entropic concept caused by segmental motions in the polymer backbone and pendant side groups. Transport, therefore, occurs not by bulk flow but by a solution / diffusion mechanism. The mobility of water molecules may exceed that of proteins being less soluble in the membrane phase than the water molecules. Non-ionic solutes are more readily soluble in such membranes. The exclusion of these solutes being due to their low mobility relative to water molecules. Reverse osmosis membranes tend to be asymmetric in structure or in the form of thin film composites where a thin, homogeneous solute rejecting skin (20-50nm thick), known as the 'active layer' is deposited on a porous substrate that acts as a support.

7.2.4 Dialysis

In a broad sense, dialysis refers to a process separating one chemical species from another in a liquid solution through semipermeable membrane, by means of their unequal diffusion rates through the membrane[2]. In ordinary dialysis the transport of the solute through the membrane is achieved by imposing a concentration gradient across the membrane - there is no pressure differential in dialysis. If the mixture contains more than one electrolyte, and the inter ionic interaction amongst ions of the same sign is insignificant then the governing equation in ordinary dialysis is the diffusion equation.

7.2.5 Donnan Equilibrium

In Donnan dialysis the inter ionic interaction plays an important role and the Donnan equilibrium is maintained at the membrane-solution interface. Normally, Donnan dialysis is limited to the dialysis of electrolyte solutes with an ion exchange membrane. The term can be extended to all cases where the Donnan equilibrium has a significant effect such as in neutral membranes where the membrane is permselective with respect to one of the ions

present in the solution. However, the Donnan effect may be subsumed if the solvent on the low-concentration side is continually renewed.

7.2.6 Electrodialysis

The driving force in dialysis is a chemical potential caused by a transmembrane concentration gradient. In the case of electrodialysis there is a second force: an electrical potential difference. This electrical potential is usually applied opposite to the concentration gradient in order to create a more concentrated salt solution. Consequently, this process is sometimes used as an alternative to reverse osmosis. Neutral membranes are not used since they would tend to pass anions and cations in opposite directions in the electric field and thus fail to achieve the desired concentration of solute. The membranes employed are made of poly electrolytes which selectively allow for the passage of ions of counter-charge to the polymer, thus cation transport is selected for by anionic membranes and anion transport by cationic membranes. The electrical potential used in such systems is typically in the range of 1-2V per cell pair.

7.2.7 Physical Factors

A membranes' morphology dictates the mode of permeation and separation[170,174-180]. The basic morphologies are isotropic (dense or porous) and anisotropic with a tight surface extending from a highly porous wall structure. Figure 7.6 shows a SEM trace of the porous structure of a typical Group IV lens (Acuvue) after critical point drying. The tight surface can be a dense, selective skin, permitting only diffusive transport or a porous skin, allowing viscous flow to permeate, as in conventional ultrafiltration. Such techniques such as membrane separation is achieved by manipulation of these basic morphologies.

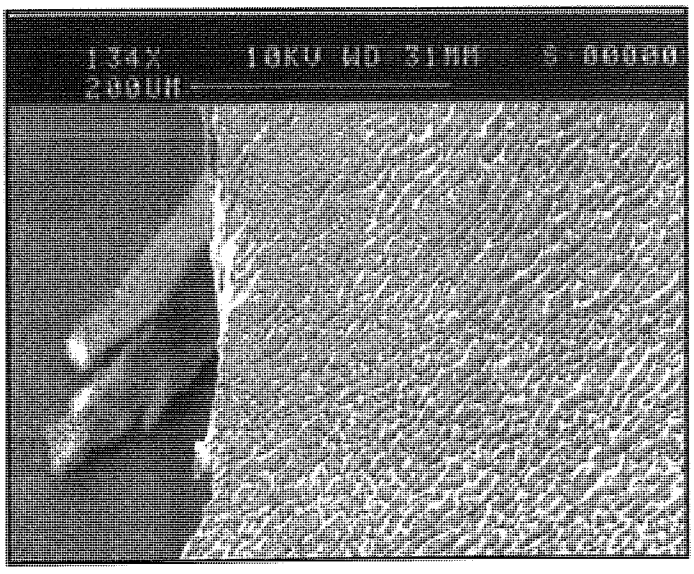

Figure 7.6: SEM Trace of Porous Network of a Typical Group IV Lens

Permeation through a homogeneous film can be thought of as resulting from two distinct processes:

(i) solubility of the penetrant in the polymer, which is a thermodynamic quantity (lipid),

and (ii) diffusion which is a kinetic quantity relating to the mobility of the penetrant species within the macromolecular matrix (protein).

Structure and morphology have important influences on the selectivity and rate of diffusion through a polymer membrane:

(i) On the macroscale you have membrane: thickness, lamination, asymmetry as well as the size, type and size distribution of pores.

(ii) On the microscale, degree of crosslinking, chain stiffness, crystallinity, degree of swelling as well as fixed charges, hydrogen bonding, polar group interactions or even simple Van Der Waal attractions will all affect the rate of transport of the penetrant. In general, it can be said that factors which decrease the segmental mobility of the polymer chains will decrease the diffusion rate.

Various studies have been made into the basic nature of transport through hydrogels, particularly for small molecular weight species[170-172,181]. An understanding of transport, and thus an ability to influence permeability and permselectivity, is important in applications such as reverse osmosis, kidney dialysis, sensors and drug release. A universally satisfactory transport model has not yet been realised but they mainly all try and relate the permeability or diffusivity to the overall amount of water in the gel matrix. In a study of dissolved oxygen permeability through a range of hydrogels, Tighe and Ng[183] found the log of permeability coefficient to be linearly related to the overall equilibrium water content (EWC)[189]. This empirical observation was later confirmed by Feurer et al[190] and Refojo and Leong[170]. All these studies indicated that the oxygen permeabilites were dependant upon the water content alone and were independent of the type of monomer used in the polymer.

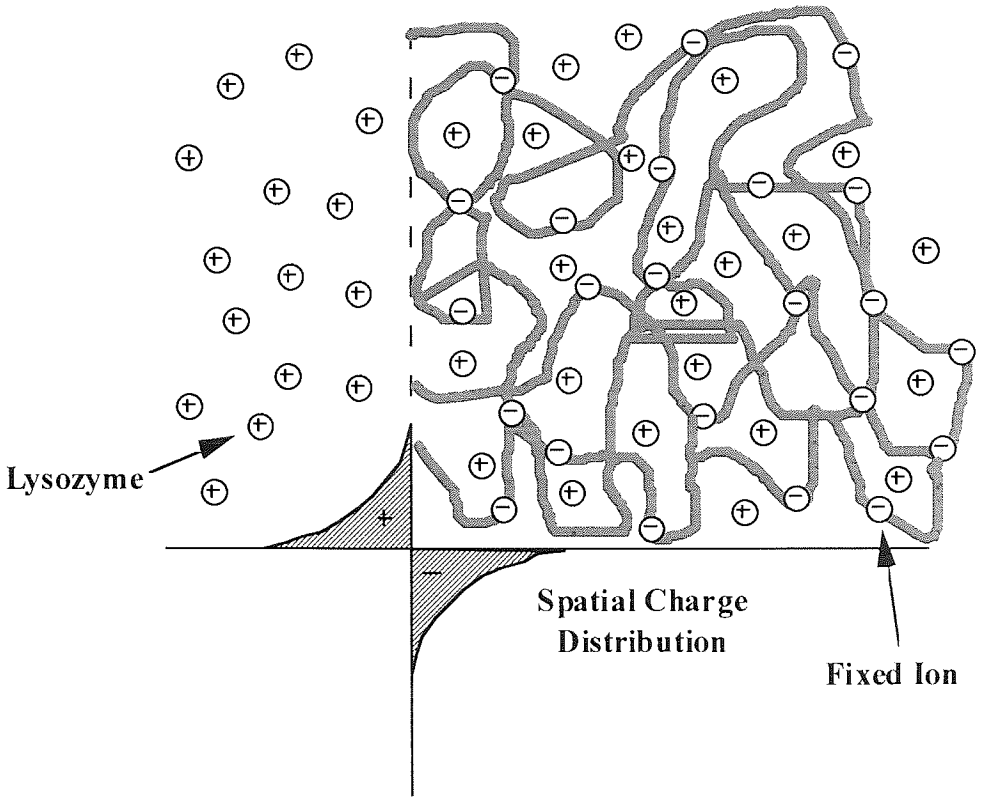

Figure 7.7: Ion Distribution Near the Membrane - Solution Interface

With the initial experiment carried out in Chapter 6, a similar observation may be detailed, that the higher the material's water content the greater the amount of protein spoilation and the deeper the depth of penetration. Section 6.7 investigates the role of monomer constituents as compared to the polymer. But it is necessary to actually look at the polymers overall charge to gain a true perspective. For example, FAP1 and 2 have a greater overall negative charge than FAP3 and they absorb more protein. FAP4 and FAP 3 have no charge and there is no protein uptake.

Our studies show that for a larger, charged molecule (e.g. lactofferin) this does not hold true, and that the driving force is actually the polymer's composition, with water actually acting as a 'mobile phase'.

A feature of hydrogel membranes in gas transport studies, that distinguishes them from hydrophobic membranes, is their significantly reduced 'boundary layer effect'. In the case of hydrophobic polymers the 'gaseous' oxygen permeability coefficient is greater than the corresponding 'dissolved' permeability coefficient (transport of oxygen across a membrane separating two aqueous phases). This is due to hydrophobic polymers possessing an added resistance to transport known as the 'boundary layer effect' which is caused by the high interfacial tension between the polymer and water. This can be reduced by increasing the surface hydrophilicity of the membrane[170], so reducing the additional affects that may be felt by a protein molecule. This is supported by work carried out in section 6.7 and 6.5.

The free volume model proposed by Yasuda et al[185], is perhaps the one that has been applied most successfully to the study of solute transport in hydrogels. This model applies to homogeneous water swollen polymer matrices. In such hydrogels, pores are fixed neither in size nor location but results from the random fluctuations of chain segments that may exhibit a high degree of mobility due to the plasticing effect of water. The pores and channels in such systems are therefore in a constant state of flux. The free volume or 'hole' model takes a partly thermodynamic partially statistical approach. It assumes that the transported species is associated only with the water phase, with its diffusion being located next to a suitable hole that is both unobstructed and large enough to accept the penetrant. The energy required to form a 'hole' being the Helmoltz free energy. This diffusion into the polymer occurs by local activated jumps of the penetrant molecules from one to another unoccupied 'hole'. The activation energy takes into account rotation of a few monomer segments near the penetrant and perhaps some bond stretching. The term 'holes' does not refer to actual voids in the matrix but is meant entropically to indicate the probability of creating either sorption sites for the penetrant or diffusion channels in the hydrogel matrix through which the penetrant species can move from one site to another. In the free-volume model the flux from high to low concentrations reflects that act that fewer holes are occupied in the less concentrated regions and the penetrant has a higher probability of jumping to an unoccupied hole in the low concentration regions. The model predicts a linear relationship between InP and 1/H, where P is the permeability coefficient in the hydrogel and H is the degree of hydration. It also predicts the permeability decreases exponentially with increasing solute size and that the permselectivity of solutes increases as the degree of membrane hydration decreases.

More recently, Peppas and Moynian[186] have proposed a theoretical model for the diffusion of solutes through moderately swollen hydrogels which makes use of topological features as well as free-volume characteristics of the network[187]. It yields a general expression which shows the dependence of the normalised diffusion coefficient on factors such as the degree of swelling, the radius of the solute, the number average molecular weight between crosslinks and a function related to the mesh size which takes into account the effects of barriers such as those due to crosslinking and entanglements.

By choice of monomer composition or polymerisation technique the amount of water, porosity and consequent permeability characteristics can be controlled, that is, heterogeneous hydrogels with a fixed macroporous structure can be generated as well as the homogeneous type mentioned above. This allows hydrogels to be permeable not only to small molecular weight species but also to macromolecules such as the protein hormones. Davies[88] in one of the early studies on the use of hydrogels for the controlled release of high molecular weight species, such as bovine pancreatic insulin, found the diffusion coefficient of

the hydrogel D, to be governed by the molecular weight of the penetrant and the degree of hydration of the polymer.

The polymers were based on polyacrylamide (PA) and polyvinylpyrrolidone (PVP). Langer and Folkman[181] studied the release of the macromolecular species, soybean trypsin inhibitor (molecular weight 21,000) from poly HEMA, PVA and ethylenevinyl acetate copolymer based systems. They found that the release mechanisms of such high molecular weight species could not be determined, and in the case of the ethylene vinyl acetate copolymer, simple diffusion could not explain the release behaviour. Such species that were studied do not diffuse through a homogeneous film of pure polymer. This may be indicative that these macromolecular species permeate out through heterogeneities (flaws and cracks) that are formed during the manufacture of the polymer devices. Indeed, this concept of a heterogeneous 'drug-modified polymer' was used by Brook and van Noort[189] to explain the release characteristics of hydrocortisone sodium succinate from acrylic gels. Contrary to the expectations of the free volume model of Yasuda[80] which would predict an increase in the rate of release with an increase in the degree of hydration of the polymer, the opposite was found. The authors concluded that diffusion of the drug through the polymer matrix was therefore insignificant but occurred, instead, by surface release and the dissolution into and diffusion through cracks and channels that were formed due to the presence of the drug within the polymer system.

The semi-permeability of porous membranes is based on the spatial cross section of the permeating species, that is, small molecules exhibit a higher permeation rate than large molecules, and linear chain molecules permeate better than those with a globular shape. The semi-permeability of the dense membrane or a membrane that exhibits anisotropic morphology with a dense skin is obtained primarily through a solution-diffusion mechanism. The permeating species interact chemically with a dense polymer matrix and selectivity dissolve in it, resulting in a diffusive mass transport along a chemical potential gradient. So, for a dense membrane semi-permeability may be exhibited towards large molecules with which it interacts, whereas the smaller, non interacting species do not permeate.

There are also the combination of additional physical factors that may influence the process of protein absorption, such as the smoothness of the contact lens surface, the surface charge, the wettability, the chemical structure of the polymer surface, the elasticity of the lens material, and other factors such as tear flow and rate of blinking.

Take for example tear break-up which may be responsible for such high concentration on the anterior surface of a lens. The wind-screen wiper effect (blinking), will clean the surface but may increase the protein concentration due to shear. The physical pressure of blinking may force protein into the hydrogel.

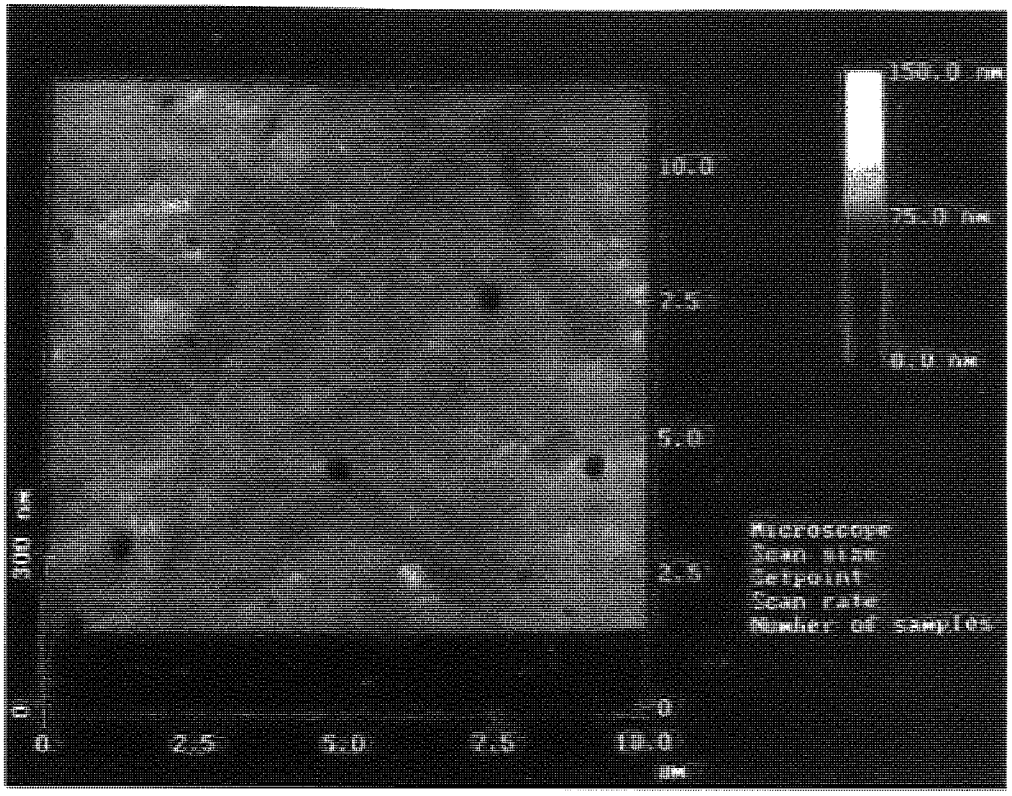

Figure 7.8: Surface of an Acuvue Lens viewed by ATM

The structure of the hydrogel may play a part, and maybe issues such as the manufacturing processes may have a part to play, i.e. lathed versus moulded. Variations in molecular structure may occur during swelling, and adsorption of protein molecules may alter the physical dimensions of the polymer matrix. Cleaning solutions may alter the molecular structure due to pH variations and imbibed solutions.

Both *in vivo* and *in vitro* studies reveal that protein (lysozyme) uptake is of the order of 1mg per lens (see Example 1). This separates to an average protein concentration throughout the lens of $1/0.0036 = 28mg/cm^3$, and to an average protein concentration in the penetration zone of $360mg/cm^3$. Firstly, these figures should be compared with that for total protein concentration in tear fluid, typically 8 mg/cm^3. Secondly, within the penetration zone, the volume occupied by protein appears to be similar to that filled by the polymer; this represents a high degree of spoilage or fouling with little effect on the optical properties of the lens. Thirdly the above findings appear to contradict the intuitive belief that molecular diffusion in Group IV hydrogels is relatively rapid. The high local concentrations of protein ($100mg/cm^3$, as compared to $500mg/cm^3$ of water and $400mg/cm^3$ of polymer), may in itself produce a 'plugged effect' from the out-set inhibiting any further permeation. Additionally localised denaturing could cause a barrier of resistance to permeation.

Initially driven to the surface of a hydrophilic polymer by electrostatic charge, a protein once encountering the surface, undergoes conformational changes to reduce the energy of the intervening system. At this stage there are mechanical influences by eyelid movement, (or solution swirling for *in vitro* studies on the shaker). These mechanical forces will squeeze and stretch the polymer on the microscopic scale this maybe as effective as the buckling of the earth's plates, but the motion being reversible (unlike the Himalayas), so undulating the distribution of pores and there size. This will cause a redistribution of any species entering the polymer network. This is borne out by carrying out *in vitro* studies without the aid of a shaker for solution distribution. Studies with experimental system used in this work showed that there is a decrease in penetration by 5 ± 1 %.

Permeation of protein may also be affected by the lipids for *in vivo* samples, and may have a transportation role to play, due to their hydrophobic nature.

1) One mechanism is simply the interactions of the carboxyl groups of fatty acids with hydrogen-bonding sites at the dynamic hydrogel interface. Both the polarity and total surface energy of these hydrogels are appreciably higher than those of natural tissue.

2) The other mechanism is similar to that occurring in discolouration reactions, where penetration arises because molecules that have some solubility in water but greater solubility in the polymers are taken into the lens matrix.

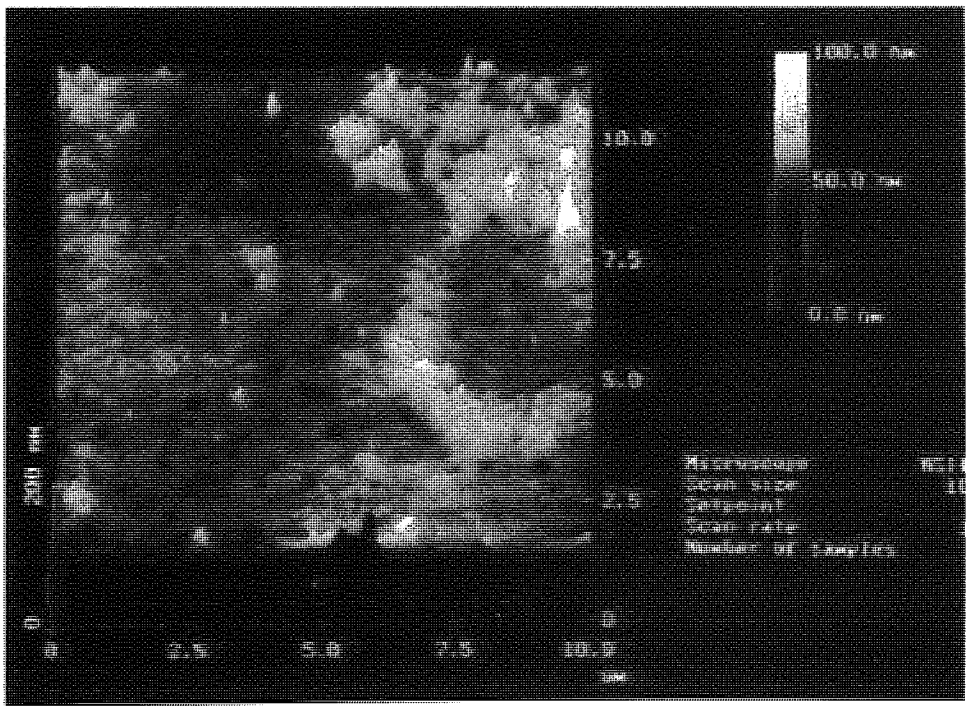

Figure 7.9: Surface of an Acuvue Lens Spoiled with Lysozyme Solution for 24 hours viewed by ATM

7.2.8 Protein Uptake

The surface of a protein is often complex in nature, with different characteristics such as hydrophilicity and charge[190-196]. The surface view of protein molecules is shown in Figure 7.10 and indicates the complexity of the surface groups that can participate in interaction with other surfaces. The fact that many real surfaces are heterogeneous together with the complex nature of the protein surface complicates the prediction of how a protein interacts with a surface.

The surface of a material demands that atoms[197], which in the bulk are surrounded by a homogeneous distribution of neighbours, be exposed to an asymmetric environment. This results in dangling bonds and unfulfilled valences - a high-energy situation. This high energy situation always leads to an attempt by the system to reduce the surface energy. This can occur through surface atomic rearrangement (to bring lower energy atoms or functional groups to the surface) or by adsorption of lower energy species to the surface. These mechanisms are very complex, and in the case of proteins involve attachment of different amino acid residues of the protein molecule to the sorbent surface. Whatever the mechanism and kinetics of adsorption, the process (at constant temperature and pressure) can occur only if the Gibbs energy G of the system decreases:

$$\Delta G_{abs} = \Delta H_{abs} - T\Delta S_{abs} < 0,$$

where, H, S and T refer to the enthalpy, entropy and absolute temperature, respectively, and Δ_{abs} indicates the change of the thermodynamic functions of state resulting from the adsorption.

Protein adsorption is the overall result of various types of interactions between the different components present in the system, i.e. the sorbent surface, the protein molecules, the solvent (water) and any other solutes such as low-molecular mass ions. Build-up of lysozyme, lactoferrin and albumin on the copolymers produced, are shown for both high and low water content polymers. It shows that lysozyme a small positively charged protein absorbs very rapidly, on high water content polymers. Absorption is also highly dependent on the polymers compositions with 1% crosslink density the water content are higher and the amount of lysozyme absorbed is about 2.5 times higher than the low water content polymers containing 10% crosslinker.

Aston University

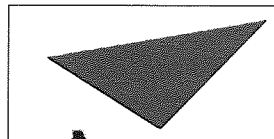

Illustration has been removed for copyright restrictions

Aston University

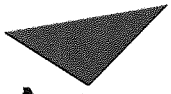

Illustration has been removed for copyright restrictions

Aston University

Illustration has been removed for copyright restrictions

Figure 7.10: Tertiary Structure of Protein Molecules (a) Prealbumin, (b) Ovalbumin,(c) Lysozyme and (d) Transferrin

The natural habitat of most proteins is an aqueous environment. When a protein solution contacts another phase (either a solid, liquid, or gas) with which it is immiscible, protein molecules tend to accumulate instantaneously at the interface between the two phases[146]. This tendency has a great effect on various natural and technological processes. The protein film which forms may then act as a substratum for subsequent adhesion of other components such as eukaryotic cells or micro-organisms.

The most basic level of protein structure, called the primary structure, is the linear sequence of amino acids. Different sequences of the acids along a chain, however, affect the structure of a protein molecule in different ways. Forces such as hydrogen bonds, disulphide bridges, attractions between positive and negative charges, and hydrophobic ("water-fearing") and hydrophilic ("water-loving") linkages cause a protein molecule to coil or fold. Figure 6.1 gives us geometric appreciation of the coiled structures produced for such molecules as (a) prealbumin, (b) ovalbumin, (c) lysozyme and (d) transferrin. Lysozyme is a tightly coiled sphere, whereas transferrin and ovalbumin posses two lobes and prealbumin is pyramidal in shape. Compared to lysozyme, lactoferrin is molecularly five times larger, with a lower charge distribution, and albumin is a magnitude larger than lysozyme with a smaller, negative charge density (Table 5.6 and 6.2).

Chemical structure of the monomer used for copolymerisation has a distinct effect on the behaviour of the protein spoilation levels, and locality. From the data obtained above it can be seen that material composition and type of protein have an effect on material absorption. This may be expected as it is the outermost surface atoms of a membrane (or implant) material that directly interface with the surrounding media. The absorption follows a pattern, where Group I materials (low water content, non-ionic) have a lower absorbance for all the proteins studied, compared to Group IV materials (high water content, ionic) (Figure 6.2). The trend with both material types is that a small, highly charged molecule, lysozyme, has a higher degree of attraction than (Figure 7.5(c) and Table 6.2), lactoferrin and then albumin.

In the case of lactoferrin (a positively charged, larger protein), the increase in the absorption of protein with the increase of MAA and water content is less pronounced and the quantities are much lower than lysozyme. Same applies for albumin. Due to the negative charge on albumin, the driving force to head for the surface of the lens is less but once having adhered to the surface, it shows signs of absorption, probably due to the hydrophobic interactions.

Protein	Ellipsoid Dimensions (Å)	Molecular Weight (kD)
Lysozyme	45 * 30 * 30	14
Lactoferrin	55 * 42 * 42	78
Bovine Serum Albumin	140 * 38 * 38	86
IgG	235 * 44 * 44	160
Fibrinogen	450 * 90 * 90	400

Table 7.3: Structural Parameters of Proteins[193-196]

The use of PEEMS technique show a dramatic contrast in the protein location. From these studies it was found that water content of the hydrogel affects most of its potential contamination by protein. Group II lenses have shown an affinity for protein which is greater than Group I, but significantly less than Group IV. However, the non-ionic polymer matrix prevents additional favourable interactions between the protein and the lens.

The PEEMS study confirms the all ionic PCLM materials are subject to protein penetration and the tear film stability has a clearly discernible effect on spoilation. PCLM materials are all subject to lipid penetration and in broad terms non-ionic PCLM materials resemble Group II materials. The PCLM lenses show lower levels of protein adhesion than typical Group IV lenses, with lower levels of tear debris penetration.

The PEEMS study of polyurethanes show protein adsorption levels to one tenth of that of Group IV materials, with lysozyme and lactoferrin adsorption and limited albumin absorption. There is no protein absorption detectable. PU are impenetrable to protein, and only undergo surface deposition. With a hydrogel, which consists of a water swollen polymer matrix, the concentration of 'pores' has a different physical meaning to that of the fixed pores of heterogeneous membranes. In hydrogels, pores are fixed neither in size nor location but result from the random movement of chain segments which may exhibit a high degree of mobility due to the plasticing effect of the water. The pores and channels in such systems are, therefore, in a constant state of flux.

Lipids in contrast to proteins, are non-water soluble and hydrophobic, and prefer the relatively hydrophobic environment of the polymer, to that of the aqueous tear layer. They therefore partition out of the tear layer into the hydrogel, as if being absorbed by a sponge. Because lipid cannot be measured by UV transmission techniques it is necessary to use surface fluorescence, which gives a useful additional check on the protein profiles. Take for example oxygen permeability: it indicates the proportion of oxygen that is dissolved or partitioned out of the atmosphere and into the lens material. In the case of hydrogels, the

oxygen is no more soluble in the water polymer part of the hydrogel at all. This is why the oxygen permeability of hydrogels is governed by water content.

Although the polymer segments of conventional hydrogels have low partition values for oxygen they have much higher partition values for organic molecules. This is because 'like dissolves like'. This migration process is substantiated by the fact that relatively hydrophobic steroids, such as progesterone, are some two hundred times more soluble in polyHEMA hydrogel than in water soluble sugar molecules of similar size such as sucrose. This was substantiated by the BRU [14] when they took hydrogel materials and exposed them to low concentration dye solutions for a period of time and then placed them in saline for several days. The colour of the lenses after exposure were more intense than the colour of the solution they were soaked in. This is because the dyes preferred the organic environment of the polymer rather than the aqueous environment of the solution, i.e. the partition value for the dye and the polymer is higher than the partition value for the dye and water. In the same way lipids with some water affinity and many other organic species are taken up into the hydrogel network. They cannot be seen by the naked -eye like the dyes as they have no light-absorbing or chromophoric groups. They do have implications for other spoilation processes.

7.3 Key Points

- Permeation through a polymeric membrane is a complex system dependent on a number of transport mechanisms, simple diffusion cannot explain the uptake mechanism.

- As in gas transport studies hydrophilic membranes have a reduced boundary layer effect compared to hydrophobic membranes

- Penetration is governed by the molecular weight of the penetrant and the degree of hydration of the polymer.

- The semi-permeability of porous hydrogel membranes is based on the spatial cross section of the permeating species, i.e. small molecules exhibit a higher permeation rate than large molecules, and linear chain molecules permeate better than those with a globular shape.

- The permeating species interact chemically with a dense polymer matrix and selectivity dissolve in it, resulting in a diffusive mass transport along a chemical potential gradient.

- Data analysis shows for both *in vitro* and *in vivo* studies protein uptake per lens can be of the order of 1mg and that protein concentrations in the narrow penetration band can reach levels of around $300mg/cm^3$ (concentration of protein in tears is approximately $10mg/cm^3$).

- Another key aspect of data analysis concerns the apparent depth of penetration. Etched samples reveal that protein penetration depth is typically 10 to 30 etches, which equates to 3.6 - 10.8 μm.

- Increased hydrophobicity of the system minimises the driving force for penetration (Section 6.3.12).

- Data analysis suggests that penetration is restricted (Section 7.2.4).

- Fluorescence Spectroscopy is able to show localised protein and lipid penetration, whereas UV/visible spectroscopy can give residual and localised protein penetration, (Section 7.2.3).

Chapter 8

Advances in PEEMS and Future Work

8.1 Introduction

Traditionally, the plasma etch processes employed in the microelectronics industry have relied on a stable and well - characterised process for repeatable automatic operation. Due to the inherent complexity of the process, few processes had this stability. Even fewer machines actually had the required sophistication of control systems to ensure repeatable operation, with process termination being determined using an etch timer or by eyeball from the operator. PEEMS proved successful in analysing the amount of protein present and the depth of penetration; relying on gravimetry to assess the 'end-point'. By successively removing small quantities of material from the surface of the sample (Chapter 4-7), information on the amount of spoilant attracted to the sample's surface and matrix were ascertained using extrinsic and intrinsic surface characterisation techniques (e.g. UV and fluorescent spectroscopy). Interesting information about protein and lipid location and concentration were obtained, but PEEMS was not been able to yield any further data on protein and lipid competition, heterogeneity or conformation at the biological-material interface (Chapter 3). For example, if a solution contains a displacer or any other protein with molecules that have an affinity for absorption any desorbing segment can be replaced by another. Desorption of the molecule is now virtually an exchange process and the Gibbs energy for exchange is lower than that of the Gibbs energy for desorption ($\Delta G_{exchange} < \Delta G_{desorption}$) the process is more likely to occur. Brash[199] reported examples of exchange between adsorbed and dissolved protein molecules upon dilution where desorption did not take place. It is the competitive processes, which will eventually correlate with such phenomena as blood coagulation, cell adhesion and so providing us with a more representative model of processes occurring at the biological interface. One hyphenated technique considered early on to help answer some of the questions generated by PEEMS was based on Optical Emission Spectroscopy (section 8.2) although theoretically workable practically this proved to be difficult. In conjunction to the glass-PEEMS based system, was a high vacuum system produced by co-workers[163] with a reduced volume reaction chamber (Chapter 4) that was envisaged as a starting base for further investigative work.

reduced volume reaction chamber (Chapter 4) that was envisaged as a starting base for further investigative work.

8.2 Optical Emission Spectroscopy

Optical emission spectroscopy (OES)[211-214] is one of several optical diagnostic techniques for plasma discharges. It has the advantages of being non-invasive, capable of operating in real-time, and of being relatively straightforward to implement. The emissions from a plasma are characteristic of those species present in an excited state. OES is used to record the intensity of those emissions as a function of wavelength, most usually in the UV/visible region. The resultant spectra (Figure 8.2) may, if they have suitable emission, be fully analysed to unequivocally identify atoms, ions, free radicals and molecular species (Table 8.1) present in the plasma. However, the vast majority of species are present in their ground state, and the relationship between emission intensity and ground state concentration is not straightforward. If a species can be pin-pointed within the reaction chamber then a decay curve can be generated for the lifetime of this species (Figure 8.3).

Species Monitored	Wavelength (nm)	Reference
CN*	387.1	79
N_2*	337.1	79
N*	674	78
CO*	483.5	79
CO*	519.5	79
OH*	308.9	78
H*	656.3	78

* indicates a species in an excited state.

Table 8.1: Common species and emission wavelengths

Within the above mentioned groups using OES, it is usually straightforward to follow qualitative changes in discharge properties. However, the minute concentrations of species evolved when etching a small cross-sectional area of 1.4cm^2 within a vessel of volume 100cm^3 is hardly above that of background levels. To overcome this as the technique proved reliable and uniform it was considered feasible to etch on mass to see if concentrations were of a detectable level. Reasonable results were obtained if approximately 22 lenses were placed within the chamber, (21 arranged in three's on the grounded electrode

and one on the cradle of the micro-force balance). This would allow maximum coverage of etchable area without causing loading effects. Peaks were observed for CO*, OH* and NO*. Unfortunately time was not permitting to follow up enhancement techniques which are addressed in Section 8.3.

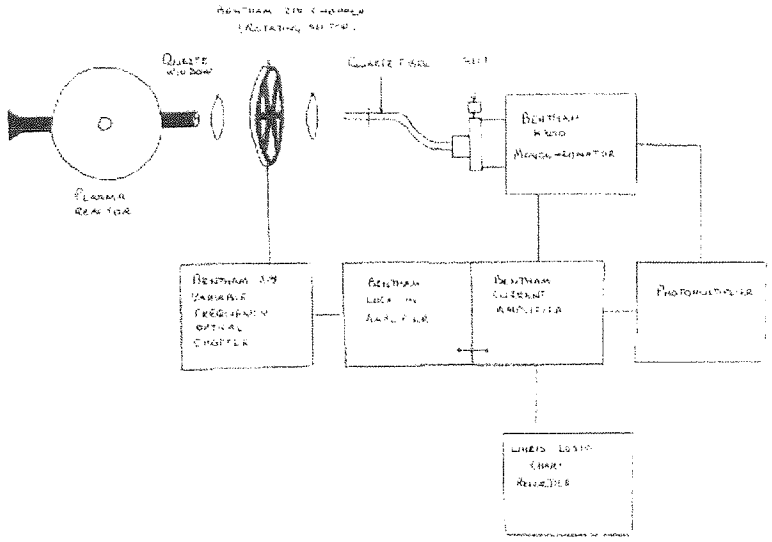

Figure 8.1: Schematic Representation Of Optical Emission Spectrometer (OES) Laboratory Set-up

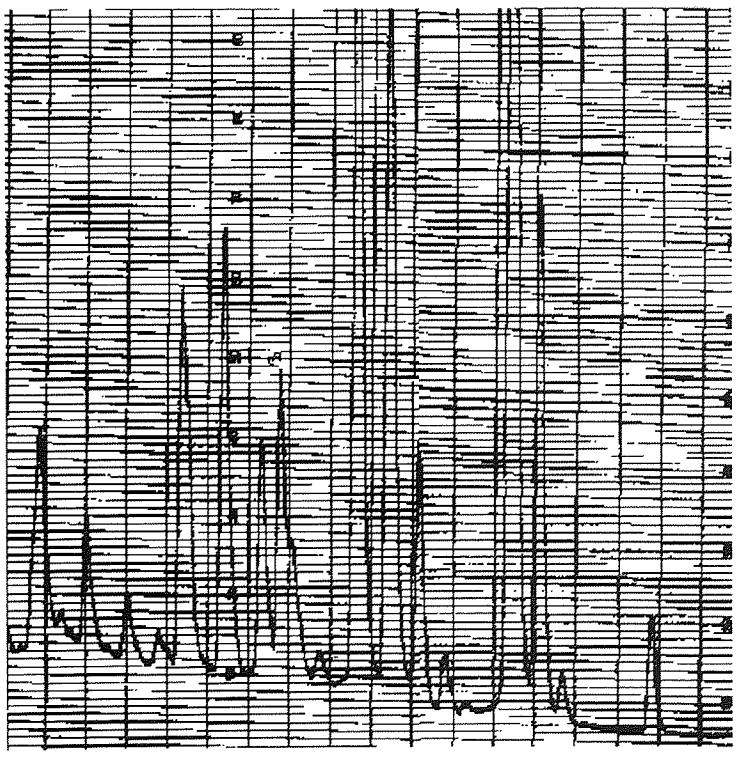

Figure 8.2: Typical Output from OES for an Acuvue Polymeric Contact Lens (unspoilt)

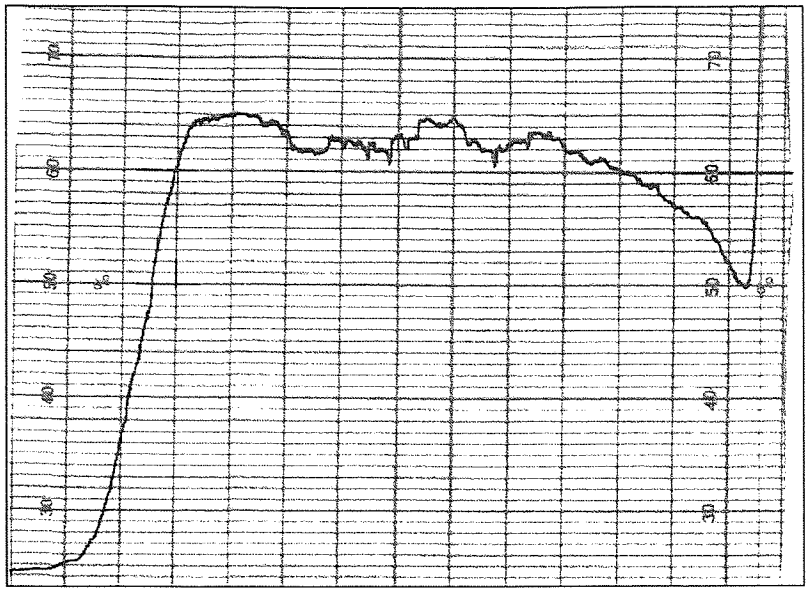

Figure 8.3: Typical Decay Curve Measured at 208nm for CO*

8.3 Enhancement Techniques

Many techniques are available as diagnostic techniques for plasma systems[217-220] such as OES. This section discusses other possible methods available that may help in assessing the breakdown products from a glow discharge.

8.3.1 Actinometry

Harshberger et al[163] first used OES to study silicon and silicon nitride etching in CF_4-O_2 mixtures. They found that oxygen additions to a CF_4 plasma enhanced the etch rate of these materials by the liberation of atomic fluorine. Their results, though, were qualitative as the emission intensity of an excited species is a function of both its ground state concentration and the electron energy distribution function (EEDF) of the plasma. The EEDF may very with changes in the plasma parameters. In order to overcome this problem, Coburn and Chen[122] devised a method, referred to as 'actinometry', for correlating emission intensities to reactive particle density. It involves the deliberate addition of a small constant amount of noble gas, the actinometer, to a plasma and monitoring the noble gas emission concurrently with those of the reactive particle. If the excited state is responsible for the noble gas emission matches closely in energy with the level of the reactive particle, then the same group of electrons will be responsible for the excitation of both levels. By comparing the emission intensities from the actinometer and reactive particle, the relative changes in ground state concentration of the latter can be assessed. Ideally the excited states should also be produced by direct electron impact only, and decay exclusively by photoemission. Coburn and Chen applied their method to atomic-F (703.7 nm; 14.5 eV) with argon as an actinometer (750.4 nm; 13.5 eV).

In practice, it may be possible for actinometry to be used even when the above conditions are violated. For example, d'Agostino[107,216] et al studying the CF_4-O_2 system validated the use of argon actinometry for the measurement of F, O, CO and CO_2 concentrations from emitting levels in the range 8-20 eV by comparing two actinometers Ar (750.4 nm; 13.5 eV) and N_2 (380.5 nm; 11.5 eV). The trends in the two actinometers were coincident, implying that their relative emission intensities were proportional to the electron density in a broad energy range. The technique was similarly extended to CF_2 (4.5 eV).

Argon actinometry for the determination of O-atom concentrations in CF_4-O_2 plasma has been tested directly using two-photon induced fluorescence (LIF) by Walkup et aldb70. They found that at high O_2 concentrations the O(844.6 nm)/Ar (750.4 nm) intensity ratio followed the changes in O-atom concentration observed by LIF but the O(777.4 nm)/Ar(750.4 nm) ratio did not. Both O(777.4 nm) and O(844.6 nm) are produced by direct electron impact excitation of atomic oxygen and dissociative excitation of molecular oxygen. However, the O(844.6 nm) emission line is a much better indicator of O-atom concentration than the O(777.4 nm) emission line because the cross section for direct excitation of O(844.6 nm) is much larger than that for O(777.4 nm) whereas the opposite is true for the dissociative excitation cross section.

Coburn and Chen also used OES with argon actinometry to study changes in relative fluorine-atom concentration in a CF_4 discharge as a function of pressure and flow rate. In their pressure dependence studies, they kept the CF_4 and Ar flow rates constant and varied the chamber pressure by adjusting the pumping speed. The procedure ensured that the percentage of Ar in CF_4 remained constant, but allowed the total Ar pressure to increase with the CF_4 pressure. In order to have a reference Ar emission is constant Ar density the Ar emission data was divided by the Ar pressure.

8.3.2 Laser Induced Fluorescence

To gain more quantitative information about plasma processes, an optical technique such as laser induced fluorescence (LIF) can be employed. LIF has the advantage that it can directly detect ions, molecules and atoms which are in the electronic ground state. LIF combines the high spatial and spectral resolution of a laser technique with the high sensitivity, which allows the detection of low concentrations of reactive radicals and ions.

This method uses a tuneable dye laser beam to pass through a discharge chamber and resonantly excite atoms or molecules, which subsequently fluoresce. A significant limitation of this approach is that the targeted species must fluoresce with a reasonable quantum efficiency. This is not necessarily true for the larger polyatomic molecules

which are present in plasma. Background light must also be kept to a minimum when using LIF and discharge emissions as well as scattered laser light can cause problems. A LIF spectrometer also relies on a laser source of an appropriate wavelength being available to match the spectroscopic transition of the species to be detected. This is not always possible.

8.3.3 Optical Reflection

Optical reflection makes use of either the differences in reflectivity of an a incident light source at a material layer boundary, or it looks at the interference effects in the thin film being etched. In the optical reflection mode, the change in reflectivity is monitored as a function of time. As the boundary point is reached, there is a change in the intensity of the reflected signal. The magnitude of the change is proportional to the ratio of the material layers which are encountered. If a film is transparent, then the reflected intensity various approximately sinusoidally as the interference conditions vary with decreasing film thickness. The periodicity of the reflected signal against time plot varies with the both the etch rate and the refractive index of the film being etched.

This type of diagnostic implementation is highly suitable for endpoint detection and various different forms of this technique have been successfully used. Both coherent and non-coherent light sources have been employed with in-situ laser interferometry emerging as one of the most common systems.

8.3.4 Mass Spectrometry

Mass spectrometer[220-225] seems to have similar sensitivity to OES but can provide more information on ions, radicals and polyatomic molecules within the discharge. One of the major advantages is that when operating as a neutral sampler, mass spectrometry allows process control and monitoring to be implemented before the discharge has been struck.

Mass spectrometers are used to measure the ratio of mass to electric charge of a molecule or atom. They can be used in several ways to monitor glow discharges:

(i) Analysis of the discharge gas without line of sight to the chamber. This includes sampling of the exhaust gas with the spectrometer mounted in the pumping line between the chamber and the pumping system; and sampling through a controlled leak valve from the chamber. This set-up is relatively simple to install but does not allow reactive species detection. There is a time lag involved between the chamber process reactions and the

neutral species detection, with the result that endpoints tend to be non-reproducible or non-existent. Some researchers have reduced the time delay and increased the sensitivity by sampling through a small quartz capillary tube which was directly attached to the spectrometer probe head. Reactive species could be detected using this technique despite its markedly invasive nature.

(ii) Line of sight sampling of neutral species. This set-up allows the detection of reactive species, but is not very sensitive. The major disadvantage is that mounting the apparatus is very complex in terms of cost and modifications to the etching machine. Line of sight neutral sampling is most often used to provide information for basic studies of plasma chemistry.

(iii) Direct sampling of positive ions which is also known as in-situ SIMS[217]. This is a very high sensitivity technique which has previously been used for ion-molecule reaction studies and to characterise the discharge[219]. However, the apparatus required is complex and the ions sampled are not representative of the neutral species concentrations[225].

Mass spectrometry usually consists of three stages, ionisation, mass separation and detection. Various methods have been used for each of these stages. The most sophisticated spectrometers are capable of differentiating small fractional mass differences. Most commonly implemented are systems which can resolve peaks which are 1 amu apart. These systems are often referred to as residual gas analysers (RGA).

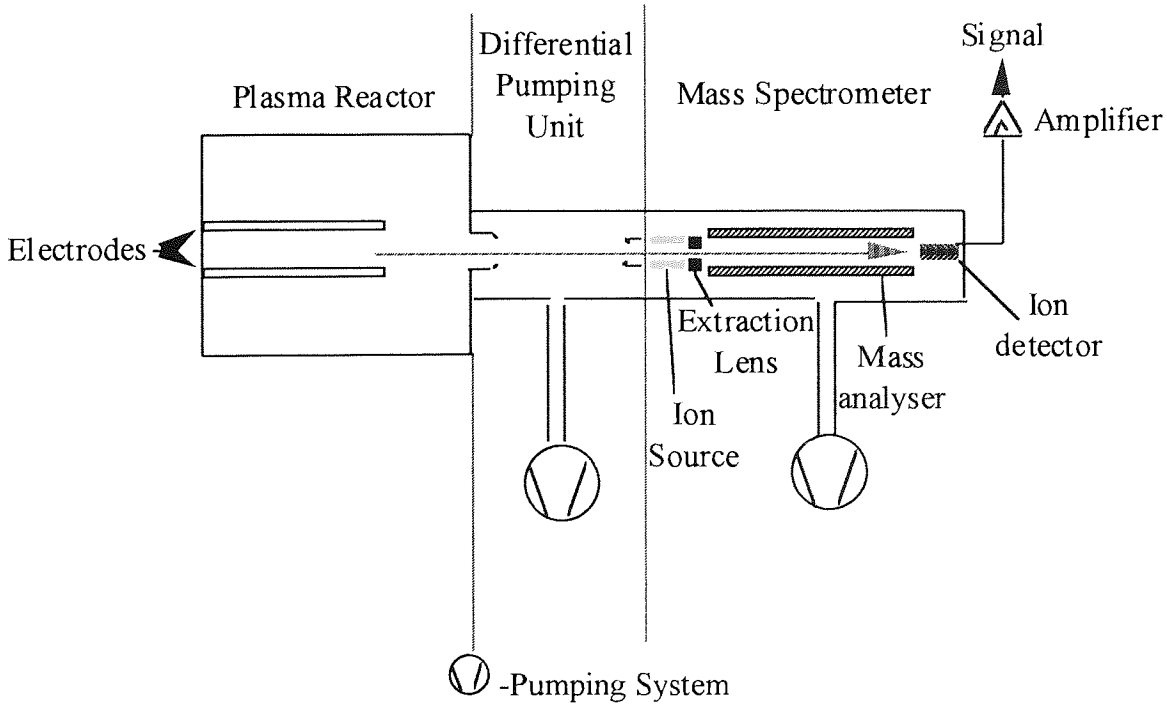

Figure 8.4: Schematic View of Mass Spectrometer set-up for Plasma Diagnostics

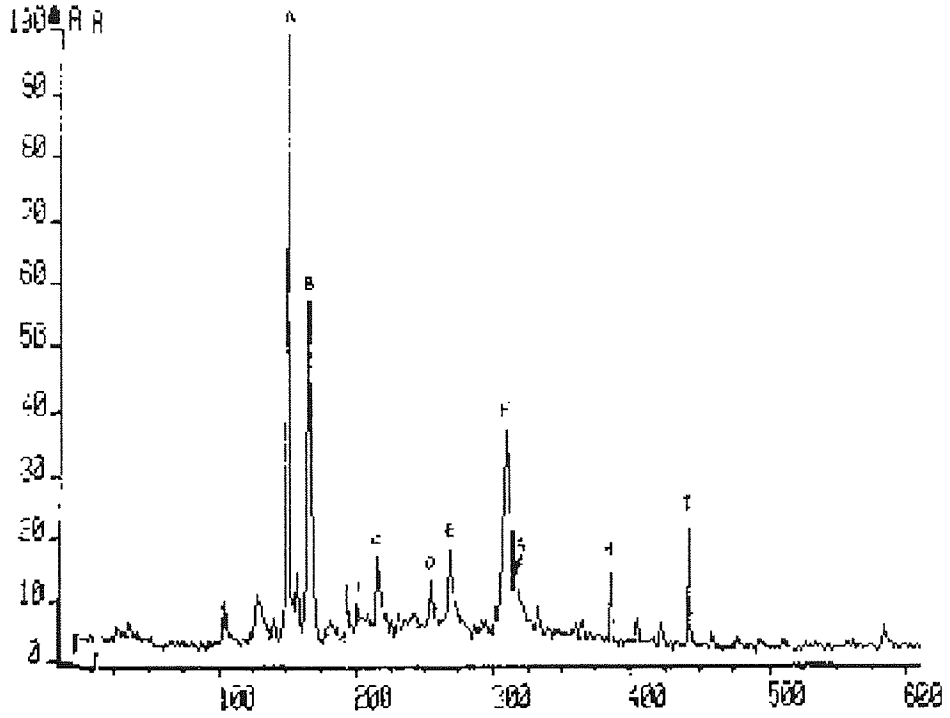

Peak	Scan No.	Assignment
A	150	A C8 phenol
B	166	A C8 phenol
C	215	A C12 phenol
D	254	Dibutylphthalate
E	268	Palmitic acid plus alkyl phenol
F	310	Linoleic acid
G	316	Stearic acid
H	385	di-2-ethylhexyphthalate
I	442	Aliphatic alcohol

Figure 8.5: MS Total Ion Chromatogram for Lipid Deposit

A schematic view of the stages involved in mass analysis is shown in Figure 8.4. Ion production is almost always implemented by electron impact ionisation. Electrons from a hot filament cross the chamber to an anode and collide with gas molecules as they cross. This creates positive ions. The next stage of the analysis is a mass separation of the ions, using either a magnetic sector or a RF quadrople. The magnetic sector technique accelerates the ions through a uniform magnetic field which then separates the different mass to charge ratios. The Quadrople technique uses four electrodes to filter the different masses one pair of electrodes in the Quadrople acts as a low pass filter. A more comprehensive review of these techniques is beyond the scope of this work but is

available[102]. Detection is typically carried out using a combination Faraday cup - electron multiplier arrangement.

Each gas species has a unique mass/charge ratio, while the peak amplitudes are dependent on the gas and instrumental conditions. The different peaks which can be obtained from a gas sample are created primarily by isotopic mass differences, multiple ionisation and dissociative ionisation. The particular species which are monitored during the process depends on the etching equipment used, the way in which the mass spectrometer has been employed, the gas chemistry, and the layer(s) to be etched. Figure 8.5 shows lipid analysis using a mass spectrometer, similar interpretations are expected for our system.

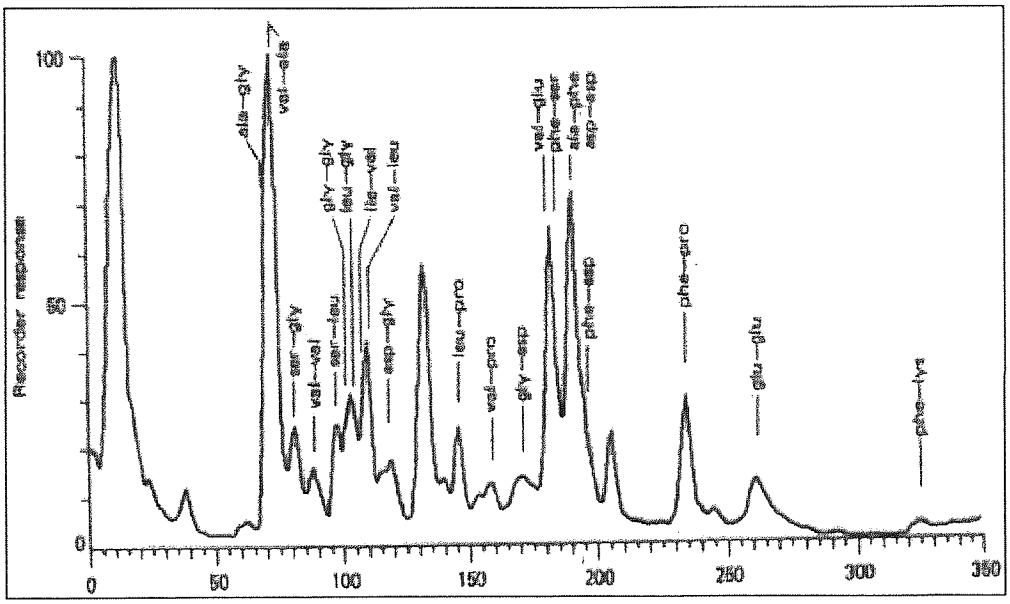

Figure 8.6: Mass Spectrum of Spinach analysed down to it's amino acid constituents[225]

Mass spectrometry appears to have similar sensitivity to OES but can provide more information on ions, radicals and polyatomic molecules (e.g. lipids and proteins) within the discharge. One of the major advantages is that when operating as a neutral sampler, mass spectrometry allows process control and monitoring to be implemented before the discharge has been struck.

This particular technique was envisaged as a possible way forward for future work. A photograph of the system employed is shown in Figure 8.7. This is a modified set-up, originally used by Dr. S Moss and Graham Allison for plasma deposition studies. The system consists of a plasma reactor with controlled and monitored pressure, gas flows, electrode temperature and radio-frequency power supply.

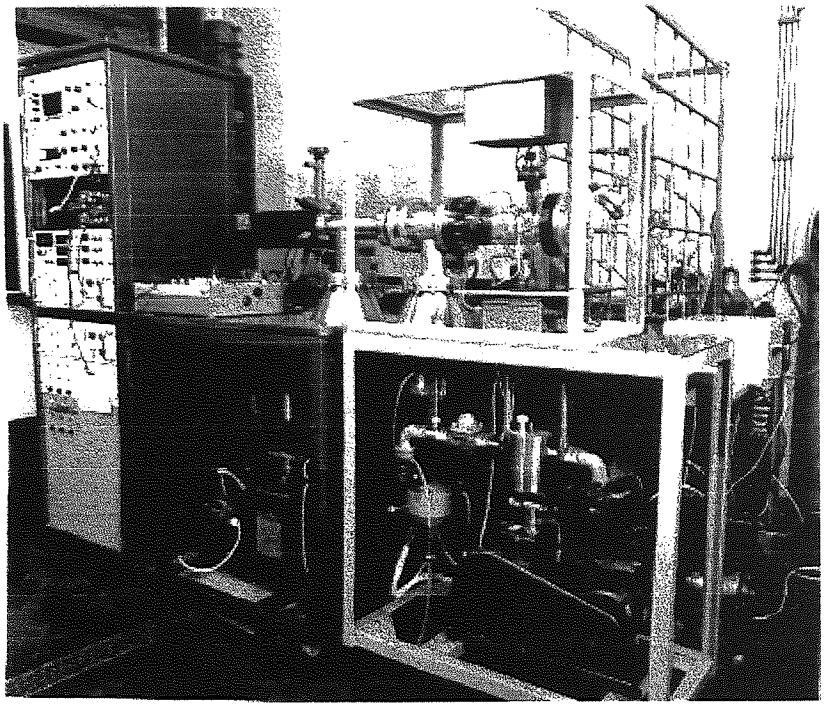

Figure 8.7: Photograph of Laboratory Set-up for a Pulsed-Plasma Discharge linked to a Quadrople Mass Spectrometer

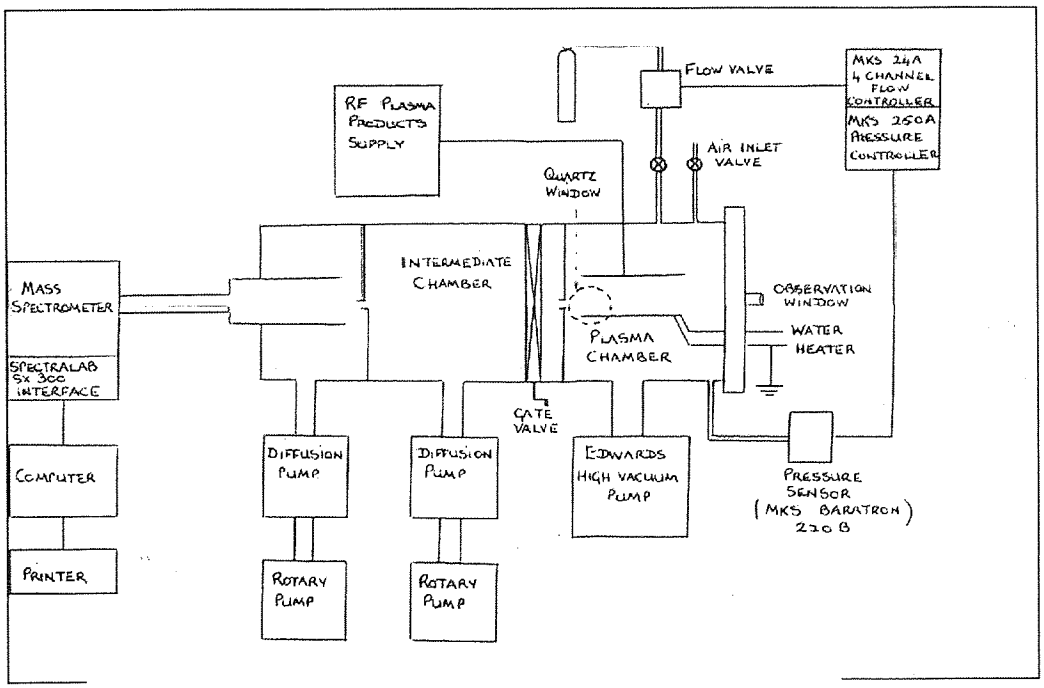

Figure 8.8: Schematic of Mass Spectrometer and Plasma Equipment

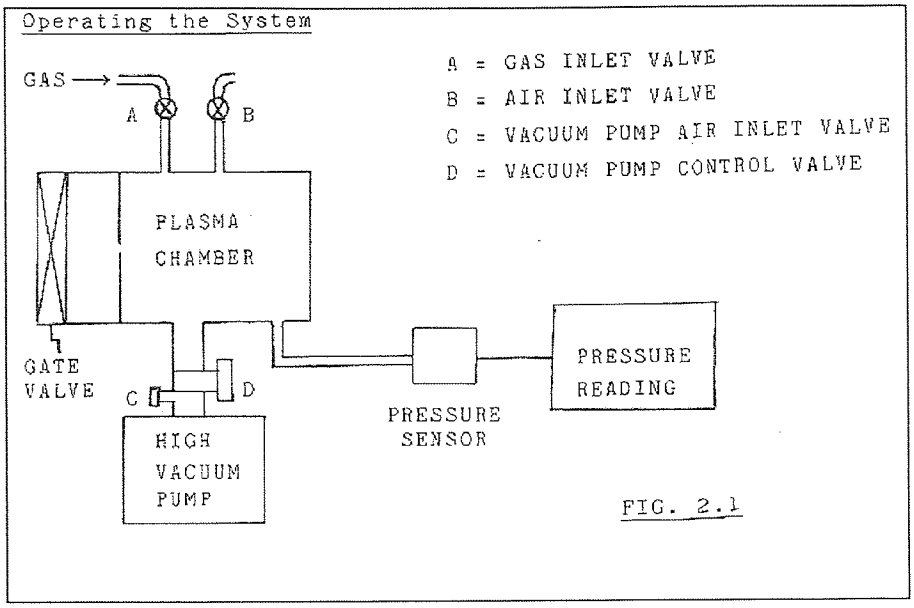

Figure 8.9: Gas Handling and Pressure Control

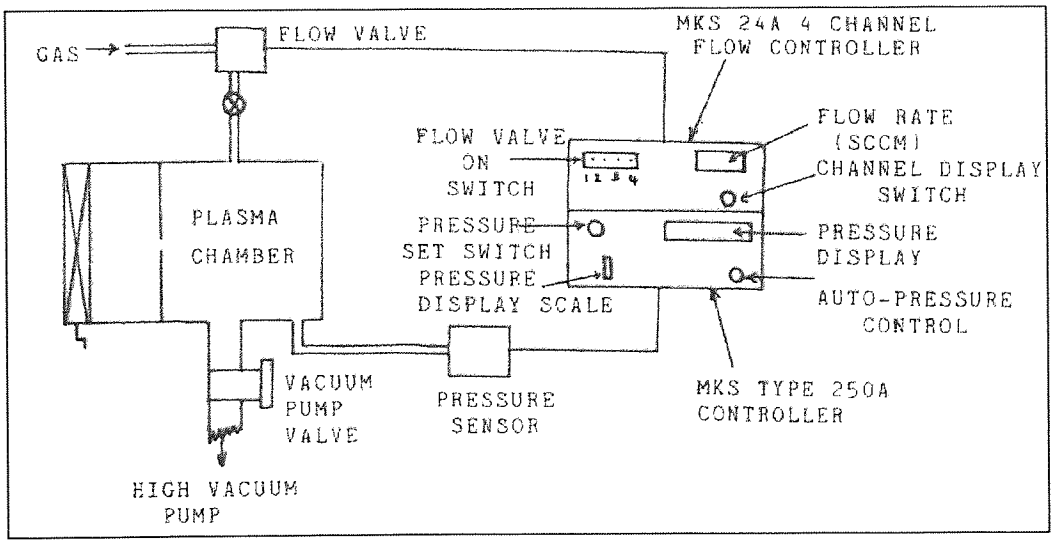

Figure 8.10: Gas Flow Controller for Plasma Etching

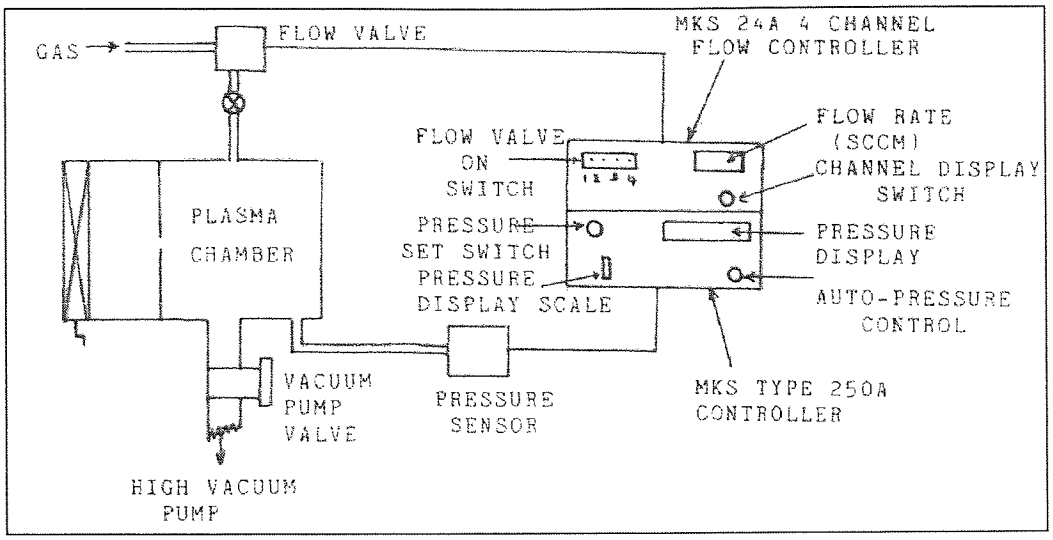

Figure 8.11: Species Detection Using the Mass Spectrometer

The system is quite complex and initially sensitive to commission. The Mass Spectrometer will only operate at pressures $< 10^{-6}$ torr and as the plasma chamber usually operates at ~0.1 - 1 torr, the intermediate chamber (at $< 10^{-4}$ torr) acts as a transition stage. It prevents the pressure in the mass spectrometer rising to a value $> 10^{-6}$ torr by a pressure surge through the pin-hole from the plasma chamber, when the gate valve is opened.

The mass spectrometer detector and the pin-holes are all aligned, therefore a collimated beam is produced which gives greater sensitivity. N.B. The number of species detected depends on the width of the second pin-hole and the distance between the pin-holes.

Atoms and molecules pass out of the plasma chamber and those travelling in a parallel direction pass through the second pin-hole into the mass spectrometer detector and are ionised. The ions are accelerated down the mass analyser and only species with appropriate m/e ratio are detected by the multiplier or faraday cup. The output from the detector is then passed into the electronics of the mass spectrometer.

8.3.5 Other Techniques

Many other techniques have been used to monitor boundary changes in plasma processes. These include discharge impedance monitoring; optogalvanic spectroscopy; pressure monitoring; absorption spectroscopy and chemiluminescence.

Discharge impedance monitoring is useful for boundary detection as it monitors the change in impedance across the plasma as layer boundaries are reached. Optogalvanic spectroscopy monitors the change in discharge characteristics (current, voltage, electron density) which are induced by the absorption of light. One of the simplest techniques is the monitoring of chamber pressure, although the usefulness of this technique has been reduced by the easy availability and widespread use of constant pressure control systems. Absorbance spectroscopy in the infra-red, visible or ultra-violet can allow detection of ground state species. Information regarding the absorbance coefficients can be obtained from the species that do not fluoresce or give rise to an optogalvanic effect, but the sensitivity is limited. Chemiluminescence is a downstream technique which detects the emission of light from the reaction products of a chemical reaction, and is used primarily to study heterogeneous reaction mechanisms.

Chapter 9
Conclusions

When a contact lens is placed in contact with the tear film, the lens immediately becomes coated with biological debris. This is not necessarily bad, because it can contribute to improved biocompatability of the contact lens. Thus, the problem is not that a contact lens adsorbs biological species, but the build-up that occurs thereafter. The nature of the initial adsorption is influenced by a combination of factors related to the contact lens, such as the smoothness of the contact lens surface, the surface charge, the wettability, the chemical structure of the polymer surface, the elasticity of the lens material, and other factors such as tear flow and rate of blinking.

At the outset of the project the ultimate aim was to attempt to establish a technique based on gas plasma etching, that would aid in the understanding of the matrix-surface deposition process, since these patterns are believed to influence the more troublesome contact lens complications e.g. GPC, along with less significant, although no less clinically important, problems such as lens wear discomfort.

The absorption of tear proteins to hydrogel contact lenses is a complex phenomena which includes the diffusion of the protein particle through the aqueous solution and the collision and interaction of the protein at the interface. In the case of small proteins with charges opposite to the high water content hydrogels the primary absorption is followed by the penetration of the protein into the hydrogel matrix. The protein absorption depends on many factors such as the protein concentration, protein type, size and charge, the chemical structure of the sorbent surface. Temperature and the pH of the spoilation solution also influence the absorption, as the pH affects the charge of the protein and the hydrogel surface.

This work suggests that it is primarily the ionic nature of a hydrogel and secondarily its water content that determines the extent of its potential contamination by proteins. After the protein has been permeated the water of the lens, favourable polar interactions with an ionic polymer matrix further enhance the deposition process. Thus, the Groups I and

II lenses show relatively little protein deposition due their non-ionic nature. Group II lens materials shows higher protein deposition compared to Group I due to its higher water content, but shows lower deposition compared to a Group IV which is also ionic. Group IV lenses are able to absorb relatively large amounts of protein because of their ionic character and high water content. In the case of group IV lenses, once the protein has permeated the lens, the chances of its remaining are enhanced by binding to the ionic polymer matrix.

The following conclusions are made about the absorption of the proteins to various hydrogel materials:

- The use of the PEEMS technique shows dramatic contrast in protein location.
- PEEMS can additionally be used to monitor lipid absorption.
- All materials studied are subject to lipid penetration to a similar extent.
- The uptake of different proteins into the matrices of Group IV lenses is greatly influenced by the charge and size of proteins.
- Lysozyme and lactoferrin adsorb onto the surface of Group IV materials to a higher degree compared albumin which is adsorbed to a lesser extent.
- Lactoferrin, as well as lysozyme, penetrates into the matrix of Group IV lenses despite its greater size.
- Lysozyme is mobile and can be leached out of the matrices of Group IV lenses stored at pH > 7.
- The biological activity of lysozyme shows no marked change during absorption, but is reduced by 20% on material preparation in the PEEMS technique (i.e. microwave dehydration and etching).

- Polyurethanes show protein adsorption levels to one tenth of that of Group IV materials, with lysozyme and lactoferrin adsorption and limited albumin adsorption. There is no protein absorption detectable.

- The higher the molecular weight of PEG in the PEG: PTMO system, the greater the water contents.

- The greater the molecular weight of PTMO, the greater the protein deposition.

- Increasing the concentration of PTMO in the copolymer increases the protein adsorption.

- The higher the molecular weight of PEG and PPG in the PEG: PPG system, the higher the water content.

- Molecular size did not make a significant difference in protein deposition for PPG: PEG copolymers. An increase in water content resulted in an increase in lysozyme absorption/adsorption levels.

- Increasing the concentration of PEG increased the protein adsorption, but increasing the concentration of PPG decreased the protein adsorption.

- PU are impenetrable to protein, and only undergo surface deposition within the scope of this study.

- Tear film stability is clearly discernible within a penetration profile.

- Non-ionic PCLM materials resemble Group II materials, with no protein penetration, as PU.

- A simple diffusion model cannot be employed to describe the absorption principles occurring in a hydrophilic polymer. The system has many parameter complexities. Although there is no conclusive proof of the mechanism occurring without further

experimental data, a hypothesis can be presented from the data produced and basic engineering principles of permeability as described in Chapter 7.

- Typical depth of penetration of a Group IV materials is 4 microns on the anterior surface and 6 microns on the posterior surface.

- Calculations suggest that penetration is restricted. Both *in vivo* and *in vitro* studies reveal that protein (lysozyme) uptake is of the order of 1mg per lens. This is equivalent to an average protein concentration throughout the lens of 1/0.0036 = 28mg/cm^3, and to an average protein concentration in the penetration zone of 360mg/cm^3.

Suggestions for Further Work

Arising from the experimental work carried out in this thesis and the results obtained some suggestions can be made for future work:

◊ Enhancement of OES within PEEMS and within the Pulsed Plasma Discharge - Mass Spectroscopy system would yield complimentary data for surface absorption studies. A potential link between the process parameters and etch quality is most readily provided through an understanding of the plasma chemistry- both gas-phase chemistry and gas-surface interactions. Had the system had a reliable OES system up and running, it would have been interesting to assess the chemical processes occurring i.e. concentrations of components altering as power, flow rate and pressure are altered.

◊ The extraction methods used here only extracted up to 65 % of the proteins while it may be possible to extract most of the proteins using a mixture of the extraction solvents and care methods.

◊ Some copolymers with positive charged surfaces should be synthesised and their protein up-take monitored, as well as reviewing other novel copolymers which was touched upon in Chapter 6.

◊ The negative charges on the Group IV lenses can be neutralised by pre-soaking the lens in acidic solution before it is worn. Some *in-vitro* experiments should be carried out to examine the lens characteristics after soaking in acidic solution.

◊ It has been shown that the activity of lysozyme is unaffected due to different experimental conditions and concluded that lysozyme is a stable enzyme. The biological activity of other tear proteins such as lactoferrin should be measured. Lactoferrin can also penetrate into the matrices of high water content anionic contact lenses and, therefore, its stability can be important.

◊ Most of the clinical studies were carried out for short periods. Therefore their reproducibility was not assessed. Some clinical studies should be done over longer periods (such as one year) to show the accuracy and reproducibility of the results.

◊ Tear analysis undertaken along with PEEMS analysis could help review data due to patient variation.

References

1. Andrade J. D., Surface and Interfacial Aspects of Biomedical Polymers, Plenum Press, New York, 1985.

2.Kane P. F., Larrabee G. B., Characterisation of Solid Surfaces, Plenum Press, New York, 1974.

3.Williams D. F., Fundamental Aspects of Biocompatability, Vols. I and II, CRC Press, Boca Raton, FL, 1981.

4. Tripathi R. C., Tripathi B. J., & Ruben M., The Pathology of Soft Contact Lens Spoilage, Opthalmol, 87, p. 365-380, 1980.

5. Allansmith M. R., Immunologic Effects of Extended Wear Contact Lenses, Ann. Ophthamol, 21:465-474, 1989.

6. Franklin V. J., Horne A., Jones L., Tighe B. J., Early Deposition Trends on Group I (Polymacon and Tetrafilcon A) and Group III (Bufilcon A) Materials, CLAO J., 17(4):244-248), 1991.

7. Franklin V. J., Bright A., Pearce E., Tighe B. J., Hydrogel Lens Spoilation:Part5: Tear Proteins and Proteinaceous Films, Optician, 5367(204):16-22, 1992.

8. Lyman D., "Biomaterials", Encyclopaedia of Polymer Science and Engineering, Wiley & Sons., USA., 1985, Vol. 2, p. 267 - 286.

9. Lowther G. E., Hammack G. O., Wissner S., Alvord L, Quantification of Visible Deposits on Hydrogel Contact Lenses, ICLC, 18:219-225, 1991.

10. Bilbaut T., Gachon A. M., Dastugue B., Deposits Discovered On Soft Contact Lenses: Electrophoresis And Scanning Electron Microscopic Examination, Expt. Eye Res., 1986; 43:153-165.

11. Willard H. H., Merritt L. L., Dean J. A., Settle F. A., Instrumental Methods of Analysis, 6th Edition, Wadsworth Pub. Co., Belmont, California, 1981.

12. Sack R. A., Jones B., Antignani A. et al, Specificity and biological activity of the protein deposited on the hydrogel surface, Invest. Opthamolocial Sci., 1987; 28:842-849.

13. Myers R., Larsen DW., Tsao M., et al, Quantity of Protein Deposited on Hydrogel Contact Lenses and its Relation to Visible Protein Deposits, Optom. Vis. Sci., 1991, 68: 776-782.

14. Allansmith M. R., Korb D. R., Greiner J. V., Henquez A. S., Simon M. A., Finnemor V. M., Giant Papillary Conjunctivitus in Contact Lens Wear, Am. J. Ophthamol., 1997, 83:697-708.

15. Readers' Digest Eurodata -Consumer Survey of 17 European Countries - Personal Products, The Readers' Digest Association Ltd., London, 1991, p.214-215, tables 144-145.

16. Ratner B. D., Hoffman A. S., American Chemical Society Symposium Series, 31:1, 1976-5.

17. Fowler S. A., Korb D. R., Allansmith M. R., Deposits on Soft Contact Lenses with various water contents, CLAO J., 1985; 11:124-127.

18. Office of Dentistry, Dental Implant Registry History and Findings, Int. Jour. Oral Implant., 1991:8(1), 81-93.

19. Paavolaninen P. et al, Registration of Orthoplastics in Finland, Acta Orthopaedica Sacndinavica Suppllementum, 1991: 241, 27-30.

20. Bruck, S. D., Biomaterials, Medical Devices, Artificial Organs, 1973:1, 79.

21. Ratner, B., Biomedical Applications of Synthetic Polymers, Encyclopaedia of Advanced Materials, 1991.

22. Tighe B. J., Towards the Bionic Man, Biomaterials, 1987:7, 204-210.

23. Goldie I., Total Hip and Knee Replacement, Acta Orthopaedica Scandinavia Supplementum, 199:241, 23-26.

24. Tighe B. J., "Hydrogels as Contact Lens Materials", Hydrogels in Medicine and Pharmacy, CRC Press, 1987.

25. Williams D. F., Biomaterials and Biocompatability In Fundamental Aspects of Biocompatability, CRC Press, Florida, 1981.

26. Ratner, B., Biomedical Applications of Synthetic Polymers, Encyclopaedia of Advanced Materials, 1991, 7, p202.

27. Piskin R., Biodegradable Polymers as Biomaterials, J. Biomater. Sci. Polymer Ed., 1994, Vol. 6, No. 9, p. 775-795.

28. Tighe B. J., Towards the Bionic Man - a new biomedical technology?.J. Biomedical Technology, p.186-192.

29. Phillips A. J., Stone J., Contact Lenses, Butterworths, London, 3rd edition, 1989.

30. Larke J. R., Tears and Lens Deposits, The Eye in Contact Lens Wear, Butterworths, London, 1985, 22-51.

31. Meadows D. L., Paugh J. R., Use of Confocal Microscopy to Determine Matrix and Surface Protein Deposition Profiles in Hydrogel Contact Lenses, CLAO Journal, 20(4): 237-241, 1994.

32. Corkhill PC., Fitton JH., Tighe BJ., Towards a Synthetic Articular Cartilage, J. Biomaterial Sci., Polymer Ed., In Press.

33. Corkhill P. H., Hamilton C. J., Tighe B. J., The Design of Hydrogels for Medical Application, Critical Reviews in Biocompatability, 5(4), 392-395, 1990.

34.

35. Smith MEB., Design and Synthesis of Novel Hydrogels for Biological Applications, PhD thesis, Aston University, 1994.

36. Wilson G., Bachman WG., Call PL., A Nutritional Role for Tears, The Pre-Ocular Tear Film, ed. Holly F., Dry Eye Institute, Texas, 1996.

37. Farris RL., Tear Osmolarity in Contact Lens Wear, The Pre-Ocular Tear Film, ed. Holly F., Dry Eye Institute, Texas, 1996.

38. Holly F. J., Tear Physiology and Contact Lens Wear II. Contact Lens-Wear Film Interaction, Am. J. of Optom. Physiol. Opt., 58:331-341, 1982.

39. Marshall E. C., Begley C. G., Nguyen C. H. D., Frequency of Complications among Wearers of Disposable and Conventional Soft Contact Lenses, ICLC 19:55-60, 1992.

40. Baker D. et al, "Polymers In Contact Lens Applications (VIII), The Problem of Biocompatability", Contact Lens Journal, 3-14.

41. Franklin V. J., & Tighe B. J., Hydrogel Lens Spoilation: Deposit Formation and the Role of Lipids, Optician, 202:5305, 19-25, 1991.

42. Franklin V. J., & Tighe B. J., Hydrogel Lens Spoilation: The Structure and Composition of Surface Films and Plaques, Optician, 1991.

43. Franklin V. J., & Tighe B. J., Hydrogel Lens Spoilation: Discolouration and Staining Processes Within the Lens Matrix, Optician, 16-22, 1991.

44. Bright A. M., Tighe B. J., The Composition and Interfacial Properties of Tears, Tear Substitutes and Tear Models, J. British Contact Lens Assoc., 16(2):57-66, 1993.

45. Fowler S. A., Allansmith M. R., Evolution of Soft Contact Lens Coatings, Arch. Ophthalmol., 98, 95-99, 1980.

46. Abbott J. M., Bowers R. W. J., Franklin V. J., Tighe B. J., Studies in the Ocular Compatability of Hydrogels (IV): Observations on the Role of Calcium in Deposit Formation, J. Brit. Contact Lens Assoc., 14(1): 21-28, 1991.

47. Tripathi R. C., Tripathi B. J., & Ruben M., The Pathology of Soft Contact Lens Spoilage, Opthalmology, 1980; 87:365-380.

48. Hart D. E., Shih K., Surface Interactions on Hydrogel Extended Wear Contact Lenses:Microflora and Microfauna on Lenses in situ, J. Optom. Physiol. Opt, 64:10, 1987.

49. Bowers R. W. J., Tighe B. J., Studies Of Ocular Compatability Of Hydrogels: White Spot Deposits-Chemical Composition And Geological Arrangement Of Components, Biomaterials, 1987; 94:1315-1321.

50. Hill R. M. and Fatt I., Science , 142, 1295 (1978).

51. Guillon M., Acuvue Clinical Research Update, Optician, 202(5317):13-15, 1991.

51. Ivins P., Disposability and Planned Replacement-A personal view, Optician, 201(5290):18-22, 1991.

52. Chrisite C., Edwards K., Frequent Replacement of Soft Contact Lenses, Optician 201(5286):26-31, 1991.

53 . Grant G., A Breakthrough in Soft Contact Lens Technology, Optician, 204(5383):21-26, 1992.

54. Marren S. E. Contact Lens Wear, Use of Eye Cosmetics, and Meibomian Gland Dysfunction, J. Opt. Vis. Sci., 71(1):60-62, 1994.

55. Guillon M., Allary J. C., Guillon J., Orsborn G., Clinical Management of Regular Replacement: Part 1: Selection of Replacement Frequency, ICLC, 19:104-120, 1992.

56. Lin S. T., Mandell R. B., Leaby C. D., Newell J. O., Protein Accumulation on Disposable Extended Wear Lenses, CLAO J., 17(1):44--51, 1991.

57. Hart D. E., Surface Interactions on Hydrogel Contact Lenses: Scanning Electron Microscopy, J. Am. Optom. Assoc., 1987.

58. White G. L., Thiese S. M., Olafsson H. E., Lundergan M. K., Disposable Contact Lenses, Amer. Family Practitioner, 43(5):1643-1646, 1991.

59. Borassa S., Benjamin W. J., RG Wettability: The First Day Could Be the Worst Day!, ICLC, 19:25-34, 1992.

60. Mertz G., Nason R., Brewitt H., Guillon M., Lutcher B., Alberti R. M., Rutten H., Van der Linden J. W., Gleit J., Yi F., A Monthly Replacement Soft Lens, Optician, May1st, p19-29, 1992.

61. Snyder C., Hammack G. G., Daily Disposed Hydrogel Lenses- a comparison with biweekly Replacement, J. Am. Optom. Assoc., 65(3):164-169, 1994.

62. Marshall E., Disposable vs. Non-Disposable Contact Lenses- the relative Risk of Ocular Infection, J. Am. Otom. Assoc., 63(1):28-34, 1992.

63. Quinn G., Clinical Experience of Two Disposable Lenses for Daily Wear, Optician 202(5308):24-26, 1991.

64. Pseudovs K., Phillips A. J., A Clinical Comparison of the Johnson & Johnson Acuvue, the Barnes-Hind Calendar and the Bausch & Lomb Medalist Disposable Contact Lenses, Lcin. Exp. Optom., 77(6):264-271, 1994.

65. Watanbe R. K., Ridder W. H., Tomlinson A., Visual Performance of Three Disposable Soft Contact Lenses, ICLC, 20:106-112, 1993.

66. Hu J., Tartaglia L., Kohler J., Lett J., Shih K., Gentle Touch, a Lens Material Resistant to Protein Deposition, CLAO J., 21(2):93-95, 1995.

67. Llabres C. M., Antunez D. M., Evaluating Protein Deposits on Preference and CSI Lenses, Spectrum Dec:23-29, 1994.

68. Davies I., Davies G., Tinted Soft Contact Lenses-A Review, Optician, 206(5476):18-25, 1994.

69. Laxter M., "Soft Tinted Contact Lenses and Colour Discrimination", ICLC, 17:88-91, 1990

70. Kaminski E. J., Oglesby R. J., Wood N. K., Sandrik J., The Behaviour of Biological Materials at Different Sites of Implantation, J. Biomed. Mater. Res., 2:8188, 1968.

71. Pye D. C., Current Australian Attitudes to Contact Lens Extended Wear, Clin. Exp. Optom., 70(3):85-90, 1987.

72. Bergmanson J. P. G., Benjamin W. J., Fungal Deposition: A Sign Of The Times, ICLC 17:42-44, 1990.

73. Miller D., Optics and Refraction- A User Friendly Guide, Vol1, Textbook of Ophthamology, p.11.2-11.3.

74. Guyton A. C., Textbook of Medical Physiology, 8th Ed., W. D. Saunders Co., US, p.534-545, 1991.

75 Davson H., Physiology of the Eye, 5th ed., p. 792-794, Pergamon Press, New York, 1990.

76. Guillon J & M, Tear Film Examination of the Contact Lens Patient, Contact Lens Monthly, 206(5421), 21-29, 1993.

77. Mishima S., Gasset A., Klyce S. D., Baum J. L., "Determination of Tear Volume and Tear Flow", Invest. Ophthamol., 5(3):264-276, 1966.

78. Carney L. G., Hill R. M., Human Tear Buffering Capacity, Arch. Ophthamol., 97:951-952, May 1979.

79. Nicolades 1986. Recent Findings on the Chemical Composition of the Lipids of Steer and Human Meibomian Glands, In Holly F. J. (Ed.), The Precorneal Tear Film in Health, Disease, and Contact Lens Wear, Lubbock, TX:Dry Eye Institute, p. 570-596, 1986.

80. Holly F., Tear Film Formation and Rupture: An Update, The Pre-Ocular Tear Film, ed. Holly F., Dry Eye Institute, Texas, 1996.

81. Carney . G., Hill R. M., Human Tear pH, Arch. Ophthamol., 94:821-824, May 1976.

82. Fischer F. H., Wiederholt M.., Human Precorneal Tear Film pH Measured by Microelectrodes, Graefe's Arch. Clin. Exp. Ophthamol., 218:168-170, 1982

83. Mishima, S. and Maurice D.M., The Oily Layer of the Tear Film and Evaporation from the Corneal Surface, Experimental Eye Research, 1, 39, 1961.

84. Hoffman A. S., Ratner B. D., Garfinkle A. M., et al, Polymers in Medicine II - Biomedical and Pharmaceutical Applications, Plenum Press, New York, 157-173, 1985.

85. Holly FJ., Surface Chemistry of Tear Components Analogs, J. Colloid Interface Sci., 1974:49, 221-231.

86. Whikehart D. R., "Biochemistry of the Eye", Butterworth-Heinemann, p.98, New York, 1994.

87. Nicolaides 1989. Nicolaides N., Santose E. C., Smith R. E., Jester J. V., Meibomian Gland Dysfunction III: Meibomian Gland Lipids, Invest. Ophthamol. Vis. Sci., 30:946-951, 1989.

88. Hart D. E., Lipid deposits which form on extended wear contact lenses, Int. Contact Lens Clin., 11:348-62, 1984.

89. Hart D. E., Tisdale R. R., Sack R. A., Origin and Composition of Lipoidal Deposits on Soft Contact Lenses, Ophthamology, 93:495-503, 1986.

90. Tripathi R. C., Ruben M., Trpathi B. J., Soft Lens Spoilation in Soft Contact Lenses Clinical and Applied Technology, ed. M. Ruben, Wiley, New York, 1978.

91. Fischer FH., Wiederholt M., The pH Dependency of Sodium and Chloride Transport in the Isolated Human Cornea, Invest. Opthal. Vis. Sci., 1978:17, 810-813.

92. Gachon A. M., Bilbaut T., Dastugue B., Adsorption Of Tear Proteins On Contact Lenses, Exp. Eye Res., 1985; 40:105-116.

93. Wedler F. D., Illman B. L., Horensky D. S., Mowrey-McKee M., Analysis of Protein and Mucin Components Deposited on Hydrophilic Contact Lenses, Clinical & Expt. Optom., 70(2):59-68, Mar/Apr 1987.

94. Temel A., Kazokogul H., Taga Y., Orkan A., The Effect of Contact Lens Wear on Tear Immunoglobulins, Clao J., 17(1):69-71, 1991.

95. Gachon AM., Verrelle P. Betail G., Datugue B., Immunological and Electrophoretic Studies of Human Tear Proteins, Exp. Eye Res., 1979:29, 539-553.

96. Moore JC., Tiffany JM., Human Ocular Mucus Origins on Preliminary Characterisation, Exp.Eye Res., 1979:29, 291-301.

97. Wedler F. C., Illman B. L., Horensky D. S., et al, Analysis Of Protein And Mucin Components Deposited On Hydrophilic Contact Lenses, Clinical Experimental Optometry, 1987; 70:59-68.

98. Rapp J., Broich J. R., Lipid Deposits On Worn Contact Lenses, CLAO J., 1984; 10:235-239.

99. McCully J. P., Dougherty J. M., Meibomian Lipids in Chronic Blepharitis, In Holly F. J. (Ed.), The Precorneal Tear Film in Health, Disease, and Contact Lens Wear, Lubbock, TX:Dry Eye Institute, p. 626-631, 1986.

100. Bonavida B., Sapse A. T., Human Tear Lysozyme - II. Quantitative Determination with Standard Schirmer Strips, Am. J. of Ophthamology, 66(1):70-79, July 1968.

101. Tripathi P. C., Tripathi R. C., Analysis of Glycoprotein Deposits on Disposable Soft Contact Lens, Invest. Ophthamol. Vis. Sci., 33(1):121-125, 1992.

102. Andrade J. D., and Hlady V., Vroman Effects, Techniques and Philosophies, J. Biomater. Sci. Polymer Edn., 2(3):161-172, 1991.

103. Jones L. W. J., Contact Lens Deposits: Their Causes and Control, Contact Lens Journal, 20(1):6-13, 1991.

104. Pallassana N.V., Surface Functionisation by RF Plasma Treatment of Polymers for Immobilisation of Bioactive-Molecules, J. Biomater. Sci. Polymer Edn., 6(2):181-193, 1994.

105. Panchalinghma V., Poon B., Huo H., Savage C. R., Timmons R. B., Eberhart R. C., Molecular Surface Tailoring of Biomaterials Via Pulsed RF Plasma Discharges, J. Biomater. Sci., Polymer Edn., 5(1/2):131-145, 1993.

106. Golander C. G., Lassen B., Nilsson-Ekdahl K., Nilsson U. R., RF-Plasma-Modified Polystyrene Surfaces for Studying Complement Activation, Journal of Biomaterials Science, Polymer Edition, 4(1):25-30, 1992.

107. Favia P., Fracassi F., D'Agostino R., X-ray Photoelectron Spectroscopy of Plasma Polymerised Films From Tetramethylsilane-Containing Feeds, Journal of Biomaterials Science, Polymer Edition, 4(1):61-73, 1992.

108. Planck H., Egbers G., Syre I., Polyurethanes in Biomedical Engineering, Elsevier, Amsterdam, 1984.

109. Lelah M. D., Cooper S. L., Polyurethanes in Medicine, CRC Press, Boca, Raton, FL., 1986.

110. Piskin E., "Plasma Processing of Biomaterials", Journal of Biomaterials Science, Polymer Edition, 4(1):45-60, 1992.

111. Planck H., Syre I., Dauner M., Egbers, Polyurethanes in Biomedical Engineering II, Elsevier, Amsterdam, 1987.

112. Dekker A., Reitsma K., Beugeling T., Banjtes A., Feijen J., Van Aken W. G., Adhesion of Endothelial Cells and Adsorption of Serum Proteins on Gas Plasma-Treated Polytetrafluoroethylene, Biomaterials, 12(2):13-138, 1991.

113. Chapman B., Glow Discharge Processes, John Wiley & Sons, New York, 1980.

114. Butler H. S., Kino G. S., Plasma Sheath Formation by Radio-Frequency Fields, The Physics of Fluids, 6(9):1346, Sept. 1963.

115. Nasser E., Fundamentals of Gaseous Ionisation and Plasma Electronics, Wiley Interscience, London, 1971.

116. Ephrath L. M., Etching Needs for VLSI, Solid State Technology, 5:87, Jul. 1982.

117. Coburn J. W., Plasma Assisted Etching, Plasma Chemistry and Plasma Processing, 2:1, 1982.

118. Coburn J. W., Kay E., Positive Ion Bombardment of Substrates in RF Diode Glow Discharge Sputtering, J. Appl. Phys. 43:4965, Dec. 1972.

119. Bruce R. H., Frequency Dependence of CCl4 Etching, Plasma Processing: Symposium on Plasma Etching and Deposition, May 1980, 81:243.

120. Koenig H. R., Maissel L. I., Application of RF Discharges to Sputtering, IBM Journal of Research and Development, 168, Mar. 1970.

121. Chapman B. N., Minikiewicz, Flow Rate Effects in Plasma Etching, J. Vac. Sci. Technol., 15:329, Mar. / Apr. 1978.

122. Coburn JW., Chen M., Dependence of F atom density on pressure and flow rate in CF_4 glow discharges as determined by emission spectroscopy , J. Vac. Sci. Technol., 1981:18, 353-6.

123. Okano H., Yamzaki T., Horiike Y., High Rate Reactive Ion Etching Using a Magnetron Discharge, Solid State Technology, 25:166, Apr. 1982.

124. Flamm D. L., Donnelly V. M., Ibbotson D. E., Basic Chemistry an Mechanisms of Plasma Etching, Semiconductor International, 6(3):136, Apr. 1983.

125. Flamm D. L., Mucha J. A., Plasma Etching, The Chemistry of Semiconductor Industry, Blackie & Son Ltd., Glasgow, 1987.

126. Flamm D. L., Donnelly V. M., Ibboson D. E., Basic Principles of Plasma Etching Silicon Devices, Microstructure Science, 8:189, Academic Press, 1984.

127. Battey JW., Swain H. H., A Review of Plasma Processing Fundamentals, Solid State Technology, 28(4):211, Apr. 1985.

128. Pennebaker W. B., Influence of Scattering and Ionisation on RF Impedance in Glow Discharge Sheaths, IBM Journal of Research and Development, 23:16, Jan. 1979.

129. Truesdale E. A., Smolinsky G., Mayer T. M., The Effect of Added Acetylene on the RF Discharge Chemistry of C_2F_6: A Mechanistic Model For Fluorocarbon Plasma, J. Appl. Phys., 51:2909, May 1980.

130. Williams T., Empedocles, Collins Biographical Dictionary of Scientists, Harper Collins, Glasgow, 1994, p.156.

131. Blakley D.C.W., Chemical Studies of Plasma Etchants Used in Integrated Circuit Manufacture, The University of Aston in Birmingham, 1991.

132. Ratner B. D., Plasma Deposition for Biomedical Applications: A brief Review, Journal of Biomaterials Science, Polymer Edition, 4(1):3-11, 1992.

133. Oeher C., Bauser H., Hellwig G., Muller M. and Schindler B., Plasma Polymerisation and Grafting of ethylene oxide on polysiloxane surfaces, Journal of Biomaterials Science, Polymer Edition, 4(1):13-23, 1992.

134. Mogab C. J., Dry Etching, VLSI Technology, McGraw-Hill, London, 303, 1983.

135. Terlington J. G. A., Feijen J., Hoffman A. S., Immobilisation of Surface Active Compounds on Polymer Supports Using a Gas Discharge Process, Journal of Biomaterials Science, Polymer Edition, 4(1):31-34, 1992.

136. Kiaei D., Hoffman A. S., Horbett T. A., Tight Binding of Albumin to Glow Discharge Treated Polymers, Journal of Biomaterials Science, Polymer Edition, 4(1):35-44, 1992.

137. Anderson A. J., Multiple Processing: A Systems Overview, Prentice-Hall, London, 1989.

138. Vossen J. L., Glow Discharge Phenomena in Plasma Etching and Plasma Deposition, J. Electrochem. Soc.: Solid State Science and Technology, 126:139, Feb. 1979.

139. Bell A. T., An Introduction to Plasma Processing, Solid State Technology, 20(4):89, Apr. 1985.

140. Battencourt J. A., Fundamentals of Plasma Physics, Pergamon Press, Oxford, 1988.

141. Szycher M., Poirier V. L., Ind. Eng. Chem. Prod. Res. Dev., 22:588, 1983.

142. Burggraaf P., Solutions for 'pump damaging' etch and CVD processes, Semiconductor International, 66-71, Oct. 1986.

143. Duval P., Problems in pumping aggressive, poisonous and explosive gases, Vacuum, 38:651-8, 1988.

144. Gorowitz B. Saia R. J., Reactive ion Etching, VLSI Electronics: Microstructure Science", Academic Press, 8:297, 1984.

145. Bell A. T., Abstract: Fundamentals of Plasma Chemistry, J. Vac. Sci. Technol., 16(2):118, Mar/Apr. 1979.

146. Cadogan J. I. G., Principles of Free Radical Chemistry, The Chemical Society, London, 1973.

147. Irving S. M., Plasma Oxidation Process for Removing Photoresist Films, Solid State Technology, 14(6):47, Jun. 1971.

148. Deshmukh V. G. I., Cox T. I., Physical Characterisation of Dry Etching Plasma Used In Semiconductor Fabrication, Plasma Physics and Controlled Fusion, 30(1):21, 1988.

149. Reinberg A. R., Plasma Processing With a Planar Reactor, Circuits Manufacturing, 25, Apr. 1979.

150. Dautemont-Smith W. C., Gottscho R. A., Plasma Processing Mechanisms and Applications, Semiconductor Materials and Process Technology Handbook, Noyes Publications, Park Ridge, New Jersey, USA, 1988.

151. Schultz R. J., Reactive Plasma Etching, VLSI Technology, McGraw-Hill, 184, 1988.

153. Boenig H. V., Fundamentals of Plasma Chemistry and Technology, Technomic Pub. Co., Lancaster, 1988.

154. Smith E. B., Basic Chemical Thermodynamics, Oxford University Press, Oxford, 42-4, 1973.

155. Hutchinson I. H., Principles of Plasma Diagnostics, Cambridge University Press, 1987.

156. Fonash S. J., Advances in Dry Etching Processes: A Review, Solid State Technology, 28(1):150, Jan. 1985.

157. Emslie B., May P., Oil Free Vacuum Pumping System for Semiconductor Processes, CIPG 87, Antibes, France, Conference Proceedings, 93-7, 1987.

158. Gokan H., Onishin Y., Saigo K., Micro Electronics, 1985:1, 251.

159. Moss SJ., Ledwith FF., The Chemistry of Semi Conductors, Balckie and Sons, New York, 1987.

160. Shabushing J. G., Demko P.R., Savage R. N., Applications of Optical Emission Spectroscopy to Semiconductor Processing, Mat. Res. Soc. Symp. Proc., 38:77, 1985.

161. Metcalfe E., Atomic Absorption and Emission Spectroscopy, John Wiley & Sons, 1987.

162. Box G. E. P., Hunter W. G. , Hunter J. S. Statistics for Experimenters, Wiley, New York, 1978.

163. Pearse R. W. B., Gaydon A. G., The Identification of Molecular Spectra, Chapman and Hall, London, 1965.

164. Sariri R., Tear Protein Interaction with Hydrogel Contact Lenses, thesis, Aston University, 1995.

165. Mirejovsky D., Bakhit P., Patel AS., Stability of Lysozyme Absorbed in High Water Content Lenses, Contact Lens Research Allergan Inc., Irvin CA, Poster.

166. M. A. Lemp and J. R. Hamil, Arch. Opthamol., 89, 1973, 103.

167. S. P. Lin and H. Brenner, J. Col. Interface Sci., 89(1), 1982, 226.

168. A. Sharma and E. Ruckenstein, J. Col. Interface Sci.,

169. A. Sharma and E. Ruckenstein, Am. J. of Optometry and Physiological Optics, 62(4), 1985, 246.

170. M. F. Refojo, p.195 in Encyclopaedia of Polymer Science and Technology, ed. R. N. Bikales, Wiley Interscience, New York, 1976.

171. Meares P. (Ed.), Membrane Separation Processes, Elsevier, Amsterdam, 1974.

172. Wedler F. C., Analysis Of Biomaterials Deposited On Soft Contact Lenses, J. Biomed, Mater. Res., 1977; 11:525-535.

173. Mandelkern, L. An Introduction to Macromolecules, Springer-Verlag, New York, 1972).

174. Phillips A. J., Surface Deposition and Cracking of a Tinted Hydrogel Contact Lens, Clinic. Exp. Opt., 77(5):210-214, 1994.

175. Gudmundsson O. G., Woodward D. F., Fowler S. A., et al, Identification Of Proteins In Lens Surface Deposits By Immunoflurescence Microscopy, Arch. Ophthamol., 1985; 103:196-197.

176. Andrade J.D., Hlaly V., "Vroman effects, techniques and philosophies", Journal of Biomaterials Science- Polymer Edition, 2(3):161-172, 1991.

177. Norde W., Lyklema J., Why Proteins Prefer Interfaces, J. Biomater. Sci. Polymer Edn., 2(3):183-202, 1991.

178. Andrade J. D., "Surface and Interfacial Aspects of Biomedical Polymers", Vol. 2: Protein Adsorption, Plenum Press, New York, 1985.

179. Tighe B. J., Hydrogels as Contact Lens Materials, Hydrogels in Medicine and Pharmacy, CRC Press, 1987.

180. Wong H. J., Quinn J. A., "Colloidal and Interfacial Aspects of Biomedical Polymers", Vol. 2., Protein Adsorption, Andrade J. D. (Ed.), Plenum Press, New York, 1985.

181. Cheng K. H., Kok J. H., Van Mil C., Kiljstra A., Selective Binding of a 30 kD Protein to Disposable Hydrophilic Contact Lenses, Inv. Ophthamol. Vis. Sci., 31(11):2244-2247, 1990.

182. Leninger, A.L., Biochemistry, Second Edition, Worth Publishers, Inc., (1975).

183. Ng CO., Larke JR., Tighe BJ., Polymers in Contact Lens Applications: Hydrogel Polymer II, Optician, 1971:12, 162.

184. Ng CO., Corkhill PH., Jolly AM., Tighe BJ., Synthesis ofHydrohels 1: Copolymers of Hydroxylalkyl Acrylates and Methacrylates: Water Binding Studies, Polymer, 1987:28, 1758.

185. Yasuda G., Nyquist G., Caldwelll K. D., Payor R., McCraw E. C., "Quantification of Total Protein Deposits on Contact Lenses by Means of Amino Acid Analysis", Inv. Ophthamol. Vis. Sci., 34(5):1804-1813, 1993.

186. Van Straaten J., Peppas N. A., Modelling of Protein Adsorption on Polymeric Surfaces, J. Biomater. Sci. Polymer Edn., 2(2):91-111, 1991.

187. Horbett T. A., Protein Adsorption to Hydrogels, Hydrogels in Medicine and Pharmacy ed. N. L. Peppas, CRC Press, Baco Raton, FL., 127, 1986.

187. Vroman L., Adams A. L., Peculiar Behaviour of Blood at Solid Interfaces, J. Polymer Sci.:Part C, 34:159-165, 1971.

188. Langer JR., Folkman RF., Arnebrant, T. Nylander, T., Adsorption of Insulin on Metal Surfaces in Relation to Association Behaviour, J. Colloid interface Sci., 122, 557-566, (1988).

189. Van Noort J., Brook N. A., Modelling of Protein Adsorption on Polymeric Surfaces, J. Biomater. Sci. Polymer Edn., 2(2):91-111, 1991.

190. Mannucci LL, Moro F., Cosani A., Conformational State of Lacrimal Proteins Adsorbed on Contact Lenses, Curr. Eye Res., 4(7):736, 1985.

191. Yoshimoto J., Shuzo I., Studies On The Interaction Between Contact Lenses And Tear Fluid (Viii). Phenomenon Of Human Tear Lysozyme And Lactoferrin Adsorption Onto Contact Lens Materials, J. Japan Contact Lens Sym, 1984; 26:225-229.

192. Holly F. J., Protein And Lipid Adsoprtion By Acrylic Hydrogels And Their Relation To Water Wettability, J. Polymer Science, 1979; 66:409-417.

193. Castllo E. J., Koenig J. L., Anderso J. M., et al, Protein Adsoprtion On Hydrogels. Ii. Reversible And Irreversible Interactions Between Lysozyme And Soft Contact Lens Surface. Biomaterials, 1985; 6:338-345.

194. Gok E., Kiremitci M., Serdar Ates I., Protein Adsorption to Functional Hydrophilic Polymer Beads: Role of Structural Properties and Medium Conditions, Private Communication, Ankara, Turkey, 1994.

195. Sone R. P., Mowrey-McKee M. F., Kreutzer P., Protein: A Source Of Lens Discolouration, Contact Lens Forum, 1984; 9:33-41.

196. Dillman, W.J., Miller l F., On the Adsorption of Serum Proteins on Polymer Membrane Surfaces, J. Colloid Interface Sci., 44, 221, (1973).

197. Norde W., Adsorption of Proteins From Solution at the Solid-Liquid Interface, Advances in Colloid and Interface Science, 25, 267-340, 1986.

198. Horbett, T. A., Proteins at Interfaces: Physiochemical and Biochemical Studies, ed. T.A. Horbett and J. L. Brash, American Chemical Society, Washington DC, 239, 1987.

199. Brash J. L., Hove P. T., Protein Adsorption Studies on 'Standard' Polymeric Materials, J. Biomaterial Sci. Polymer Ed., 4(8):,591-599 1993

200. Horbett T. A., and Brash J. L., Proteins at Interfaces: Current Issues and Future Prospects, ACS Symposium Series, 343, 1, 1987.

201. Fitton JH., Cells, Surfaces and Adhesion: PHD. Thesis, University of Aston in Birmingham, 1993.

202. Brash J. L., Interaction of Blood with Natural and Artificial Surfaces, ed. E. W. Saltzman, Dekker, New York, 37, 1981.

203. Hench L. L., The Interfacial Behaviour of Biomaterials, 1979, J. of Biomedical Material Research, 14:803-811, 1980.

204. Adams D. J., Evans M. T. A. Evans, Mitchell J. R., Phillips M. C., Rees P. M., Adsorption of Lysozyme and Some Acetyl Derivatives at the Air-Water Interface, J. Polymer Sci:Part C, 34:167-179, 1971.

205. Sakuri Y., Akaike T., Kataoka K., Okano T., Interfacial Phenomena in Biomaterials Chemistry, Biomedical Polymers, Academic Press, p.335-343, 1980.

206. Bezkorovainy A., Iron Proteins, Iron and Infection, Bullen J. J., Griffiths E. (Ed.), John Wiley & Sons, 1987.

207. Pitt, W.G., Cooper, S.L., Albumin Adsorption on Alkyl Chain Derivatized Polyurethanes: 1. The Effect of C-18 Alkylation, J. Biomed,. Mater. Res., 22, 359-382, (1988).

208. Lensen, H.G.W., Bargeman, D., Bergveld, P., Smolders, C.A., Feijen, J., High Performance Liquid Chromatography as a Technique to Measure the Competitive Adsorption of Plasma Proteins onto Lattices, J. Colloid interface Sci., 99, 1-8, (1984).

209. Wood, W.G., Gadow, A., J. Clin. Chem. Clin. Biochem., 21, 7X9-797, (1983).

U8. Kesting R. B., Synthetic Polymeric Membranes, Wiley Interscience, New York, 2nd ed.:1, 1985.

210. Boonstra A., Van Haeringen N., Kijlstra A., Human Tears Inhibit the Coating of Proteins to Solid Phase Surfaces, Curr. Eye. Res., 4(1):1137-1144, 1985.

211. Greene J. E., "Abstract: Optical Spectroscopy for Glow Discharge Sputtering Diagnostics and Process Control", J. Vac. Sci. Technol., 15(2):203, 1978.

212. Curtis B. J., Optical end-point Detection for the Plasma Etching of Aluminium, Solid State Technology, 23:129, Apr. 1980.

213. Harshbarger W. R., Porter R. A., Miller T. A., Norton P., A Study of the Optical Emission from a RF Plasma During Semiconductor Etching, J. Applied Spectroscopy, 31(3):201, 1977.

214. Marcoux P. J., Foo P. D., Methods of end point Detection For Plasma Etching, Solid State Technology, 24(4):115, Apr. 1981.

215. Krogh O., Slomowitz H., Melaku Y., Blom H., Summary Abstract: Spectroscopic Diagnostics of Photoresists Erosion in an Aluminium Etch Plasma, J. Vac. Sci., Technol. A, 5(4):1929, Jul/Aug. 1987.

216. Favia P., Fracassi F., D'Agostino R., X-ray Photoelectron Spectroscopy of Plasma-Polymerised Films form Tetramethylsilane-Containing Feed, J. Biomater. Sci. Polymer Edn., 4(1):61-73, 1992.

217. Pelletier J., Cook M. J., "Microwave Plasma Etching of Si and SiO_2 in Halogen Mixtures: Interpretation of Etching Mechanisms", J. Vac. Sci. Technol. B, 7:59-67, 1989.

218. Felts J. Lopata E., "Measurements of Electron Temperature in a Capacitively Coupled Plasma Using Emission Spectroscopy", J. Vac. Sci. Technol. A, 6(3):2051, May/Jun. 1988.

218. Coburn J. W., Hen M., Optical Emission Spectroscopy of Reactive Plasma; A Method for Correlating Emission Intensities to Reactive Particle Density, J. Appl. Phys., 51(6): 3134, Jun. 1980.

219. Webb A. P., Smith J. A., Applications of in-situ SIMS During Processing of Electronic materials, Surface and Interface Analysis, 12:303, 1988.

220. Coburn J. W., Mass Spectrometric Studies of Positive Ions in RF Glow Discharges, Thin Solid Films, 171:65-80, 1989.

221. O'Hanlon J. F., A User's Guide to Vacuum Technology, Wiley Interscience, New York, 1989.

222. Raby B. A., Mass Spectrometric Study of Plasma Etching, J. Vac. Sci. Technol., 15(2):205, Mar/Apr. 1978.

223. Lehman H. W., Heeb E., Frick K., Plasma Diagnosis by Time Resolved Mass Spectrometry, Solid State Technology, 24:69, Oct. 1981.

224. Taylor G. N., Wolf T. M., Oxygen Plasma Removal of Thin Polymer Films, J. Polymer Engineering Science, 20(16): 1087-1092, 1980.

225. M.A. Cohen Stuart, G. J. Fleer and J.M.H.M. Scheutjens, J. Colloid Interface Sci., 97 (1984) 526.

Appendices

Appendix 1: Alternative Methods of Expressing Various Physical Quantities

Mass (SI unit : kg)

g	=	10^{-3} kg		
mg	=	10^{-3} g	=	10^{-6} kg
μg	=	10^{-6} g	=	10^{-9} kg

Length (SI unit : m)

cm	=	10^{-2} m
A	=	10^{-10} m
nm	=	10^{-9} m
pm	=	10^{-12} m

Volume (SI unit : m^3)

l	=	dm^3	=	10^{-3} m^3
ml	=	cm^3	=	10^{-6} m^3
μl	=	10^{-3} cm^3		

Concentration (SI unit : $molm^{-3}$)

M	=	$moll^{-1}$	=	$moldm^{-3}$	=	10^3 $molm^{-3}$
mgl^{-1}	=	$mgcm^{-3}$	=	ppm	=	$10^{-3}gdm^{-3}$

Pressure (SI unit : $Nm^{-2} = kgm^{-1}s^{-2}$)

Pa	=	Nm^{-2}	
atmos	=	101 325 Nm^{-2}	
bar	=	105 Nm^{-2}	
torr	=	mmHg	= 133.322 Nm^{-2}

Energy (SI unit : $J = kgm^2s^{-2}$)

cal	=	4.184 J
erg	=	10^{-7} J
eV	=	1.602 * 10^{-19} J

Appendix 2: Geometrical Perspective

An attempt has been made to integrate information from a number of Sources by developing a lens model:

Density	g/cm^3
Water (P_W)	1.0
Polymer (P_P)	1.28
Hydrated Polymer (P_G)	1.17

Source: Ng C. O., PhD Thesis 1974

Initially the actual water content of the polymer-protein system is calculated, to assess the actual linear swelling of the system, and the actual thickness of the hydrated material:

Ww = , W_G = water content of hydrated polymer

ρ_P = density of polymer, ρ_G = density of hydrated polymer

V_P = volume of polymer, V_G = volume of hydrated polymer

Water content of hydrated polymer:

$$\frac{W_W}{W_G} = \frac{\rho_P - \rho_G}{\rho_G \left(\frac{\rho_P}{\rho_W} - 1\right)}$$

$$= \frac{1 - \frac{\rho_G}{\rho_P}}{\rho_G \left(\frac{1}{\rho_W} - \frac{1}{\rho_P}\right)}$$

$$= \frac{1 - \frac{1.17}{1.28}}{1.17 \left(\frac{1}{1.10} - \frac{1}{1.28}\right)}$$

$$= 0.336$$

Volume Swell between hydrated polymer and dehydrated polymer:

$$\frac{V_G}{V_P} = \frac{W_G}{W_P} \times \frac{\rho_P}{\rho_G}$$

$$= \frac{1}{(1 - \frac{W_W}{W_G})} \times \frac{\rho_P}{\rho_G}$$

$$= \frac{1}{(1 - 0.336)} \times \frac{1.28}{1.17}$$

$$= 1.647$$

Linear Swelling of hydrated polymer compared to dehydrated polymer:

$$= (\frac{V_G}{V_P})^{\frac{1}{3}}$$

$$= 1.18$$

Model of Lens Geometry

	Diameter (mm)	Thickness (mm)
Dehydrated	12.3	0.1
Hydrated	14.5	0.118

$$\frac{V_G}{V_P} = \frac{(\frac{\pi}{4}) \times 14.5^2 \times 0.118}{(\frac{\pi}{4}) \times 12.3^2 \times 0.10}$$

$$= 1.64$$

So in region 2 the mass of sample removed per etch is 0.019 μg/s for 1800 seconds which is equivalent to 34.2 μg per etch. So the volume of sample removed per etch is:

$$\frac{34.2 \times 10^{-6}}{1.28} = 2.67 \times 10^{-5} \text{ cm}^3$$

This is equivalent to:

$$2.67 \times 10^{-5} \times 1.64 = 4.38 \times 10^{-5} \text{ cm}^3$$

And relating this to the hydrated polymer is 0.265 μm per etch:

$$\frac{4.38 \times 10^{-5}}{\frac{\pi}{4} \times 1.45^2} = 2.65 \times 10^{-5} \text{ cm}$$

$$= 0.265 \quad \mu\text{m}$$

So from the data above this equates to a lysozyme penetration of ~ 2.7 microns.

Appendix 3: Statistical Treatment of EWC Determination Technique

The correlation of the sample points between the five samples lies at a 5% deviation, using the Mettler digital balance and 7% for the micro-force balance

Sample	EWC (%)
1	35.9
2	36.4
3	36.4
4	35.8
5	36.2
6	36.1
7	36.1
8	35.9
9	36.5
10	36.4
11	36.6
12	35.9
13	34.9
14	36
15	35.9
16	36
17	35.2
18	36.3
19	36
20	35.1
21	36.1
22	35.8
23	35.7
24	36.4
25	36.4
26	36.1
27	36.7
28	35.9
29	36.2
30	36.1
31	37
32	36.2
33	36.2

Appendix 2: Statistical Treatment of Error of Equilibrium Water Content (EWC) Determination Technique.

The important polymer, poly HEMA was chosen for a careful determination as to the accuracy of the technique foe EWC determination. Using two hydrated poly HEMA sheets, ninety nine discs (1.1 cm diameter) were cut. Using three discs for each determination thirty three EWC's were calculated at 37oC.

A statistical treatment of the above results reveals that this sample size of n = 33 yields a mean, x = 36.1 with a standard deviation, s n-1 = 0.4

Appendix 4: Statistical Treatment of Weight Determinations Between Mettler Balance and C. I. Electronics Microforce Balance

Mettler Balance(g)	Microforce Balance (g)	standard deviation
31.9801	32	0.014
31.7712	31.7	0.050
31.4679	31.5	0.023
31.2109	31.17	0.029
31.088	31	0.062
30.866	30.8	0.047
30.556	30.62	0.045
30.489	30.5	0.008
30.112	30.2	0.062
29.871	29.99	0.084
29.84	29.85	0.007
29.6456	29.66	0.010
29.431	29.51	0.056
29.2109	29.32	0.077
28.907	29.1	0.136
29.101	29.08	0.015
28.621	28.72	0.070
28.2907	28.36	0.049
28.1389	28.15	0.008
27.977	28.04	0.045
27.645	27.69	0.032
27.566	27.66	0.066
27.666	27.61	0.040
27.5403	27.57	0.021

Appendix 5: Reproducibility of Plasma Etching

GRAPH 1	
Concentration	Weight Loss
0.179	31.7
0.175	31.4
0.173	31.19
0.17	30.87
0.161	30.7
0.15	30.5
0.142	30.32
0.136	30.14
0.129	29.96
0.124	29.78
0.112	29.54
0.099	29.36
0.092	29.21
0.073	29.02
0.059	28.88
0.05	28.78
0.035	28.65
0.024	28.56
0.015	28.45
0.014	28.34

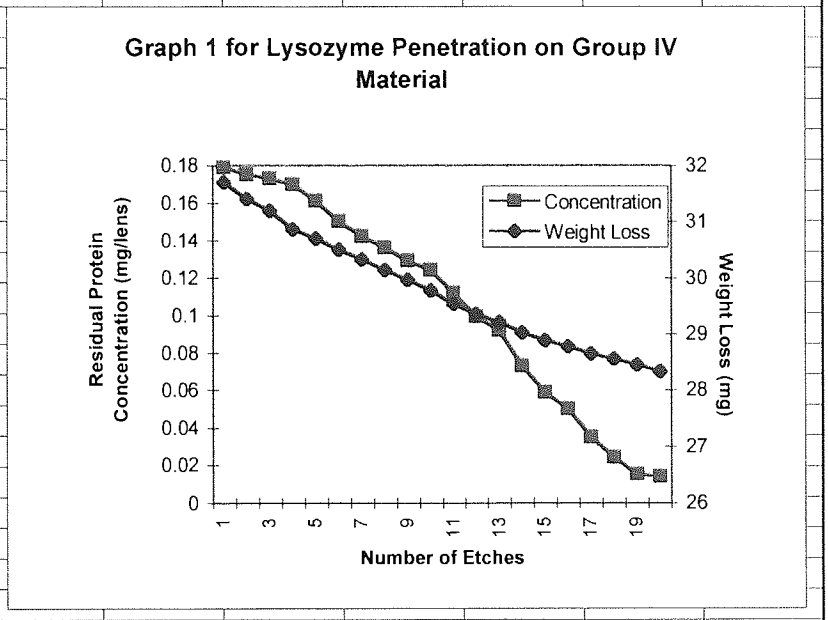

GRAPH 2	
Concentration	Weight Loss
0.181	31.21
0.179	31.01
0.173	30.85
0.17	30.6
0.161	30.4
0.155	30.2
0.148	29.99
0.136	29.84
0.129	29.7
0.124	29.48
0.112	29.24
0.099	29.06
0.092	28.81
0.073	28.72
0.059	28.58
0.05	28.48
0.035	28.35
0.024	28.26
0.015	28.15
0.014	28.04

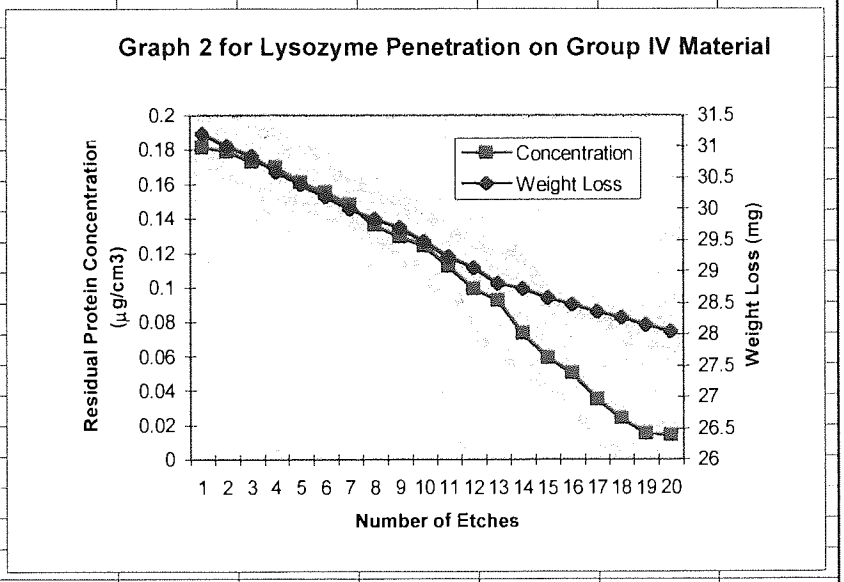

GRAPH 3	
Concentration	Weight Loss
0.181	31.21
0.179	31.01
0.173	30.85
0.17	30.6
0.161	30.4
0.155	30.2
0.151	29.99
0.146	29.84
0.14	29.7
0.136	29.48
0.131	29.24
0.129	29.06
0.125	28.81
0.118	28.72
0.112	28.58
0.099	28.48
0.092	28.35
0.073	28.26
0.059	28.15
0.05	28.04
0.035	27.99
0.024	27.96
0.015	27.91
0.014	27.87

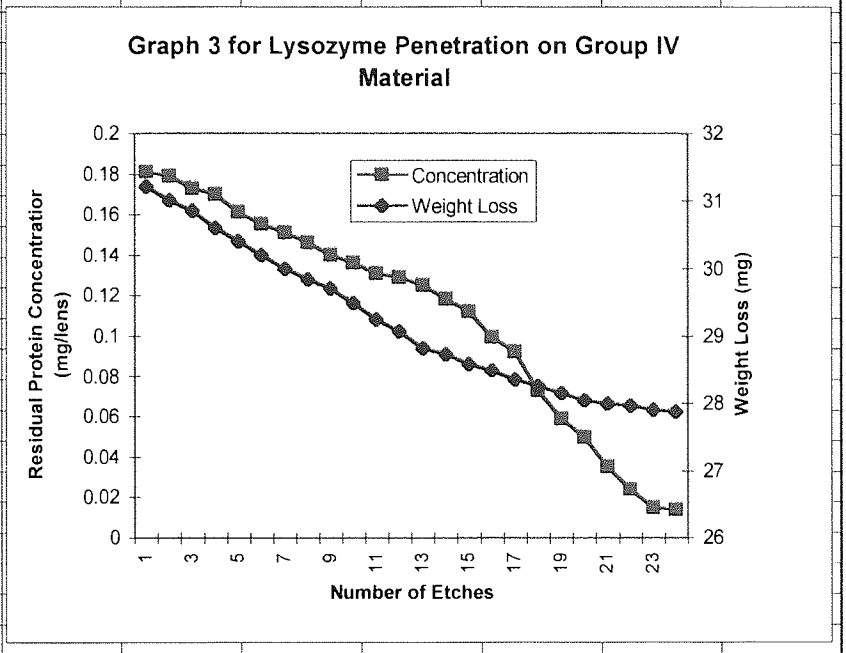

GRAPH 4	
Concentration	Weight Loss
0.201	32
0.199	31.7
0.193	31.5
0.19	31.17
0.181	31
0.175	30.8
0.171	30.62
0.166	30.5
0.16	30.2
0.156	29.99
0.149	29.85
0.138	29.66
0.125	29.51
0.119	29.32
0.097	29.1
0.086	29.08
0.08	28.72
0.069	28.36
0.057	28.15
0.044	28.04
0.036	27.69
0.021	27.66
0.015	27.61
0.014	27.57

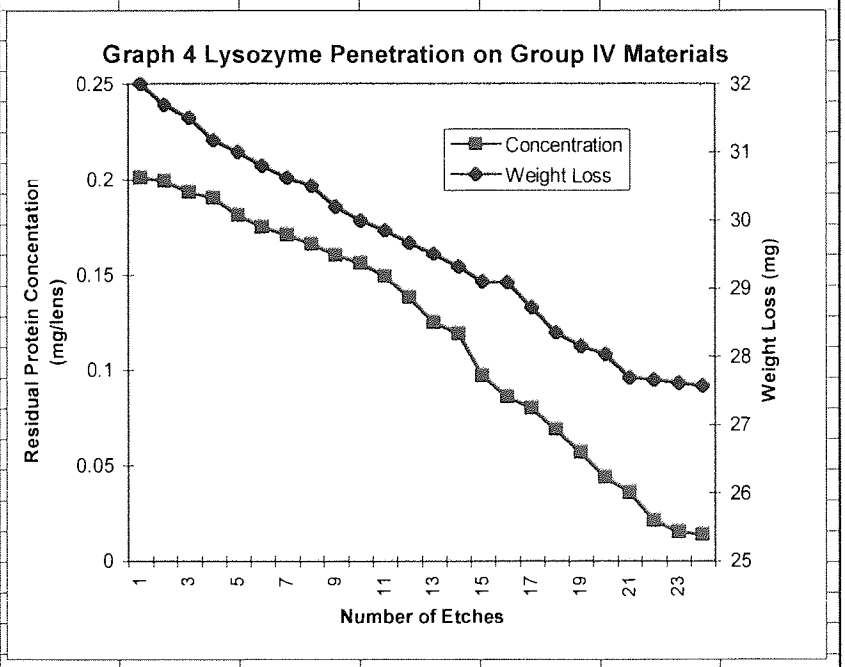

GRAPH 5	
Concentration	Weight Loss
0.201	32
0.199	31.7
0.196	31.5
0.192	31.17
0.188	31
0.183	30.8
0.176	30.62
0.17	30.5
0.166	30.2
0.158	29.99
0.15	29.85
0.138	29.66
0.125	29.51
0.112	29.32
0.097	29.1
0.086	29.08
0.08	28.72
0.069	28.36
0.057	28.15
0.044	28.04
0.036	27.69
0.021	27.66
0.015	27.61
0.014	27.57